



Comparison of Spacecraft Contamination Models with Well-Defined Flight Experiment

G.H. Pippin

Boeing Information Space & Defense Systems, Seattle, WA

Prepared for Marshall Space Flight Center
under Contract NAS8-40581
and sponsored by
the Space Environments and Effects Program
managed at the Marshall Space Flight Center

National Aeronautics and
Space Administration

Marshall Space Flight Center • MSFC, Alabama 35812

Available from:

NASA Center for AeroSpace Information
800 Elkridge Landing Road
Linthicum Heights, MD 21090-2934
(301) 621-0390

National Technical Information Service
5285 Port Royal Road
Springfield, VA 22161
(703) 487-4650

Table of contents	Page
Figure Titles	v
Introduction	1
Flight	2
Geometry of the Experiment	2
Vent locations	6
Materials	6
Contamination Sources	6
Outgassing	14
Computer Modeling of Exposure Levels	17
Analysis Results	25
Tray A4 Results	26
ESCA Measurements Location Map	26
Photographs	27
ESCA Data	28
Sputter Depth Profiles	29
Background Contamination	29
Tray C6 Results	30
ESCA Measurements Location Map	30
Photographs	31
ESCA Data	35
Sputter Depth Profiles	35
Tray E10 Results	35
Photographs	37
Surface Analysis Results	41

Table of contents (continued)	Page
Summary	44
Silicon Distribution	44
Coating Depths	44
Separation of Contributions from Different Contamination Sources	45
Summary of Modeling Calculations	46
ISEM Model Results	46
NASTRAN/NASAN Model Results	47
Plume Impingement (PLIMP) Model Results	48
Analysis	49
Conclusions	55
Model Comparison	55
Measured Results	56
Appendix A Detailed Results of ESCA Measurements from all Surfaces Examined under Contract NAS8-40581.	
Appendix B ESCA Depth Profiles Obtained for Selected areas from LDEF Tray Locations E10-8, C6-2, and A4-9.	
Appendix C Plots of Solar UV and Atomic Oxygen Exposure Levels at Selected Locations on the LDEF Trays being Examined.	
Appendix D SEM images from Tray E10-9	
Appendix E Contamination Deposited on LDEF Surfaces	
Appendix F Contamination Prediction Model (ISEM) Calculation for Selected LDEF Trays	

Figure Titles		Page
Figure 1.	Drawing of LDEF thermal blanket assembly showing velcro™ attachment locations and vent locations.	4
Figure 2.	Cross-section drawing of details of the UHCRE trays showing orientation of blanket with respect to tray walls.	5
Figure 3.	Vent location numbering system for tray E10.	7
Figure 4.	Vent location numbering system for tray C6.	8
Figure 5.	Vent location numbering system for tray A4.	9
Figure 6.	Dimensional details for areas of trays near side blanket vents.	10
Figure 7.	Cross-sectional detail of tray E10 side wall, frame holding thermal blankets, and cylinders holding experiment.	11
Figure 8.	Dimensional details for areas of trays near Earth and space end blanket vents.	12
Figure 9.	Cross-sectional detail of tray E10 end wall, rivet, and frame holding thermal blankets.	13

Figure Titles	Page
Figure 10. Outgassing measurements for DC6-1104™ adhesive and velcro™ fasteners used on the UHCRE.	16
Figure 11. Solar exposure on tray A4.	18
Figure 12. Solar exposure on tray C6.	19
Figure 13. Solar exposure on tray E10.	20
Figure 14. Atomic oxygen exposure on tray C6.	21
Figure 15. Atomic oxygen exposure on tray E10.	22
Figure 16. Range of Exposure Conditions for Tray Surfaces Examined.	23
Figure 17. Surface Properties Used for Solar Exposure Modeling.	24
Figure 18. Mission average values used for atomic oxygen modeling.	24
Figure 19. Surface Properties Used for Atomic Oxygen Fluence Modeling.	25

Figure Titles	Page
Figure 20. NASA post-flight photograph of tray A4.	27
Figure 21. NASA post-flight photograph of tray C6 with the thermal blanket removed.	31
Figure 22. Close-up photograph of area C6-2 (NASA PHOTO)..	32
Figure 23. NASA post-flight photograph of area C6-2 showing discoloration pattern.	33
Figure 24. Close-up photograph of area C6-2 showing relative position of the velcro™ and adhesive to the discolored area on the tray side and curved region of the tray lip (NASA PHOTO).	34
Figure 25. NASA post-flight photograph of tray E10.	37
Figure 26. NASA post-flight photograph of side of E10 towards row 11 showing discoloration at vent areas and along the tray wall(above the rivets).	38
Figure 27. NASA post-flight photograph showing close up of blanket vent at location E10-7.	39

Figure Titles	Page
Figure 28. NASA post-flight photograph showing exterior of one corner of tray E10.	40
Figure 29. Total Deposition at Typical Locations on E10-3, E10-8, and C6-2 from NASAN Model in Å	48
Figure 30. Orifice Flow Streamlines In Fraction of Total Mass Flow.	50
Figure 31. Orifice Flow Mass Flux In gm/cm ² /sec.	51
Figure 32. Mass Flux in gm/cm ² /sec. to Cylindrical Portion of Tray Edge.	52
Figure 33. Mass Flux in gm/cm ² /sec. to Flat Plate Portion of Tray Edge.	53
Figure 34. Fluence in gm/cm ² to Cylindrical Portion of Tray Edge.	53
Figure 35. Fluence in gm/cm ² to Flat Plate Portion of Tray Edge.	54
Figure 36. Silicon vs Aluminum Surface Content for Tray C6-2 ESCA Measurement Locations.	57
Figure 37. Silicon vs Aluminum Surface Content for Tray E10-8 and E10-3 ESCA Measurement Locations.	58

Figure Titles	Page
Figure 38. Silicon vs Aluminum Surface Content for Tray A4-9 ESCA Measurement Locations.	59
Figure 39. Si 2p Peaks from profile 1 on E10-8 piece B.	62
Figure 40. Normalized Si 2p Peaks from profile 1 on E10-8 piece B.	63

Introduction

This final report covers all activities carried out as part of NAS8-40581, "Comparison of Spacecraft Contamination Models with Well-Defined Flight Experiment," between April 16, 1995 and April 30, 1998. The objective of this contract was to analyze selected surface areas on particular experiment trays from the Long Duration Exposure Facility (LDEF) for silicone based molecular contamination. The trays chosen for examination were part of the Ultra-Heavy Cosmic Ray Experiment(UHCRE). These particular trays were chosen because each tray was identical to the others in construction, and the materials on each tray were well known, documented, and characterized. In particular, a known, specific source of silicone contamination was present on each tray. Only the exposure conditions varied from tray to tray.

The results of post-flight analyses of surfaces of 3 trays were compared with the predictions of three different spacecraft molecular contamination models. Phase one tasks included 1) documenting the detailed geometry of the hardware, 2) determining essential properties of the anodized aluminum, velcro™, silverized teflon™, silicone gaskets, and DC6-1104™ silicone adhesive materials used to make the trays, tray covers, and thermal control blankets, 3) selecting and removing areas from each tray, 4) and beginning surface analysis of the selected tray walls. Phase two tasks included 1) completion of surface analysis measurements of the selected tray surfaces, 2) obtaining auger depth profiles at selected locations, 3) running versions of the ISEM, MOLFLUX, and PLIMP (Plume Impingement) contamination prediction models and making comparisons with experimental results.

Flight

The LDEF mission flew from April 4, 1984, 17:27:4652 GMT through January 12, 1990, 15:16:00 GMT. The Long Duration Exposure Facility flew in a fixed orientation with respect to the direction of motion for 69 months, at 28.5 degrees, in low Earth orbit. The fixed orientation over time allows well-defined environmental exposure conditions. The specific trays from the Ultra Heavy Cosmic Ray experiment (UHCRE) at LDEF locations A4(trailing edge, UV exposure), E10(leading edge, UV and atomic oxygen exposures) and C6(side, UV and small amounts of atomic oxygen) were selected for several reasons. The locations, and therefore environmental exposures, are well defined. The tray geometry's are well-defined and virtually identical, the silicone sources are well characterized and defined, and the anodized aluminum surface shows only aluminum oxide as a background.

Geometry of the Experiment

The analyses being discussed in this report concern results of examination of essentially three surfaces at each tray location. The surfaces of interest are referred to as the tray lip, which is the surface around the edge of each tray, the interior tray wall, and the curved region between the lip and wall. Along the sides of the tray, the angle between lip and wall is 75 degrees. At each end of the tray (Earth and space), the angle between lip and wall is 90 degrees. Each UHCRE tray was covered by a silverized teflon™ blanket. Each blanket was held in place by about 44 pairs of velcro™ strips, one strip of each pair

bonded to the underside of the blanket and an identical sized strip bonded to an aluminum lattice framework on the top of three steel canisters containing the actual experiment.

Figure 1 is a drawing showing the location of the velcro™ fasteners and associated silicone adhesive relative to the keyhole shaped vents around the edge of the silverized teflon™ thermal control blankets which covered each tray of the UHCRE. At the center vent locations along each of the long sides, and at the end locations (along the short sides) the velcro™ fasteners are positioned so as to allow line-of-sight outgassing normal to the tray wall. At the other vent locations on the long side of the trays, the line of sight from silicone adhesive source through the vent slot to the tray wall is not normal to the tray wall. However the discolored areas on C6 and E10 walls are essentially directly across from the vent slots indicating that silicone molecules underwent multiple bounces within the tray, on average, before exiting at the vent and condensing on the tray wall.

Figure 2 is a drawing showing details of the experiment assembly. In particular, detail A shows how the silverized teflon™ blanket contacts the tray side. This detail indicates that the tray wall below the piece of aluminum that forms the tray lip is exposed to outgassing products from silicone adhesive patches holding the velcro strips, but not to atomic oxygen or solar UV, except at vent locations. Below the vent locations on trays E10 and C6, a plume of faint discoloration can be seen extending down the tray wall several centimeters below the end of the Ag/FEP blanket.

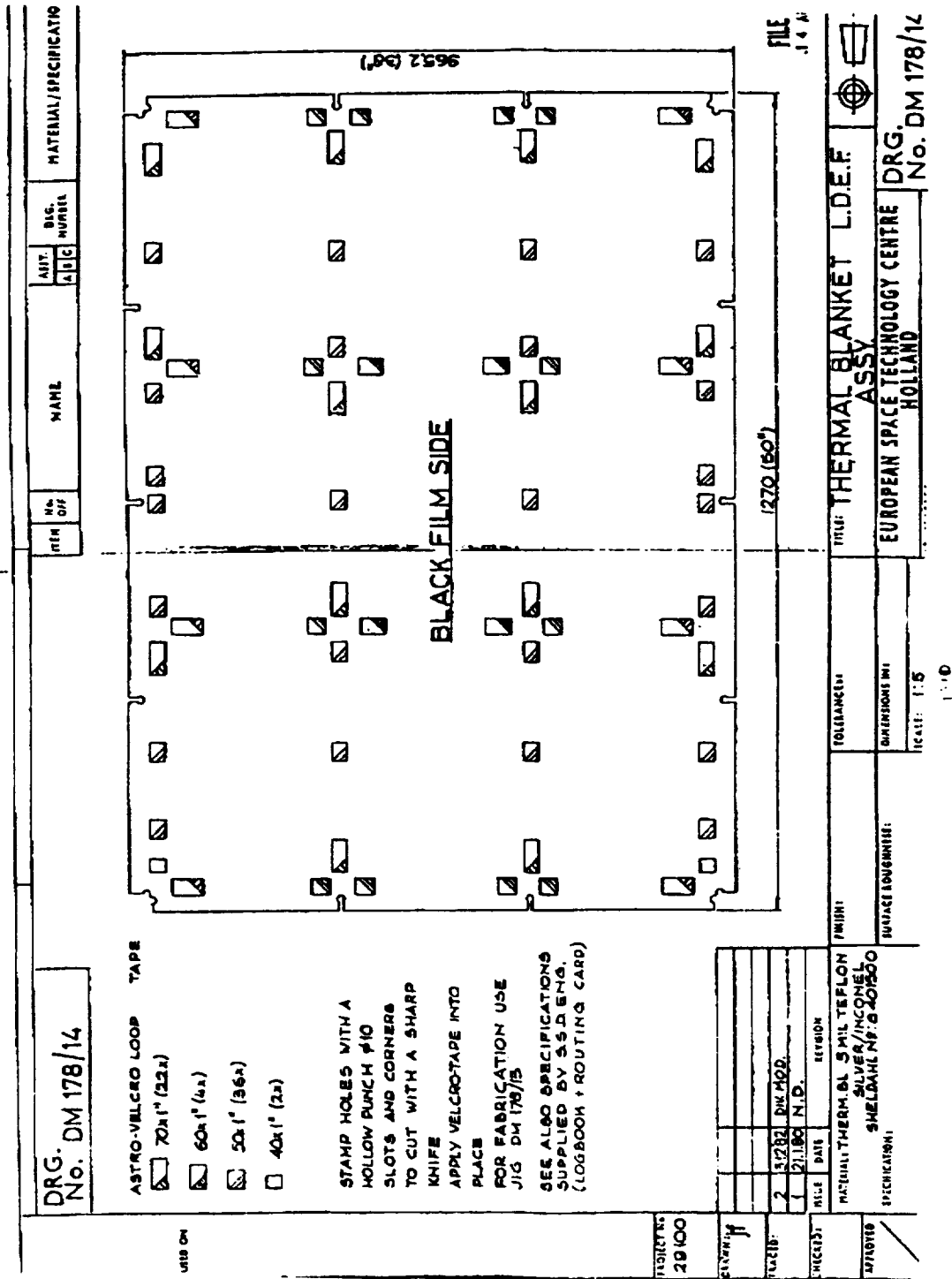


Figure 1. Drawing of LDEF thermal blanket assembly showing velcro™ attachment locations and vent locations.

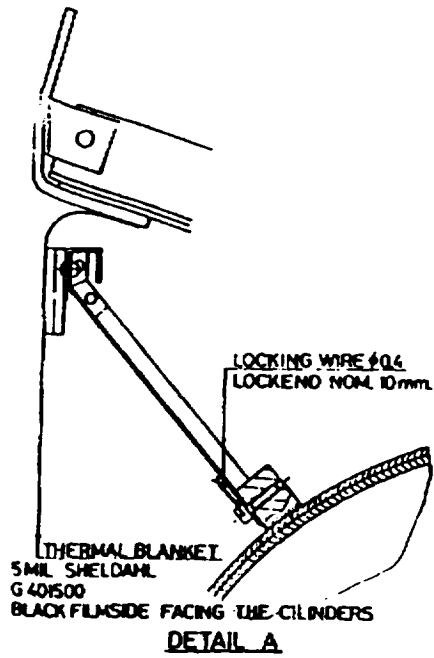
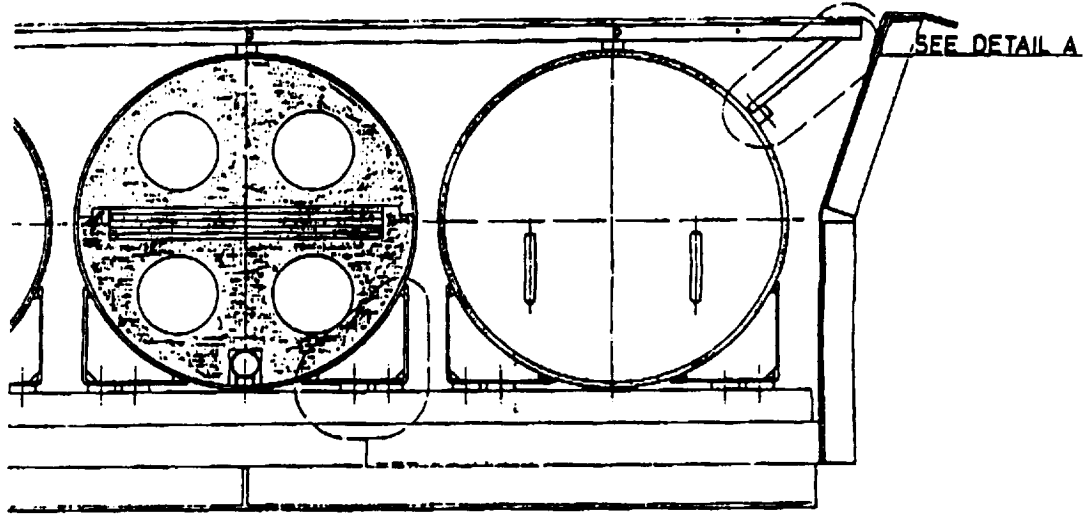


Figure 2. Cross-section drawing of details of the UHCRE trays showing orientation of blanket with respect to tray walls.

Vent Locations

Figures 3, 4, and 5 show the numbering system used for the vents in blankets E10, C6, and A4, respectively. Figure 6 shows dimensions of selected vent slots in the Ag/FEP blankets and relative positions of the tray lip and blanket material in cross-section at location AA. Figure 7 shows the cross-section at location BB and includes more dimensional details needed for modeling. Figure 8 shows the dimensions and geometry of vent slots at the Earth and space ends of the trays, including a cross-section at location CC. Figure 9 shows the details of the cross-section DD marked in figure 8.

Materials

Contamination Sources

Silicone based contamination films were the primary focus of this work. Organic based contamination was examined primarily with respect to how it masked or altered the apparent amount of silicon present. In particular, the Z306 black thermal control paint, used on the UHCRE stainless steel cyclinders within the tray, is polyurethane based. This material outgasses carbon based products, but contains no silicones. Depth profiles from discolored areas on trays E10 and C6 show clearly the effects of carbon-based material outgassing simultaneously with the silicone-based material.

Potential silicon contamination sources for the surfaces being examined include pre-flight outgassing from the tray cover gaskets, outgassing from the Space Shuttle during deployment and retrieval, outgassing from other LDEF experiments, outgassing from the

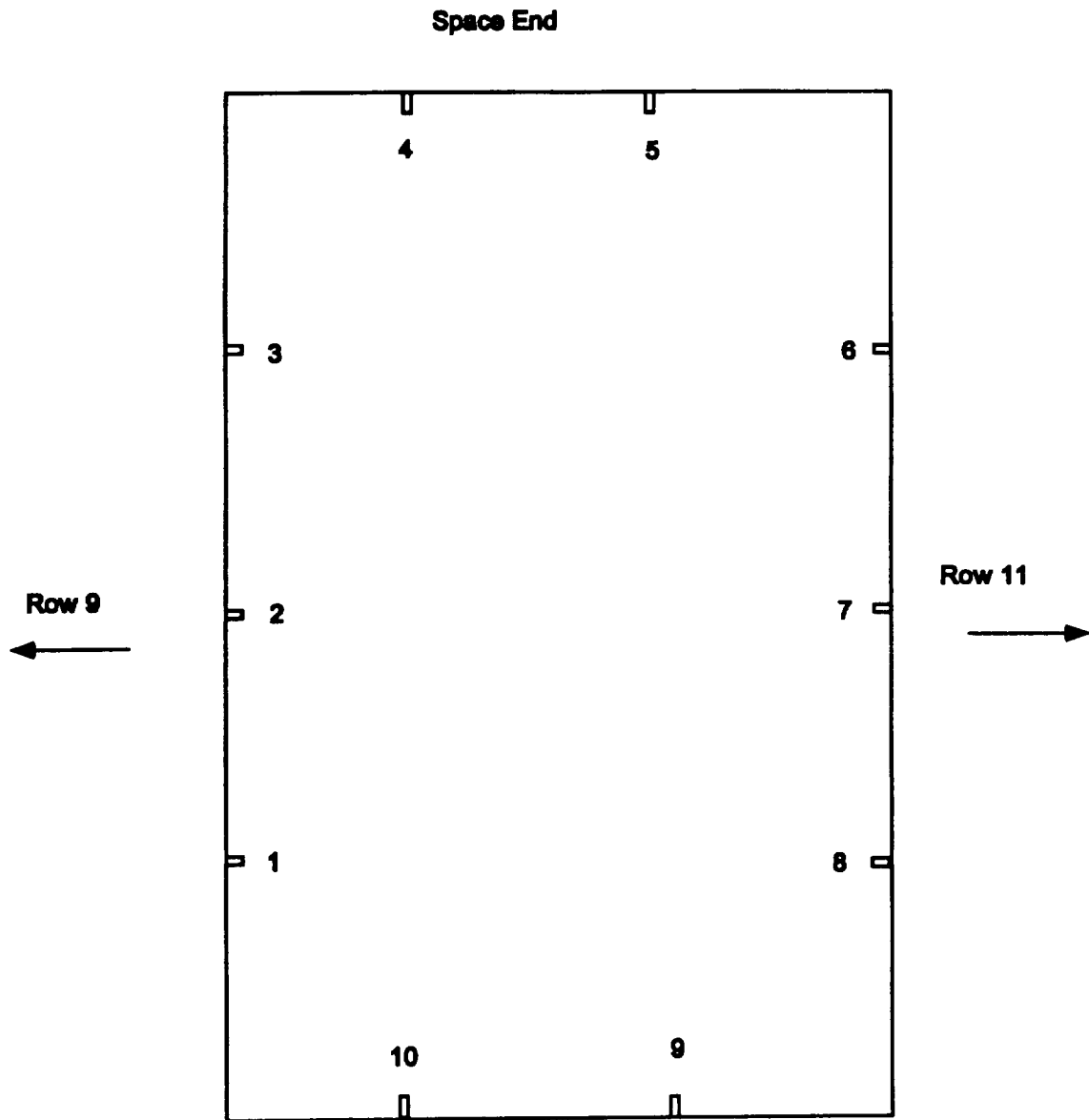


Figure 3. Vent location numbering system for tray E10.

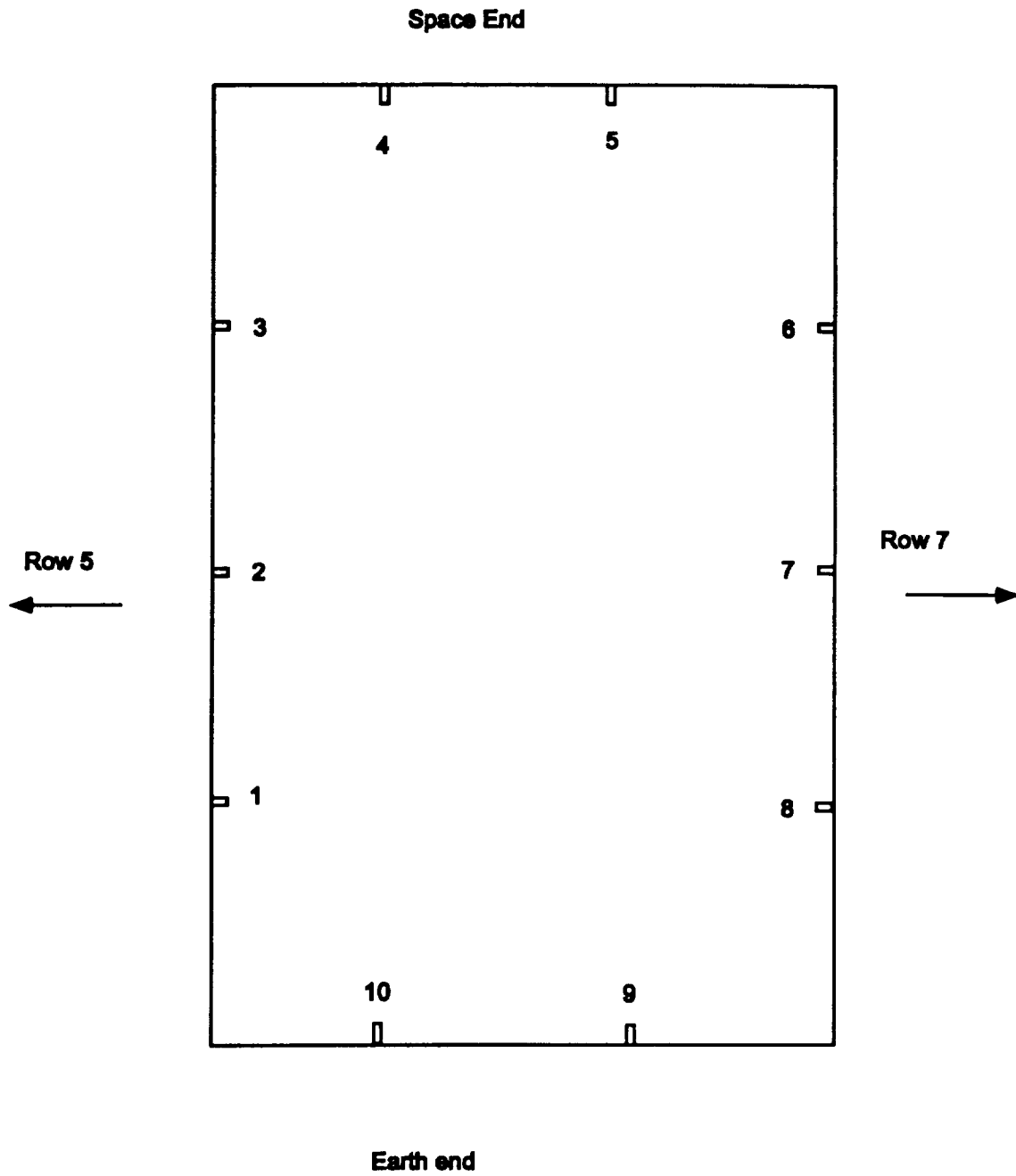


Figure 4. Vent location numbering system for tray C6.

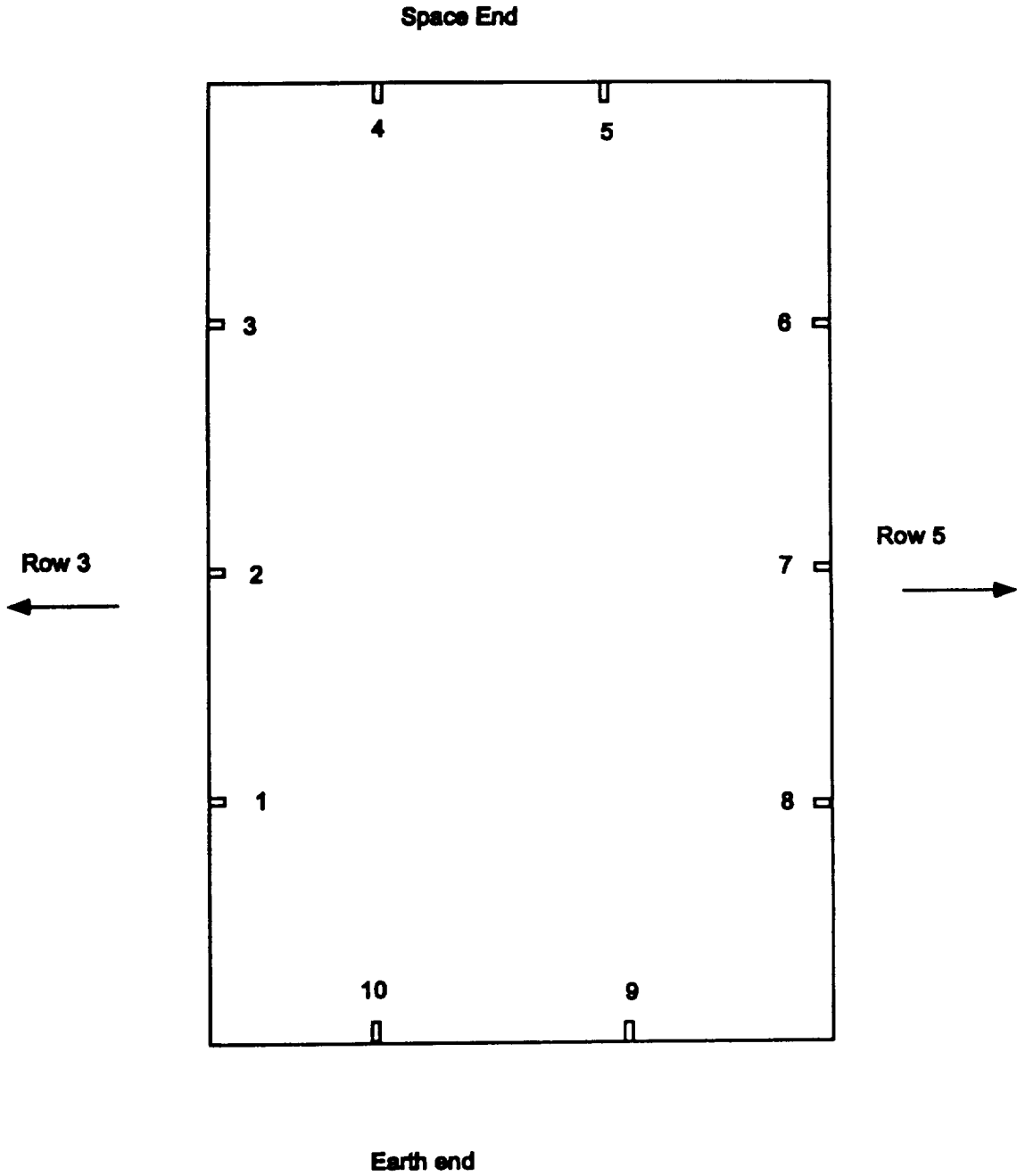
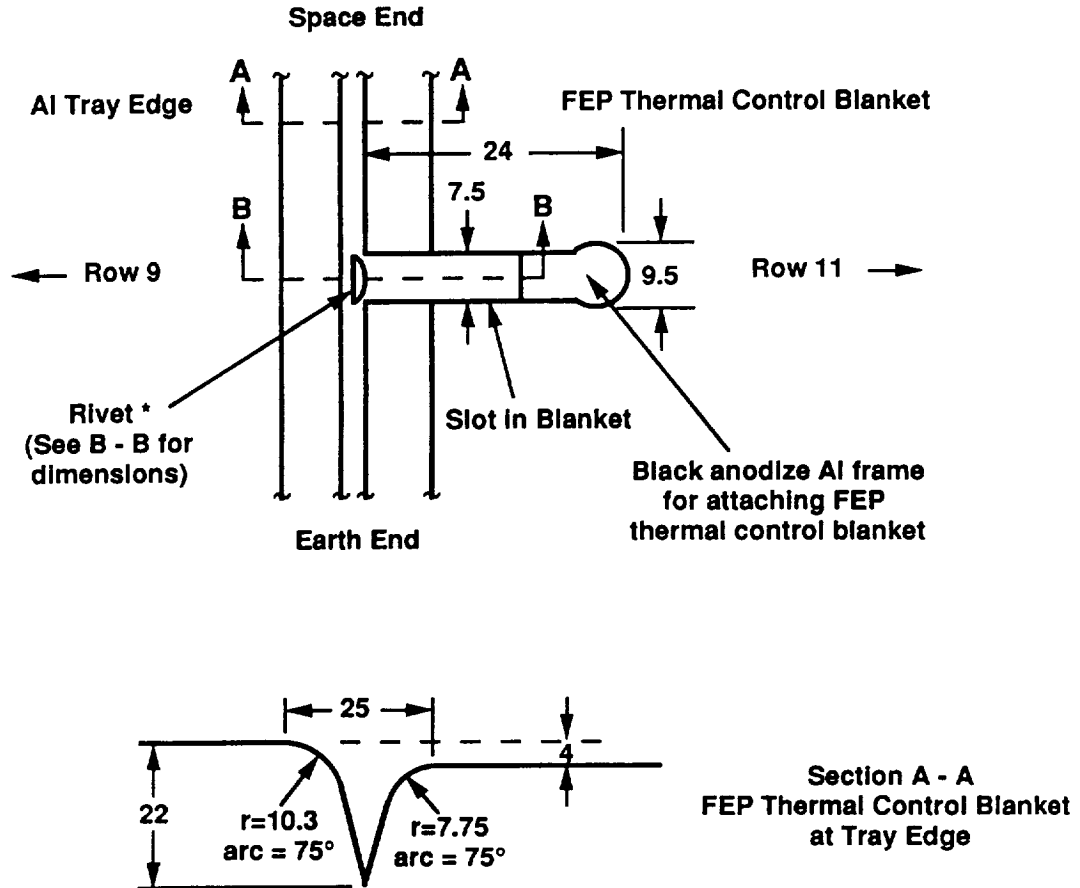


Figure 5. Vent location numbering system for tray A4.

Detail of E10 Tray and FEP Thermal Control Blanket
 at 6, 7, 8 (3, 2, 1 are symmetric facing row 11)
 (All dimensions in mm)



* location of rivet center relative to horizontal centerline of slot

1	7 above	6	8 below
2	no rivet	7	no rivet
3	6 below	8	3 above

Figure 6. Dimensional details for areas of trays near side blanket vents.

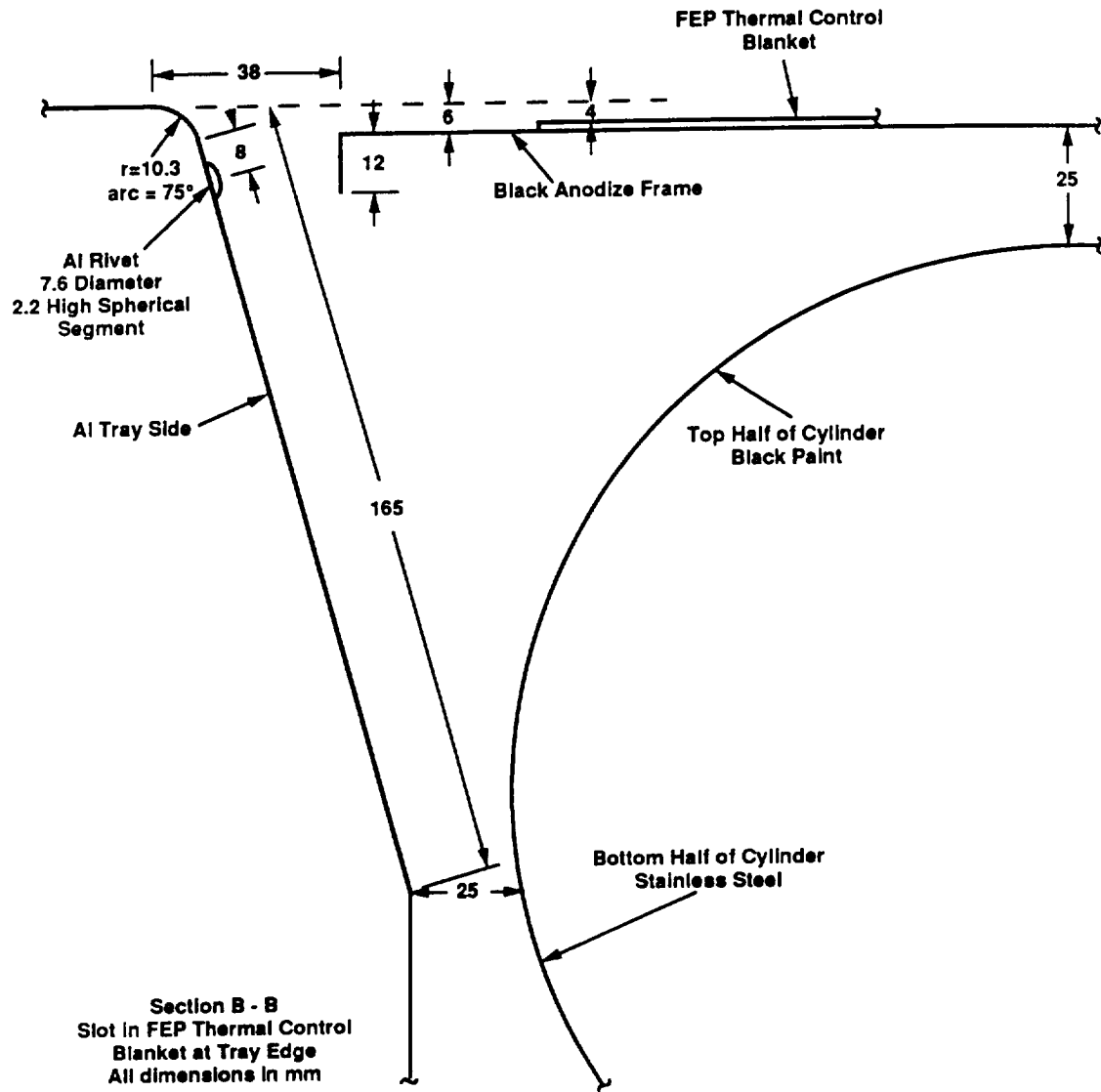
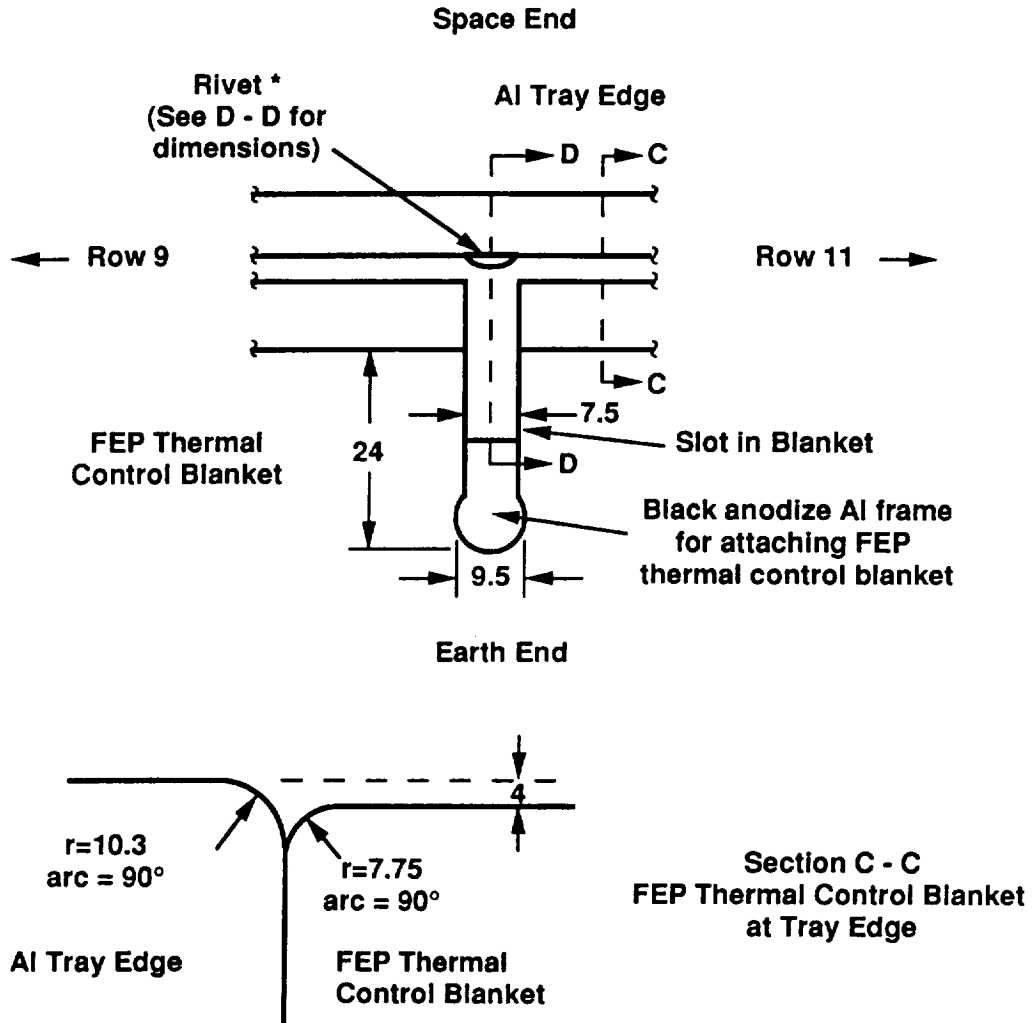


Figure 7. Cross-sectional detail of tray E10 side wall, frame holding thermal blankets, and cylinders holding experiment.

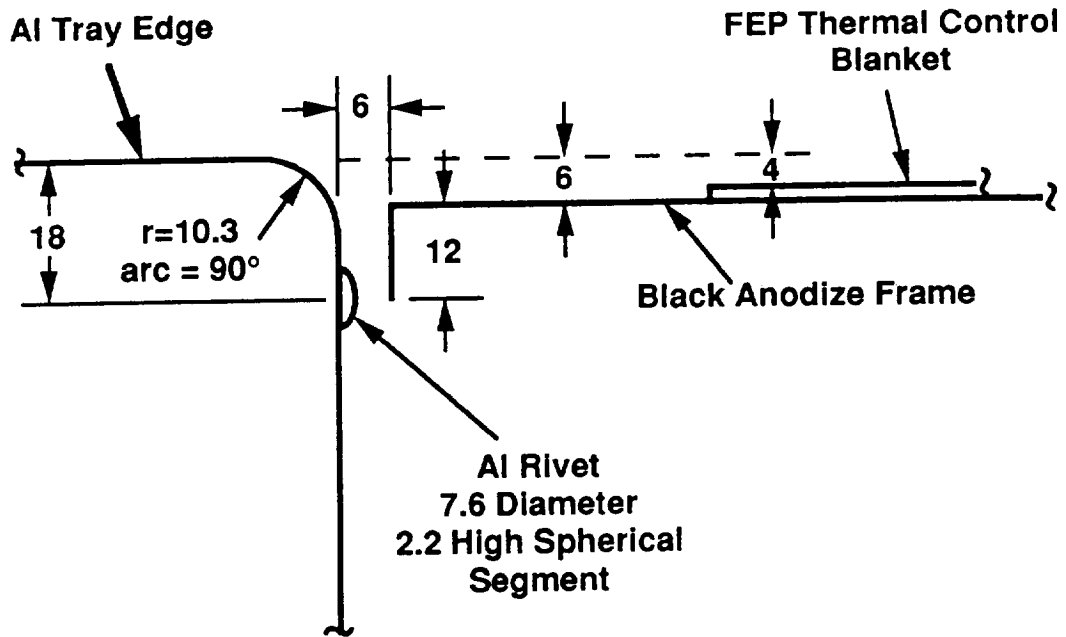
**Detail of E10 Tray and FEP Thermal Control Blanket
at 9 and 10 (5 and 4 are symmetric facing Earth End)
(All dimensions in mm)**



* location of rivet center relative to vertical centerline of slot

4	4 right	9	3 right
5	7 right	10	1 left

Figure 8. Dimensional details for areas of trays near Earth and space end blanket vents.



Section D - D
Slot in FEP Thermal Control
Blanket at Tray Top
All dimensions in mm

Figure 9. Cross-sectional detail of tray E10 end wall, rivet, and frame holding thermal blankets.

DC6-1104™ adhesive used by the UHCRE, and post-flight outgassing from new tray cover gaskets. The tray side walls near vent locations were chosen for examination because this gives the best opportunity to minimize all sources of contamination except the DC6-1104™. By comparison, the geometry around the vent locations at the corners of the trays allows for a large potential contribution from the tray cover gaskets. These specific locations are therefore being excluded from the current study. Previous examination of LDEF stainless steel bolt heads(NASA CR 4662, “Effects of Space Exposure on Metals Flown on the LDEF”) indicates some silicon based material is outgassed from the Space Shuttle. However, even near the top of tray interior walls the view factor to the Space Shuttle was very small. Thermal control blankets physically blocked any potential Space Shuttle sources from over 90% of the tray wall. Previous studies on LDEF hardware do not indicate tray-to-tray molecular cross-contamination was significant. In summary, the significant sources to consider for this study are the DC6-1104™ adhesive and the silicone gaskets for the tray covers. The outgassed gasket material may extend down onto the curved portion of the tray lip.

Outgassing

The distributed nature of the adhesive locations within the individual trays suggests the outgassed product is likely deposited fairly uniformly around the entire tray interior. The 12 inch depth of the tray, the metal lattice supporting the thermal control blanket, and the large stainless steel cylinders served to partially block exposure to the lower portions of the walls. However, plumes, visible at locations with substantial atomic oxygen exposure, created by the interaction of the space environment with contamination on the

tray walls, extend from just below the blanket vent holes to near the bottom of the tray walls. The presence of such plumes suggests that the contamination layer within each tray is well distributed.

The gasket material used for the tray covers was not space grade material and a silicon based film was left where this material contacted the tray lips. This is shown by both ESCA and SEM measurements. This material also had line of sight to both the tray interior and tray exterior walls at the corner of each tray. This pre-flight exposure created an outgassed layer which was darkened by the on-orbit environmental exposure, particularly on the exterior surfaces where the exposure was most severe. This darkening effect was seen on virtually all LDEF leading-edge tray corner areas exposed to both atomic oxygen and solar UV, including those trays containing experiments with no source of silicones.

Average values of outgassing properties of the DC6-1104™ adhesive and velcro used to hold silverized teflon blankets to tray frames of LDEF experiment AO138 are reported in figure 10. These numbers are taken from NASA CR 4646, "Evaluation of Adhesive Materials Used on the Long Duration Exposure Facility." Also included in this figure are results of individual measurements on material taken from the specific trays being examined under this contract.

DC6-1104™ Silicone Adhesive

LDEF Location	TML	CVCM
C6-2	0.47/0.46	0.02/0.02
C6-7	0.49/0.46	0.02/0.02
E10-2	0.40/0.41	0.03/0.03
A4-2	0.38/0.37	0.03/0.03
A4-7	0.50/0.49	0.06/0.05
E10-7	0.39/0.33	0.04/0.03

Velcro™

LDEF Location	TML	CVCM
E10-7	0.17/0.16	0.05/0.02
E10-2	0.10/0.17	0.01/0.02
C6-2	0.14/0.17	0.07/0
C6-7	0.14/0.17	0.01/0.02
A4-7	0.22/0.23	0.05/0.05
A4-2	0.17/0.18	0.01/0.02

DC6-1104™ Silicone Adhesive, Tray Averages

LDEF Location	TML	CVCM
C8	0.29	0.02
B7	0.36	0.03
C6	0.51	0.03
B5	0.35	0.03
F2	0.54	0.08
A2	0.33	0.04

Velcro™, Tray Averages

LDEF Location	TML	CVCM
B7	0.22	0.01
A2	0.24	0

Figure 10. Outgassing measurements for DC6-1104™ adhesive and velcro™ fasteners used on the UHCRE.

Computer Modeling of Exposure Levels

Preliminary plots showing the AO and UV exposure on each tray are shown in figures 11-15. There is no plot for AO exposure for tray A4, the E+5 atoms/cm² exposure level is insignificant for any materials property change.

The LDEF row 10 baseline exposure is 8.43E+21 atoms/cm² AO and 10700 ESH solar UV radiation. For row 6 the exposure is 4.94E+19 atoms/cm² AO and 6400 ESH solar UV radiation. The row 4 atomic oxygen (AO) exposure is essentially zero and the solar UV exposure is 10500 Equivalent Sun Hours(ESH). The trays are subject to mild thermal cycling each orbit. The specific exposure levels are a very strong function of location on each surface. For a given tray, the primary surface of each side wall is 75 degrees, and the tray end walls are 90 degrees, to the plane of the tray surface.

Figure 16 gives the approximate range of exposures for each tray surface examined.

These values were obtained by running the same detailed modeling program used to estimate the exposure levels for all rows of the LDEF.

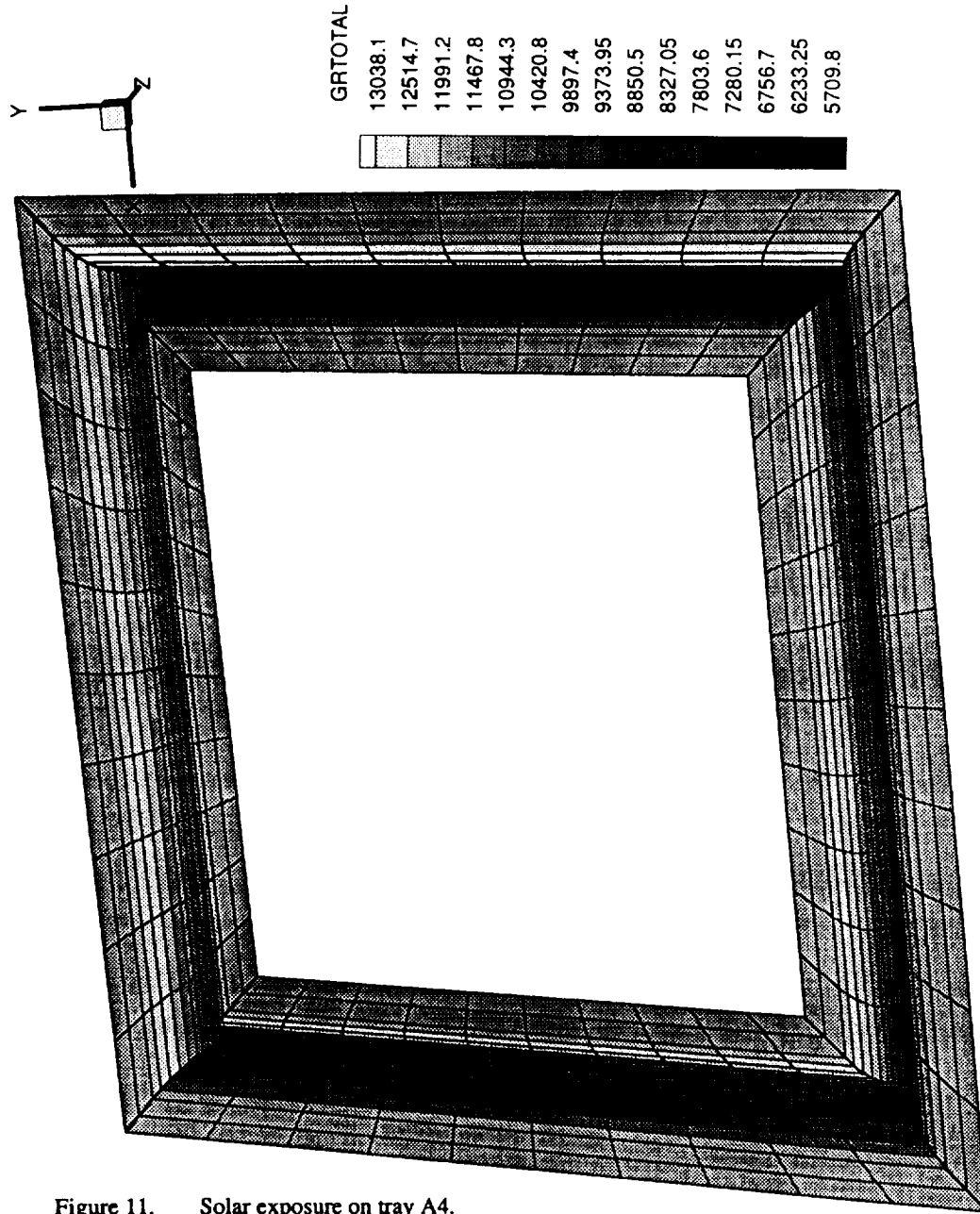


Figure 11. Solar exposure on tray A4.

Figure 11. Solar exposure on tray A4.

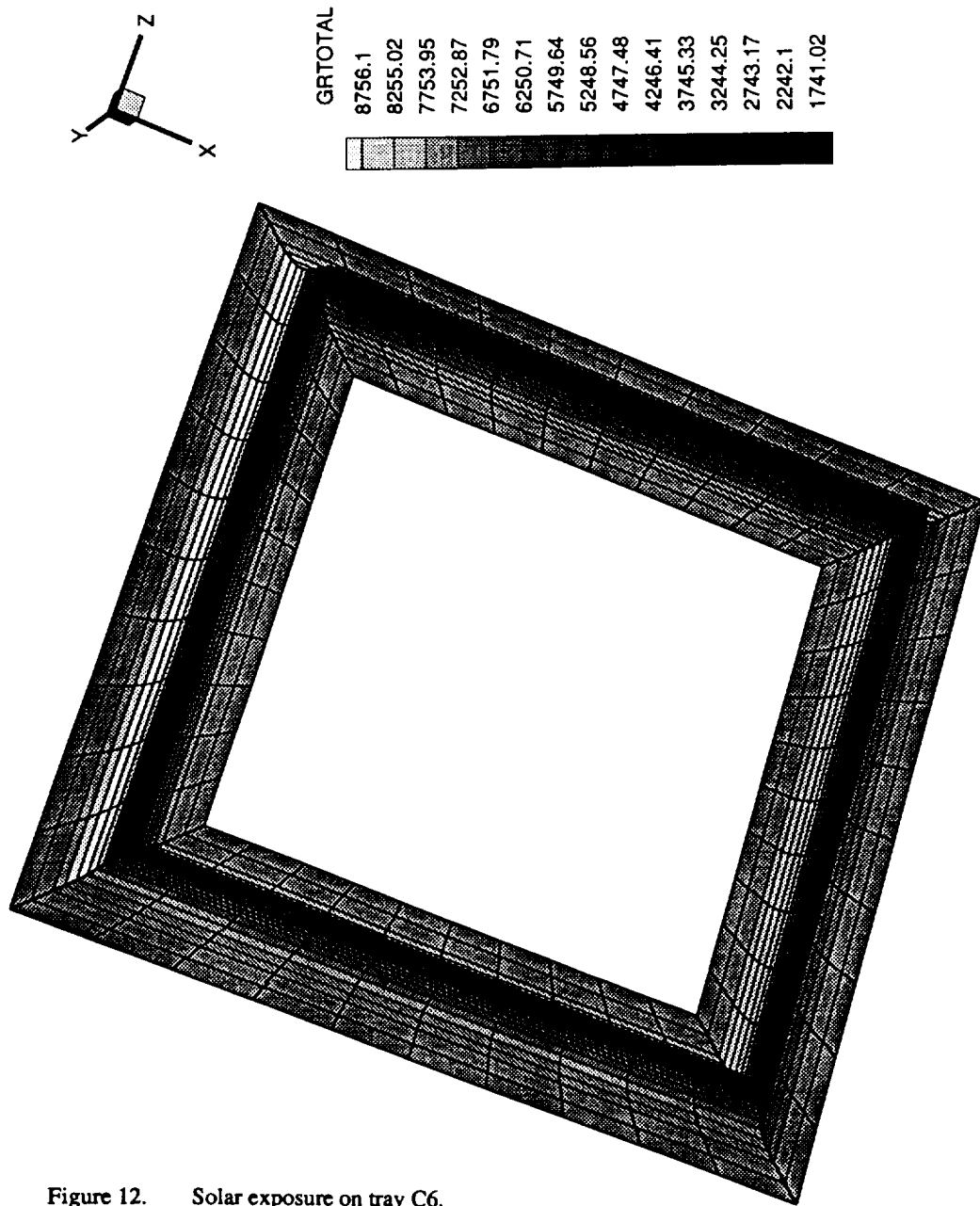


Figure 12. Solar exposure on tray C6.

Figure 12. Solar exposure on tray C6.

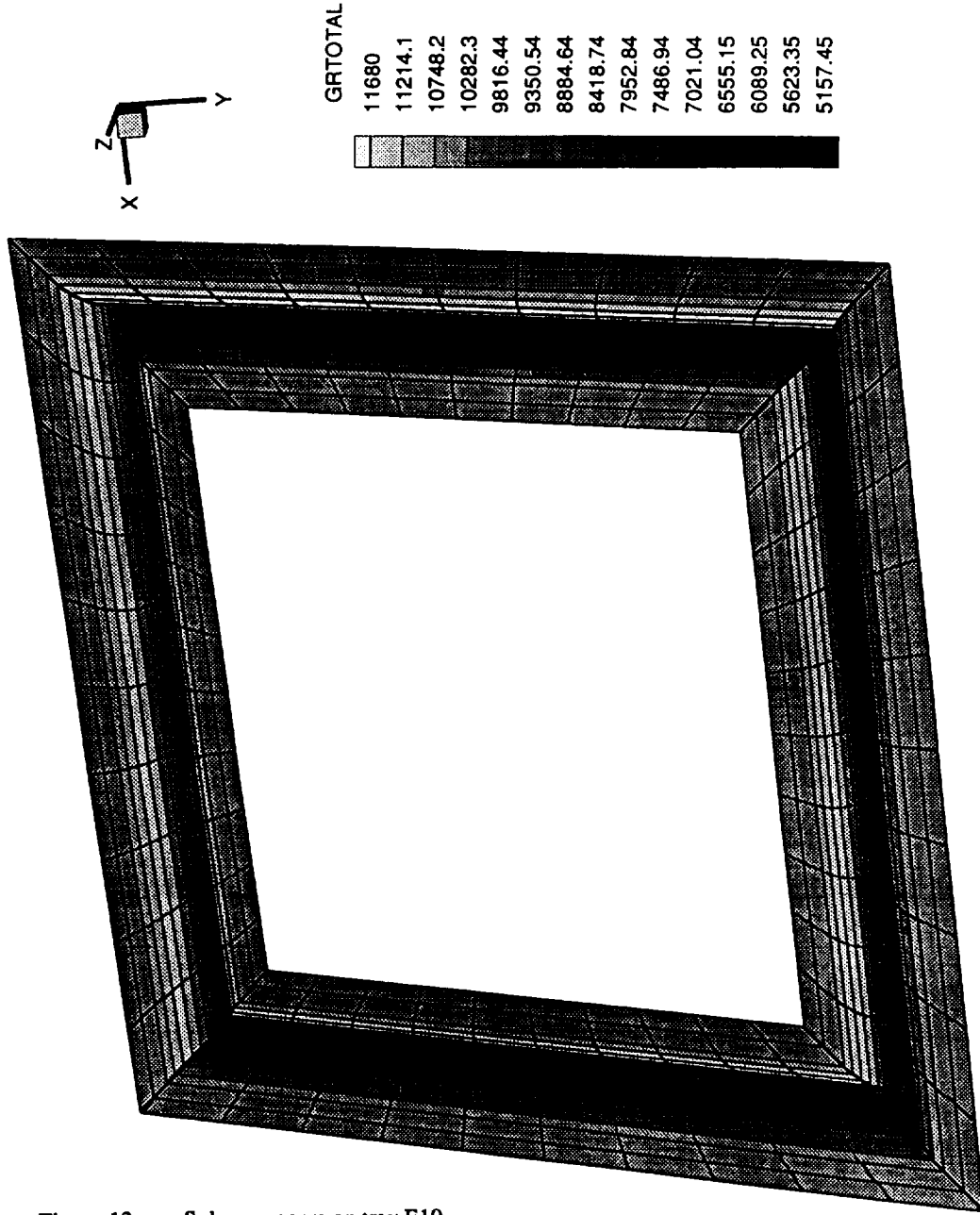


Figure 13. Solar exposure on tray E10.

Figure 13. Solar exposure on tray E10.

(3D) || Print || 16 Dec 1994 || a:tray6c.ip7 || LDEF tray 6C with fep blanket

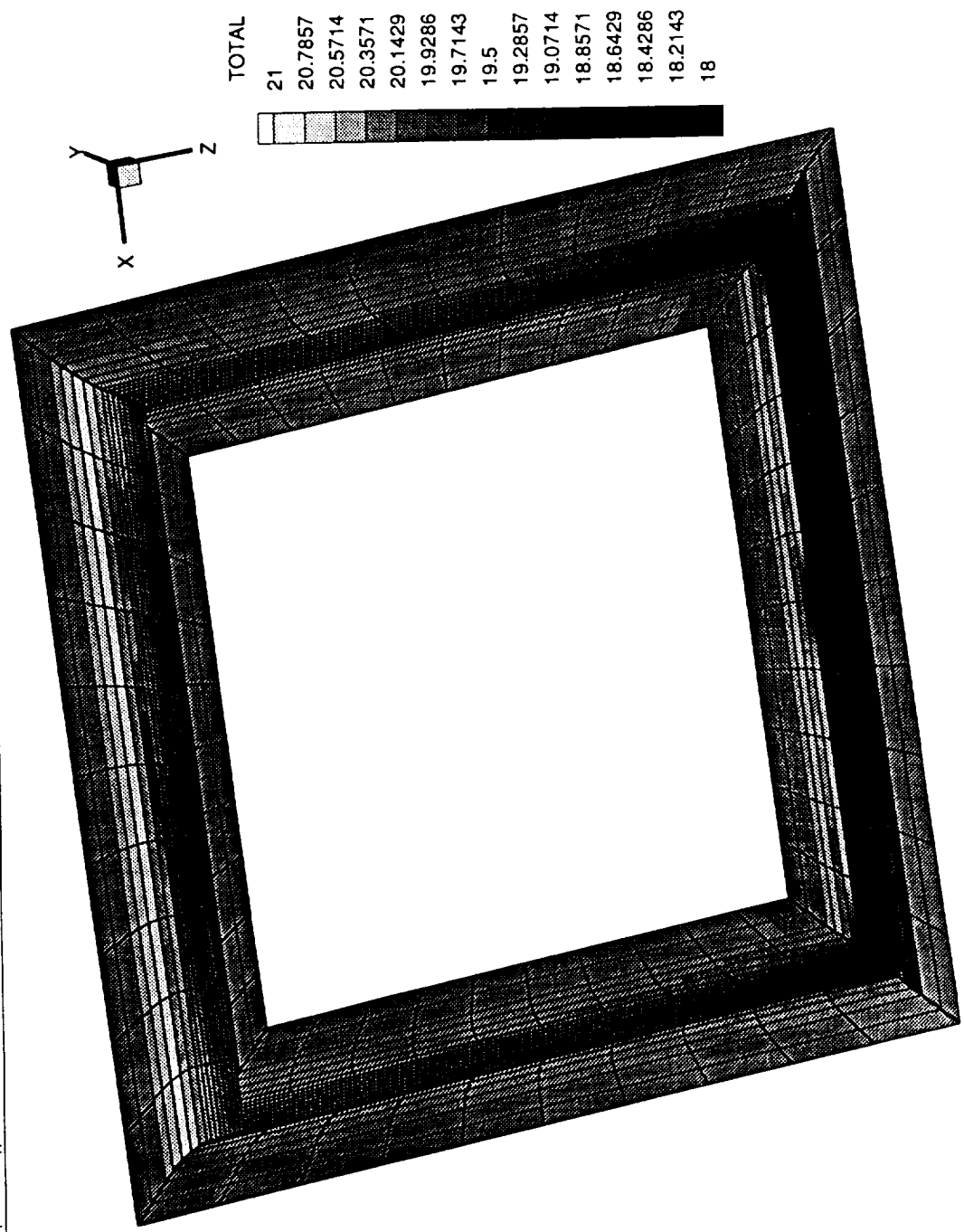


Figure 14. Atomic oxygen exposure on tray C6.

Figure 14. Atomic oxygen exposure on tray C6.

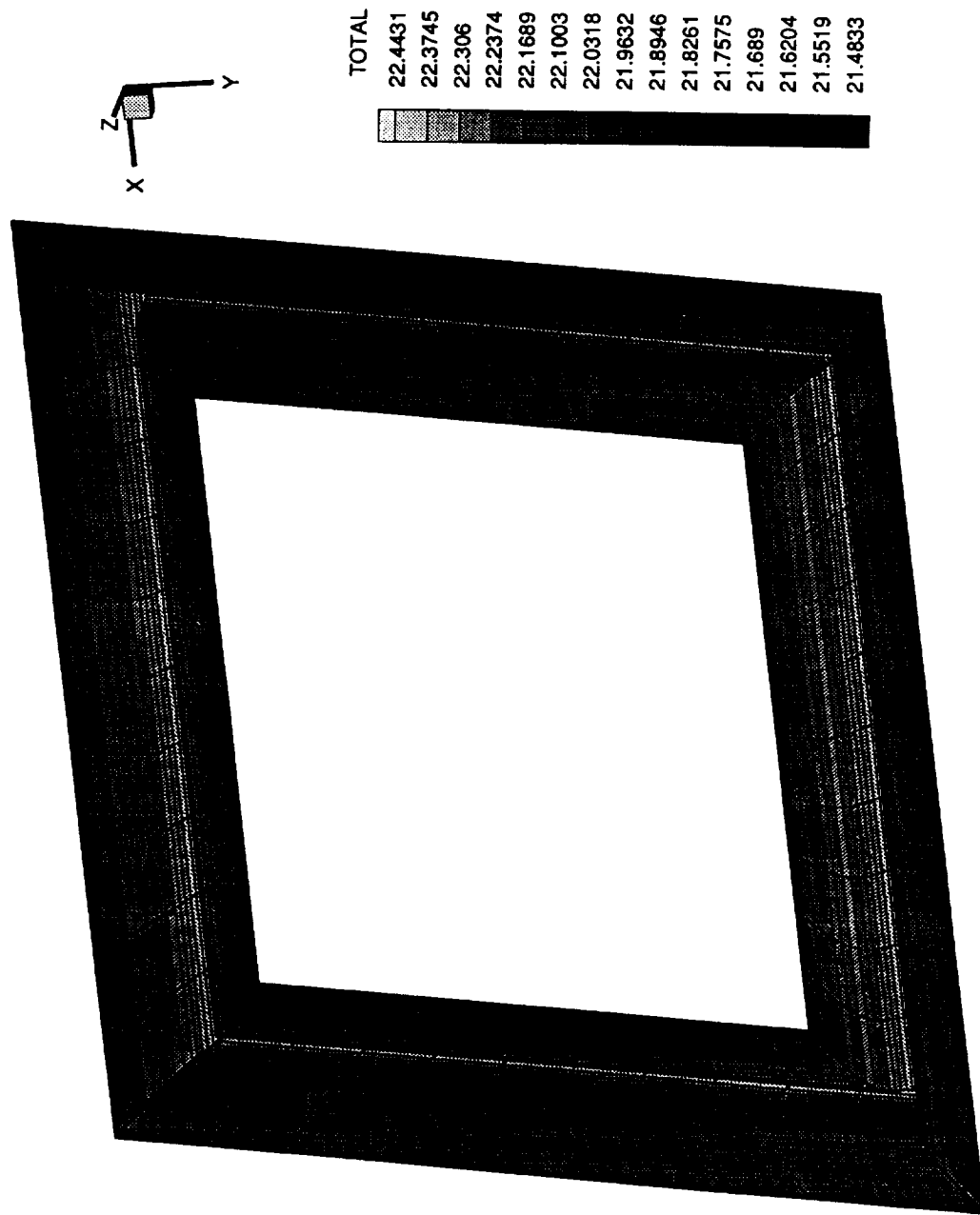


Figure 15. Atomic oxygen exposure on tray E10.

Figure 15. Atomic oxygen exposure on tray E10.

Location	Atomic Oxygen (10^{21} atoms/cm ²)	UV(ESH)
A4	-	5700-13000
C6	0.001->1	1700-8700
E10	1->10	5000-11700

Figure 16. Range of Exposure Conditions for Tray Surfaces Examined.

During solar exposure modeling the LDEF orbit was allowed to precess randomly and all LDEF orbit positions were allowed. 1000 LDEF and Sun position pairs were used to model solar exposure. An average orbit altitude of 400 km and an average Earth albedo under the LDEF of 0.246 were assumed. The modeled solar exposure is the total of direct and Earth reflected exposure, including photons reflected from one LDEF surface to another. Material properties and average conditions used for modeling the exposure levels are shown in figures 17-19.

Material	Specular Reflectivity	Diffuse Reflectivity	Absorbivity y
Aluminum	0.06	0.60	0.34
FEP	0.83	0.10	0.07

Figure 17. Surface Properties Used for Solar Exposure Modeling.

The following mission average values used for atomic oxygen modeling were derived from calculations of detailed on-orbit atomic oxygen fluence to unshielded surfaces calculations.

Average resultant ram speed (average speed of satellite through the atmosphere, which rotates with the Earth.	7.21E5 cm/s
Average atmospheric temperature	1182.9 K
Average atomic oxygen density times mission time (used to calculate fluence rather than flux)	1.17E16 AO/(cm ² s)

Figure 18. Mission average values used for atomic oxygen modeling.

The atomic oxygen fluences modeled are the total of direct and reflected exposure to surfaces.

Material	Specular Reflectivity	Diffuse Reflectivity	Recombination Efficiency	Surface Reactivity
Aluminum	0.50	0.46	0.04	0.0
FEP	0.49	0.49	0.0	0.02

Figure 19. Surface Properties Used for Atomic Oxygen Fluence Modeling

At each location examined, evaluation of atomic oxygen fluence and cumulative equivalent sun hours (CESH) of solar exposure show the aluminum surface (tray wall) directly across from a vent has slightly decreased exposure relative to the remainder of the tray wall. This is because there is no FEP to scatter the solar radiation and atomic oxygen back on to this area. The exposure around the rivets does vary. The rivets create shadow patterns and in each case one side clearly is more exposed. This can be seen in figures A-3 and A-7 in appendix A.

Analysis Results

All ESCA measurement results for each of the six areas examined are reported in Appendix A. Auger depth profiles are reported in Appendix B. Selected locations from areas E10-8, C6-2, and A4-9 were used for depth profile measurements. Appendix C is a set of figures showing results of atomic oxygen and solar UV exposures as functions of location on specific tray walls. The calculated exposure levels were used to assess the role of the environmental factors in fixing the contaminant on the surface. Appendix D is a set of figures showing SEM images of areas from tray location E10-9. Small pieces

from this tray location were fractured and examined under SEM to provide an independent look at the nature of the contaminant layers on the tray surfaces.

Tray A4 Results

Photographs

Figure 20 is a NASA post-flight photograph of tray A4. Position 9 is at the top left of the photo. No visible discoloration was seen on the interior walls near any of the vent areas on this tray.

ESCA Measurements Location Map

Figure A-16 shows the labeling of the small pieces from tray A4-9 cut to fit into the ESCA vacuum chamber. The designation MLR stands for middle left rivet, the other rivet in the diagram is the leftmost rivet on the large section. The small pieces were cut by hand with a jewelers saw to minimize the amount of material destroyed in the process. An area approximately 1mm wide is destroyed by the cutting. This technique was used for all surfaces examined as part of this work. Figure A-17 in appendix A shows the coordinates at the center of each ESCA measurement location on tray area A4-9. Tables of ESCA data and depth profile sputtering graphs for tray area A4-9 refer to this coordinate system. The vent slot is roughly centered between the two rivets. One group of measurements was conducted on the surface as directly across from the large circular



Figure 20. NASA post-flight photograph of tray A4.

portion of the vent as possible. Background measurements were taken at surface locations 4-5 inches below, and slightly to the right of the rivet centered about coordinates (37,10) in figure A-17. To make the ESCA measurements, small pieces about 1-1.5 cm by 2 cm were cut from the roughly 25 cm by 30 cm sections.

ESCA Data

Each analysis area is a 0.6 mm diameter circle centered on the location defined by the (x,y) coordinate pair. The silicon percent generally increases the closer to the top of the tray wall the measurement is made. The measurements around the rivet on the right show some shadowing due to this structure. The 25+ percent silicon measurements at the top are from the tray lip surface (~90 degrees from the tray wall). The next two pairs of measurements are about 60 and 30 degrees from the tray wall, respectively. Background silicon levels are at about 3-3.5%.

Measurements on the A4-9 piece show silicon % is essentially a function of solar exposure. Maximum silicon %'s occur near the tray lip in areas seeing the most sunlight, with decreasing silicon % levels observed as measurement locations move down the tray wall from the tray lip. This is expected because the lower on the tray wall, the less solar exposure.

Measurements from the A4-1 location showed similar results to measurements on A4-9. The elemental %Si on A4-1 varied with solar exposure. Decreasing amounts of silicon were detected observed as measurement locations moved down the tray wall from the tray lip. Aluminum was detected at each surface measurement site, implying very thin, or

patchy silicon based coatings. The A4-1 location showed no discoloration due to contaminant deposition. The silicon was also distributed over a wide area. This was as expected, and is similar to results from locations on trays E10 and C6.

Sputter Depth Profiles

Repeated cycles of sputtering to remove material followed by ESCA measurements produced a profile of the composition of the material at the A4-9 locations examined as a function of depth. The silicon containing films appear to be quite thin. Surface measurements show 10-15% aluminum and the silicon % dropping rapidly within 5-10 nm of the surface at most locations not directly aligned with the vent. Depth profiles of locations near the vent show thicker silicon containing films. The locations referred to as light sputter are locations immediately adjacent to areas that have previously been sputtered. These “adjacent” areas were exposed to the edge of the sputtering beam and some surface material is removed prior to any ESCA measurements. The process essentially “cleans” surfaces by partially removing the layer of carbon based contamination found on any surface that has been exposed to ambient atmosphere

Background Contamination

The post-flight exposure to air allows deposition of carbon based material. This layer is extremely thin, as seen by examining the sputter depth profiles. For A4-9 locations it is difficult to separate the contributions from the adhesive and the tray gasket because there was no conversion of silicone to silicate material due to atomic oxygen.

Tray C6 Results

The surface from tray C6 was exposed to less than 1% of the atomic oxygen exposure received by tray E10. Tray C6 was exposed to about 60% of the solar exposure level received by tray E10.

Photographs

The pattern of velcro fasteners and the aluminum frame holding the fasteners are visible in figure 21. Only areas by the vents on the side of tray C6 closest to row 5, that have some direct exposure to atomic oxygen show discoloration due to the contaminant layer. These discolored areas are visible along the left side of the figure. Figure 22 shows a close-up view of vent area 2. Surface analysis measurements have been carried out in this area of the tray. Figures 23 and 24 show the discolored region at C6-2. Figure 23 shows that the discoloration extends into the curved portion of the tray lip and is well centered between the side wall rivets. Figure 24 shows the relative position of the aluminum tray frame, velcro™ and tray wall. The velcro™ piece on the right is essentially at the vent.

ESCA Measurements Location Map

Figures A-12 and A-13 show the dimensional details of area tray C6-2 and the coordinates at the center of each ESCA measurement location. Tables of ESCA data and depth profile sputtering graphs for tray C6-2 use this coordinate system. Figure A-12 also shows the labeling of the small pieces cut to fit into the ESCA vacuum chamber. The angles are relative to the tray wall, section Eb is the tray lip.

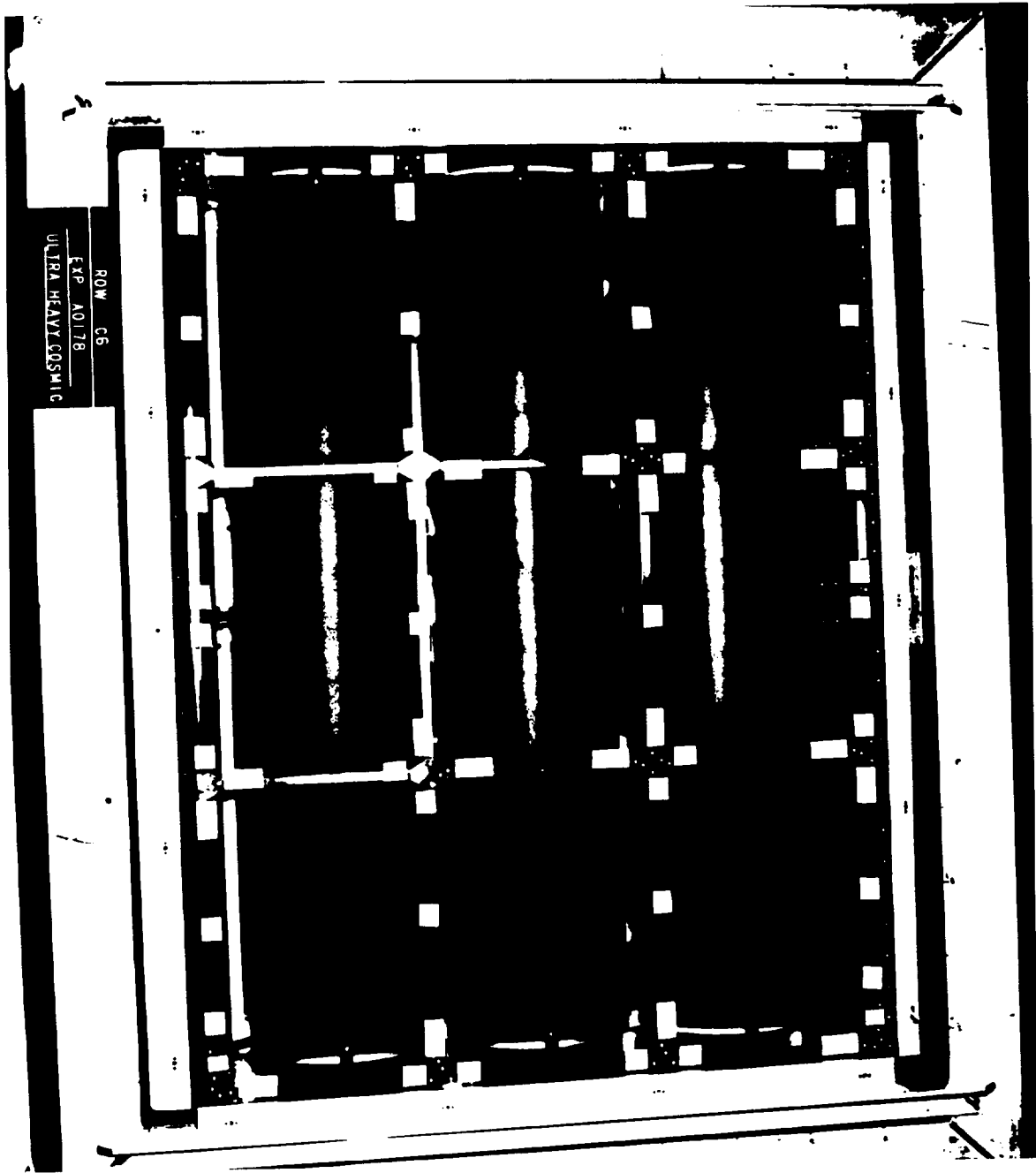


Figure 21. NASA post-flight photograph of tray C6 with the thermal blanket removed.



Figure 22. Close-up photograph of area C6-2 (NASA PHOTO).

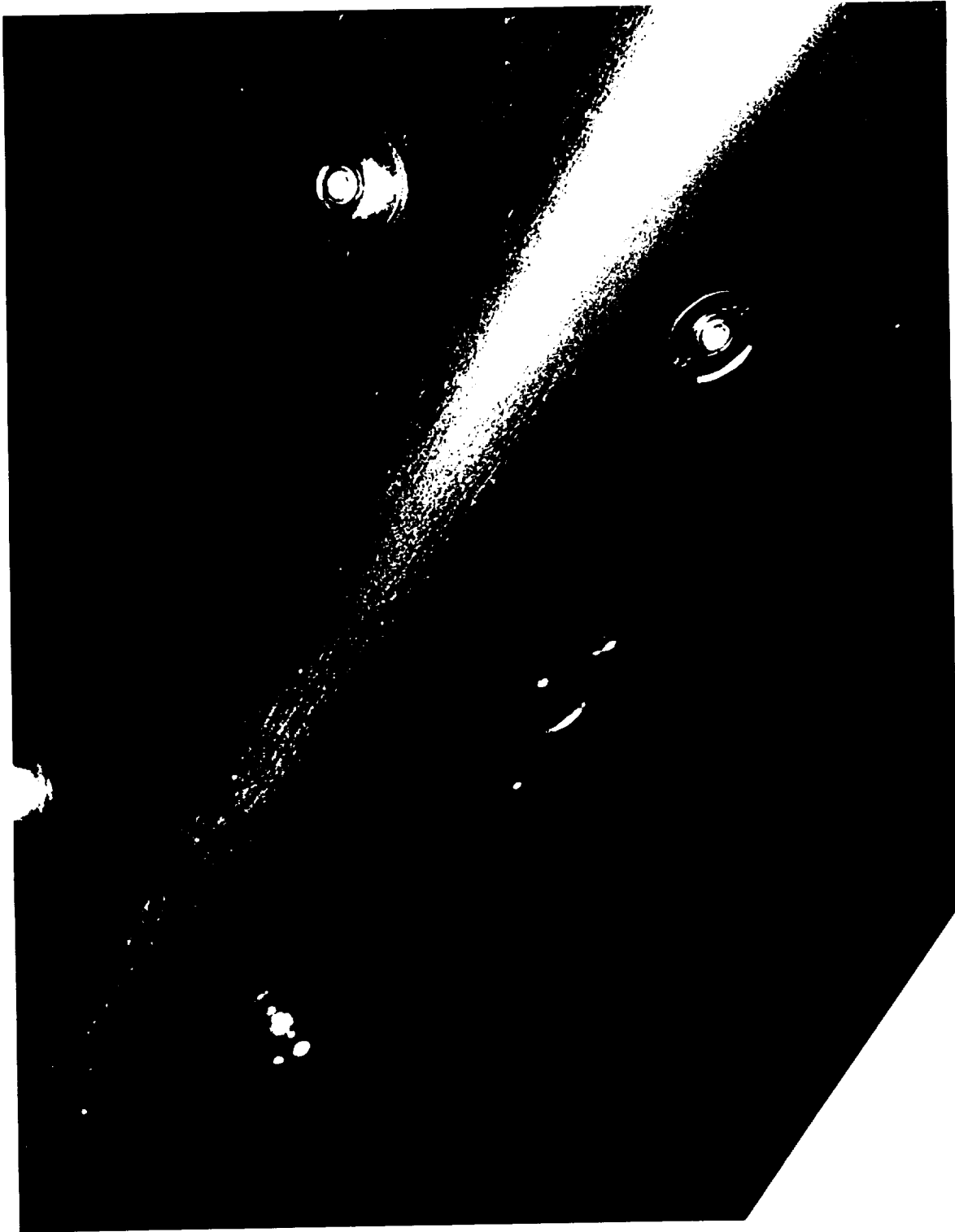


Figure 23. NASA post-flight photograph of area C6-2 showing discoloration pattern.

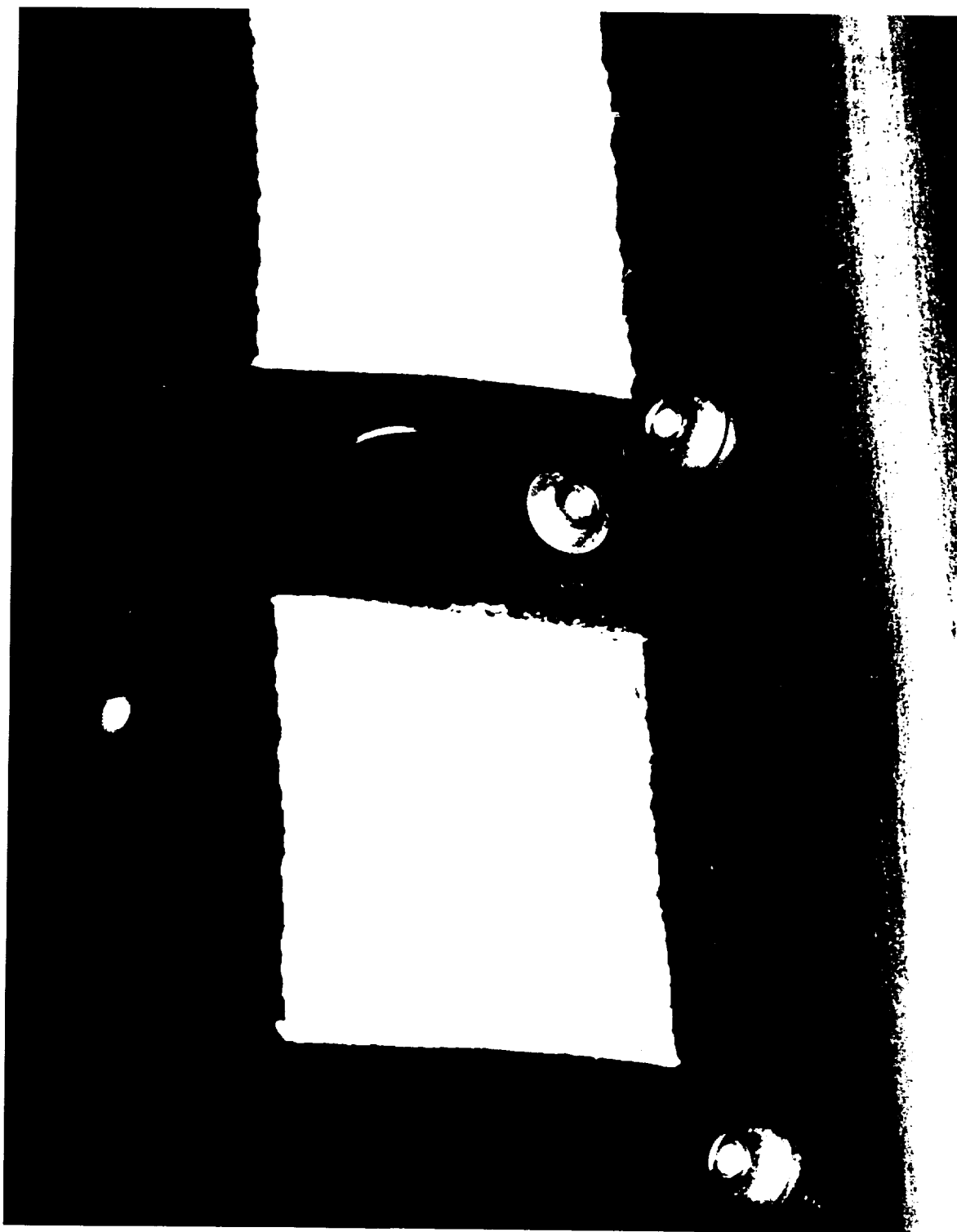


Figure 24. Close-up photograph of area C6-2 showing relative position of the velcro™ and adhesive to the discolored area on the tray side and curved region of the tray lip.

ESCA Data

Figure A-14 shows the surface percent silicon for locations measured on C6-2. Areas “B” and “G” on C6-2 show high levels of silicon on the surface. These areas are relatively near the vent and also show some evidence of silicon residue left from the cover gasket(locations 70) around the tray lip). Area “H”, located a large distance from the vent, shows some measurement values decreasing toward background levels. On the C6-2 surface, as on the A4-9 surface, the silicon deposition increases with exposure severity.

Sputter Depth Profiles

For areas not directly across from the vent, depth profiles show thin layers(ranging from ~200 to 500 nm) of essentially constant composition with underlying material showing a rapid decrease in silicon content with depth. The depth profiles carried out within the discolored areas directly across from the vent shows an extremely thick contaminant layer with wide variations in relative amounts of silicon, carbon, and oxygen as a function of depth.

Tray E10 Reports

Photographs

Figure 25 is a NASA post-flight photograph of tray E10. Figure 26 is a close-up of deposits along the side of E10 closest to row 11. The deposition pattern from vent location E10-7 extended over a copper grounding strap and along the top edge of the wall. A gap in the discoloration is seen in the area from where the copper strap has been

removed. Figure 27 shows a post-flight close up of this area. It is clear from this photograph that the blanket material around the vent is skewed so as to provide a better line of sight to the right of the vent (toward the discolored area) than to the left, where little discoloration is seen. Figure 28 shows the exterior of a corner of tray E10. The discoloration pattern induced by the on-orbit environmental exposure is apparent. The likely source of the material on the surface is pre-flight outgassing from the tray cover silicone gaskets. The view factor of the gaskets to the surface can be seen in the photograph.

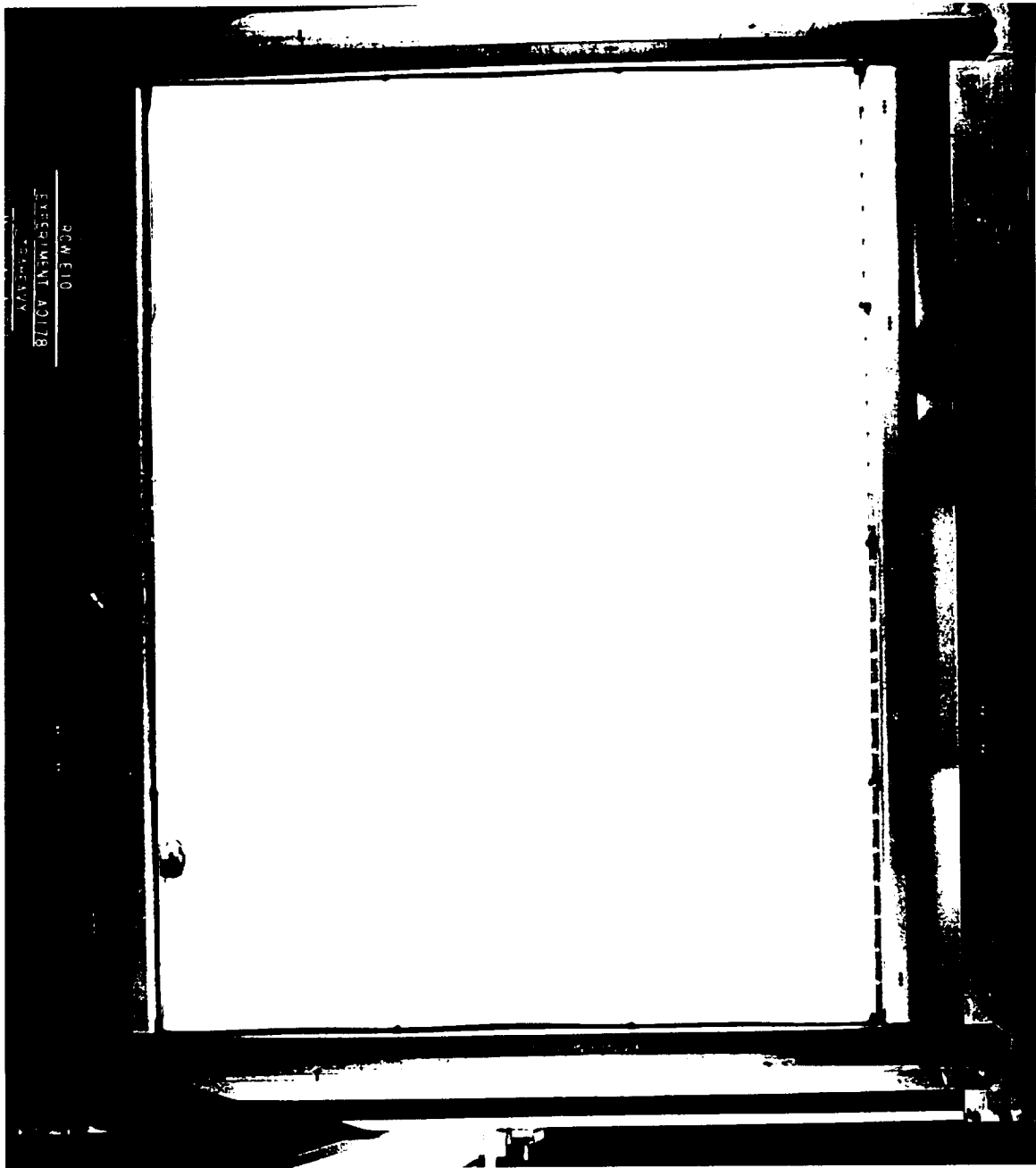


Figure 25. NASA post-flight photograph of tray E10 (NASA PHOTO).

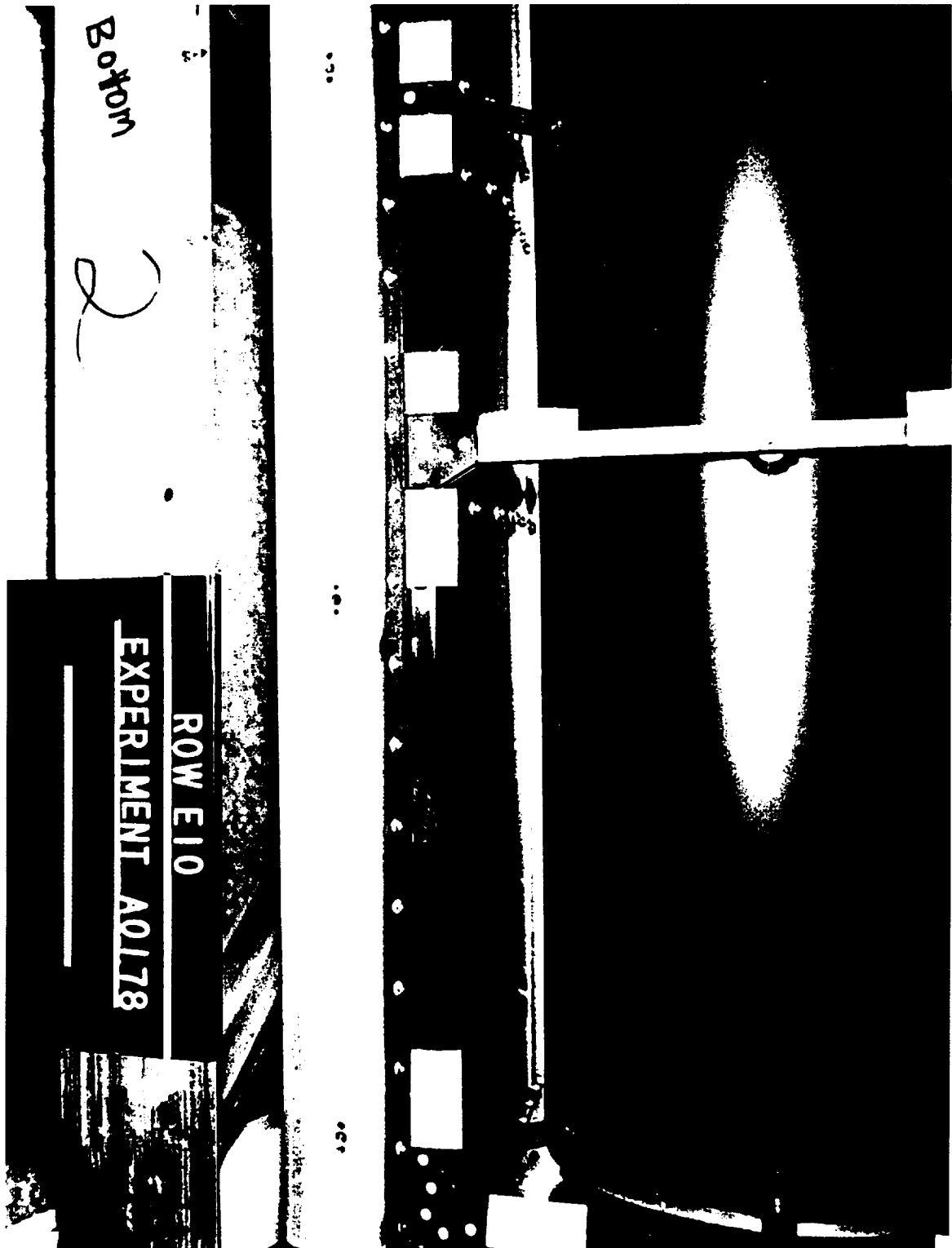


Figure 26. NASA post-flight photograph of side of E10 towards row 11 showing discoloration at vent areas and along the tray wall (above the rivets).

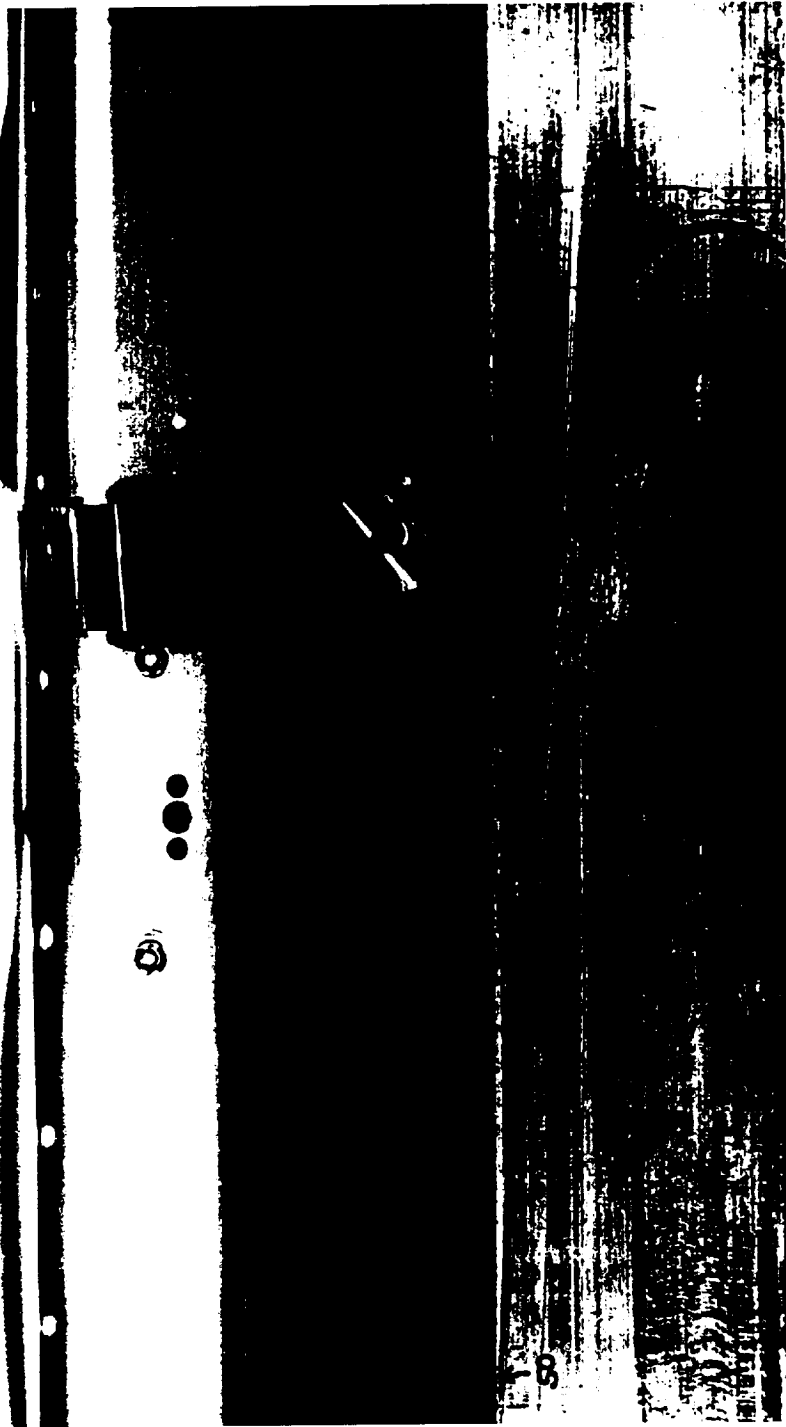


Figure 27. NASA post-flight photograph showing close up of blanket vent at location E10-7.

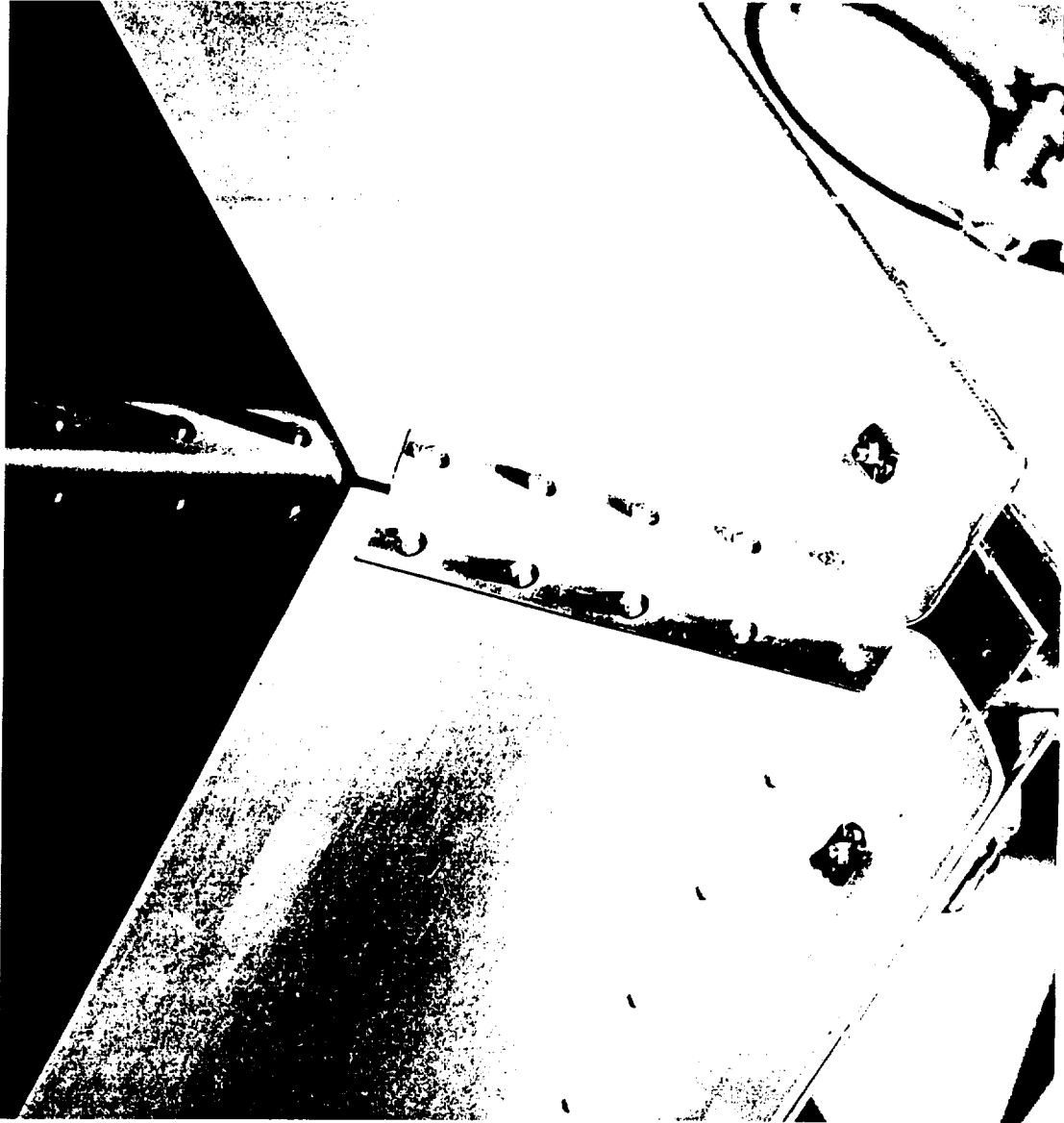


Figure 28. NASA post-flight photograph showing exterior of one corner of tray E10.

Surface analysis results

The E10-8 location had a distinctly discolored area and showed evidence of relatively thick films compared with the C6 and A4 locations. Measurement sites which have surface % Si >30% show no aluminum signal, indicating the film is thick enough to completely cover the substrate material. For stoichiometric films of SiO₂, the Si content should be ~33 mol%. Many readings within the discolored areas on E10 have values close to 33% indicating a completely oxidized silicate film remains on these leading edge locations

For tray E10-8, profiles taken at locations labeled C-1 through -5, and C-8, show thin layers which appear to be essentially silicon dioxide. The ratio of silicon to oxygen is approximately 1 to 2. The carbon profile shows a little surface carbon, as expected from exposure to the atmosphere post-flight, and then extremely low carbon levels in the silicon dioxide layer. At the depths where the silicon intensity begins to decrease, the aluminum peak begins to increase. This indicates the top of the aluminum oxide(anodized) coating. The profile for location C-6, which is quite close to the discolored region, shows a much thicker silicon dioxide layer(almost 1500 angstroms) but otherwise is similar to the previously discussed peaks. The depth profiles from locations C-7 and B-1 are quite complex. The silicon and carbon profiles show periodically varying intensities. These profiles represent very thick deposits from both the silicone based adhesive and hydrocarbon based outgassing sources, such as the polyurethane based paint from the interior of the tray, covered by a silicon dioxide layer. Because the sputtering system is calibrated for SiO₂, the sputter rate becomes more difficult to interpret as the carbon content of the material increases. This means the

depths shown on the profiles are not very accurate after the first several thousand angstroms of sputtering. The vent at location E10-8 is essentially at a rivet location and the rivet does not provide any effective shielding in this case. The silicon % on the surface at locations on pieces B and C is generally over 30%, except for the extreme left edge of piece B. The measurements on piece A from E10-8 show decreases in silicon % relative to surfaces closer to the vent, but still show silicon well above background levels. The visible discoloration is to the left of, and above, the rivet. The extreme left edge of piece B does not show discoloration. There seems to be a distinct difference between the levels of silicon present on piece B correlated with the visible deposits.

Measurements on E10-8 show a gradual drop-off from the high levels of silicon observed at locations near the vent. Area "E" is to the right of the vent. These locations were not well shielded by the vent by the rivet, in contrast to area "A", that is located to the left of the vent. Measurements in area "A" show much lower silicon % than for measurements in area "E", due to the rivet partially shadowing of area "A" from the vent.

Measurements from E10-3, cut piece labeled "E", each show a high silicon content. This area is a highly discolored area directly across from the vent and the measurements were made on the darkest part. Cut piece D has some dark areas (with Silicon above 32%) and lighter regions, which appear to be thinner, and show less Si elemental %. These areas show some aluminum on the surface, suggesting the films are thinner than the darker areas. The area directly across from the E10-3 vent location and around the rivet by the vent area shows uniformly high silicon deposition on the surface (>30%). The silicon % at locations on the E10-3 piece labeled B shows a large decrease in Si content relative to

the areas of E10-3 piece labeled C. Piece C was located closer to the vent. The lowest portion of piece B shows surface silicon in excess of 30%. Most other measurements from pieces B and G show very low surface silicon amounts (<3%).

At each tray location examined, there is a strong correlation between the silicon and aluminum detected. Locations with relatively high silicon %s (roughly 30% and higher) did not show an aluminum peak. Results consistently show the lower the silicon value, the higher the aluminum value.

The silicon % measured at locations on the piece labeled C show large variations between locations in close proximity. The lower portions of this piece show surface silicon in excess of 20%. Immediately above this area are measurements showing very low surface silicon (<2%). These measurements may represent a specific highly directed vent path from the vent hole in the FEP blanket; however, this has not been proved.

Scanning electron microscope images of fracture specimens from tray E10-9 show a flexible elastomeric contaminant layer covering the anodized aluminum layer on the tray lip. This is essentially material deposited from the silicone gasket post-flight. The contaminant layer along the tray wall has a very brittle structure, suggesting an oxidized material from the on-orbit exposures. The sequence of photos in figure 16 shows a view of a discolored area from an area near position E10-9(a surface at the Earth end of the tray facing space) and locations from which fracture samples were taken. The remaining photos show views of the surface at selected locations and edge-on views to show the structure of the contaminant layers on top of the anodized aluminum.

Summary

Silicon Distribution

Linear fits to the data for both A4-9 and C6-2 at locations on the tray wall between the two rivets(no shielding) closest to the vent opening show strong correlations with distance from the top of the wall (y-direction), but not with distance along the wall(x-direction). The correlation of silicon elemental % with y-position is 0.92 and 0.96 for trays A4 and C6, respectively. These preliminary findings are based on locations near the vent openings. The silicon sources were in a plane with the top of the tray side wall. Experiment hardware within the tray blocks the line of sight of some source areas from the lower portions of the tray walls.

Coating Depths

For the A4-9 locations which were sputter depth profiled, the higher on the tray wall, the “thicker” the silicon containing film. However, all the silicon containing films are extremely thin, by 30 nm depth the levels of silicon are quite low, and give the appearance of filling the voids in the anodize layer. For the C6-2 locations the coatings are thicker than for A9. However, like the A9 locations, those locations away from the C6-2 vent also show that the higher on the tray wall, the “thicker” the silicon containing film. The depth profiles for locations directly across from the C6-2 vent show complex films of varying composition with depth. The films across from vent location E10-8 are even thicker than films at comparable locations on C6. The presence of significant carbon based deposition made quantitative thickness determinations impossible. The

sputter rate was calibrated for SiO₂ but the high levels of other species made sputter rate estimates invalid.

Separation of Contributions from Different Contamination Sources

The contamination sources for the deposits examined under this contract are the following:

- 1) The DC6-1104 silicone adhesive used to hold the Velcro™ fasteners to the tray frames and thermal control blankets.
- 2) The silicone tray cover gaskets, which were used both pre- and post-flight.
- 3) Outgassing from the Space Shuttle.

The contributions from the tray cover gaskets and the Space Shuttle are negligible on the interior walls of the experiment trays. The contaminant films are extremely thin in all cases. This is in spite of the fact that the films at the discolored areas on E10 are many times the thickness of the film at A4 locations. At A4 locations the silicone based contaminant did not really build up any thickness, but essentially occupies the pores in the anodize layer. Silicone containing films are distributed over wide areas on the LDEF tray surfaces being examined, but the films are only visible in areas which were exposed to both atomic oxygen and solar UV.

The background measurements from the tray lip to the wall help separate the gasket contribution from the adhesive outgassing. The gasket contribution is relatively small in the areas near vents. On E10 and C6 the remainder of the curved regions and tray lips do not show the discoloration observed near the vents. At locations on E10 and C6 which

received both atomic oxygen and solar exposure, the discoloration pattern is so distinct as to show the shape of the vent.

Summary of Modeling Calculations

The reports provided by the organizations which carried out the modeling using the ISEM and NASTRAN/NASAN codes are included as stand alone documents with this report.

The results obtained by running the Plume Impingement (PLIMP) model are contained entirely within this report. The following sections are summaries of findings from each specific modeling effort.

ISEM MODEL RESULTS

A review of a previous calculation for the entire LDEF structure was made prior to conducting the detailed modeling calculations for the specific locations of interest. The review of the previous calculations show that the background ambient contamination from the general LDEF environment was negligible relative to the specific, local sources at each tray location of interest. The model used for the ISEM based calculation assumes that atomic oxygen will fix the silicon containing species in place when sufficient oxygen is available. This condition is true for the E10 tray surfaces examined. Based on the data provided, and using the simplifying assumptions detailed in the report provided by ROP, Inc., the worst case deposition estimate (assuming a source at 125C and complete outgassing and re-deposition) is 28,500 angstroms. At certain locations directly across from vent locations, depositions in apparent excess (calibration of sputtering rate has some uncertainty) of 10,000 angstroms were measured. Measured deposits had considerable carbon-based material deposition in addition to the silicon-based material. While it is not possible to determine exactly the fraction of deposited material which came from the

silicone-based adhesive and from the Z306 paint binder, it is clear there is considerable contribution from each source. It is also likely that the on-orbit source temperature was not as high as the standard 125C used in ground based outgassing measurements. The 75C outgassing source temperature is likely closer to the actual on-orbit source temperatures. The temperature of the tray wall where the contaminants deposited was also likely colder than 25C during a portion of each orbit while the LDEF was within the Earth's shadow. The model estimates are well within reason. The values of maximum deposition of silicone-based materials on surfaces at locations E10 and C6 are probably slight over-estimates, but given the complexity of actual exposure conditions and uncertainty in temperatures, the model represents the experimental results rather well.

NASTRAN/NASAN MODEL RESULTS

Outgassing temperatures for source and collection surface were estimated from LDEF on-orbit measurements and the outgassing rate from ground-based measurements at 125C and 75C was adjusted to the estimated on-orbit conditions of 24C average source temperature and 10C collection plate temperature. From these estimates a mission average outgassing rate was determined. Details of this determination are discussed in a companion stand-alone document "Contamination Deposited on LDEF Surfaces" (MDC 97H0867R1). An average density of contaminant material was estimated and a total deposited mass per cm² determined. From this model worst case estimates of contaminant depths of 15000 angstroms were determined for Trays E10, C6, and A4. Examples of contaminant thickness estimates from E10-3, E10-8, and C6-2 are shown in figure 29. The predicted distribution of Si from this analysis is similar to the distribution seen in pictures of the silicone deposition on the LDEF trays in terms of contamination

shape. The predicted thickness of the contamination layer at tray location A4-9 is much more than the amount actually measured. The predicted thickness of layers at E10 and C6 locations are much closer to the measured values.

E-10-3 Total Deposition modeled with NASAN in Å	E-10-8 Total Deposition modeled with NASAN in Å	C6-2 Total deposition modeled with NASAN in Å
45	100	1100
83	2200	430
230	1700	2400
1900	28000	2400
5700	6300	3300
15000	29000	5400
12000	13000	9100
3600	1600	5000
8200	150000	10000
2200	100000	5900
120	43000	7500
76	27000	8500

Figure 29. Total Deposition at Typical Locations on E10-3, E10-8, and C6-2 from NASAN Model in Å

Plume Impingement (PLIMP) Model Results

The ISEM and MOLFLUX computer models contain rather detailed geometric models to support prediction of contaminant flows on spacecraft. In addition to the detailed ISEM and MOLFLUX models, it was decided to also use a set of less complicated computer models that incorporate simple geometries to evaluate the quality of the results that could be obtained in a quick and inexpensive analysis. A description of the method used and the results of that analysis are described in the section below.

Analysis

The Method of Characteristics (MOC) computer code was used to define the vent mass flow.

The MOC code is a code used for modeling axisymmetric, supersonic flows whose pressures are in the continuum flow range. The flow in this case is nearly two dimensional and is free molecular. In keeping with the goal of simplicity, it was decided not to try to make any modifications to the MOC code; but, instead, to make appropriate adjustments to the input and to accept whatever resulted. The slot that was modeled was approximately 7.5 mm wide and 25 mm long with a total area of 187.5 mm^2 . A circular orifice of equivalent area will have a radius of 7.73 mm.

In determining the mass flow through each vent, it was assumed that there was a total of 250 gm of adhesive under the blanket and that one percent of that mass outgassed over a period of 2106 days. These assumptions give a mass flow rate of $9.8 \times 10^{-10} \text{ gm/sec/vent}$ for each of the 14 vents. The MOC code requires the stagnation pressure of the flow as an input. An initial guess as to the stagnation pressure was made and then iterated until the vent flow was matched. This resulted in a stagnation pressure of $9.2 \times 10^{-12} \text{ atm}$. A molecular weight of 200 was assumed for the vent gas. In a Maxwellian flow with an average velocity of zero, the average molecular speed is equal to 1.24 times the speed of sound. In the flow calculations, the Mach number input for the flow at the orifice was chosen to be 1.24. The flow angle of the vent flow was varied from 0° relative to the flow centerline at the center of the orifice to 85° relative to the flow centerline at the edge of the orifice. The flow field calculated by the MOC code is shown in Figures 30 and 31. In figure 1 the numbers represent the fraction of the total mass flow which is between the labeled line and the centerline of the flow. In figure 2, the numbers represent the mass flux in $\text{gm/cm}^2/\text{sec}$.

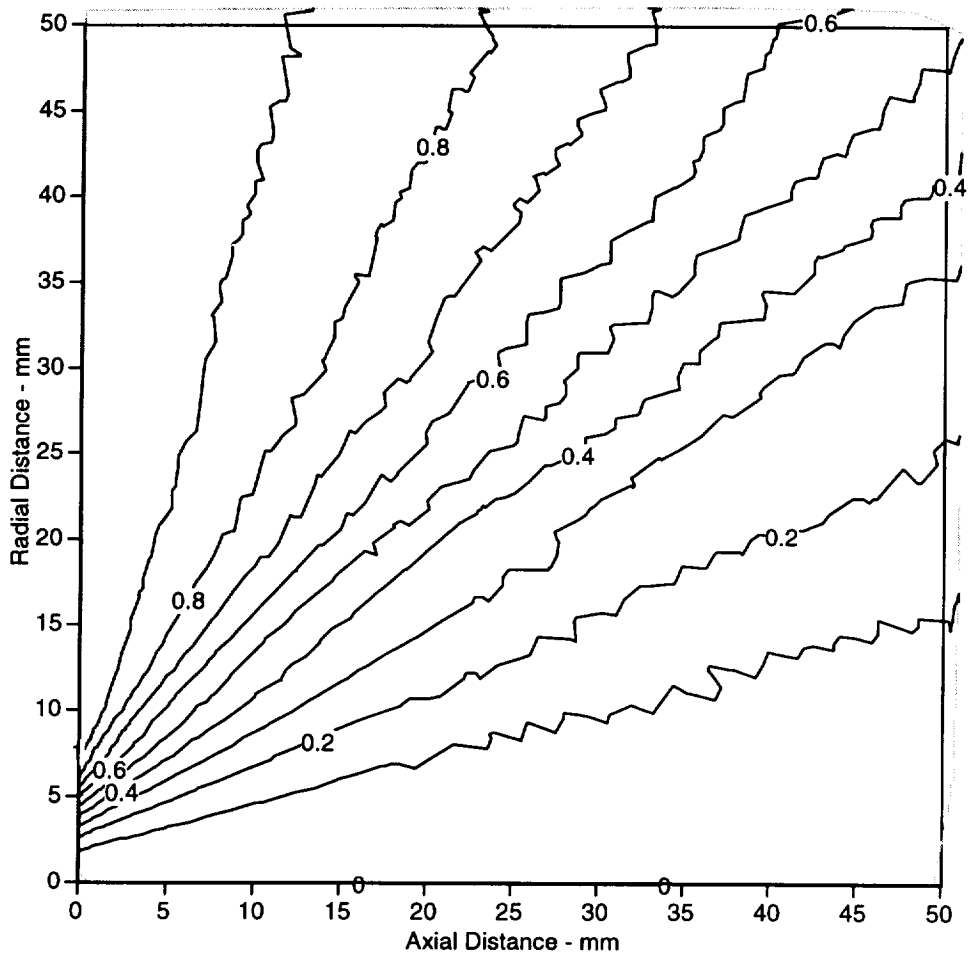


Figure 30. Orifice Flow Streamlines In Fraction of Total Mass Flow.

The Plume Impingement (PLIMP) computer code was used to calculate the mass flux impingement on the tray side. The side was modeled in the PLIMP code as a 14.9 mm wide flat plate (tilted 15° from the vertical) which transitions smoothly into a cylinder with a radius of 10.3 mm. The vent orifice was located on the centerline of the vent and at a distance of 12.5 mm along the MLI measured from the intersection of the MLI and the tray side. The centerline of the orifice flow was oriented so that it was perpendicular to the surface of the MLI.

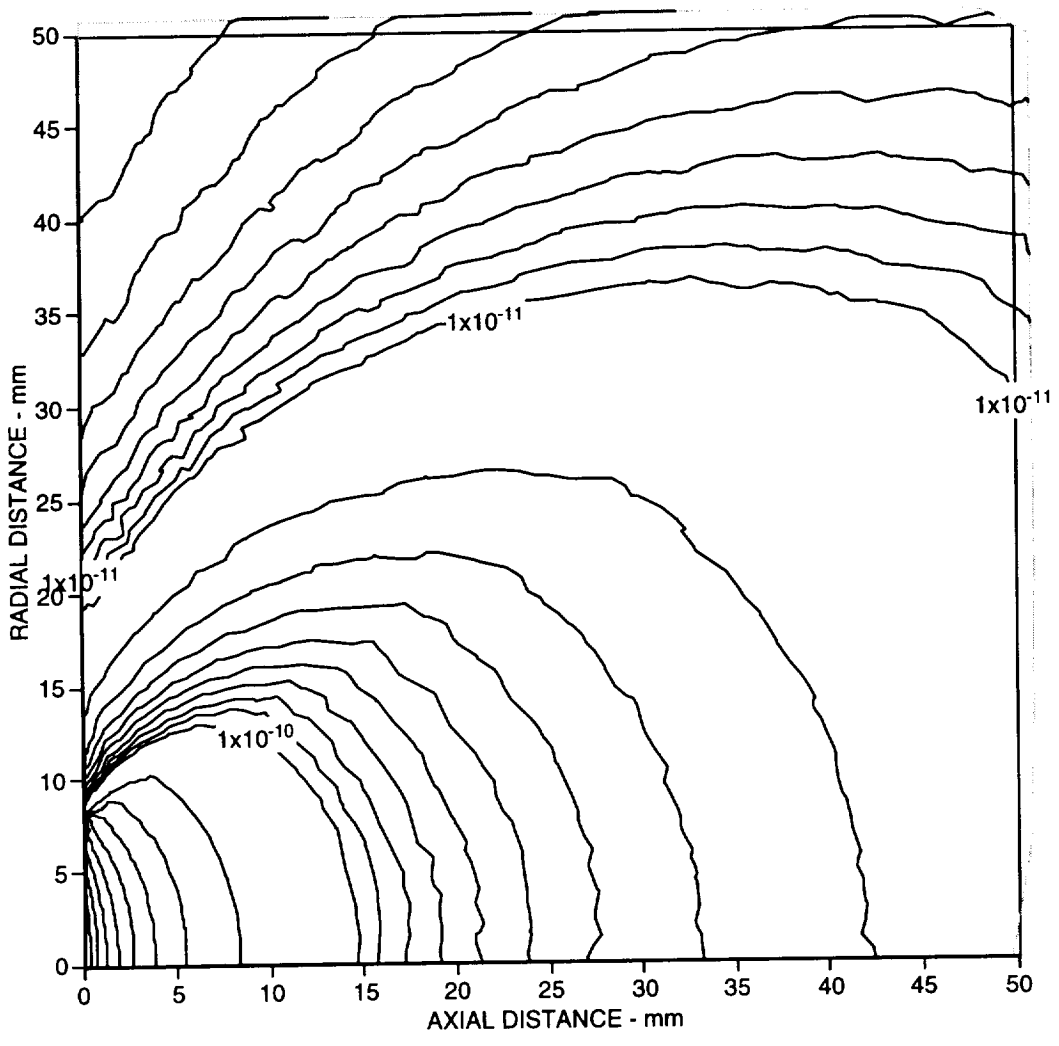


Figure 31. Orifice Flow Mass Flux In $\text{gm/cm}^2/\text{sec}$.

The mass fluxes to the cylinder and the flat plate in $\text{gm/cm}^2/\text{sec}$. are shown in Figures 32 and 33 respectively. The vertical distances shown are measured along the tray edge surface and, for the flat plate, start at the location where the blanket meets the tray side. The total mass fluence is given by multiplying the plotted results by the total exposure time of 2106 days. The results of this calculation are shown in Figures 34 and 35 for the cylinder and flat plate respectively.

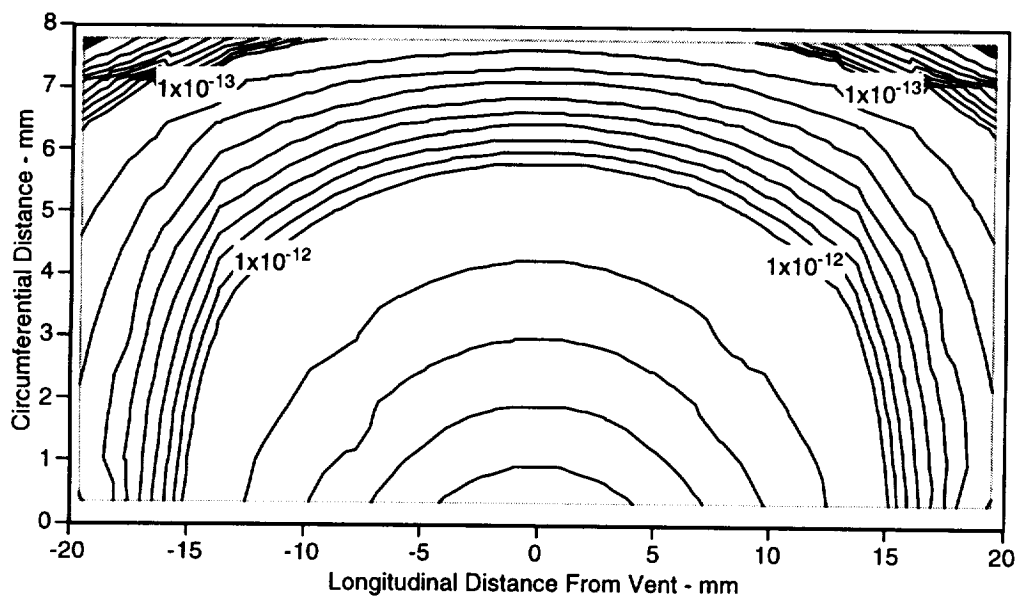


Figure 32. Mass Flux in $\text{gm/cm}^2/\text{sec}$. to Cylindrical Portion of Tray Edge.

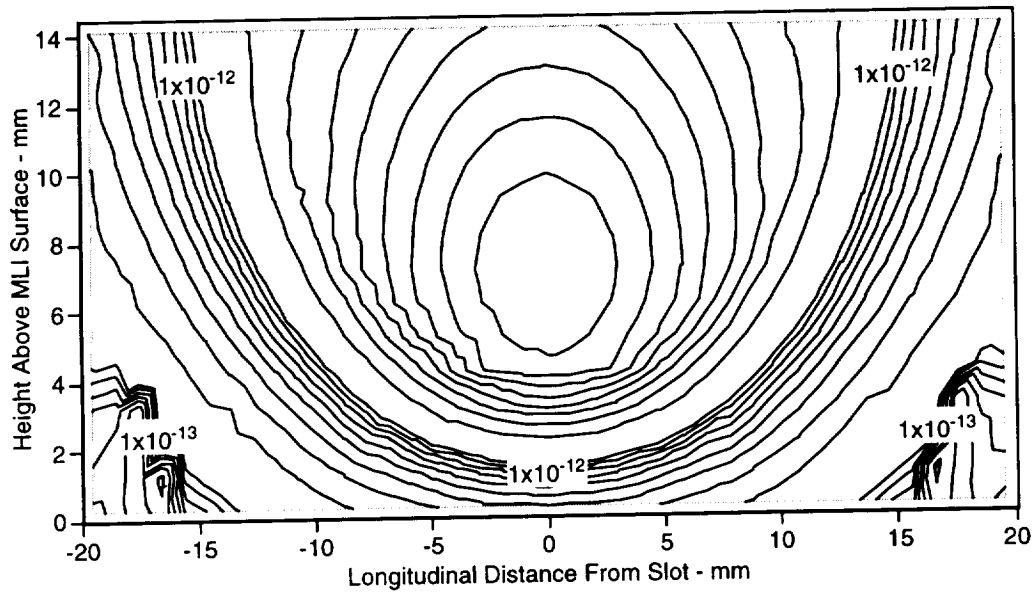


Figure 33. Mass Flux in $\text{gm/cm}^2/\text{sec.}$ to Flat Plate Portion of Tray Edge.

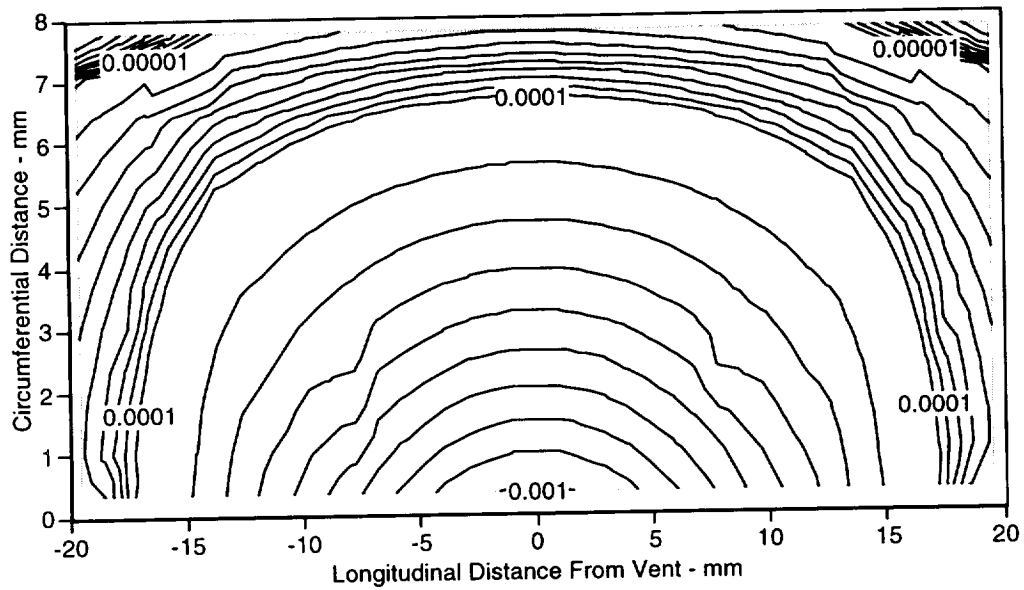


Figure 34. Fluence in gm/cm^2 to Cylindrical Portion of Tray Edge.

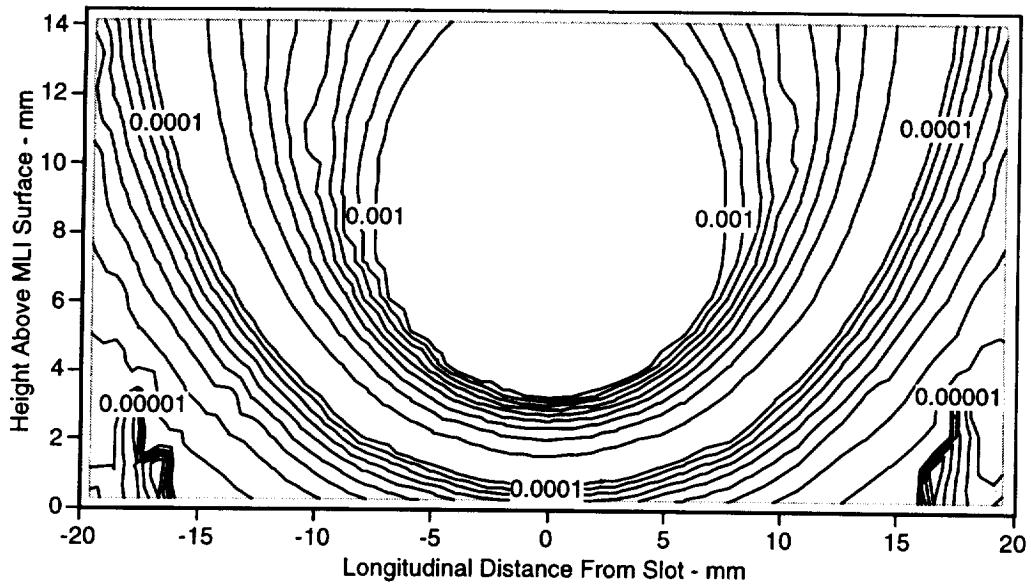


Figure 35. Fluence in gm/cm^2 to Flat Plate Portion of Tray Edge.

Calculations that produced the results shown in Figures 30 through 36 were made without any prior knowledge of the LDEF flight results. The calculations represent typical results obtainable from a rough estimate of contaminant fluxes on a spacecraft. The thickness estimates from the PLIMP model range from 10^3 to 10^5 Å for the current surfaces being modeled. The thicknesses predicted using PLIMP are of similar order of magnitude to values predicted using the more elaborate models. This similarity in results is at least partially due to the relative simplicity of the geometry and the fact that outgassing rates were all determined rather empirically using the similar assumption of ~250 gms of silicone-based adhesive with ~1% total outgassing by mass.

Conclusions

Model Comparison

The ISEM model analysis assumes explicitly that atomic oxygen must be present for contamination build-up. The other two models essentially assume outgassing rates and the (implied) value for the “sticking-coefficient” is 1.

For a simple geometry, the PLIMP model appears to give estimates similar to the more detailed models. For order-of-magnitude estimates the PLIMP model appears to be sufficient. The ISEM model has a “mechanism” for varying the sticking coefficient by making the sticking coefficient a function of atomic oxygen fluence, but this only works for LEO orbits. There is no atomic oxygen at higher orbits. The NASAN model uses mass depositions directly and converts to thickness using an assumed density. The density of the contamination layers is really unknown, probably varies widely with composition, and conversions from mass to thickness are subject to uncertainty due to specific assumptions made about the density. The complexity of the outgassed mixture,

with large carbon-based components, in addition to the silicon source, precludes any more than qualitative estimates about “sticking-coefficients”.

Measured Results

To interpret the measured depth profiles, it should be kept in mind that the mission time essentially goes from “right to left” as the profiles are being viewed. The first material deposited is the material with the very high carbon content. A periodic change was observed in the relative amounts of oxygen and silicon as a function of depth at both the C6 and E10 locations. The observed periodicity in the intensity levels may be a function of seasonal variation of the sun orientation with respect to the surface, causing long term thermal cycling of the entire LDEF, however this has not been proved. The oxygen flux rate was much greater toward the end of the LDEF flight relative to the first 3-4 years, so much of the surface oxidation could have occurred over the last few months of the flight. In summary, the contamination deposits directly across from the vents are complex mixtures of materials and the mechanisms by which they may have been changed, once deposited on the surface, are not yet clear.

For each tray surface examined there was a very strong correlation between the amount of silicon and amount of aluminum detected. The greater the mol% of silicon observed, the less the mol % of aluminum. The correlation coefficients for plots of silicon elemental % vs aluminum elemental % are 0.82 for A9-4, 0.87 for C6-2, and >0.98 for E10-3 and E10-8. The correlation coefficients were determined for locations away from the discolored area. Plots comparing aluminum and silicon elemental %'s are shown in figures 36-38.

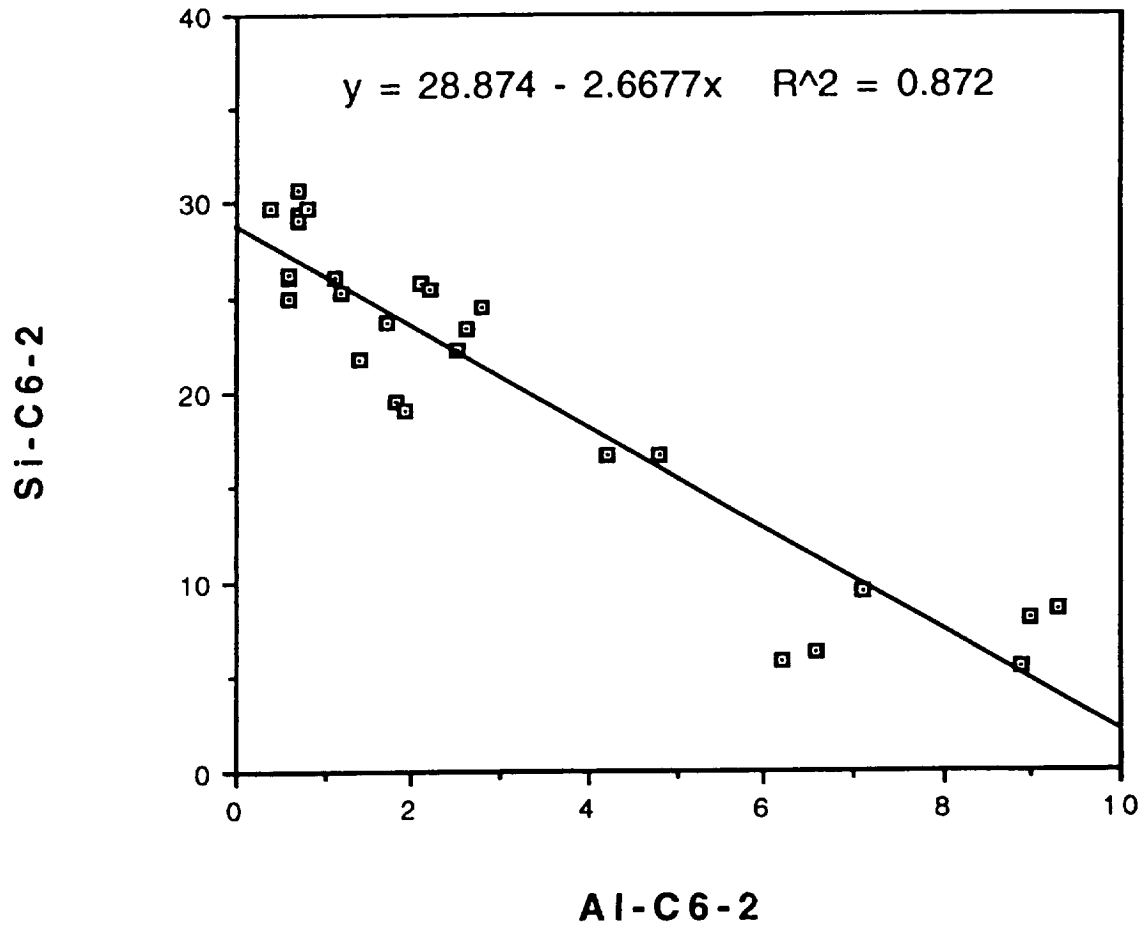


Figure 36. Silicon vs Aluminum Surface Content for Tray C6-2 ESCA Measurement Locations.

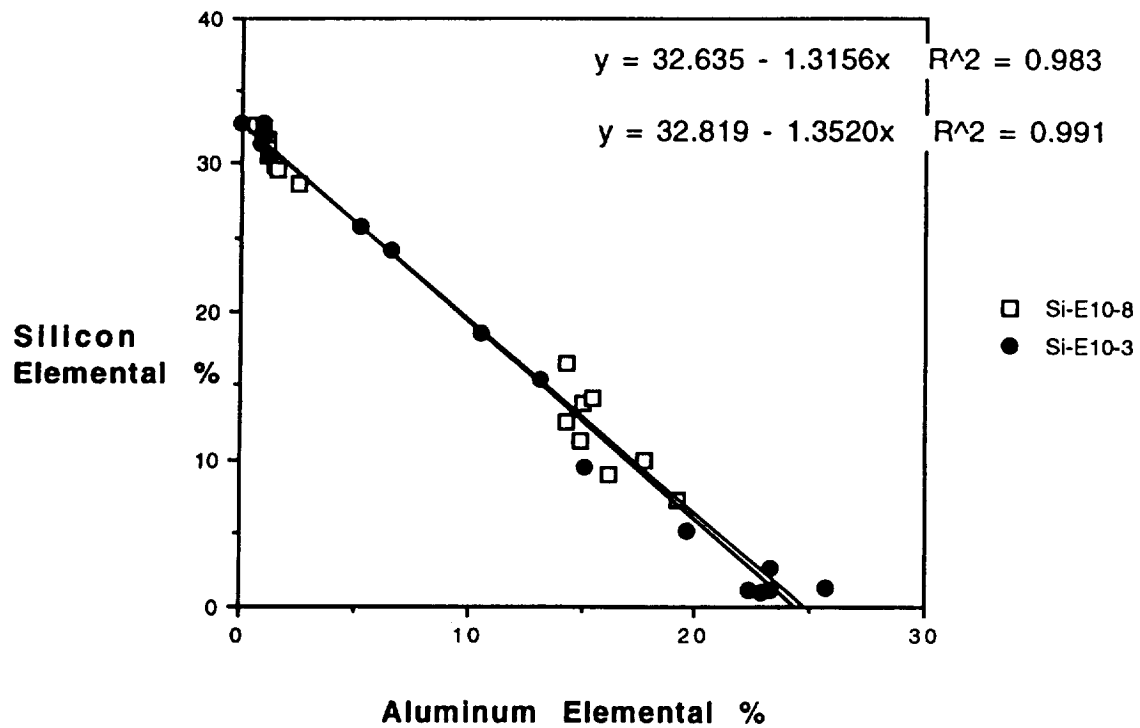


Figure 37. Silicon vs Aluminum Surface Content for Tray E10-8 and E10-3 ESCA Measurement Locations.

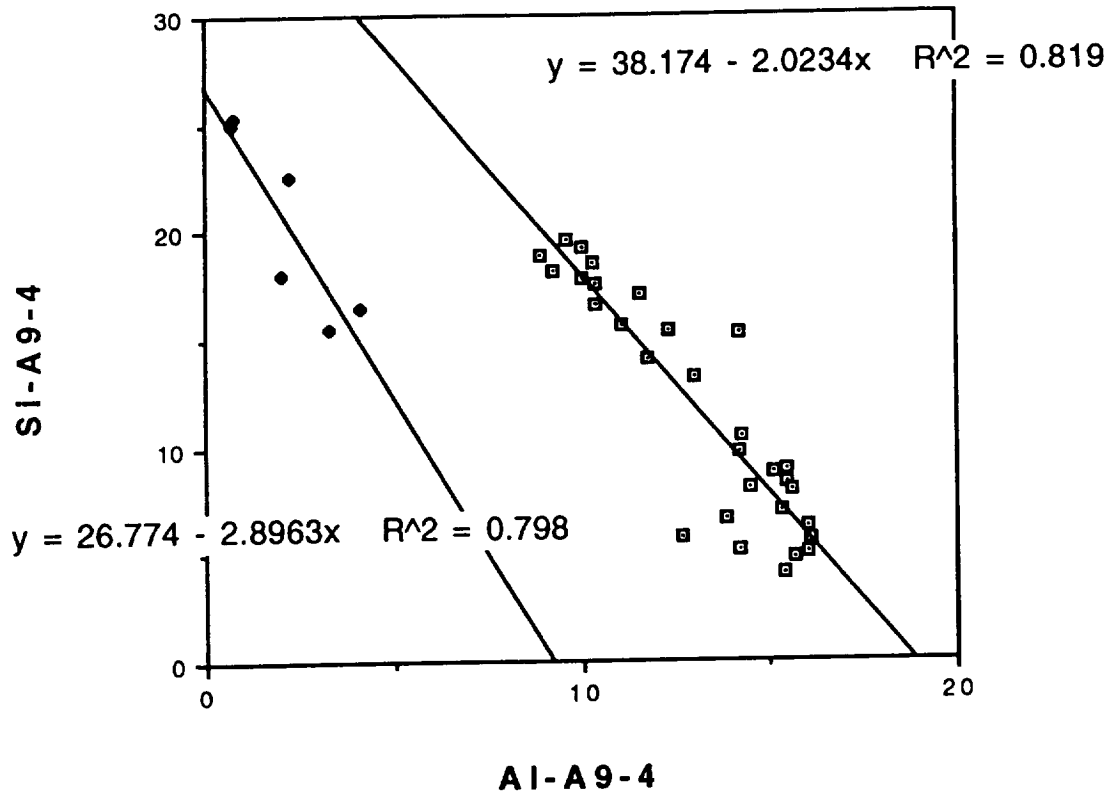


Figure 38. Silicon vs Aluminum Surface Content for Tray A4-9 ESCA Measurement Locations.

No silicon source induced discoloration appears on the interior tray walls of A4 around the vent areas. The most discoloration observed on C6 and E10 tray walls are on the sides that receive the most direct atomic oxygen. The tray lip on the side of C6 that is closest to row 7 curves away from the ram oxygen. No discoloration is seen on this side of the tray. The contaminant film on the examined area of A4 is extremely thin.

Discolored areas on E10-8 had such a thick contaminant film that sputter profiles barely reached the anodized aluminum surface.

Figures 39 and 40 show peak energies and peak shapes for silicon ESCA peaks at different sputtering depths. The peak positions have not yet been corrected for possible charging effects. The position of the Carbon peak has also been measured at each of the nominal depths, but this data is not yet available. The areas under the peaks reflect the relative amounts of silicon at the different depths. Figure 40 shows the peaks normalized to identical areas in order to show the relative shapes of the peaks. For areas which are visibly dark, the peaks at a nominal depth of 101.5 nm suggest at least two very different materials mixed at this level.

Appendix D contains scanning electron microscope images of fracture specimens from tray E10-9. These images in figures D-1 through D-3 show a flexible elastomeric contaminant layer covering the anodized aluminum layer on the tray lip. This is essentially material deposited from the silicone gasket post-flight. The contaminant layer along the tray wall has a very brittle structure, suggesting an oxidized material from the on-orbit exposures. The remaining images in appendix D show views of the surface at selected locations and edge-on views to show the structure of the contaminant layers on top of the anodized aluminum.

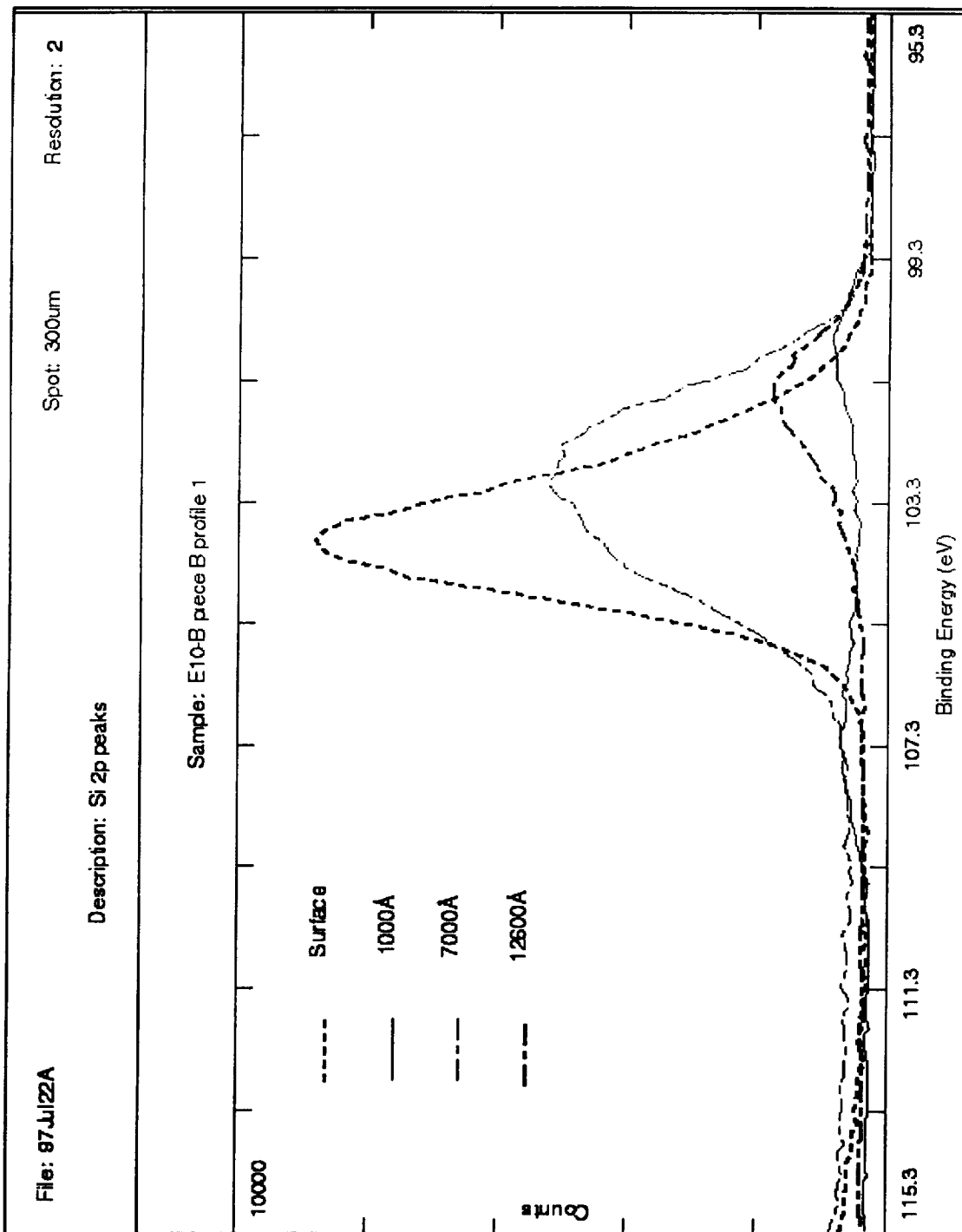


Figure 39. Si 2p Peaks from profile 1 on E10-8 piece B.

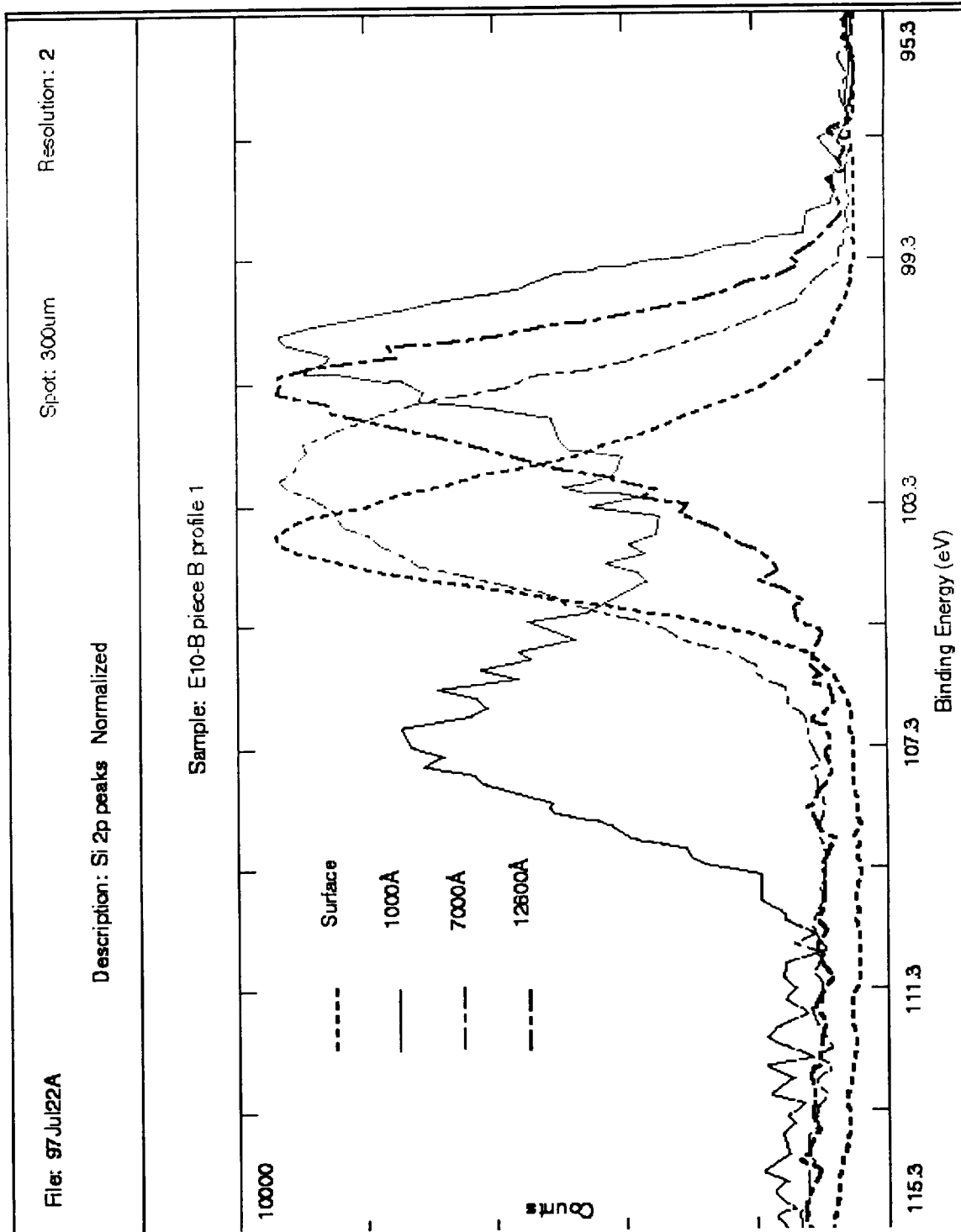


Figure 40. Normalized Si 2p Peaks from profile 1 on E10-8 piece B.

Appendix A

Detailed Results of ESCA Measurements from all Surfaces Examined under Contract NAS8-40581

Introduction

This appendix contains maps of each ESCA measurement location on each surface of interest, maps showing the %Si determined at each location, and tables of ESCA surface elemental composition at each location where measurements were conducted. These results include %C, %Al, %O, and %Si, as well as any minor constituents detected.

Data is included for LDEF tray locations E10-8, E10-3, C6-5, C6-2, A4-9, and A4-1.

Surfaces that were not exposed to atomic oxygen all show aluminum present in substantial amounts. This indicates that the contaminant layers (in trailing edge locations) are very thin and/or not-contiguous. The outgassed contaminants have essentially filled in the pores of the anodized aluminum substrate, but have not built up any substantial stand-alone layers. This implies that the photo-attachment processes for sticking this contaminant material onto anodized aluminum are very inefficient.

List of Figures

Figure A-1.	Tray E10-8 ESCA analysis areas.	A4
Figure A-2.	Tray E10-8 ESCA analysis area grid locations.	A5
Figure A-3.	Tray E10-8 Percent Silicon.	A6
Figure A-4.	Tray E10-8 Surface Composition.	A7
Figure A-5.	Tray E10-3 ESCA analysis areas.	A11
Figure A-6.	Tray E10-3 ESCA analysis grid locations.	A12
Figure A-7.	Tray E10-3 Percent Silicon.	A13
Figure A-8.	Tray E10-3 Surface Compositions.	A14
Figure A-9.	Tray C6-5 ESCA analysis areas.	A18
Figure A-10.	Tray C6-5 ESCA analysis area grid locations.	A19
Figure A-11.	Tray C6-5 Percent Silicon.	A20
Figure A-12.	Tray C6-5 Surface Composition.	A21
Figure A-13.	Tray C6-2 ESCA analysis cut sample pieces.	A25
Figure A-14.	Tray C6-2 ESCA analysis area grid locations.	A26
Figure A-15.	Tray C6-2 Percent Silicon.	A27
Figure A-16.	Tray C6-2 Surface Composition.	A28
Figure A-17.	Tray A4-9 ESCA analysis areas.	A33
Figure A-18.	Tray A4-9 ESCA analysis area grid locations.	A34
Figure A-19.	Tray A4-9 Percent Silicon.	A35
Figure A-20.	Tray A4-9 Surface Composition.	A36
Figure A-21.	Tray A4-1 ESCA analysis areas.	A41
Figure A-22.	Tray A4-1 ESCA analysis area grid locations.	A42
Figure A23.	Tray A4-1 Percent Silicon.	A43
Figure A-24.	Tray A4-1 Surface Composition.	A44

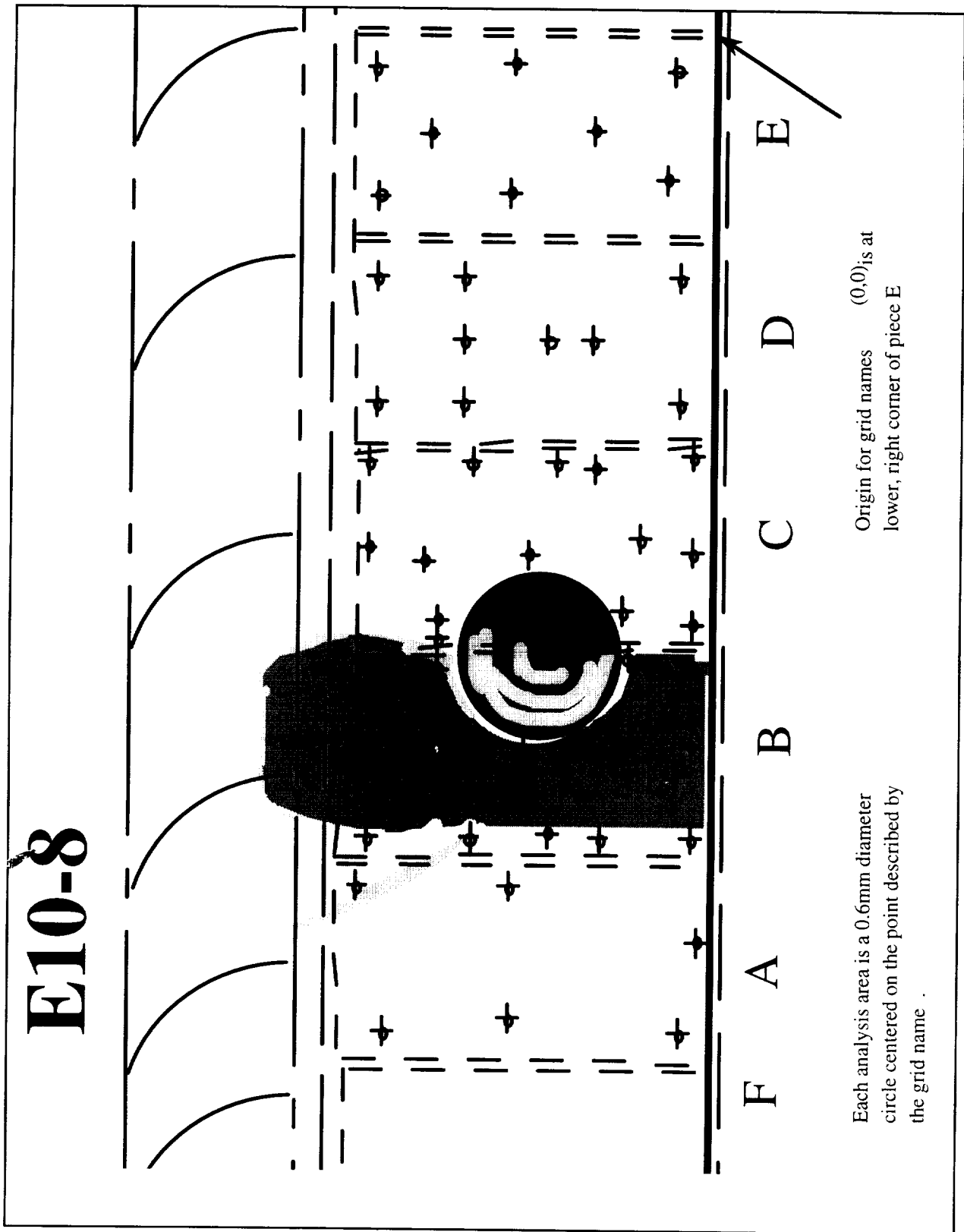


Figure A-1. Tray E10-8 ESCA analysis areas.

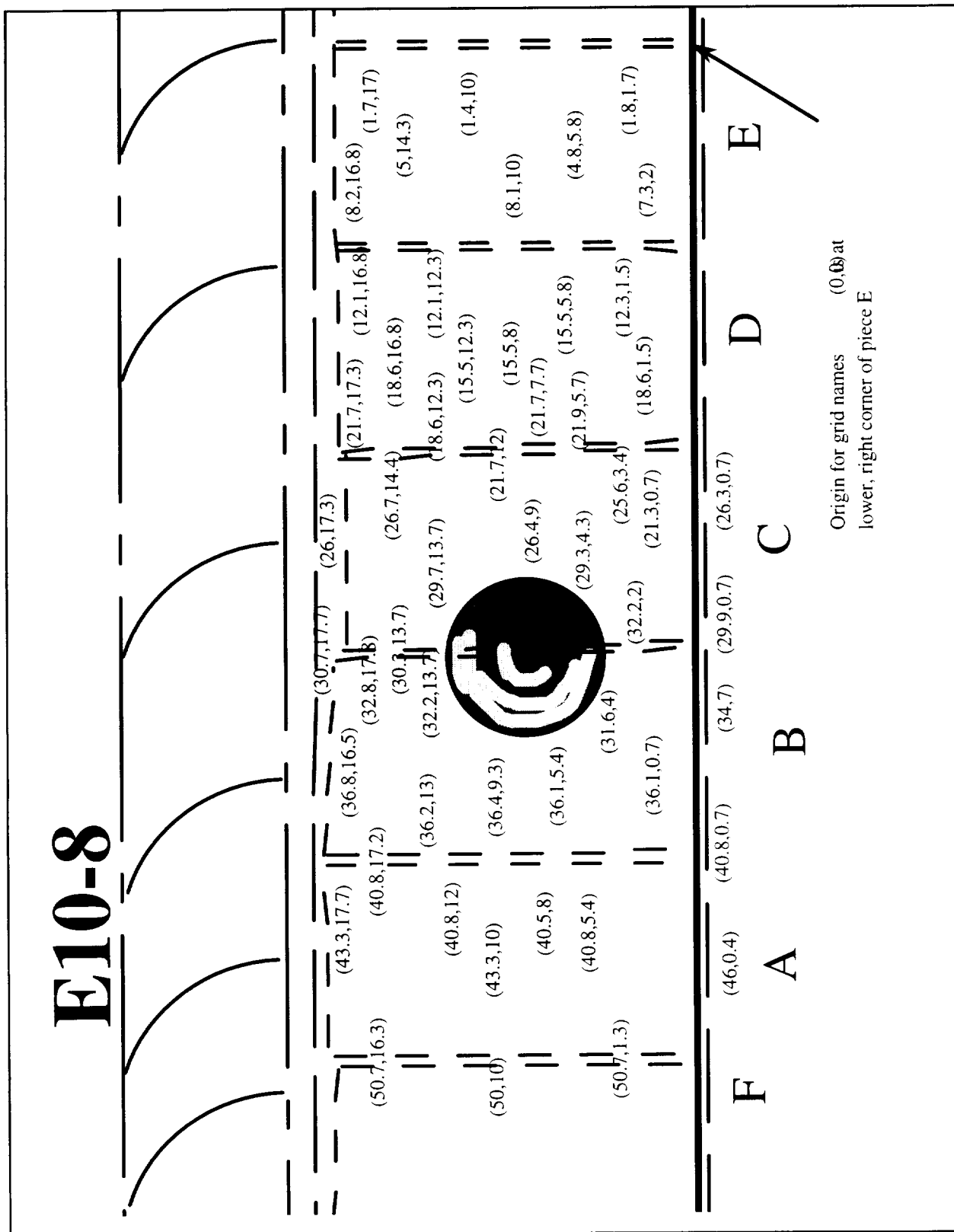


Figure A-2. Tray E10-8 ESCA analysis area grid locations.

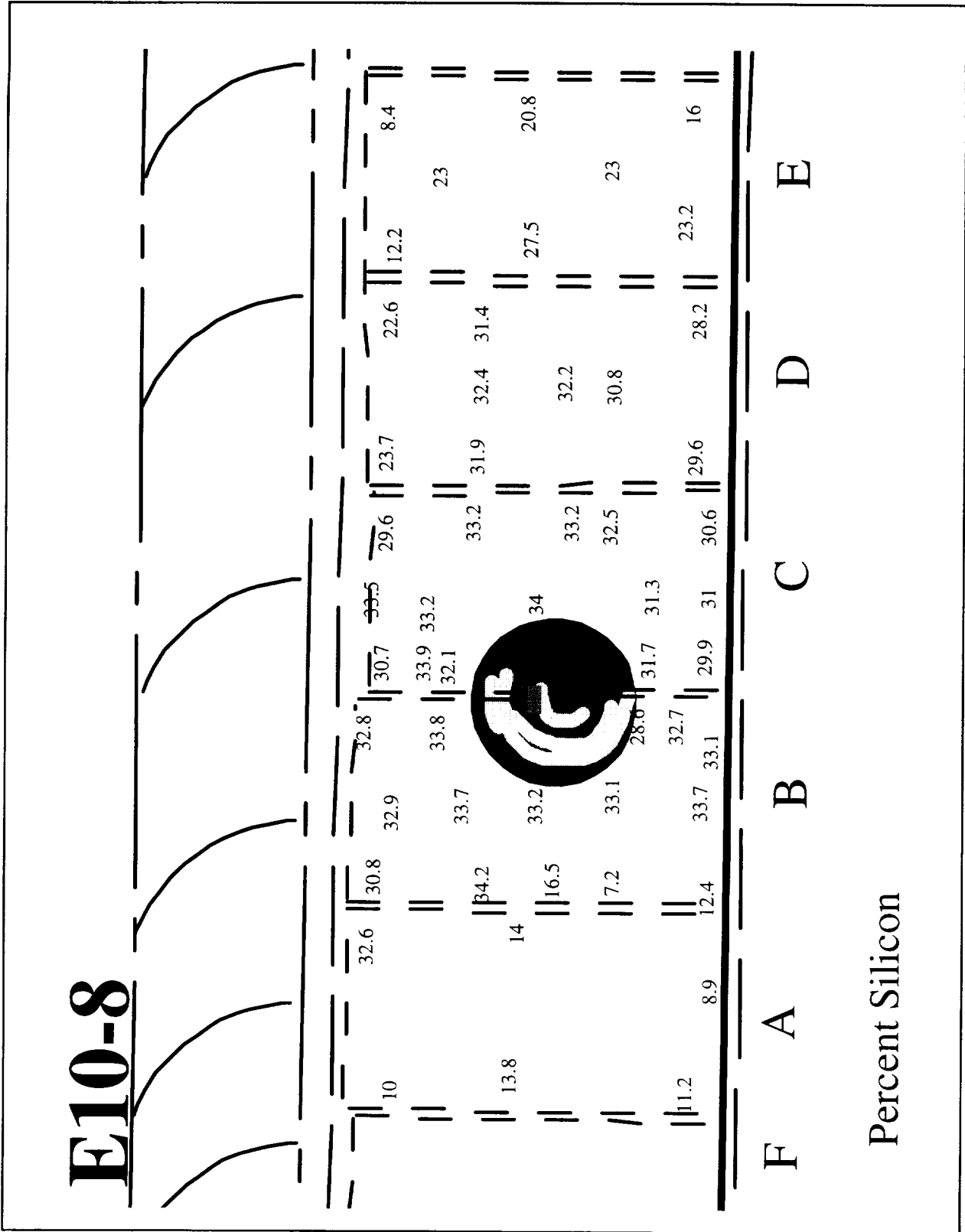


Figure A-3. Tray E10-8 Percent Silicon.

E10-8 Unspattered Surfaces only														
XPS Survey Scan Composition Table summary														
Cut Piece	A	A	A	A	A	A	A	B	B	B	B	B		
Location	46-0.4	43.3-17.7	43.3-10	50.7-16.3	50-10	50.7-1.3	40.8-0.7	36.1-0.7	36.1-5.4	40.8-5.4	40.5-8	36.4-9.3	40.8-17.2	36.8-16.5
Atomic %:	8.9%	32.6%	14.0%	10.0%	13.8%	11.2%	12.4%	33.7%	33.1%	7.2%	16.5%	33.2%	30.8%	32.9%
Silicon														
Oxygen	48.5%	55.6%	49.7%	44.1%	46.5%	48.5%	50.7%	56.9%	57.4%	49.8%	52.2%	58.6%	53.1%	54.6%
Aluminum	16.2%	0.6%	15.5%	17.8%	15.0%	14.9%	14.3%	-	-	19.2%	14.3%	-	-	-
Carbon	18.5%	10.2%	11.8%	18.4%	14.4%	14.1%	13.7%	8.8%	9.1%	13.9%	10.0%	8.2%	14.9%	12.2%
Fluorine	2.8%	0.6%	5.8%	6.4%	6.4%	2.8%	3.1%	0.4%	-	4.6%	2.7%	-	-	-
Sodium	0.6%	-	0.4%	0.2%	0.3%	0.7%	0.7%	-	-	0.8%	0.4%	-	0.6%	-
Sulfur	2.0%	-	1.7%	0.7%	1.8%	2.3%	2.0%	-	-	1.8%	2.0%	-	-	-
Nitrogen	0.8%	-	-	0.4%	0.5%	0.7%	0.9%	-	0.4%	0.8%	0.5%	-	-	-
Potassium	0.2%	-	0.3%	-	0.2%	1.1%	0.2%	-	-	-	0.4%	-	-	-
Calcium	0.3%	-	-	0.2%	0.4%	0.5%	0.4%	-	-	0.2%	-	-	-	-
Magnesium	0.5%	-	0.8%	0.5%	0.6%	1.0%	0.8%	-	-	0.8%	0.4%	-	0.3%	0.2%
Tin	-	0.1%	-	0.1%	--	0.1%	-	0.1%	0.1%	-	0.1%	-	-	0.1%
Chrome	-	0.3%	-	0.3%	-	-	-	-	-	-	-	-	-	-
Phosphorus	0.6%	-	-	0.8%	-	2.1%	0.8%	-	-	0.9%	0.5%	-	-	-
Zinc	-	-	-	0.1%	-	-	-	-	-	-	-	-	-	-
Iron	0.2%	-	-	-	-	-	-	-	-	-	-	-	-	-
Chlorine	-	-	-	-	-	-	-	-	-	-	-	-	-	0.3%

Figure A-4 (1 of 4). Tray E10-8 Surface Composition.

E10-8 Unsputtered Surfaces only													
XPS Survey Scan Composition Table summary													
Location	B	B	B	B	B	B	B	C	C	C	C	C	
Atomic %:	36.2-13	40.8-12	32.8-17.8	32.2-13.7	31.6-4	34-0.7	32.2-2	29.7-13.7	30.3-13.7	30.7-17.7	26-17.3	26.7-14.4	21.7-17.3
Silicon	33.7%	34.2%	32.8%	33.8%	28.6%	33.1%	32.7%	33.9%	32.1%	30.7%	33.5%	33.2%	29.6%
Oxygen	58.7%	58.5%	54.9%	59.4%	55.3%	56.6%	56.5%	58.0%	59.6%	51.0%	57.1%	58.8%	54.1%
Aluminum	-	-	-	-	2.5%	-	-	-	-	-	-	-	1.6%
Carbon	7.3%	6.6%	11.9%	6.5%	12.9%	10.0%	10.4%	7.7%	7.3%	16.8%	8.5%	6.7%	13.5%
Fluorine	-	0.6%	-	-	0.4%	-	-	-	-	-	0.4%	0.5%	0.5%
Sodium	-	-	-	-	0.1%	0.3%	0.3%	-	-	0.3%	0.4%	0.4%	0.1%
Sulfur	-	-	-	-	-	-	-	-	-	-	-	-	-
Nitrogen	-	-	-	-	-	-	-	-	0.7%	-	-	-	-
Potassium	-	-	-	-	-	-	-	-	-	-	-	-	0.2%
Calcium	-	-	-	-	-	-	-	-	-	-	-	-	-
Magnesium	0.2%	-	0.4%	0.2%	-	-	-	0.1%	-	0.5%	-	0.5%	0.2%
Tin	-	0.1%	0.1%	-	0.1%	-	-	-	-	-	0.1%	-	0.1%
Chromium	-	-	-	-	-	-	-	0.2%	0.2%	-	-	-	-
Phosphorus	-	-	-	-	-	-	-	-	-	-	-	-	-
Zinc	-	-	-	-	-	-	-	-	-	-	-	-	-
Iron	-	-	-	-	-	-	-	-	-	-	-	-	-
Chlorine	-	-	-	-	-	-	-	-	0.7%	-	-	-	-

Figure A-4 (cont. 2 of 4). Tray E10-8 Surface composition.

E10-8 Unspattered Surfaces only
XPS Survey Scan Composition Table summary

Cut Piece Location	C	C	C	C	C	C	C	C	C	D	D	D	D
	21.7-7.7	26.4-9	29.9-0.7	25.6-3.4	26.3-0.7	29.3-4.3	21.3-0.7	21.9-5.7	18.6-16.8	12.1-16.8	15.5-12.3	18.6-12.3	12.1-12.3
Atomic %:													
Silicon	33.2%	34.0%	29.9%	31.3%	31.0%	31.7%	30.6%	32.5%	23.7%	22.6%	32.4%	31.9%	31.4%
Oxygen	57.2%	57.4%	53.9%	58.0%	56.9%	57.0%	55.5%	57.0%	51.8%	51.5%	59.0%	56.9%	57.7%
Aluminum	-	-	1.5%	1.2%	1.2%	1.2%	1.2%	0.9%	5.4%	6.4%	-	1.0%	0.7%
Carbon	9.1%	8.0%	14.2%	8.9%	10.7%	9.9%	11.8%	9.2%	15.2%	15.0%	7.6%	8.7%	8.4%
Fluorine	0.4%	0.4%	-	0.5%	-	-	0.5%	0.3%	2.6%	3.1%	0.3%	0.9%	0.8%
Sodium	-	-	-	-	-	-	-	-	0.4%	0.5%	0.4%	0.5%	0.3%
Sulfur	-	-	-	-	-	-	-	-	-	-	-	-	-
Nitrogen	-	-	0.4%	-	-	-	-	-	-	-	0.3%	-	-
Potassium	-	-	-	-	-	-	-	-	-	-	-	-	-
Calcium	-	-	-	-	-	-	-	-	0.3%	0.2%	-	-	-
Magnesium	-	-	-	-	0.1%	-	-	-	0.5%	0.6%	-	-	-
Tin	0.1%	0.1%	0.1%	0.1%	0.1%	0.1%	0.1%	0.1%	0.1%	0.1%	0.1%	0.1%	0.1%
Chrome	-	-	-	-	-	-	0.3%	-	-	-	-	-	-
Phosphorus	-	-	-	-	-	-	-	-	-	-	-	-	-
Zinc	-	-	-	-	-	-	-	-	-	-	-	-	-
Iron	-	-	-	-	-	-	-	-	-	-	-	-	-
Chlorine	-	-	-	-	-	-	-	-	-	-	-	-	-

Figure A-4 (cont. 3 of 4). Tray E10-8 Surface Composition.

E10-8 Unspattered Surfaces only											
XPS Survey Scan Composition Table summary											
Cut Piece	D	D	D	E	E	E	E	E	E	E	
Location	15.5-5.8	12.3-1.5	18.6-1.5	8.2-16.8	1.7-17	5-14.3	8.1-10	1.4-20	4.8-5.8	1.8-1.7	
Atomic %:											
Silicon	30.8%	28.1%	29.5%	12.2%	8.4%	23.0%	27.5%	20.8%	23.2%	16.2%	23.4%
Oxygen	58.0%	58.0%	57.3%	41.2%	39.1%	55.7%	57.2%	53.6%	57.9%	53.4%	57.6%
Aluminum	1.6%	3.1%	1.9%	13.7%	15.6%	6.8%	4.3%	8.3%	6.9%	10.9%	6.7%
Carbon	9.1%	9.7%	10.9%	24.8%	25.4%	10.3%	9.1%	12.1%	8.8%	13.9%	9.5%
Fluorine	-	0.6%	-	6.6%	7.9%	3.0%	1.8%	4.3%	1.4%	1.9%	1.0%
Sodium	0.4%	0.4%	0.3%	-	-	0.5%	-	0.7%	0.7%	0.5%	0.8%
Sulfur	-	-	-	-	0.6%	-	-	-	0.3%	1.3%	0.6%
Nitrogen	-	-	-	-	0.6%	-	-	-	-	0.7%	-
Potassium	-	-	-	-	-	-	-	-	0.3%	0.4%	0.3%
Calcium	-	-	-	0.5%	0.5%	-	-	-	-	0.3%	-
Magnesium	-	-	-	0.9%	0.8%	0.6%	-	-	0.4%	0.5%	-
Tin	0.1%	0.1%	0.1%	0.1%	0.1%	-	0.1%	0.1%	0.1%	-	0.1%
Chrome	-	-	-	-	-	-	-	-	-	-	-
Phosphorus	-	-	-	-	0.8%	-	-	-	-	-	-
Zinc	-	-	-	-	-	-	-	-	-	-	-
Iron	-	-	-	-	-	-	-	-	-	-	-
Chlorine	-	-	-	-	0.2%	-	-	-	-	-	-

Figure A-4 (cont. 4 of 4). Tray E10-8 Surface Composition.

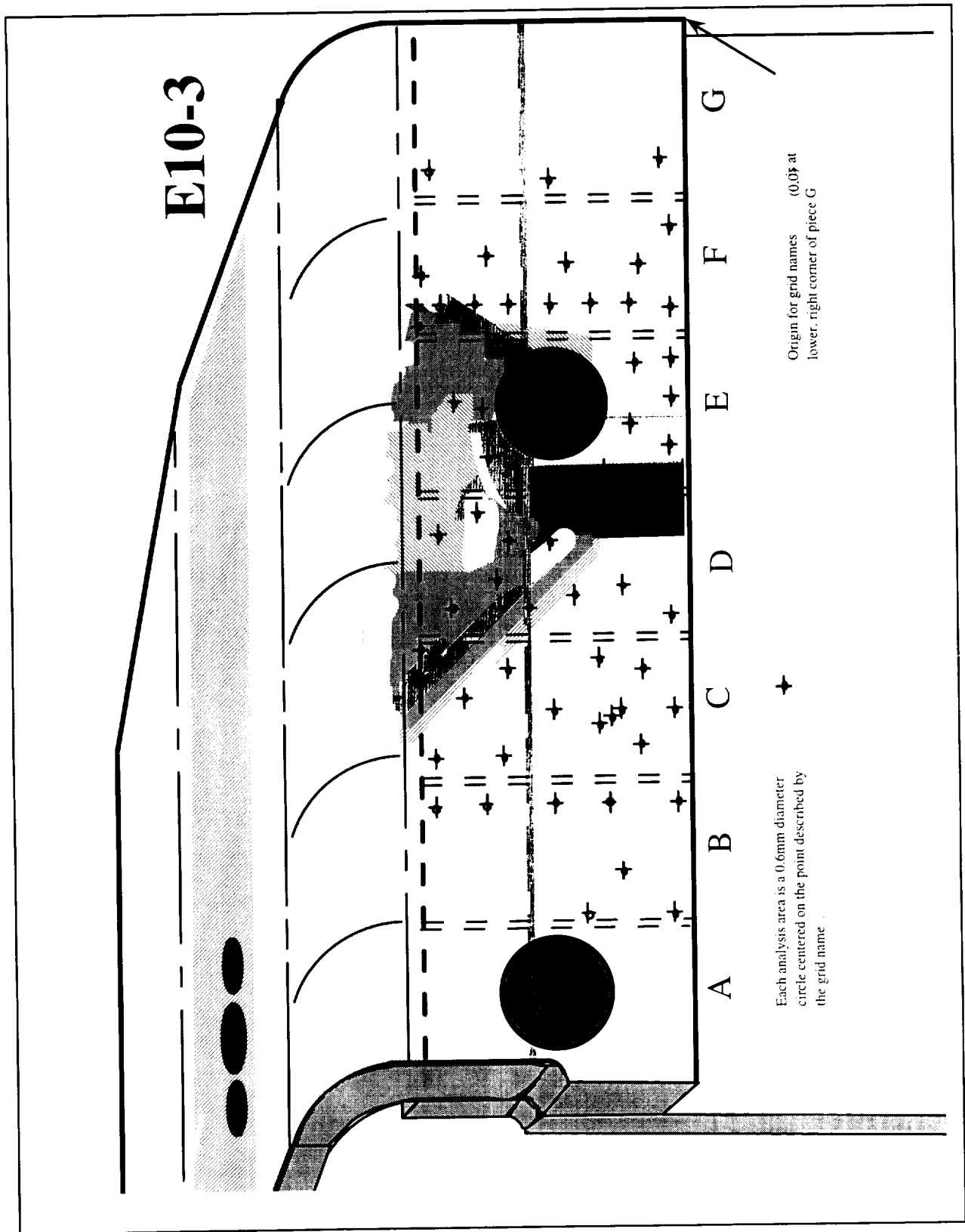


Figure A-5. Tray E10-3 ESCA analysis areas.

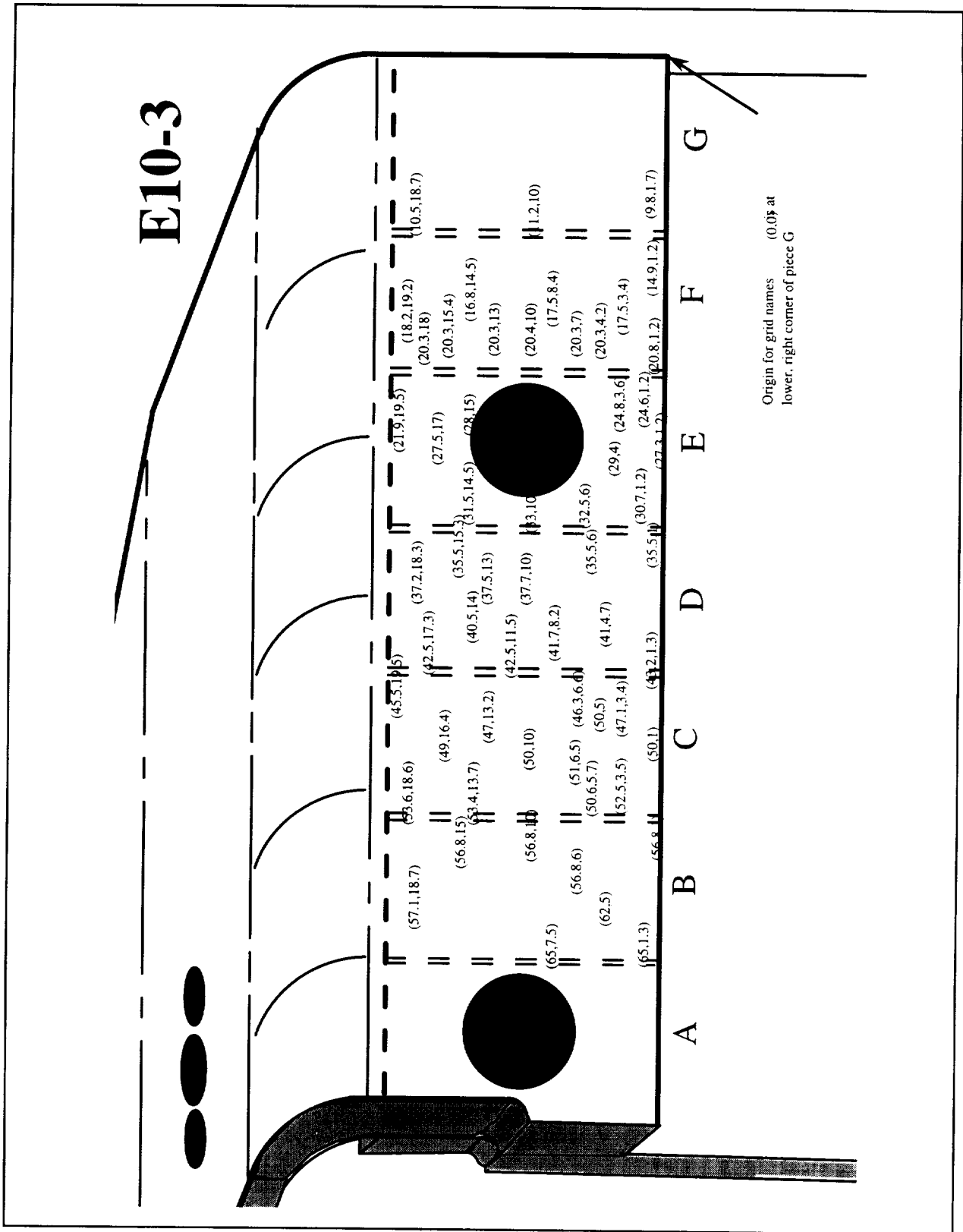


Figure A-6. Tray E10-3 ESCA analysis grid locations.

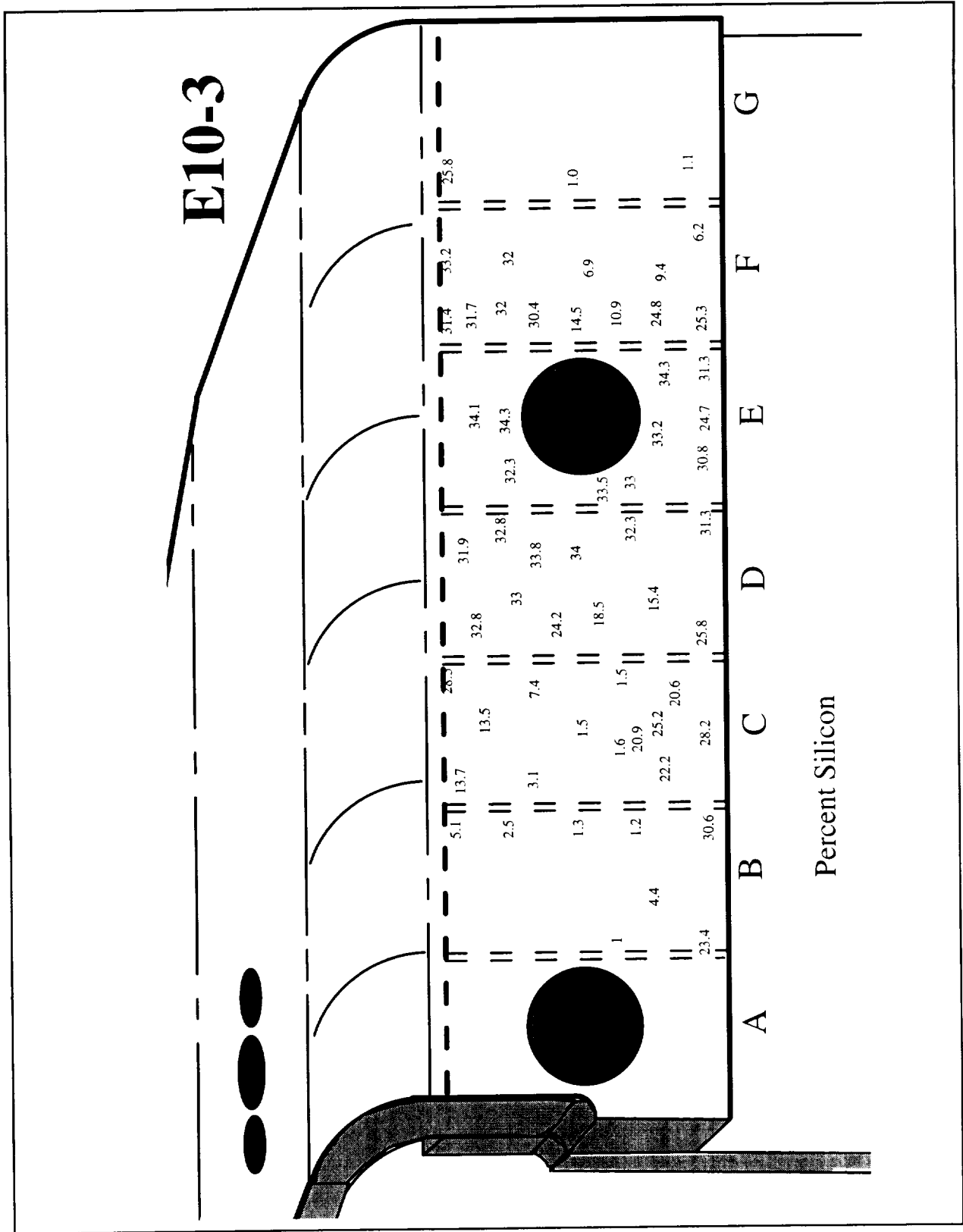


Figure A-7. Tray E10-3 Percent Silicon.

E10-3 Unspattered Surfaces only
XPS Survey Scan Composition Table summary

Location	24.8-3.6	29-4	32.5-6	33-10	31.5-14.5	28-15	27.5-17	24.6-1.2	30.7-1.2	27.3-1.2	35.5-6	41-4.7	37.7-10	41.7-8.2	37.5-13
Cut Piece	E	E	E	E	E	E	E	E	E	E	D	D	D	D	D
Atomic %:															
Silicon	34.3%	33.2%	33.0%	33.5%	32.3%	34.3%	34.1%	31.3%	30.8%	24.7%	32.3%	15.4%	34.0%	18.5%	33.8%
Oxygen	57.9%	56.2%	56.9%	56.5%	56.8%	57.8%	57.3%	56.7%	56.5%	55.9%	56.6%	45.7%	58.6%	50.2%	57.1%
Aluminum	-	-	-	-	0.9%	-	-	1.0%	-	5.8%	-	13.2%	-	10.6%	-
Carbon	6.6%	9.8%	9.5%	9.6%	8.2%	7.0%	7.5%	10.1%	12.1%	10.2%	10.3%	13.4%	6.3%	11.3%	8.5%
Fluorine	1.2%	0.5%	0.5%	0.3%	1.3%	0.8%	1.0%	0.8%	0.5%	1.3%	0.6%	10.0%	0.9%	7.5%	0.6%
Sodium	-	-	-	-	0.2%	-	-	-	-	0.6%	-	0.3%	-	0.3%	-
Sulfur	-	-	-	-	-	-	-	-	-	0.8%	-	0.8%	-	0.9%	-
Nitrogen	-	-	-	-	-	-	-	-	-	0.6%	-	-	-	-	-
Potassium	-	-	-	-	0.2%	-	-	-	-	-	-	-	-	-	-
Calcium	-	-	-	-	-	-	-	-	-	-	-	0.5%	-	0.4%	-
Magnesium	-	-	-	-	-	-	-	-	-	-	-	0.4%	-	0.2%	-
Tin	0.1%	0.1%	0.1%	0.1%	0.1%	0.1%	0.1%	0.1%	0.1%	0.1%	0.1%	-	0.1%	-	0.1%
Zinc	-	-	-	-	-	-	-	-	-	-	-	-	-	-	-
Chrome	-	0.3%	-	-	-	-	-	-	-	-	-	0.2%	0.1%	-	-

Figure A-8 (1 of 4). Tray E10-3 Surface Compositions.

E10-3 Unspattered Surfaces only
XPS Survey Scan Composition Table summary

Cut Piece	D	D	D	F	F	F	F	F	F	F	F	F	F		
Location	42.5-11.5	40.5-14	35.5-15.3	17.5-3.4	17.5-8.4	21.9-19.5	18.2-19.2	16.8-14.5	14.9-1.2	20.8-1.2	20.3-15.4	20.3-18	20.3-13	20.4-10	20.3-7
Atomic %:															
Silicon	24.2%	33.0%	32.8%	9.4%	6.9%	31.4%	33.2%	32.0%	6.2%	25.3%	31.9%	31.7%	30.4%	14.5%	10.9%
Oxygen	52.3%	56.9%	57.0%	41.5%	40.7%	53.3%	56.6%	55.7%	42.3%	54.5%	57.3%	56.0%	56.7%	48.0%	45.4%
Aluminum	6.6%	-	0.9%	15.2%	17.4%	-	-	1.0%	15.8%	5.5%	-	-	1.8%	11.1%	12.7%
Carbon	9.2%	6.9%	8.1%	17.2%	15.8%	13.5%	8.6%	8.7%	13.7%	9.3%	9.2%	10.5%	8.4%	16.4%	17.7%
Fluorine	6.4%	2.9%	1.1%	13.1%	15.4%	1.7%	1.6%	2.3%	16.8%	3.6%	1.4%	1.7%	2.5%	8.0%	10.0%
Sodium	0.4%	-	-	0.3%	0.3%	-	-	-	0.8%	1.0%	-	-	-	0.5%	0.4%
Sulfur	-	-	-	1.5%	1.2%	-	-	-	1.8%	0.5%	-	-	-	-	1.2%
Nitrogen	-	-	-	0.4%	0.6%	-	-	-	0.5%	-	-	-	-	0.6%	0.6%
Potassium	0.2%	0.2%	-	-	-	-	-	-	0.4%	0.2%	-	-	-	-	-
Calcium	0.3%	-	-	0.6%	1.0%	-	-	-	0.7%	0.1%	-	-	-	0.3%	0.6%
Magnesium	0.3%	-	-	0.4%	0.5%	-	-	0.2%	0.6%	-	-	-	-	0.6%	0.5%
Tin	0.1%	0.1%	0.1%	-	-	0.1%	0.1%	0.1%	-	0.1%	0.1%	0.1%	0.1%	-	-
Zinc	-	-	-	-	-	-	-	-	-	-	-	-	-	-	-
Chrome	-	-	-	0.2%	0.3%	-	-	-	0.5%	-	-	-	-	-	-

Figure A-8 (cont. 2 of 4). Tray E10-3 Surface Composition.

E10-3 Unspattered Surfaces only														
XPS Survey Scan Composition Table summary														
Cut Piece	F	C	C	C	C	C	C	C	C	C	C	C		
Location	20.3-4.2	45.5-19.5	49-16.4	50-10	50-5	46.3-6.6	51-6.5	50.6-5.7	50-1	52.5-3.5	47-13.2	53.4-13.7	53.6-18.6	47.1-3.4
Atomic %:														
Silicon	24.8%	28.5%	13.5%	1.5%	25.2%	1.5%	1.6%	20.9%	28.2%	22.2%	7.4%	3.1%	13.7%	20.6%
Oxygen	54.2%	53.6%	45.1%	37.8%	54.5%	38.5%	38.3%	51.3%	53.8%	52.7%	42.6%	38.7%	45.1%	52.9%
Aluminum	5.7%	2.6%	14.7%	21.2%	7.0%	22.0%	19.9%	10.1%	2.3%	8.8%	17.5%	19.4%	10.6%	9.1%
Carbon	10.9%	11.1%	14.3%	19.9%	7.7%	18.3%	20.8%	9.6%	13.6%	10.7%	17.9%	19.8%	13.7%	10.8%
Fluorine	3.8%	3.4%	9.5%	16.1%	4.9%	16.4%	15.4%	6.6%	2.1%	4.5%	11.4%	14.9%	12.1%	5.5%
Sodium	0.3%	-	0.1%	0.4%	0.4%	0.4%	0.3%	0.2%	-	0.3%	0.4%	0.8%	1.5%	0.4%
Sulfur	-	-	0.5%	1.2%	-	1.4%	1.5%	0.7%	-	0.7%	0.6%	1.1%	0.2%	0.4%
Nitrogen	-	-	0.5%	0.5%	-	-	0.3%	-	-	-	0.5%	0.6%	0.7%	-
Potassium	-	-	-	-	-	-	-	-	-	-	-	-	-	-
Calcium	-	0.3%	0.5%	0.5%	0.1%	0.5%	0.8%	0.2%	-	0.2%	0.5%	0.5%	0.6%	0.2%
Magnesium	-	0.4%	0.9%	0.7%	0.3%	0.8%	0.6%	0.4%	-	-	0.7%	0.8%	1.1%	-
Tin	-	0.1%	0.1%	-	-	-	-	-	-	-	-	-	0.1%	-
Zinc	-	-	-	-	-	-	-	-	-	-	-	-	-	-
Chrome	0.3%	-	0.3%	0.2%	-	0.3%	0.4%	-	-	-	0.5%	0.3%	0.4%	-

Figure A-8 (cont. 3 of 4). Tray E10-3 Surface Composition.

**E10-3 Unspattered Surfaces only
XPS Survey Scan Composition Table summary**

Location	35.5-1	43.2-1.3	42.5-17.3	37.2-18.3	56.8-1	56.8-6	56.8-10	56.8-15	57.1-18.7	62-5	65-1.3	65-7.5		
Cut Piece	G	G	G	D	D	D	D	B	B	B	B	B		
9.8-1.7	11.2-10	10.5-18.7	35.5-1	43.2-1.3	42.5-17.3	37.2-18.3	56.8-1	56.8-6	56.8-10	56.8-15	57.1-18.7	62-5	65-1.3	65-7.5
Atomic %:														
Silicon	1.1%	1.0%	25.8%	32.8%	31.9%	30.5%	1.2%	1.3%	2.5%	5.1%	4.3%	23.4%	1.0%	
Oxygen	36.7%	35.1%	57.0%	56.5%	54.7%	36.7%	38.0%	38.3%	38.0%	38.1%	41.3%	55.3%	38.4%	
Aluminum	22.4%	22.9%	5.2%	0.9%	0.8%	5.2%	23.3%	25.7%	23.3%	19.7%	20.8%	7.3%	23.0%	
Carbon	17.7%	22.3%	9.4%	8.4%	11.4%	9.4%	18.5%	19.7%	19.1%	20.6%	17.1%	9.7%	20.0%	
Fluorine	18.5%	15.1%	1.8%	1.7%	1.6%	1.8%	15.7%	13.4%	14.5%	13.1%	12.8%	3.7%	14.7%	
Sodium	0.4%	0.5%	-	-	-	-	-	-	-	0.4%	0.3%	-	-	
Sulfur	1.2%	0.9%	0.7%	-	-	0.7%	1.5%	0.7%	1.0%	0.9%	1.7%	0.5%	1.6%	
Nitrogen	0.6%	0.3%	-	-	-	-	0.5%	-	0.7%	0.7%	0.5%	-	0.5%	
Potassium	-	-	-	-	-	-	-	-	-	0.1%	-	-	-	
Calcium	0.5%	0.5%	-	-	-	-	0.4%	0.4%	0.4%	0.3%	0.3%	-	-	
Magnesium	0.5%	0.9%	-	-	-	-	0.4%	0.2%	0.5%	0.7%	0.4%	-	0.4%	
Tin	-	0.1%	0.1%	0.1%	0.1%	0.1%	-	-	-	0.1%	0.1%	-	-	
Zinc	-	-	-	-	-	-	-	-	-	0.2%	-	-	-	
Chrome	0.4%	0.4%	-	-	-	-	0.4%	0.3%	0.2%	-	0.2%	0.4%	0.4%	

Figure A-8 (cont. 4 of 4). Tray E10-3 Surface Composition.

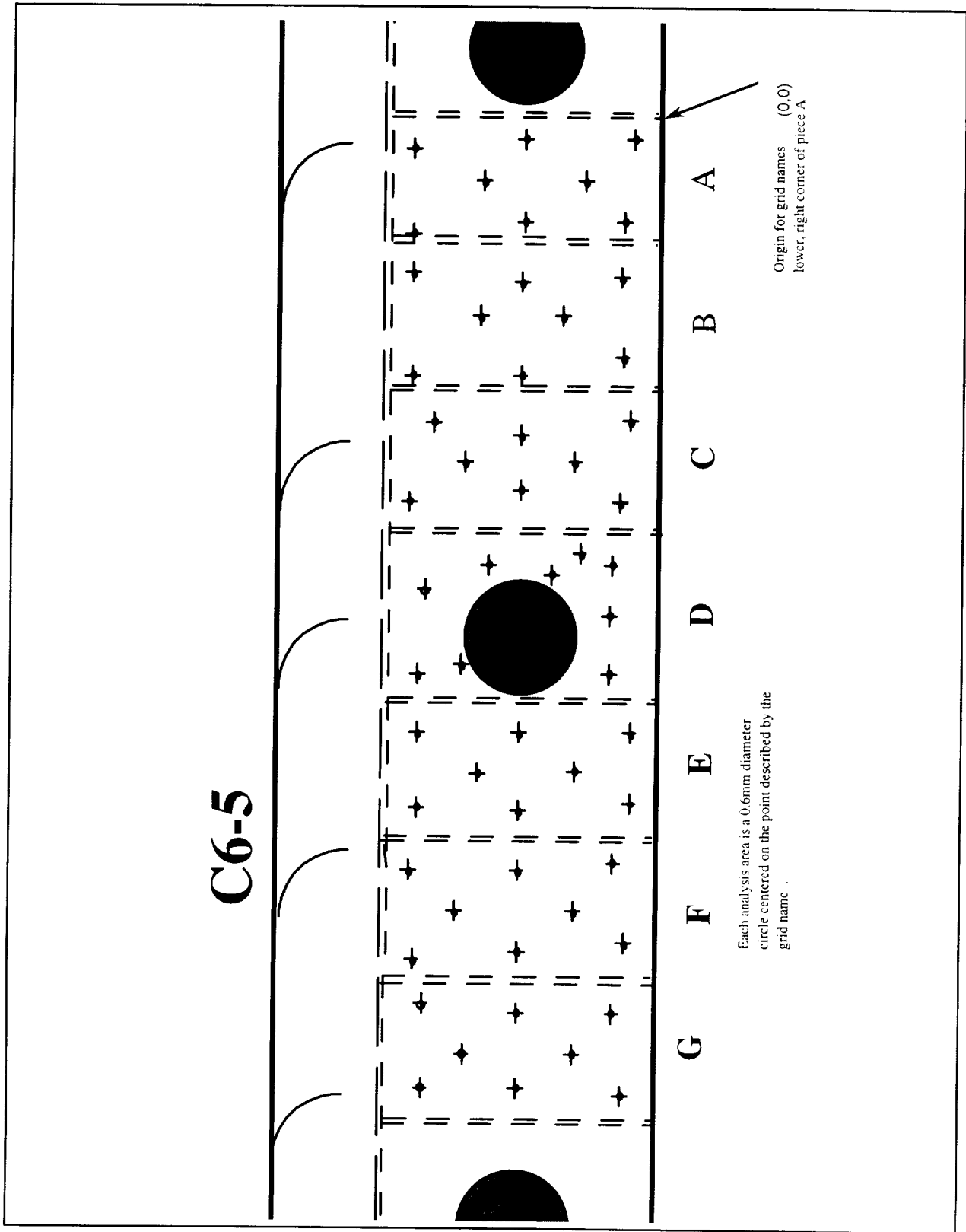


Figure A-9. Tray C6-5 ESCA analysis areas.

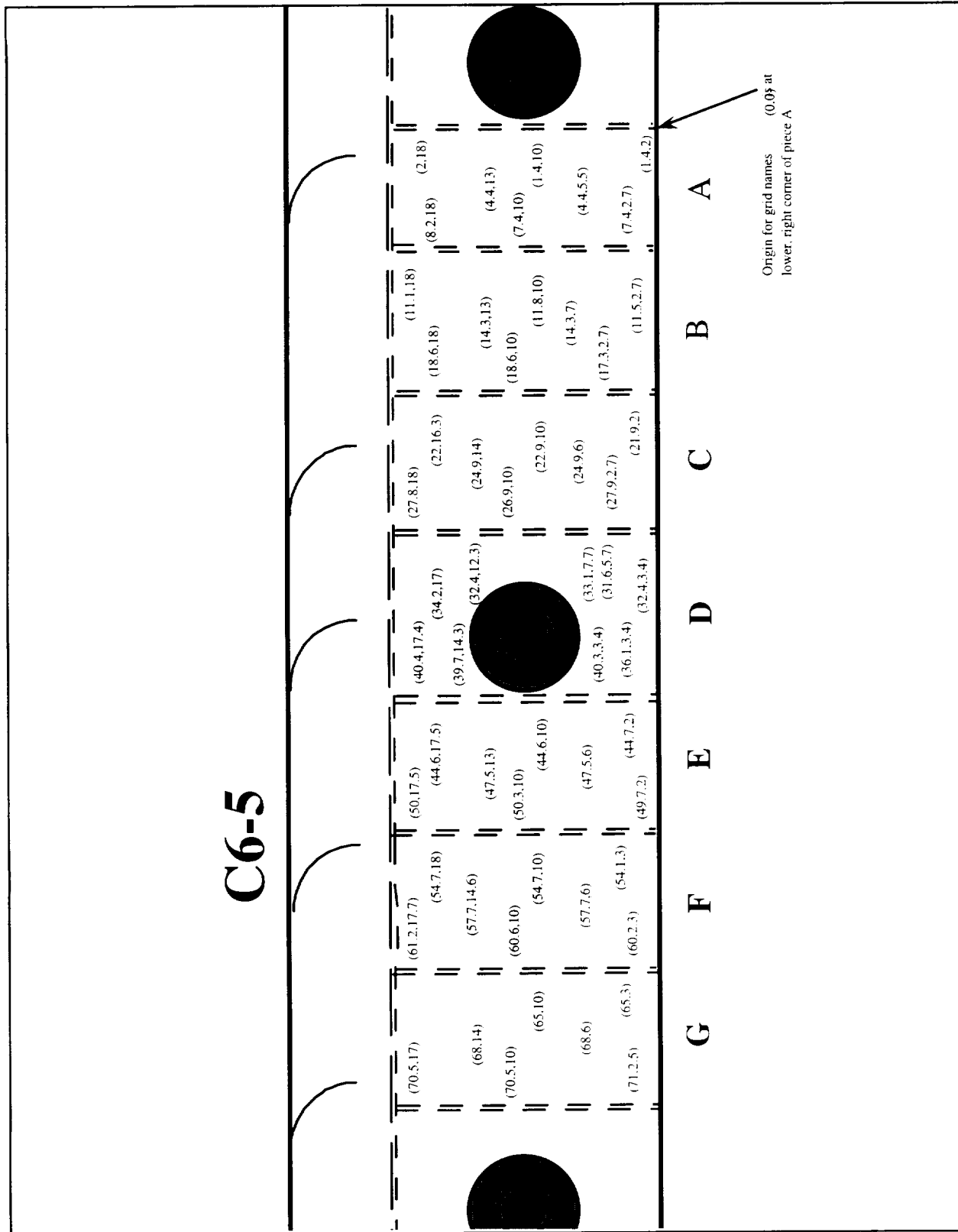


Figure A-10. Tray C6-5 ESCA analysis area grid locations.

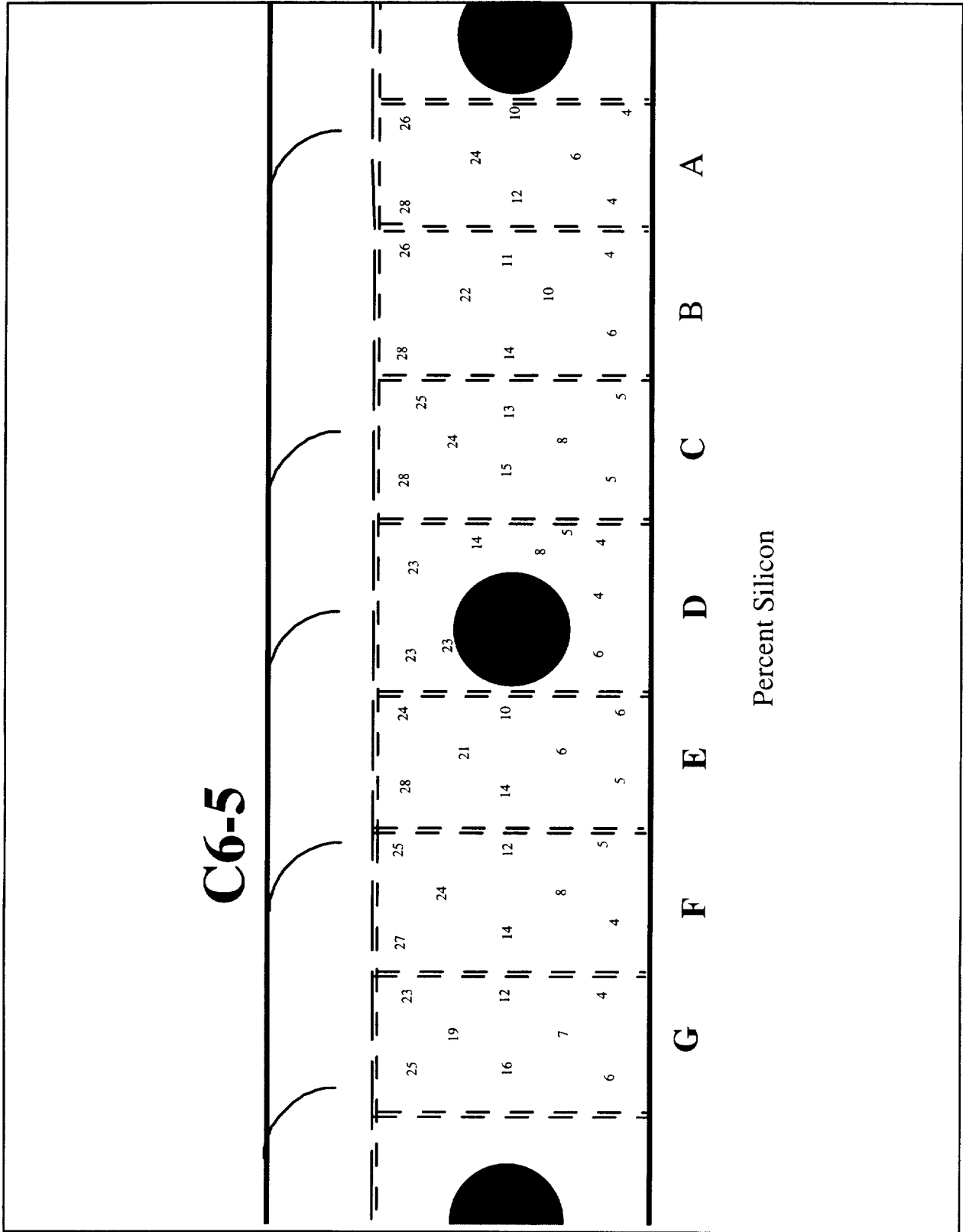


Figure A-11. Tray C6-5 Percent Silicon.

C6-5 Unspattered Surfaces only														
XPS Survey Scan Composition Table summary														
Location	A	A	A	A	A	A	A	A	B	B	B	B		
Atomic %:	8.2-18	2.0-18	4.4-13	7.4-10	1.4-10	4.4-5.5	1.4-2	7.4-2.7	18.1-18	11.1-18	14.3-13	18.6-10	11.8-10	14.3-7
Silicon	27.8%	26.2%	24.1%	12.3%	9.6%	6.4%	3.9%	4.2%	27.5%	26.1%	22.2%	13.8%	11.0%	10.0%
Oxygen	52.4%	54.7%	51.2%	46.6%	46.9%	44.1%	42.1%	42.8%	53.4%	52.9%	52.3%	49.5%	46.3%	46.2%
Aluminum	1.1%	2.3%	2.5%	7.1%	9.7%	10.6%	11.2%	11.2%	1.9%	2.2%	3.0%	6.4%	8.0%	8.3%
Carbon	16.1%	14.5%	18.2%	24.9%	23.4%	27.8%	31.6%	29.5%	15.2%	17.2%	18.2%	20.0%	25.9%	26.1%
Fluorine	1.4%	1.3%	1.7%	4.9%	5.4%	5.8%	6.5%	7.0%	1.4%	1.2%	1.9%	5.5%	4.1%	4.9%
Sodium	-	0.2%	0.4%	1.1%	1.3%	1.0%	1.0%	1.3%	0.3%	0.3%	0.8%	1.6%	0.7%	0.7%
Sulfur	-	-	0.6%	1.0%	1.4%	1.3%	1.4%	1.4%	-	-	-	1.1%	1.3%	1.1%
Nitrogen	0.7%	-	0.8%	0.9%	0.5%	0.8%	1.2%	0.9%	-	-	-	0.7%	1.0%	1.3%
Potassium	-	0.2%	0.5%	0.3%	0.6%	0.7%	-	0.5%	0.2%	-	0.8%	1.1%	0.6%	-
Calcium	-	0.2%	-	0.5%	0.5%	0.6%	0.4%	0.6%	-	-	0.2%	0.3%	0.5%	0.6%
Magnesium	-	0.4%	-	0.3%	0.5%	0.9%	0.6%	0.6%	-	-	0.4%	-	0.5%	0.2%
Tin	0.1%	0.1%	0.1%	0.1%	-	-	-	-	0.1%	0.1%	0.1%	-	-	-
Chrome	0.4%	-	-	-	-	-	-	-	-	-	-	-	-	-
Iron	-	-	-	-	-	-	-	-	-	-	-	-	-	-
Phosphorus	-	-	-	-	-	-	-	-	-	-	-	-	-	0.6%

Figure A-12 (1 of 4). Tray C6-5 Surface Composition.

C6-5 Unspattered Surfaces only													
XPS Survey Scan Composition Table summary													
Cut Piece	B	B	C	C	C	C	C	C	C	C	D	D	
Location	11.5-2.7	17.3-2.7	27.8-18	22-16.3	24.9-14	26.9-10	22.9-10	24.9-6	21.9-2	27.9-2.7	40.4-17.4	34.2-17	39.7-14.3
Atomic %:													
Silicon	4.1%	5.7%	28.2%	24.8%	24.2%	14.9%	12.5%	8.2%	4.9%	5.4%	22.7%	22.8%	22.8%
Oxygen	42.6%	42.9%	54.2%	54.9%	52.8%	48.2%	50.7%	46.4%	41.8%	42.9%	50.2%	53.1%	50.0%
Aluminum	9.3%	7.8%	1.2%	2.2%	2.6%	5.5%	7.6%	9.2%	8.0%	7.7%	2.3%	2.2%	2.1%
Carbon	31.4%	32.2%	15.0%	15.1%	18.1%	24.2%	19.4%	24.9%	31.9%	30.9%	20.7%	14.9%	20.6%
Fluorine	6.7%	6.7%	1.0%	1.1%	1.1%	3.3%	5.0%	6.3%	7.5%	7.4%	3.3%	5.0%	3.2%
Sodium	1.0%	1.1%	0.3%	0.5%	0.3%	0.6%	1.4%	1.3%	1.0%	1.2%	0.4%	0.5%	0.6%
Sulfur	1.4%	1.2%	-	0.7%	-	1.0%	1.5%	1.4%	1.5%	1.4%	-	0.9%	-
Nitrogen	1.2%	1.0%	-	0.6%	0.8%	0.8%	0.8%	0.8%	1.3%	1.2%	0.4%	-	0.6%
Potassium	0.4%	-	-	-	-	0.6%	0.2%	0.7%	0.8%	0.7%	-	0.5%	-
Calcium	0.5%	0.7%	-	-	-	0.4%	0.5%	0.6%	0.9%	0.6%	-	-	-
Magnesium	0.9%	0.6%	-	-	-	0.3%	0.3%	0.3%	0.4%	0.5%	-	-	-
Tin	-	-	0.1%	0.1%	0.1%	-	-	-	-	-	-	0.1%	-
Chrome	-	-	-	-	-	-	-	-	-	-	-	-	-
Iron	0.4%	-	-	-	-	-	-	-	-	-	-	-	-
Phosphorus	-	-	-	-	-	-	-	-	-	-	-	-	-

Figure A-12 (cont. 2 of 4). Tray C6-5 Surface Composition.

**C6-5 Unspattered Surfaces only
XPS Survey Scan Composition Table summary**

Cut Piece Location	D	D	D	D	D	D	E	E	E	E	E	E	
	32.4-12.3	33.1-7.7	31.6-5.7	32.4-3.4	36.1-3.4	40.3-3.4	50-17.5	44.6-17.5	47.5-13	50.3-10	44.6-10	47.5-6	44.7-2
Atomic %:													
Silicon	13.8%	8.3%	5.3%	4.4%	4.1%	5.5%	27.8%	23.5%	21.1%	14.2%	9.7%	5.9%	4.6%
Oxygen	46.3%	44.2%	42.8%	41.5%	42.3%	42.7%	54.1%	53.5%	52.1%	47.9%	49.4%	40.7%	37.2%
Aluminum	5.4%	7.6%	8.8%	8.2%	10.2%	9.1%	1.4%	2.8%	3.6%	6.6%	8.8%	6.5%	4.8%
Carbon	27.8%	30.4%	31.1%	34.8%	33.6%	32.5%	15.7%	16.6%	20.6%	23.5%	21.2%	34.6%	39.8%
Fluorine	3.6%	5.4%	5.9%	5.9%	5.9%	5.7%	0.8%	1.7%	1.4%	3.3%	5.9%	6.1%	7.1%
Sodium	0.8%	1.0%	1.1%	0.8%	0.9%	0.8%	-	0.5%	0.7%	0.9%	1.3%	1.0%	1.1%
Sulfur	0.9%	1.3%	1.6%	1.3%	1.0%	0.9%	-	-	-	1.1%	1.6%	1.3%	1.4%
Nitrogen	1.2%	1.0%	1.5%	1.5%	1.4%	1.4%	-	1.0%	-	0.9%	0.9%	1.2%	1.7%
Potassium	-	-	0.8%	-	-	-	-	-	-	0.8%	0.3%	0.7%	0.5%
Calcium	-	0.3%	0.5%	0.9%	0.4%	0.5%	-	-	-	0.5%	0.7%	1.6%	1.3%
Magnesium	0.2%	0.4%	0.5%	0.6%	0.2%	0.7%	-	0.3%	0.5%	0.3%	0.2%	0.3%	0.3%
Tin	-	-	-	-	-	-	0.1%	0.1%	-	-	-	-	-
Chrome	-	-	-	-	-	-	-	-	-	-	-	-	-
Iron	-	-	-	-	-	-	-	-	-	-	-	-	-
Phosphorus	-	-	-	-	-	-	-	-	-	-	-	-	-

Figure A-12 (cont. 3 of 4). Tray C6-5 Surface Composition.

C6-5 Unsputtered Surfaces only
XPS Survey Scan Composition Table summary

Cut Piece	F	F	F	F	F	F	F	F	F	G	G	G	G	G	G		
Location	61.2-17.7	54.7-1857.7-14.660.6-10	54.7-10	57.7-6	54.1-3	60-2.3				65-3	71-2.5	68-6	65-10	70.5-10	68-14	70.5-17	64.4-17
Atomic %:																	
Silicon	27.3%	24.9%	24.4%	13.8%	12.3%	7.6%	5.3%	4.3%		4.4%	5.5%	6.6%	11.9%	15.5%	19.0%	24.6%	22.7%
Oxygen	54.9%	54.6%	53.9%	46.8%	50.2%	47.0%	40.6%	41.6%		36.9%	39.0%	41.1%	46.8%	49.6%	50.8%	52.9%	52.4%
Aluminum	1.5%	3.0%	2.5%	6.2%	8.0%	10.1%	7.5%	9.3%		4.7%	4.5%	6.0%	6.4%	3.7%	3.0%	1.5%	3.6%
Carbon	14.2%	15.5%	17.4%	25.7%	22.1%	23.4%	31.6%	33.5%		40.1%	36.4%	33.6%	25.6%	21.7%	18.8%	18.1%	17.8%
Fluorine	1.5%	1.3%	1.0%	3.3%	3.7%	6.9%	8.6%	6.5%		7.4%	7.5%	6.1%	4.5%	4.6%	2.8%	1.7%	1.8%
Sodium	0.4%	0.3%	0.3%	0.7%	0.9%	1.5%	1.4%	0.9%		0.9%	1.3%	0.9%	0.9%	1.0%	1.1%	0.1%	0.3%
Sulfur	-	-	-	0.9%	1.1%	1.0%	0.9%	1.2%		1.4%	1.1%	1.3%	1.0%	1.2%	1.7%	-	-
Nitrogen	-	-	-	1.2%	0.7%	0.9%	1.4%	1.1%		1.4%	1.6%	1.3%	0.9%	0.7%	0.9%	0.7%	0.5%
Potassium	-	0.1%	0.2%	0.6%	0.2%	0.3%	1.0%	0.5%		0.7%	0.8%	0.4%	0.9%	0.2%	0.2%	-	0.3%
Calcium	-	-	-	0.4%	0.6%	0.7%	0.7%	0.8%		1.6%	1.4%	1.3%	0.6%	1.3%	1.0%	-	0.3%
Magnesium	0.1%	0.1%	0.1%	0.2%	0.3%	0.6%	0.9%	0.3%		0.4%	0.7%	0.6%	0.4%	0.5%	0.6%	0.2%	0.3%
Tin	0.1%	0.1%	0.1%	-	-	-	-	-		-	-	-	-	-	-	0.1%	0.1%
Chrome	-	-	-	-	-	-	-	-		-	-	-	-	-	-	-	-
Iron	-	-	-	-	-	-	-	-		-	-	-	-	-	-	-	-
Phosphorus	-	-	-	-	-	-	-	-		-	-	0.8%	-	-	-	-	-

Figure A-12 (cont. 4 of 4). Tray C6-5 Surface Composition.

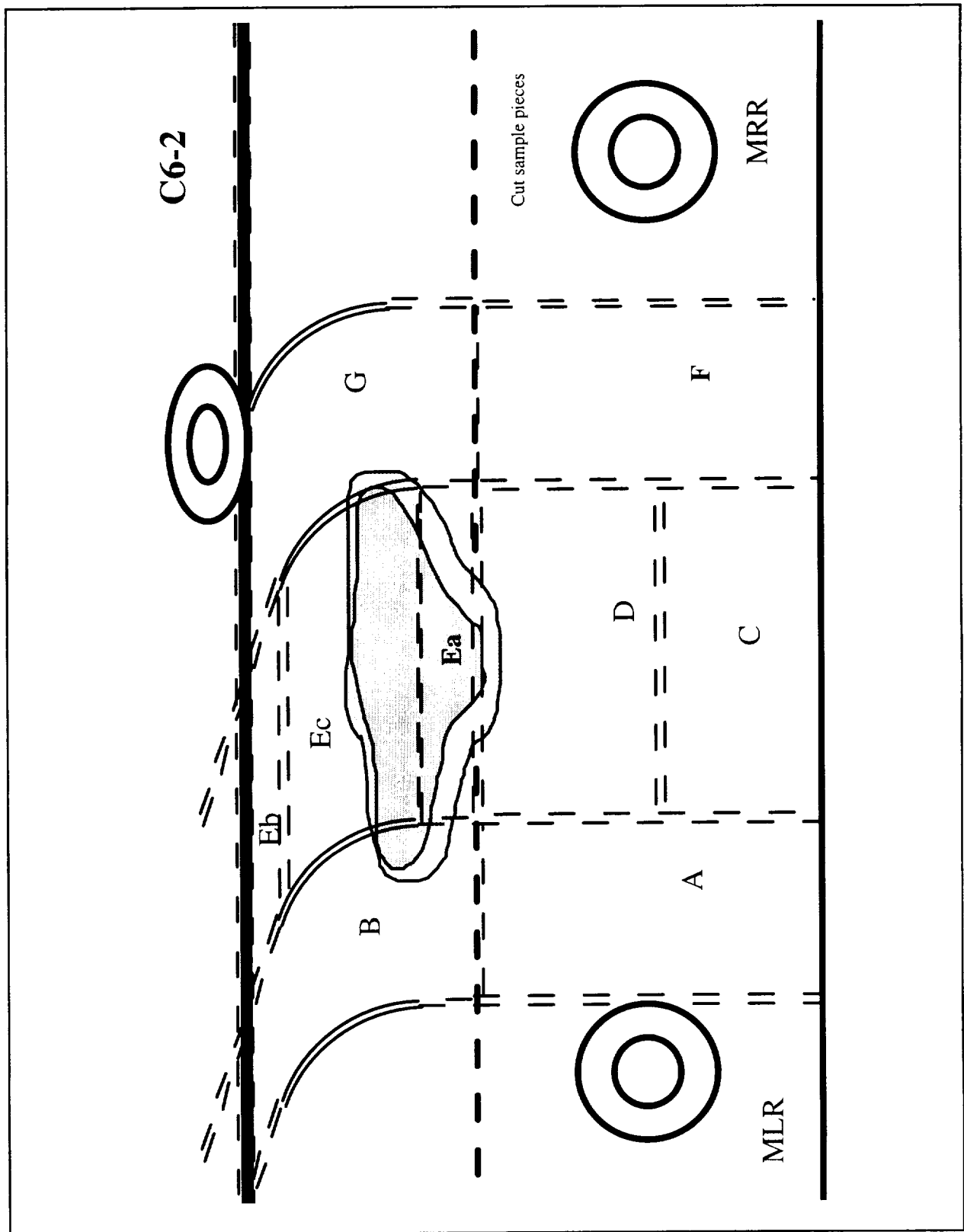


Figure A-13. Tray C6-2 ESCA analysis cut sample pieces.

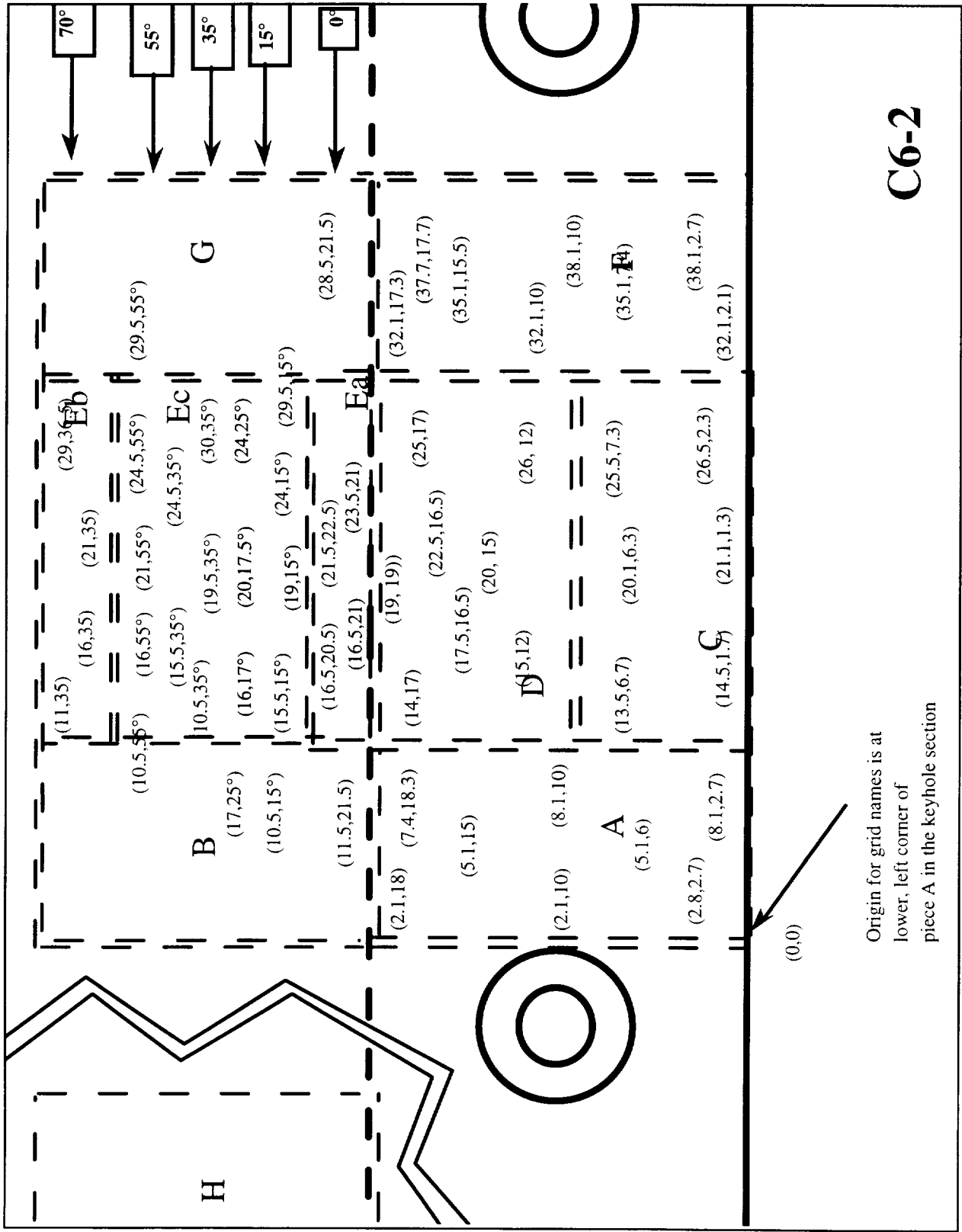


Figure A-14. Tray C6-2 ESCA analysis area grid locations.

C6-2 Unspattered Surfaces only														
XPS Survey Scan Composition Table summary														
Cut Piece	D	D	D	D	D	D	D	D	D	C	C	C		
Grid Location	19-19	22.5-16.5	20-15	17.5-16.5	25-17	26-12	15-12	14-17	21.1-1.3	20.1-6.3	14.5-1.7	13.5-6.7	25.5-7.3	26.5-2.3
Atomic %:														
Silicon	24.2%	21.7%	19.6%	19.0%	23.6%	16.7%	16.7%	22.3%	6.2%	9.4%	5.8%	8.0%	8.5%	5.5%
Oxygen	47.4%	47.0%	45.3%	45.9%	48.8%	47.6%	44.7%	48.9%	39.6%	44.4%	36.6%	44.9%	44.4%	39.4%
Aluminum	-	1.4%	1.8%	1.9%	1.7%	4.8%	4.2%	2.5%	6.6%	7.1%	6.2%	9.0%	9.3%	8.9%
Carbon	23.0%	23.4%	27.1%	24.2%	22.3%	22.1%	26.3%	21.0%	30.0%	24.6%	35.0%	26.6%	25.4%	32.6%
Fluorine	3.6%	4.6%	4.0%	5.3%	2.2%	4.1%	3.8%	3.2%	9.3%	7.7%	8.8%	6.7%	6.4%	7.2%
Sodium	0.5%	0.6%	0.6%	0.8%	0.5%	0.9%	0.6%	0.5%	1.4%	1.1%	1.2%	0.9%	1.3%	1.3%
Sulfur	-	0.4%	-	0.6%	-	2.1%	1.7%	0.5%	1.8%	1.7%	1.6%	1.7%	1.7%	1.9%
Nitrogen	0.7%	-	0.7%	1.2%	-	-	0.7%	-	1.3%	0.8%	1.0%	0.7%	0.8%	1.0%
Potassium	0.1%	0.1%	-	0.3%	-	0.4%	0.2%	0.3%	1.3%	1.1%	0.5%	0.4%	0.5%	0.9%
Calcium	0.2%	0.5%	0.5%	0.5%	0.5%	1.0%	0.7%	0.5%	1.6%	1.4%	1.7%	1.1%	1.0%	1.0%
Magnesium	0.1%	0.2%	0.3%	0.3%	0.3%	0.3%	0.4%	0.1%	0.8%	0.5%	1.0%	-	0.7%	0.4%
Tin	0.1%	0.1%	0.1%	-	0.1%	0.1%	0.1%	0.1%	-	-	-	-	-	-
Phosphorus	-	-	-	-	-	-	-	-	-	-	-	-	-	-
Chlorine	-	-	-	-	-	-	-	-	-	-	0.4%	-	-	-

Figure A-16 (1 of 5). Tray C6-2 Surface Composition.

C6-2 Unspattered Surfaces only
XPS Survey Scan Composition Table summary

Grid Location	Ec	Ec	Ec	Ec	Ec	Ec	Ec	Ec	Ec	Ec	Ec	A	A	
Atomic %:	19-15°	20-17.5°	29.5-15°	10.5-15°	15.5-15°	16-17°	16-55°	21-55°	29.5-55°	24.5-55°	10.5-55°	17-25°	2.1-18	7.4-18.3
Silicon	31.0%	30.9%	30.7%	30.6%	31.4%	30.7%	30.9%	26.2%	25.5%	23.4%	25.7%	24.5%	30.7%	30.4%
Oxygen	53.2%	51.7%	51.0%	52.2%	51.3%	52.1%	51.9%	26.4%	37.7%	33.5%	34.7%	37.1%	52.7%	52.1%
Aluminum	-	-	-	-	-	-	0.6%	2.2%	2.6%	2.1%	2.8%	-	1.4%	1.4%
Carbon	13.5%	15.2%	15.8%	15.1%	15.4%	15.2%	15.7%	45.9%	31.3%	36.6%	34.6%	32.1%	14.3%	15.3%
Fluorine	1.7%	1.5%	1.9%	1.5%	1.5%	1.4%	1.0%	0.9%	2.4%	2.1%	1.7%	1.9%	1.6%	1.3%
Sodium	0.4%	0.5%	0.5%	0.4%	0.3%	0.4%	0.4%	-	0.3%	0.2%	-	0.5%	0.6%	0.2%
Sulfur	-	-	-	-	-	-	-	-	-	-	-	-	-	-
Nitrogen	-	-	-	-	-	-	-	-	-	-	-	-	-	-
Potassium	-	-	-	-	-	-	-	-	0.5%	-	0.4%	-	0.1%	-
Calcium	-	-	-	-	-	-	-	0.4%	0.5%	0.3%	0.4%	-	-	-
Magnesium	-	-	-	-	-	-	-	0.2%	-	0.6%	0.6%	-	-	-
Tin	0.1%	0.1%	0.1%	0.1%	0.1%	0.1%	0.1%	0.2%	0.2%	0.1%	0.1%	0.1%	0.1%	0.1%
Phosphorus	-	-	-	-	-	-	-	-	-	-	-	-	-	-
Chlorine	-	-	-	-	-	-	-	-	0.4%	-	-	-	-	-

Figure A-16 (cont. 3 of 5). Tray C6-2 Surface Composition.

C6-2 Unspattered Surfaces only
XPS Survey Scan Composition Table summary

Grid Location	5.1-15	2.1-10	8.1-10	A	A	5.1-6	8.1-2.7	A	A	32.1-17.3	37.7-17.7	35.1-15.5	32.1-10	38.1-10	35.1-7.4	38.1-2.7	32.1-2.1
Cut Piece	A	F	F	F	F	F	F	F	F								
Atomic %:																	
Silicon	21.8%	12.3%	11.0%	8.8%	4.9%	5.6%	24.2%	23.0%	22.0%	10.4%	10.2%	8.2%	3.9%	4.5%			
Oxygen	51.0%	47.8%	48.4%	47.6%	41.1%	42.1%	50.1%	51.0%	51.0%	45.0%	49.1%	46.2%	42.3%	40.8%			
Aluminum	3.5%	7.1%	8.8%	9.2%	8.3%	7.1%	1.7%	2.8%	3.1%	7.7%	9.1%	8.8%	7.7%	8.5%			
Carbon	20.8%	22.8%	22.9%	22.7%	31.5%	27.5%	20.9%	18.9%	19.8%	26.4%	20.2%	24.2%	27.2%	33.1%			
Fluorine	1.7%	3.9%	3.9%	6.3%	7.8%	8.9%	1.8%	1.7%	1.8%	4.7%	5.6%	5.6%	9.3%	6.8%			
Sodium	0.4%	0.8%	0.9%	1.1%	1.1%	1.8%	0.3%	0.4%	0.4%	1.1%	1.0%	0.9%	1.2%	1.1%			
Sulfur	-	1.3%	1.3%	1.5%	1.5%	2.3%	-	-	0.7%	1.3%	1.5%	1.4%	2.0%	1.5%			
Nitrogen	-	0.7%	1.1%	0.9%	1.1%	1.1%	-	0.5%	-	0.9%	0.9%	1.1%	1.6%	1.0%			
Potassium	0.1%	0.6%	0.5%	0.4%	0.5%	0.8%	0.2%	0.4%	0.3%	0.6%	0.7%	0.5%	1.3%	0.7%			
Calcium	0.4%	1.3%	0.8%	1.0%	1.5%	2.0%	0.3%	0.4%	0.5%	0.9%	1.1%	1.3%	1.7%	1.4%			
Magnesium	0.2%	0.6%	0.3%	0.5%	0.7%	0.8%	0.4%	0.7%	0.3%	0.4%	0.5%	0.6%	1.1%	0.4%			
Tin	0.1%	0.1%	0.1%	-	-	-	0.1%	0.1%	0.1%	0.1%	0.1%	-	-	-			
Phosphorus	-	0.7%	-	-	-	-	-	-	-	0.5%	-	1.0%	0.7%	-			
Chlorine	-	-	-	-	-	-	-	-	-	-	-	-	-	-			

Figure A-16 (cont. 4 of 5). Tray C6-2 Surface Composition.

**C6-2 Unsputtered Surfaces only
XPS Survey Scan Composition Table summary**

Grid Location	B 2-15°	B 2-35°	B 2-55°	B 2-70°	G 32-22	G 38-22	G 38-15°	G 38-35°	G 38-55°	G 38-70°	H (-45)-22	H (-45)-15°	H (-45)-35°	H (-45)-55°	H (-45)-70°	
Cut Piece	B	B	B	B	G	G	G	G	G	G	H	H	H	H	H	
Atomic %:																
Silicon	30.0%	29.9%	22.7%	21.0%	25.3%	27.7%	29.3%	30.4%	25.2%	23.0%	25.3%	28.2%	12.0%	9.7%	10.1%	24.3%
Oxygen	54.1%	53.7%	42.5%	41.1%	25.3%	51.3%	53.9%	54.2%	46.6%	42.5%	24.6%	52.0%	44.1%	39.8%	38.3%	25.0%
Aluminum	-	0.7%	3.7%	3.5%	1.0%	-	-	-	2.8%	3.5%	1.1%	0.7%	8.1%	8.6%	8.1%	1.4%
Carbon	14.2%	13.6%	26.1%	29.0%	48.4%	18.0%	14.9%	12.8%	21.1%	25.9%	48.9%	16.7%	21.7%	26.9%	29.6%	48.7%
Fluorine	1.5%	1.7%	3.0%	3.4%	-	2.6%	1.4%	1.7%	3.0%	3.8%	-	2.3%	7.0%	8.2%	7.2%	0.5%
Sodium	-	0.3%	0.4%	0.4%	-	0.3%	0.2%	0.5%	0.4%	0.5%	-	-	0.8%	0.8%	0.7%	-
Sulfur	-	-	-	-	-	-	-	-	-	-	-	-	1.2%	1.2%	0.9%	-
Nitrogen	-	-	-	-	-	-	-	-	-	-	-	-	0.8%	0.8%	0.7%	-
Potassium	-	-	0.2%	0.3%	-	-	-	0.2%	0.3%	0.2%	-	-	0.6%	0.5%	0.4%	-
Calcium	-	-	0.6%	0.5%	-	-	-	-	0.3%	0.3%	-	-	1.4%	1.4%	1.2%	-
Magnesium	-	-	0.6%	0.6%	-	-	-	-	-	-	-	-	1.0%	1.6%	1.3%	-
Tin	0.1%	0.1%	0.2%	0.2%	-	0.1%	0.1%	0.1%	0.1%	0.2%	-	0.1%	0.2%	0.5%	0.5%	-
Phosphorus	-	-	-	-	-	-	-	-	-	-	-	-	0.7%	-	0.8%	-
Chlorine	-	-	-	-	-	-	-	-	-	-	-	-	0.4%	-	0.4%	-

Figure A-16 (cont. 5 of 5). Tray C6-2 Surface Composition.

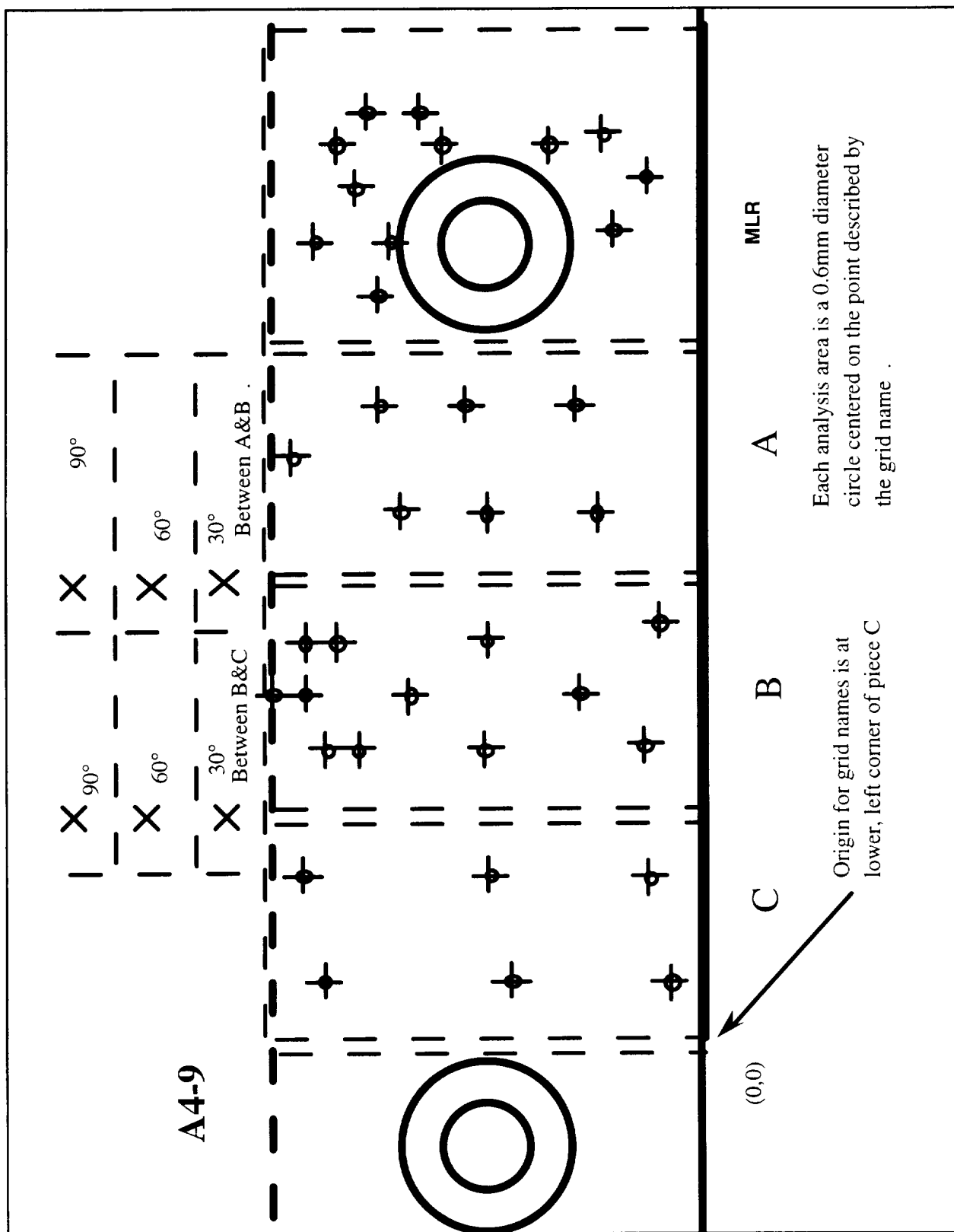


Figure A-17. Tray A4-9 ESCA analysis areas.

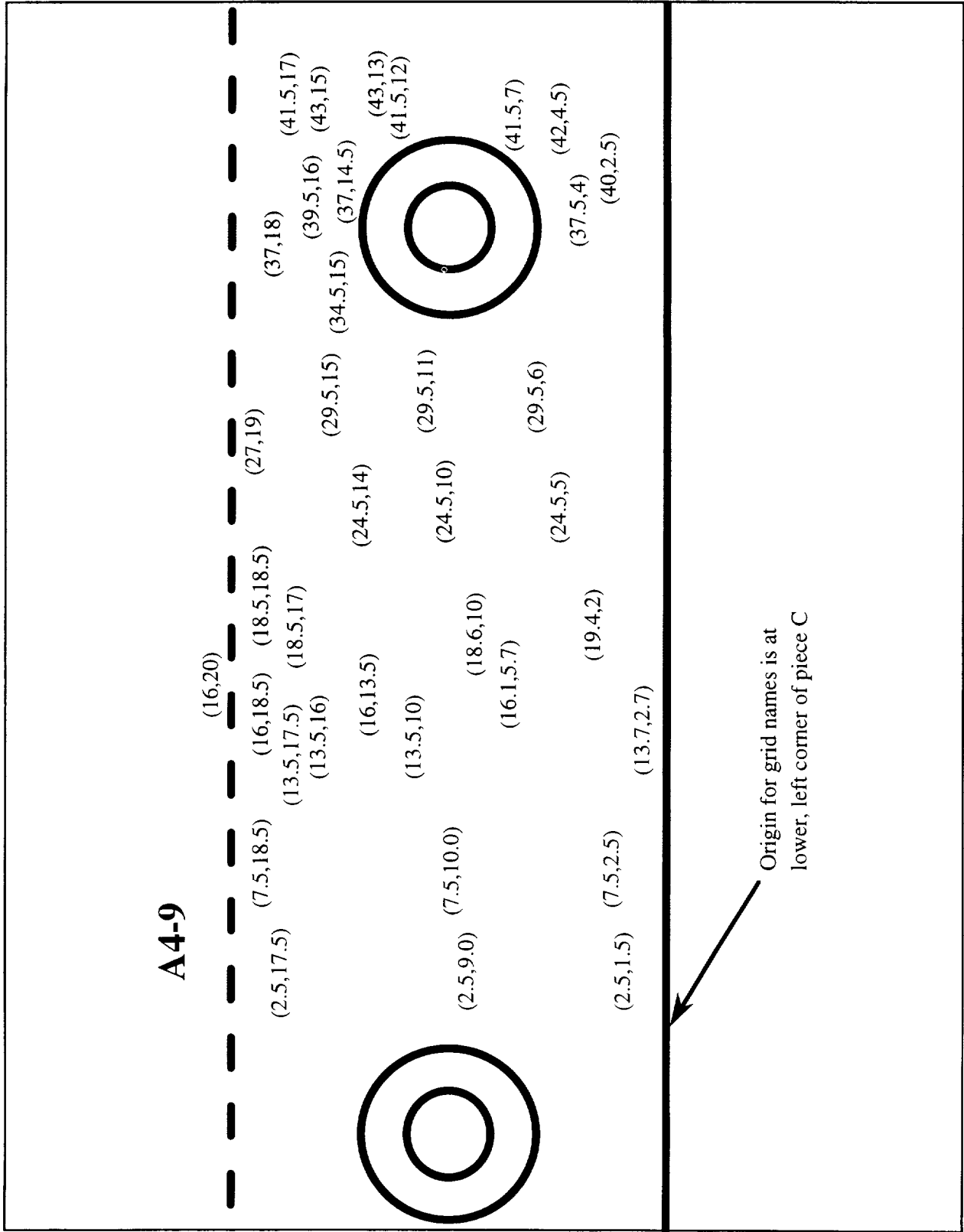


Figure A-18. Tray A4-9 ESCA analysis area grid locations.

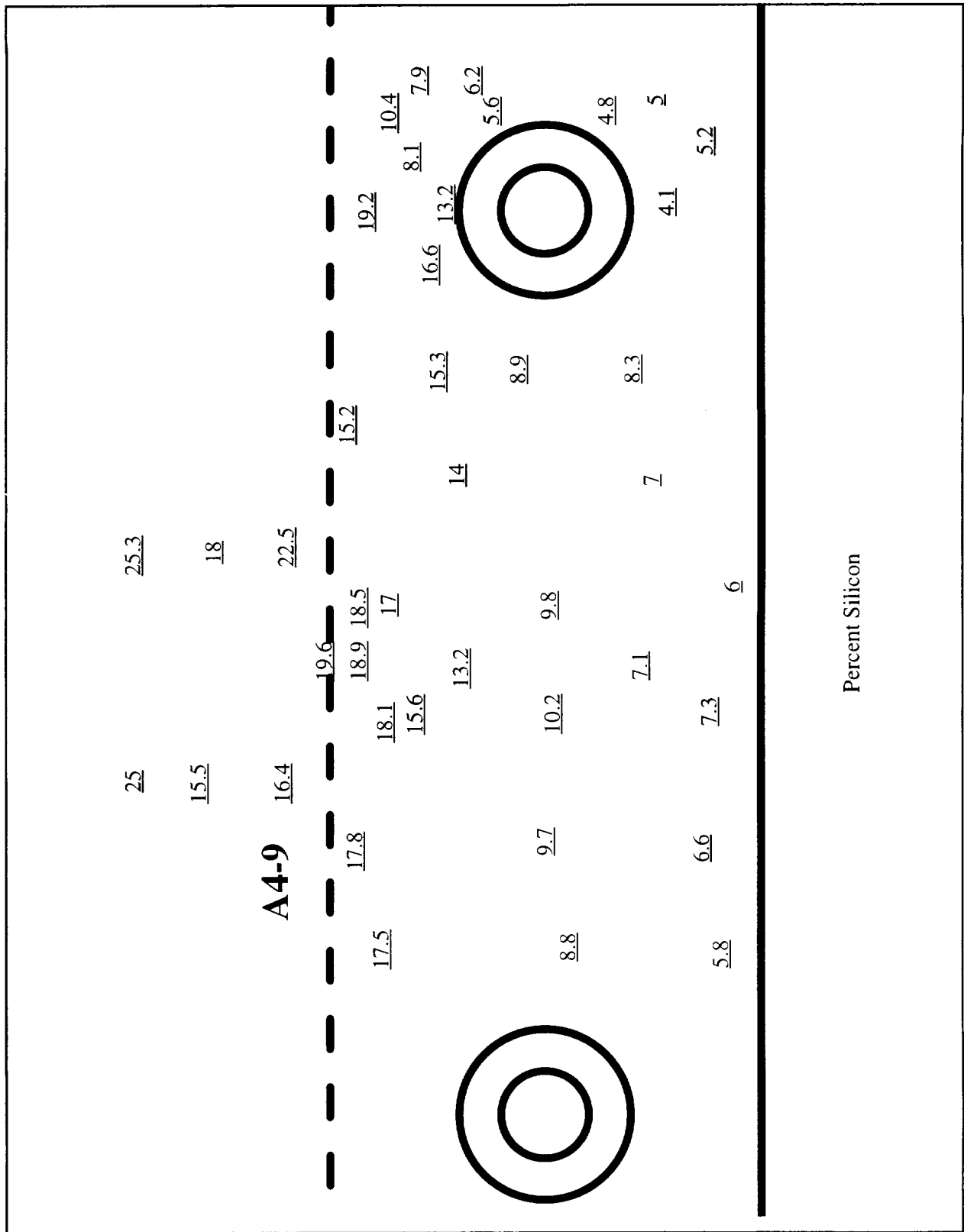


Figure A-19. Tray A4-9 Percent Silicon.

A4-9 Unspattered Surfaces only												
XPS Survey Scan Composition Table summary												
Location	A	A	A	A	A	A	A	A	C	C	C	C
Atomic %:	29.5-6	24.5-5	24.5-14	29.5-15	27-19	29.5-11	7.5-2.5	2.5-1.5	2.5-17.5	7.5-18.5	2.5-9	7.5-10
surface	surface	surface	surface	surface	surface	surface	surface	surface	surface	surface	surface	surface
Silicon	8.3%	7.0%	14.0%	15.3%	15.2%	8.9%	6.6%	5.8%	17.5%	17.8%	8.8%	9.7%
Oxygen	45.4%	44.2%	46.5%	46.9%	43.9%	40.5%	45.9%	41.9%	46.0%	45.7%	44.8%	46.8%
Aluminum	15.5%	15.3%	11.8%	12.3%	14.2%	15.5%	13.9%	12.7%	10.4%	10.0%	15.1%	14.2%
Carbon	23.2%	24.8%	20.5%	18.8%	21.9%	29.5%	20.2%	26.4%	20.3%	20.0%	23.3%	19.4%
Fluorine	3.6%	3.9%	2.4%	2.2%	1.8%	2.4%	6.4%	7.0%	2.2%	2.2%	3.5%	4.0%
Sodium	0.6%	0.8%	0.7%	0.7%	0.6%	0.6%	1.2%	1.3%	0.4%	0.4%	0.4%	1.2%
Sulfur	1.6%	1.5%	1.9%	1.8%	-	1.1%	1.7%	1.5%	1.6%	1.7%	1.7%	2.1%
Nitrogen	1.0%	0.9%	0.5%	0.8%	-	-	1.0%	0.9%	0.7%	0.5%	1.1%	0.8%
Potassium	-	-	0.7%	0.2%	0.3%	0.5%	0.9%	0.8%	0.6%	0.4%	0.3%	0.3%
Calcium	0.4%	0.5%	0.3%	0.3%	0.6%	0.4%	0.8%	0.6%	0.3%	0.4%	0.3%	0.6%
Magnesium	0.4%	0.7%	0.6%	0.6%	0.7%	0.4%	1.3%	1.0%	-	0.8%	0.7%	0.9%
Tin	-	-	0.1%	0.1%	0.1%	-	-	-	0.1%	0.1%	-	-
Chlorine	-	0.3%	-	-	0.4%	-	-	-	-	-	-	-
Argon	-	-	-	-	0.3%	-	-	-	-	-	-	-

Figure A-20 (1 of 5). Tray A4-9 Surface Composition.

**A4-9 Unspattered Surfaces only
XPS Survey Scan Composition Table summary**

	B	B	B	B	B	B	B	B	B	B	B	B	B	B	B	MLR	MLR
Location	13.5-17.5	18.5-18.5	16-20	13.5-16	18.5-17	16-18.5	16-13.5	13.5-10	18.6-10	16.1-5.7	19.4-2	13.7-2.7	41.5-17	37-14.5	43-13		
Atomic %:surface	surface	surface	surface	surface	surface	surface	surface	surface	surface	surface	surface	surface	surface	surface	surface	surface	surface
Silicon	18.1%	18.5%	19.6%	15.6%	17.0%	18.9%	13.2%	10.2%	9.8%	7.1%	6.0%	7.3%	10.4%	13.2%	6.2%		
Oxygen	48.2%	48.4%	45.4%	47.9%	48.9%	48.1%	49.4%	49.0%	51.1%	49.1%	43.5%	47.7%	46.6%	46.8%	45.3%		
Aluminum	9.3%	10.3%	9.6%	11.1%	11.6%	8.9%	13.0%	11.1%	13.5%	12.3%	10.8%	11.0%	14.3%	13.0%	16.0%		
Carbon	17.1%	16.6%	19.2%	17.7%	16.1%	16.8%	17.0%	20.2%	18.2%	19.6%	26.8%	20.9%	20.5%	18.9%	22.5%		
Fluorine	2.3%	2.0%	1.7%	2.4%	1.8%	2.0%	2.5%	3.8%	3.5%	5.9%	6.4%	7.4%	3.8%	2.9%	4.4%		
Sodium	0.7%	0.5%	0.4%	0.7%	0.5%	0.5%	0.7%	0.8%	0.6%	0.9%	1.1%	1.2%	0.6%	0.7%	1.0%		
Sulfur	2.2%	2.1%	2.3%	2.3%	1.9%	2.3%	1.7%	1.5%	1.3%	1.2%	1.5%	1.3%	1.5%	2.1%	1.7%		
Nitrogen	-	-	-	0.7%	0.6%	0.5%	0.9%	0.9%	0.5%	1.1%	1.1%	0.9%	0.7%	0.7%	0.8%		
Potassium	0.4%	0.4%	0.4%	0.3%	0.5%	0.5%	0.3%	0.8%	0.7%	0.8%	0.8%	0.8%	0.3%	0.2%	0.7%		
Calcium	0.6%	0.4%	0.6%	0.5%	0.4%	0.6%	0.5%	0.5%	-	0.6%	0.6%	0.7%	0.5%	0.8%	0.7%		
Magnesium	0.9%	0.7%	0.7%	0.8%	0.6%	0.8%	0.7%	1.0%	0.7%	1.2%	1.3%	0.7%	0.6%	0.8%	0.8%		
Tin	0.1%	0.1%	0.1%	0.1%	0.1%	0.1%	-	-	-	-	-	-	0.1%	0.1%	-		
Chlorine	-	-	-	-	-	-	-	-	-	-	-	-	-	-	-		
Argon	-	-	-	-	-	-	-	0.2%	-	-	-	-	-	-	-		

Figure A-20 (cont. 2 of 5). Tray A4-9 Surface Composition.

A4-9 Unspattered Surfaces only															
XPS Survey Scan Composition Table summary															
	MLR	MLR	On bend in plate, between pieces:												
Location	41.5-12	43-15	37-18	34.5-15	39.5-16	37.5-4	40-2.5	41.5-7	41.5-7	A&B at 30°B&C at 60°B&C at 90°	A&B at 30°B&C at 60°B&C at 90°				
Atomic %:surface	surface	surface	surface												
Silicon	5.6%	7.9%	19.2%	16.6%	8.1%	4.1%	5.2%	4.8%	5.0%	22.5%	18.0%	25.3%	16.4%	15.5%	25.0%
Oxygen	45.0%	47.1%	49.0%	47.3%	43.8%	43.9%	42.7%	44.3%	44.3%	43.5%	34.6%	23.9%	40.0%	30.4%	24.6%
Aluminum	16.1%	15.6%	10.0%	10.4%	14.5%	15.4%	14.2%	15.7%	16.0%	2.2%	2.0%	0.8%	4.1%	3.3%	0.7%
Carbon	24.4%	15.3%	17.6%	18.8%	23.7%	27.2%	27.2%	25.1%	24.5%	28.7%	43.3%	49.9%	35.2%	47.6%	49.7%
Fluorine	4.7%	8.9%	1.9%	2.3%	4.8%	5.2%	5.4%	5.4%	5.1%	1.0%	0.9%	-	1.2%	0.8%	-
Sodium	0.7%	0.8%	0.5%	0.5%	0.6%	0.8%	0.9%	0.8%	0.8%	0.2%	0.4%	-	0.3%	1.1%	-
Sulfur	1.5%	1.6%	0.6%	1.9%	1.3%	1.2%	1.2%	1.1%	1.4%	-	-	-	-	-	-
Nitrogen	0.8%	0.6%	0.5%	0.7%	1.0%	1.0%	1.1%	1.0%	1.0%	0.7%	-	-	0.9%	-	-
Potassium	0.6%	0.9%	-	0.1%	0.8%	-	0.7%	0.5%	0.6%	-	-	-	0.5%	-	-
Calcium	0.6%	0.5%	-	0.6%	0.4%	0.4%	0.4%	0.4%	0.5%	0.5%	0.5%	-	0.7%	0.3%	-
Magnesium	-	0.7%	0.6%	0.7%	0.8%	0.7%	0.9%	0.7%	0.8%	0.4%	-	-	0.5%	0.6%	-
Tin	-	-	0.1%	0.1%	0.1%	-	-	-	-	0.2%	0.2%	-	0.2%	0.1%	-
Chlorine	-	-	-	-	-	-	-	-	-	-	-	-	-	-	-
Argon	-	-	-	-	-	-	-	-	-	-	-	-	-	-	-

Figure A-20 (cont. 3 of 5). Tray A4-9 Surface Composition.

A4-9 Sputtered

XPS Survey Scan Composition Table summary

Cut Piece Location	thin sheet area 2	A	A	A	C	C
Atomic %:	light sputter	29.5-6	24.5-14	29.5-11	7.5-2.5	2.5-17.5
		light sputter				
Silicon	3.5%	8.3%	13.5%	10.3%	6.7%	17.4%
Oxygen	50.7%	52.5%	52.7%	51.3%	52.0%	51.3%
Aluminum	28.4%	25.5%	19.5%	23.4%	25.5%	16.6%
Carbon	12.0%	6.9%	7.4%	8.6%	6.4%	9.1%
Fluorine	2.5%	3.0%	2.5%	2.9%	3.1%	2.1%
Sodium	0.4%	0.7%	1.2%	0.9%	1.4%	0.7%
Sulfur	1.2%	1.5%	1.4%	0.6%	1.2%	1.1%
Nitrogen	0.8%	-	-	-	0.5%	-
Potassium	-	0.2%	0.7%	0.4%	0.7%	0.6%
Calcium	0.4%	0.5%	0.5%	0.5%	1.3%	0.5%
Magnesium	-	0.6%	0.6%	0.6%	1.1%	0.6%
Tin	-	-	0.1%	-	-	0.1%
Argon	-	0.2%	-	0.3%	-	-

Figure A-20 (cont. 4 of 5). Tray A4-9 Sputtered Surface Composition.

A4-9 After Sputter Profiles												
XPS Survey Scan Composition Table summary												
Cut Piece	thin sheet	A	A	A	A	A	A	A	A	C	C	C
Location	area 1	29.5-6	24.5-5	24.5-14	29.5-15	27-19	29.5-11	24.5-10	7.5-2.5	2.5-1.5	2.5-17.5	7.5-18.5
Atomic %:	165Å	Is+300Å	300Å	Is+300Å	300Å	Is+300Å	Is+300Å	Is+300Å	Is+300Å	300Å	Is+300Å	300Å
Silicon	1.9%	1.3%	1.1%	2.2%	2.0%	-	1.1%	1.4%	0.2%	0.9%	3.3%	3.9%
Oxygen	53.1%	53.7%	51.9%	52.3%	51.7%	52.0%	52.4%	52.4%	51.3%	50.5%	51.4%	51.5%
Aluminum	38.6%	37.5%	38.4%	37.7%	38.1%	38.2%	38.9%	36.6%	38.2%	36.5%	36.8%	35.6%
Carbon	3.3%	3.0%	3.3%	4.1%	2.9%	5.2%	2.0%	4.2%	5.7%	5.7%	4.2%	3.9%
Fluorine	1.9%	1.9%	1.9%	2.1%	1.9%	1.6%	2.2%	1.7%	1.7%	1.7%	2.3%	1.6%
Sodium	-	0.4%	1.0%	0.6%	0.9%	0.9%	0.7%	1.2%	0.7%	0.8%	0.6%	0.8%
Sulfur	-	-	-	-	-	-	0.6%	-	-	1.0%	-	-
Nitrogen	-	-	-	-	-	-	-	-	-	-	-	-
Potassium	-	-	-	-	-	-	-	-	-	-	-	-
Calcium	-	0.6%	0.8%	0.7%	0.8%	0.7%	0.5%	0.9%	0.7%	0.8%	-	0.5%
Magnesium	-	-	-	-	-	-	-	-	-	0.6%	-	0.6%
Argon	1.1%	1.3%	1.4%	1.3%	1.4%	1.6%	1.5%	1.4%	1.5%	1.4%	1.3%	1.5%

Figure A-20 (cont. 5 of 5). Tray A4-9 Sputtered Surface Composition.

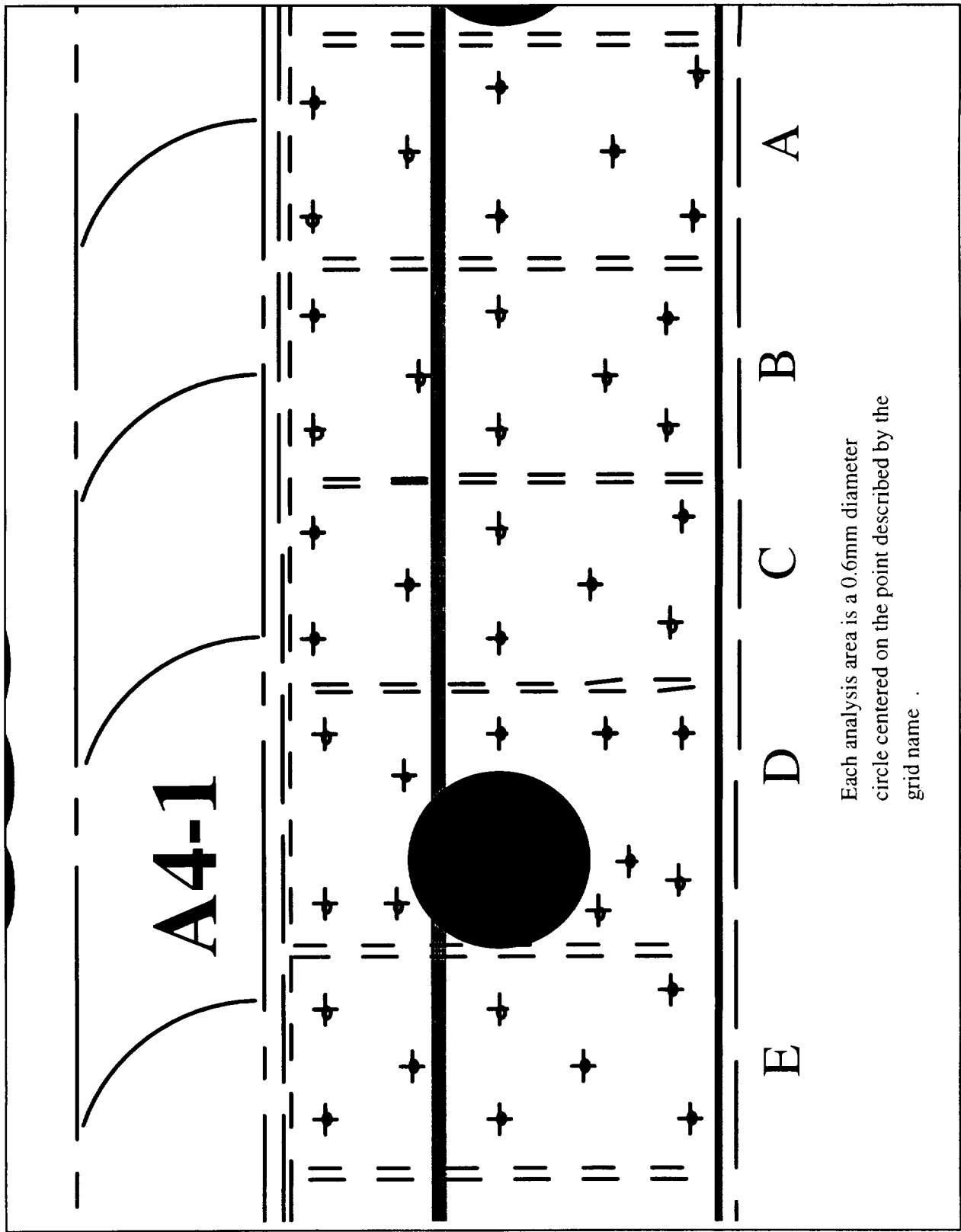


Figure A-21. Tray A4-1 ESCA analysis areas.

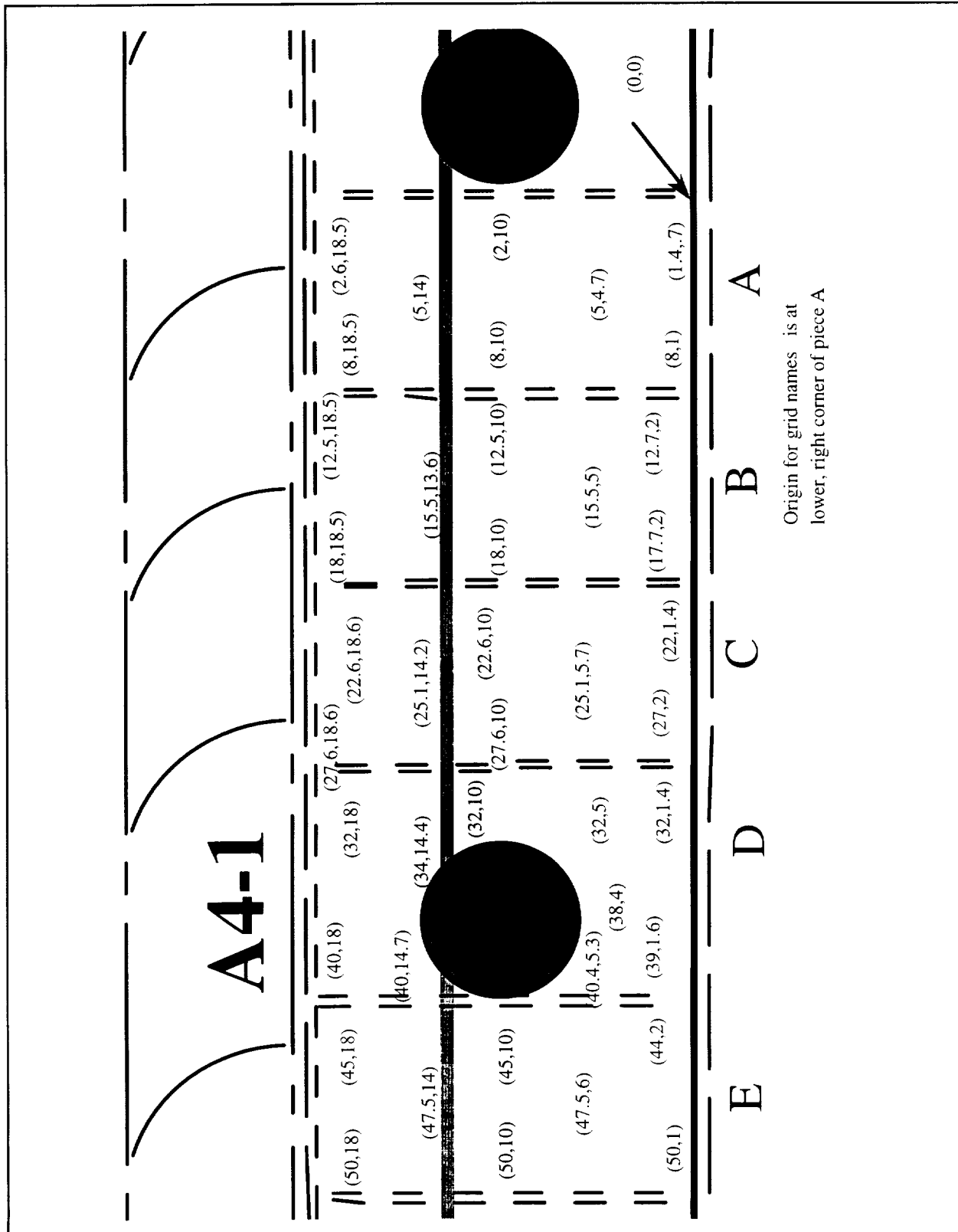


Figure A-22. Tray A4-1 ESCA analysis area grid locations.

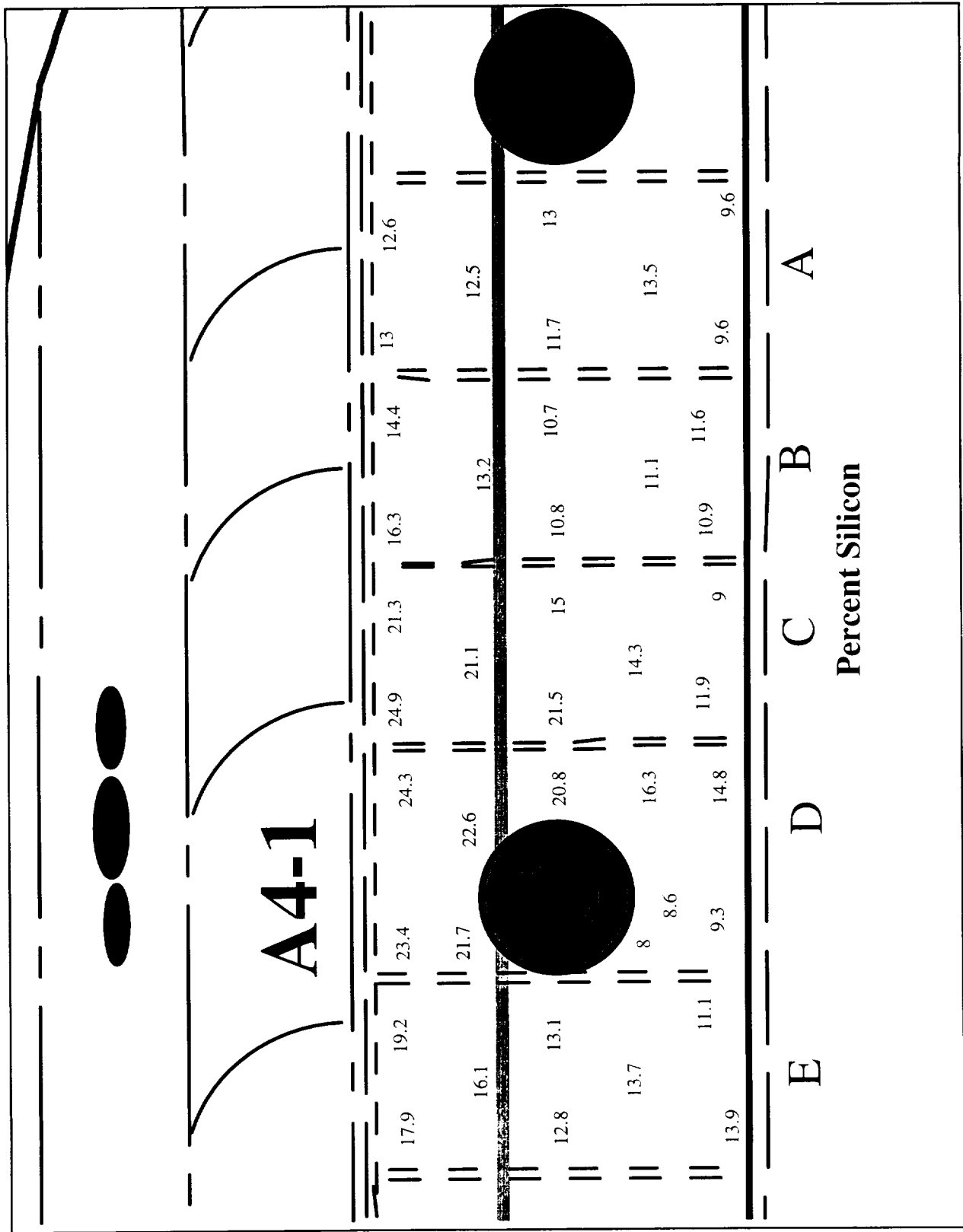


Figure A23. Tray A4-1 Percent Silicon.

A4-1 Unspattered Surfaces only															
XPS Survey Scan Composition Table summary															
Location	8-18.5	2.6-18.5	5.0-14	8.0-5	8.0-5	5.0-5	5-4.7	1.4-0.7	8.0-1	18-18.5	12.5-18.5	15.5-13.6	18-10	12.5-10	15.5-5
Atomic %:	A	A	A	A	A	A	A	A	A	B	B	B	B	B	B
Silicon	13.0%	12.6%	12.5%	11.7%	13.0%	13.5%	9.6%	9.6%	9.6%	16.3%	14.4%	13.2%	10.8%	10.7%	11.1%
Oxygen	48.1%	49.5%	49.0%	49.9%	49.9%	50.0%	46.1%	47.1%	47.1%	48.2%	48.6%	48.6%	47.7%	48.9%	48.9%
Aluminum	10.9%	12.4%	11.9%	11.8%	11.1%	10.2%	10.9%	11.7%	11.7%	8.6%	10.9%	11.6%	12.5%	12.7%	12.2%
Carbon	22.0%	18.6%	19.8%	20.5%	19.8%	20.2%	23.5%	22.0%	22.0%	20.2%	19.9%	20.0%	21.1%	21.3%	21.0%
Fluorine	2.5%	2.4%	2.7%	3.1%	2.4%	2.7%	4.7%	4.1%	4.1%	2.1%	1.9%	2.8%	3.4%	3.3%	3.0%
Sodium	1.1%	1.6%	1.2%	0.7%	1.1%	0.8%	1.6%	1.9%	1.9%	1.6%	1.6%	1.0%	1.1%	1.0%	1.0%
Sulfur	0.6%	0.6%	0.8%	1.0%	1.2%	1.0%	0.9%	1.2%	1.2%	0.9%	0.5%	0.9%	1.1%	0.9%	1.2%
Nitrogen	0.6%	0.8%	0.8%	0.7%	0.7%	1.1%	1.1%	0.9%	0.9%	-	0.6%	0.8%	0.8%	0.9%	0.9%
Potassium	-	0.6%	0.3%	-	-	-	0.5%	0.6%	0.6%	0.7%	0.5%	-	0.5%	-	-
Calcium	0.4%	0.3%	0.4%	0.4%	0.4%	-	0.4%	0.2%	0.2%	0.4%	0.3%	0.4%	0.3%	0.3%	0.4%
Magnesium	0.4%	0.4%	0.6%	-	0.4%	0.5%	0.6%	0.6%	0.6%	0.7%	0.5%	0.5%	0.6%	-	0.3%
Tin	0.1%	0.1%	0.1%	0.1%	0.1%	0.1%	-	-	-	0.1%	0.1%	0.1%	0.1%	0.1%	-
Phosphorus	-	-	-	-	-	-	-	-	-	-	-	-	-	-	-
Chrome	0.2%	-	-	-	-	-	-	-	-	-	-	-	-	-	-

Figure A-24 (1 of 3). Tray A4-1 Surface Composition.

A4-1 Unspattered Surfaces only

XPS Survey Scan Composition Table summary

Cut Piece	B	B	C	C	C	C	C	C	C	C	D	D	D
Location	12.7-2	17.7-2	27.6-18.6	22.6-18.6	25.1-14.2	27.6-10	22.6-10	25.1-5.7	22-1.4	27-2	40-18	32-18	40-14.7
Atomic %:													
Silicon	11.6%	10.9%	24.8%	21.3%	21.1%	21.5%	15.0%	14.3%	9.0%	11.9%	23.4%	24.3%	21.7%
Oxygen	48.4%	48.4%	50.0%	49.1%	49.7%	50.4%	49.8%	49.9%	46.1%	48.1%	49.2%	49.1%	49.2%
Aluminum	10.5%	10.7%	2.8%	5.7%	5.2%	5.1%	9.5%	9.9%	10.6%	9.8%	3.4%	2.4%	4.2%
Carbon	22.6%	22.3%	19.8%	20.9%	20.2%	18.6%	18.6%	19.0%	24.2%	22.8%	20.9%	21.1%	21.4%
Fluorine	3.7%	3.7%	0.8%	1.1%	0.9%	1.7%	2.8%	2.6%	4.5%	3.1%	1.2%	1.1%	1.0%
Sodium	1.1%	1.1%	0.9%	0.9%	1.1%	1.0%	1.3%	1.3%	2.1%	1.3%	1.2%	1.1%	0.9%
Sulfur	0.9%	0.9%	-	-	-	-	0.9%	0.7%	1.3%	0.8%	0.4%	-	0.4%
Nitrogen	0.8%	0.9%	0.6%	0.6%	0.6%	0.4%	0.8%	1.0%	1.0%	0.9%	-	0.7%	0.7%
Potassium	-	-	-	-	0.3%	0.5%	0.6%	0.6%	0.6%	0.6%	-	-	-
Calcium	-	0.3%	-	0.2%	0.2%	-	-	0.2%	0.3%	-	-	-	0.3%
Magnesium	0.5%	0.7%	-	-	0.5%	0.6%	0.5%	0.5%	0.4%	0.7%	-	-	-
Tin	-	0.1%	0.2%	0.1%	0.1%	0.1%	0.1%	-	-	0.1%	0.2%	0.2%	0.2%
Phosphorus	-	-	-	-	-	-	-	-	-	-	-	-	-
Chrome	-	-	-	-	-	-	-	-	-	-	-	-	-

Figure A-24 (cont. 2 of 3). Tray A4-1 Surface Composition.

Appendix B

ESCA Depth Profiles Obtained for Selected Areas from LDEF Tray Locations E10-8, C6-2, and A4-9

Introduction

This appendix contains graphs showing the composition of the contaminant layer as a function of depth from the surface for each specific location where an ESCA depth profile was conducted as part of contract NAS8-40581 activities. The individual plots each show carbon, silicon, oxygen, and (when present) aluminum atoms. All measurements show a thin layer of post-flight organic based contamination. Locations that were exposed to atomic oxygen during flight generally show "crusts" of SiO_x of fairly constant composition, but of varying thickness, depending on the exact location. Locations with a thick contaminant layer on the anodized aluminum show profiles of widely varying composition with depth. The presence of aluminum generally indicates the sputtering process has at least reached the pore structure of the anodized aluminum. Eventually the aluminum and oxygen elemental ratios reach approximately 2 to 3, signifying that Al_2O_3 has become a major constituent at the particular sputtering depth.

List of Figures

Figure B-1.	Tray E10-8 Profile locations.	B5
Figure B-2.	Tray E10-8 piece C profile 1.	B6
Figure B-3.	Tray E10-8 piece C profile 8.	B7
Figure B-4.	Tray E10-8 piece C profile 2.	B8
Figure B-5.	Tray E10-8 piece C profile 3.	B9
Figure B-6.	Tray E10-8 piece C profile 4.	B10
Figure B-7.	Tray E10-8 piece C profile 5.	B11
Figure B-8.	Tray E10-8 piece C profile 6 (0 to 4000).	B12
Figure B-9.	Tray E10-8 piece C profile 6 (0 to 2000).	B13
Figure B-10.	Tray E10-8 piece C profile 7 (0 to 6000).	B14
Figure B-11.	Tray E10-8 piece C profile 7 (0 to 2000).	B15
Figure B-12.	Tray E10-8 piece B profile 2 (0 to 15000).	B16
Figure B-13.	Tray E10-8 piece B profile 2 (0 to 4000).	B17
Figure B-14.	Tray E10-8 piece B profile 3 (0 to 15000).	B18
Figure B-15.	Tray E10-8 piece B profile 3 (0 to 2000).	B19
Figure B-16.	Tray E10-8 piece B profile 4.	B20
Figure B-17.	Tray E10-8 piece B profile 1 (0 to 15000).	B21
Figure B-18.	Tray E10-8 piece B profile 1 (0 to 2000).	B22
Figure B-19.	Tray C6-2 Profile locations.	B23
Figure B-20.	Tray C6-2 piece C profile 1.	B24
Figure B-21.	Tray C6-2 piece D profile 1.	B25
Figure B-22.	Tray C6-2 piece D profile 3.	B26

List of Figures continued

Figure B-23.	Tray C6-2 piece D profile 2.	B27
Figure B-24.	Tray C6-2 piece Ea profile 1.	B28
Figure B-25.	Tray C6-2 piece Ec profile 3 (0 to 2000).	B29
Figure B-26.	Tray C6-2 piece Ec profile 3 (0 to 4000).	B30
Figure B-27.	Tray C6-2 piece Ec profile 2.	B31
Figure B-28.	Tray C6-2 piece Ec profile 1.	B32
Figure B-29.	Tray C6-2 piece Eb profile 1.	B33
Figure B-30.	Tray A4-9 Profile locations.	B34
Figure B-31.	Tray A4-9 piece A Silicon profiles.	B35
Figure B-32.	Tray A4-9 piece C Silicon profiles.	B36
Figure B-33.	Tray A4-9 piece A profile 1.	B37
Figure B-34.	Tray A4-9 piece A profile 2.	B38
Figure B-35.	Tray A4-9 piece A profile 3.	B39
Figure B-36.	Tray A4-9 piece A profile 4.	B40
Figure B-37.	Tray A4-9 piece A profile 5.	B41
Figure B-38.	Tray A4-9 piece A profile 6.	B42
Figure B-39.	Tray A4-9 piece A profile 7.	B43
Figure B-40.	Tray A4-9 piece C profile 1.	B44
Figure B-41.	Tray A4-9 piece C profile 2.	B45
Figure B-42.	Tray A4-9 piece C profile 3.	B46
Figure B-43.	Tray A4-9 piece C profile 4.	B47
Figure B-44.	Tray A4-9 thin sheet profile 1.	B48
Figure B-45.	Tray A4-9 thin sheet profile 2.	B49

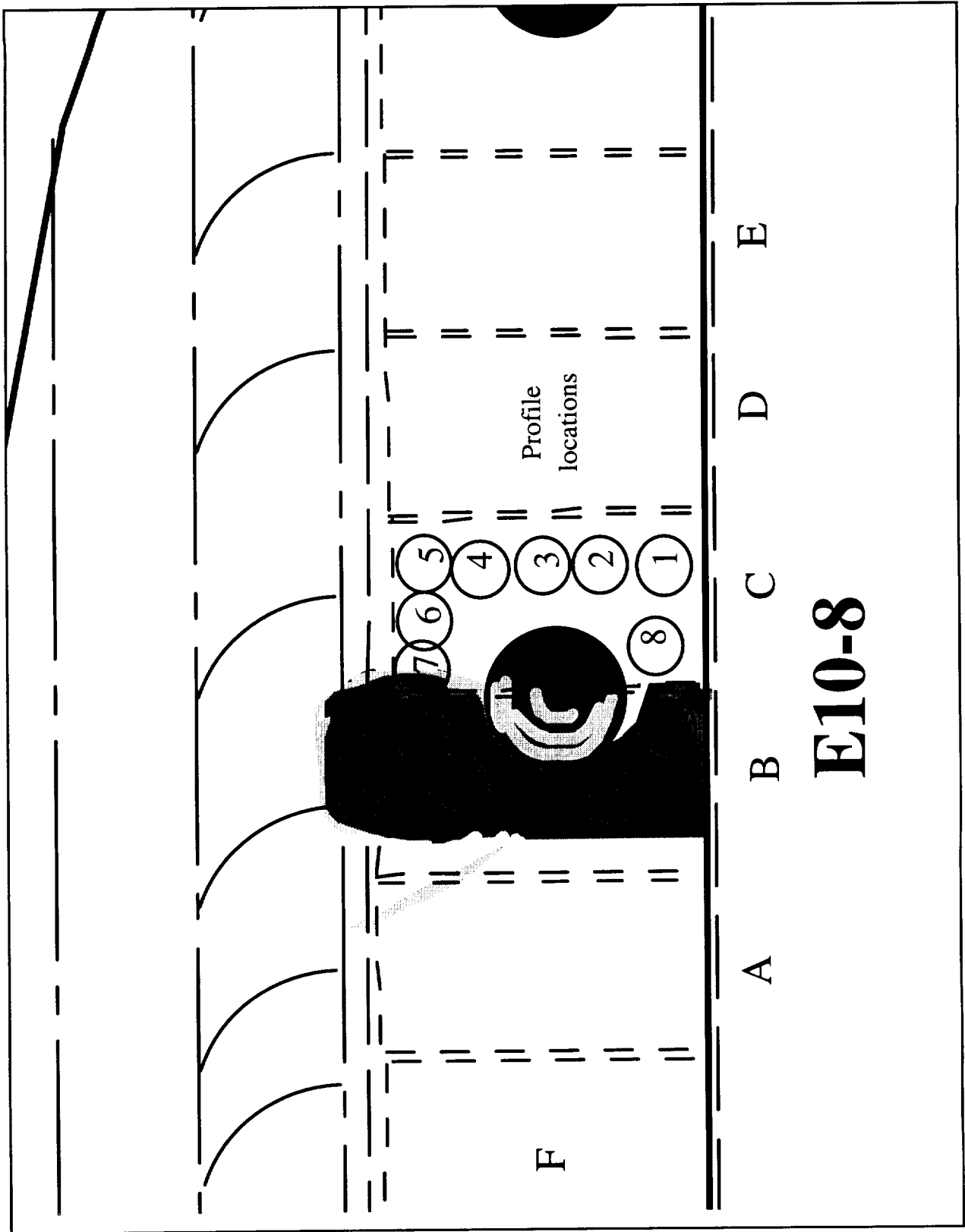


Figure B-1. Tray E10-8 Profile locations.

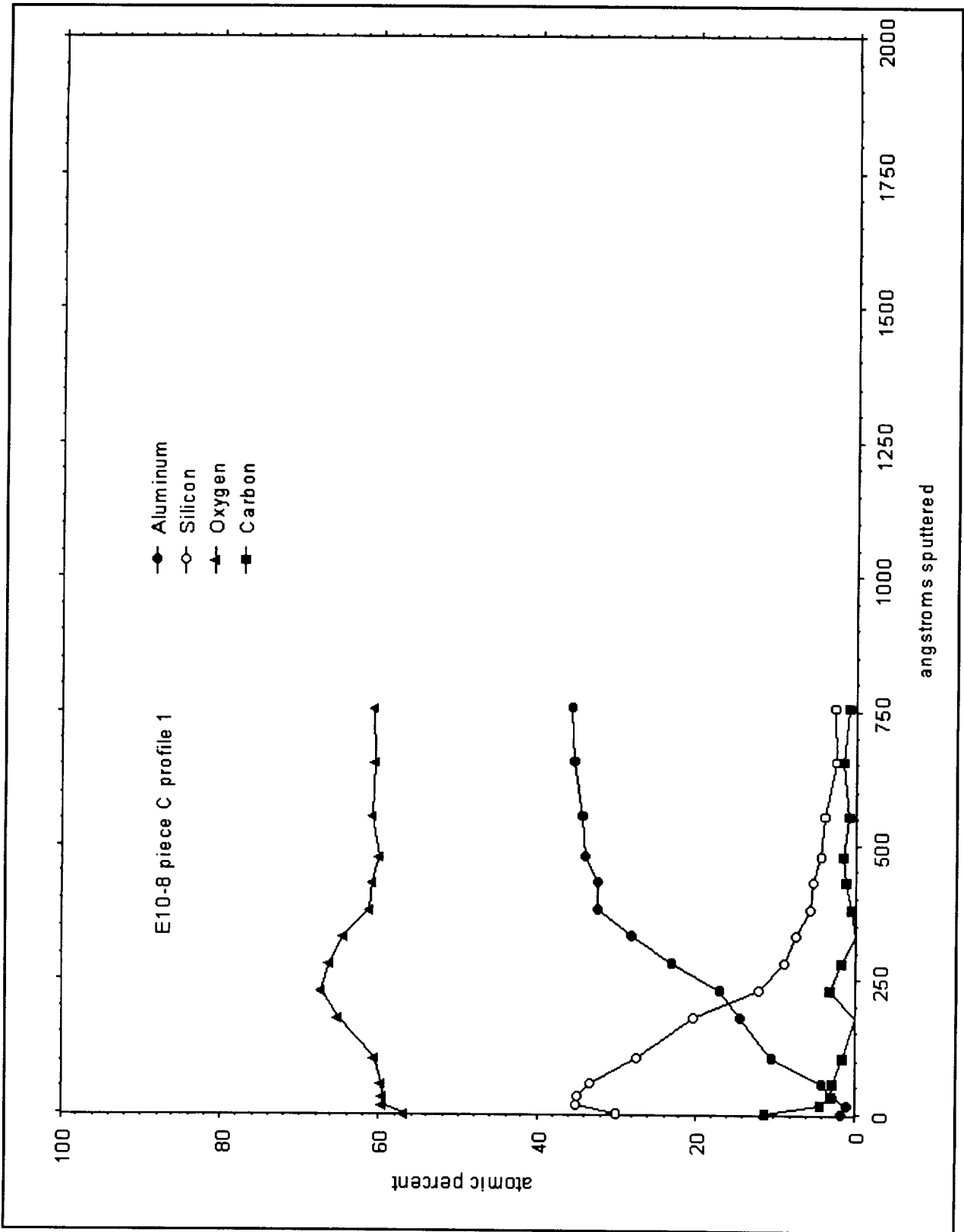


Figure B-2. Tray E10-8 piece C profile 1.

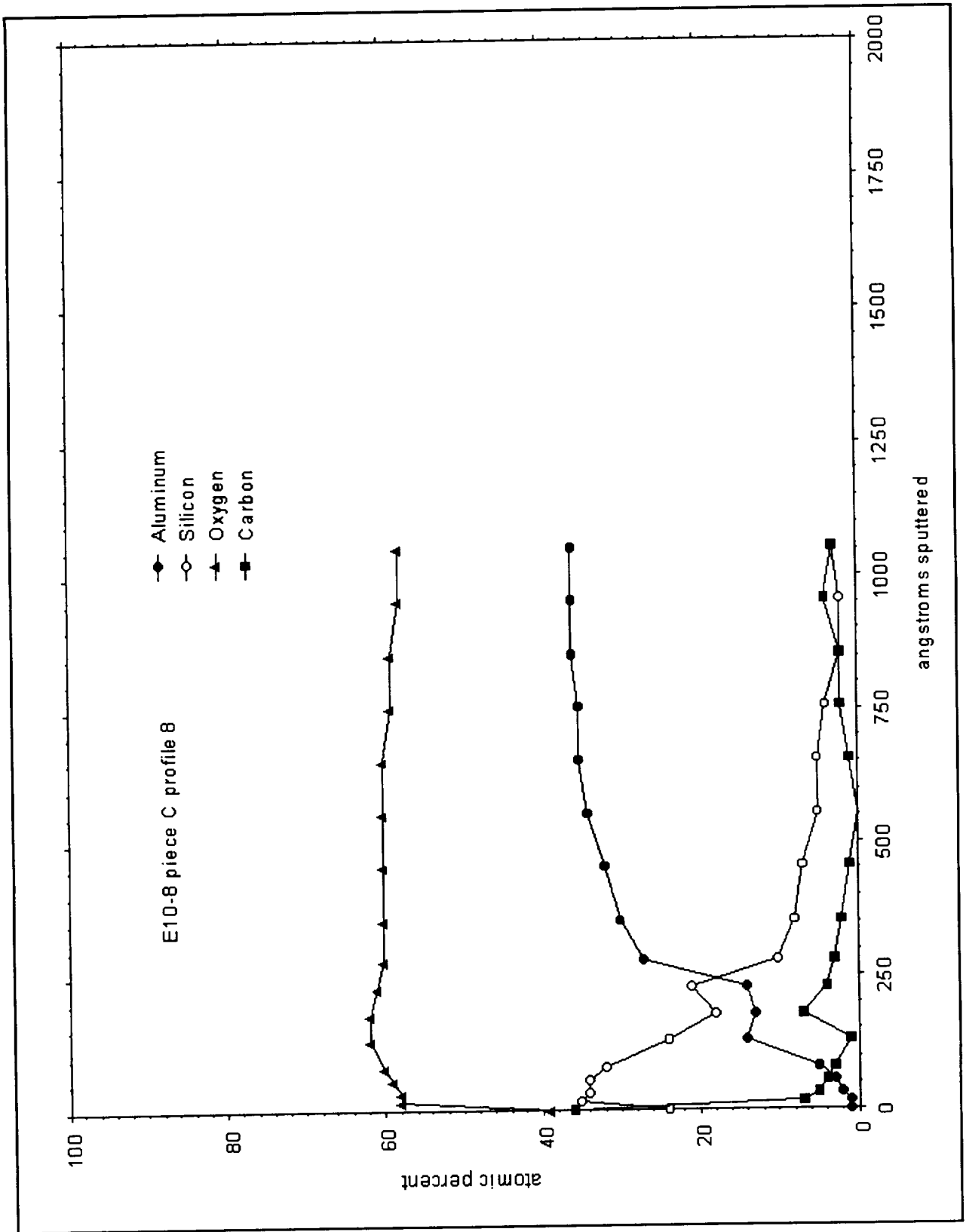


Figure B-3. Tray E10-8 piece C profile 8.

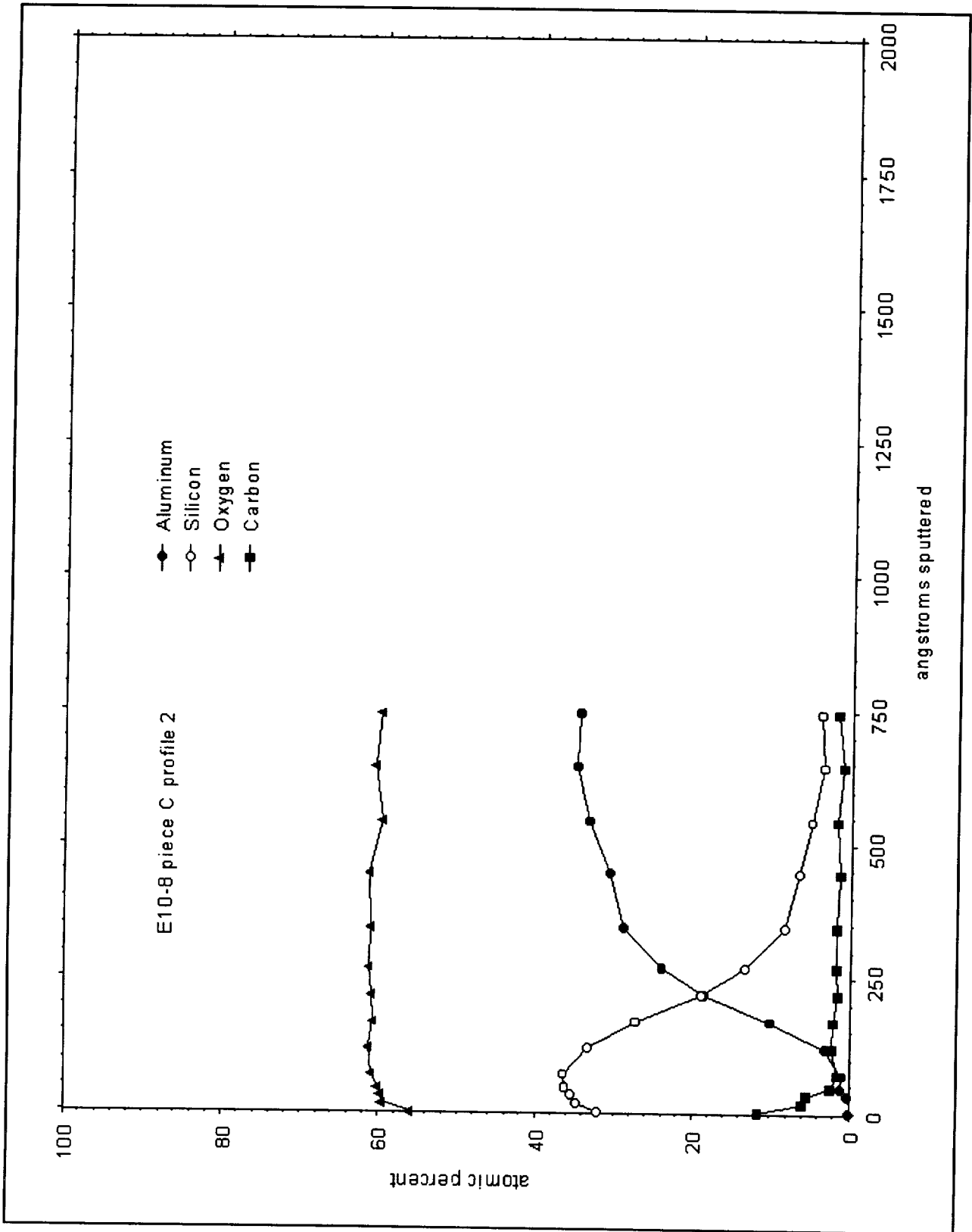


Figure B-4. Tray E10-8 piece C profile 2.

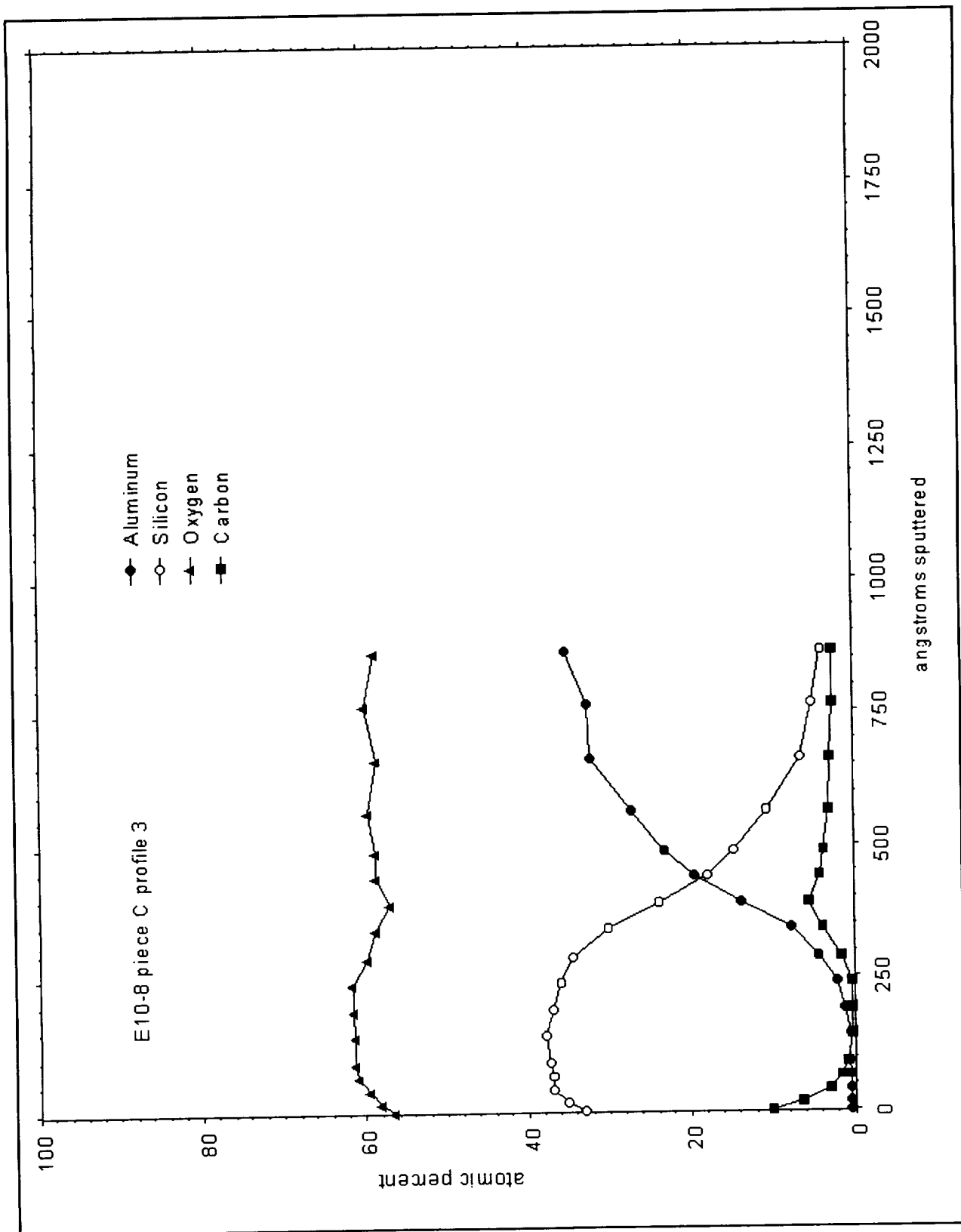


Figure B-5. Tray E10-8 piece C profile 3.

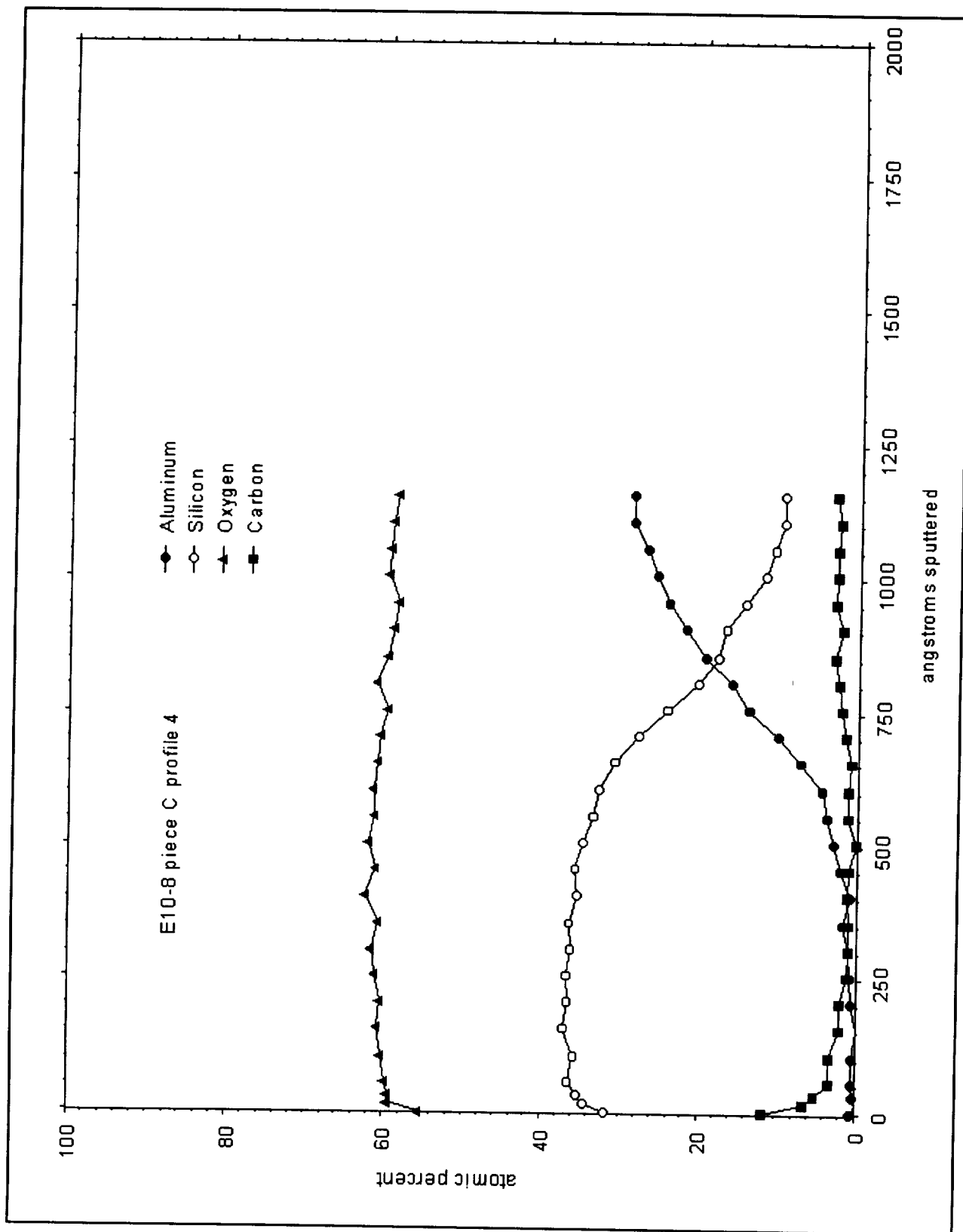


Figure B-6. Tray E10-8 piece C profile 4.

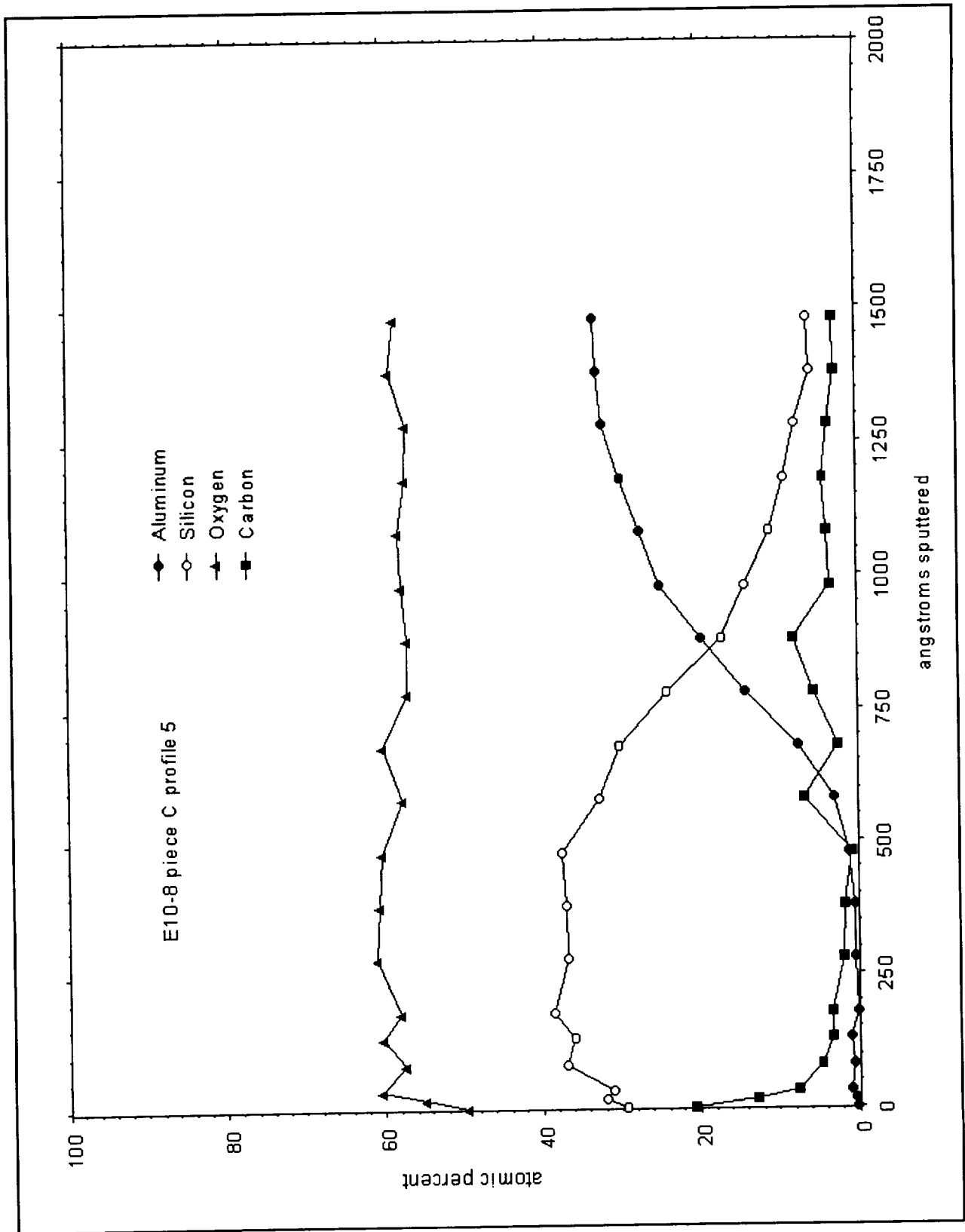


Figure B-7. Tray E10-8 piece C profile 5.

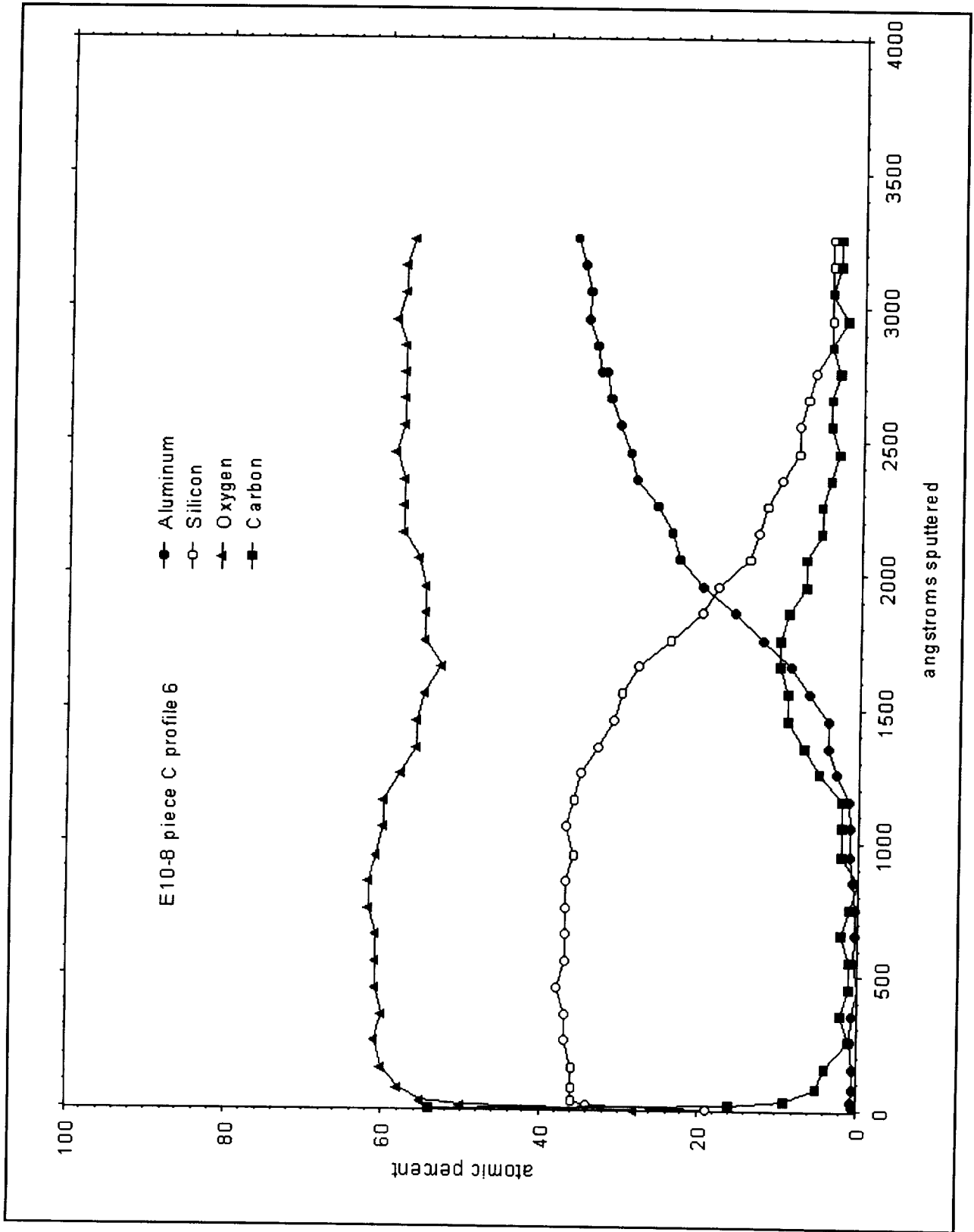


Figure B-8. Tray E10-8 piece C profile 6 (0 to 4000).

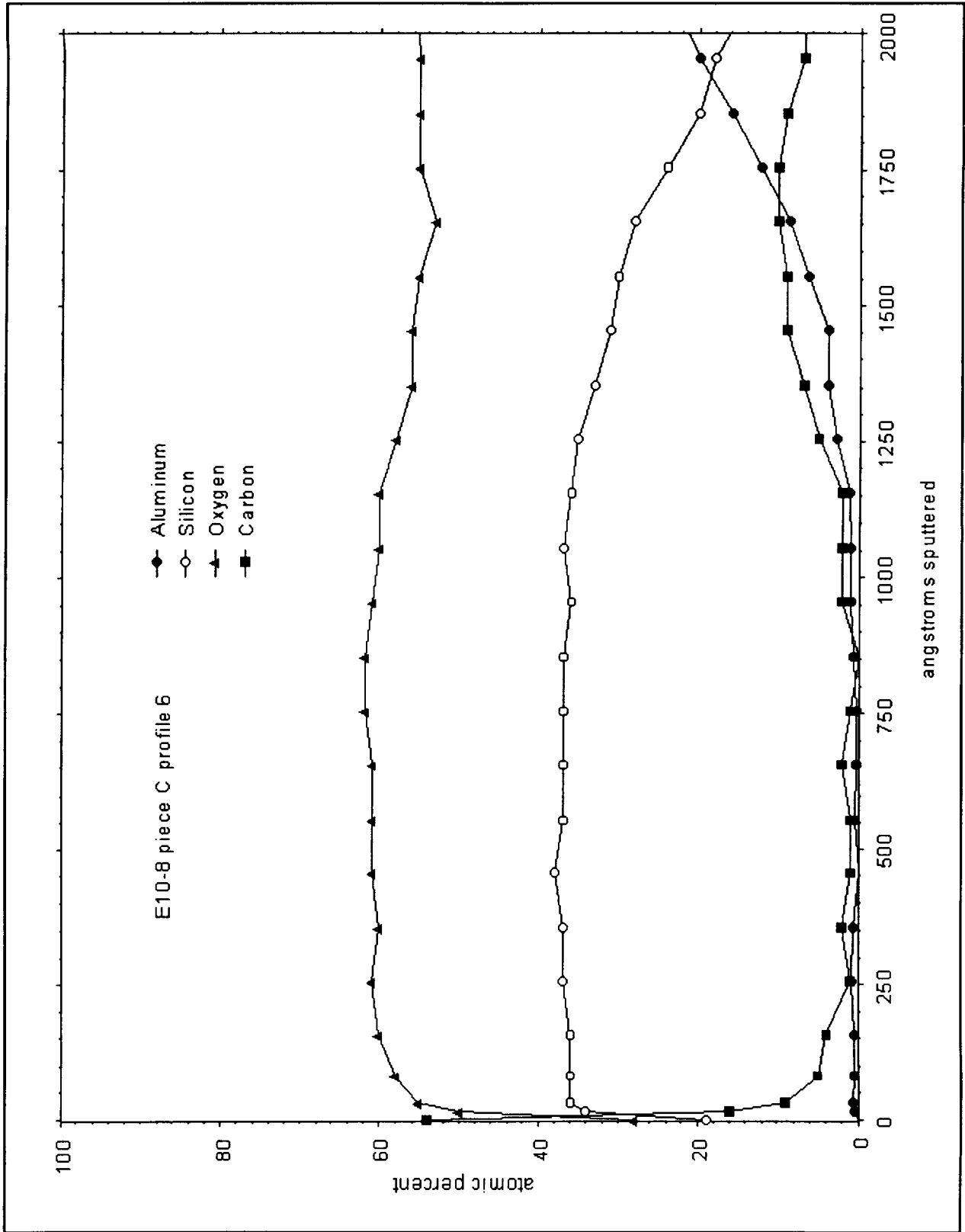


Figure B-9. Tray E10-8 piece C profile 6 (0 to 2000).

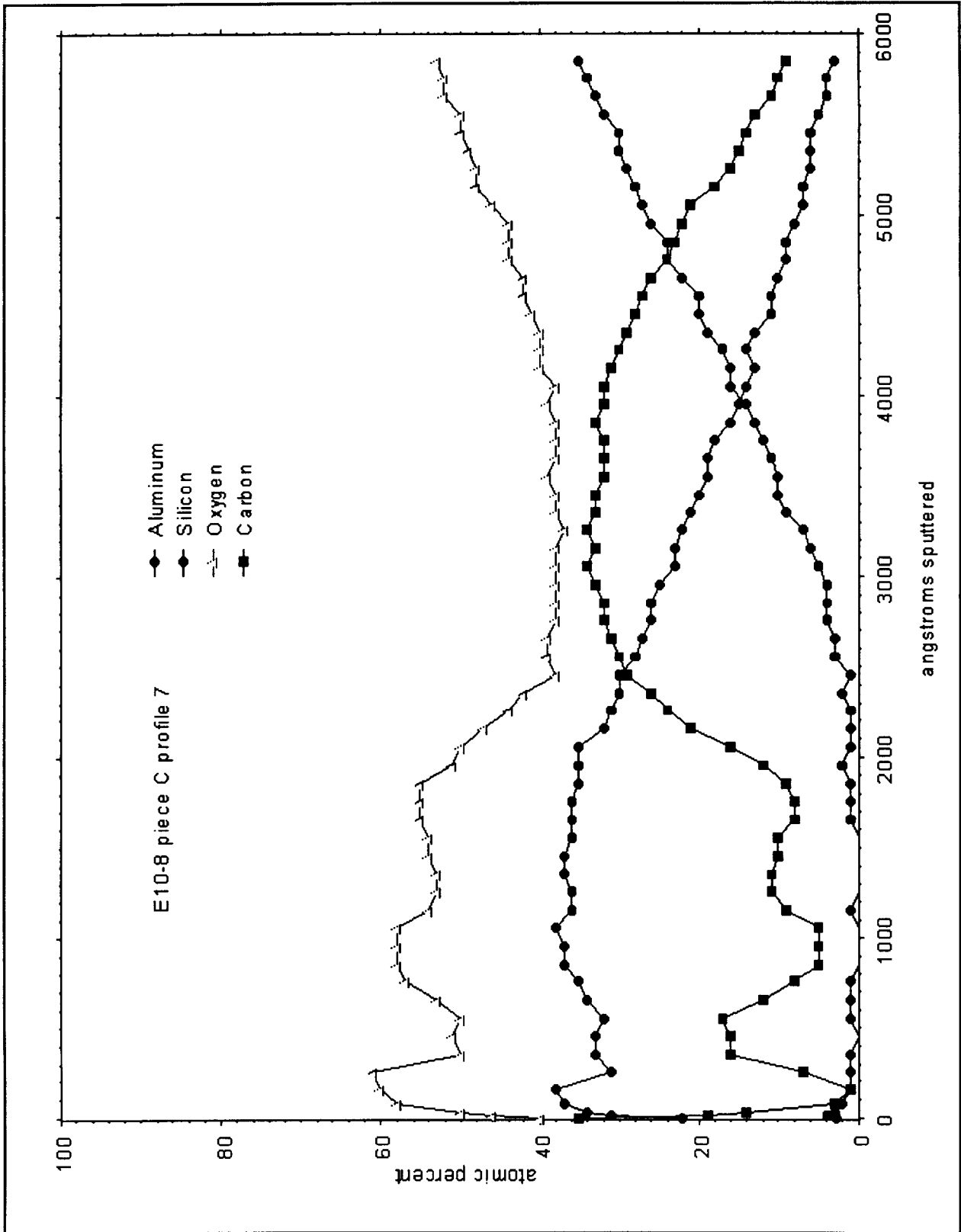


Figure B-10. Tray E10-8 piece C profile 7 (0 to 6000).

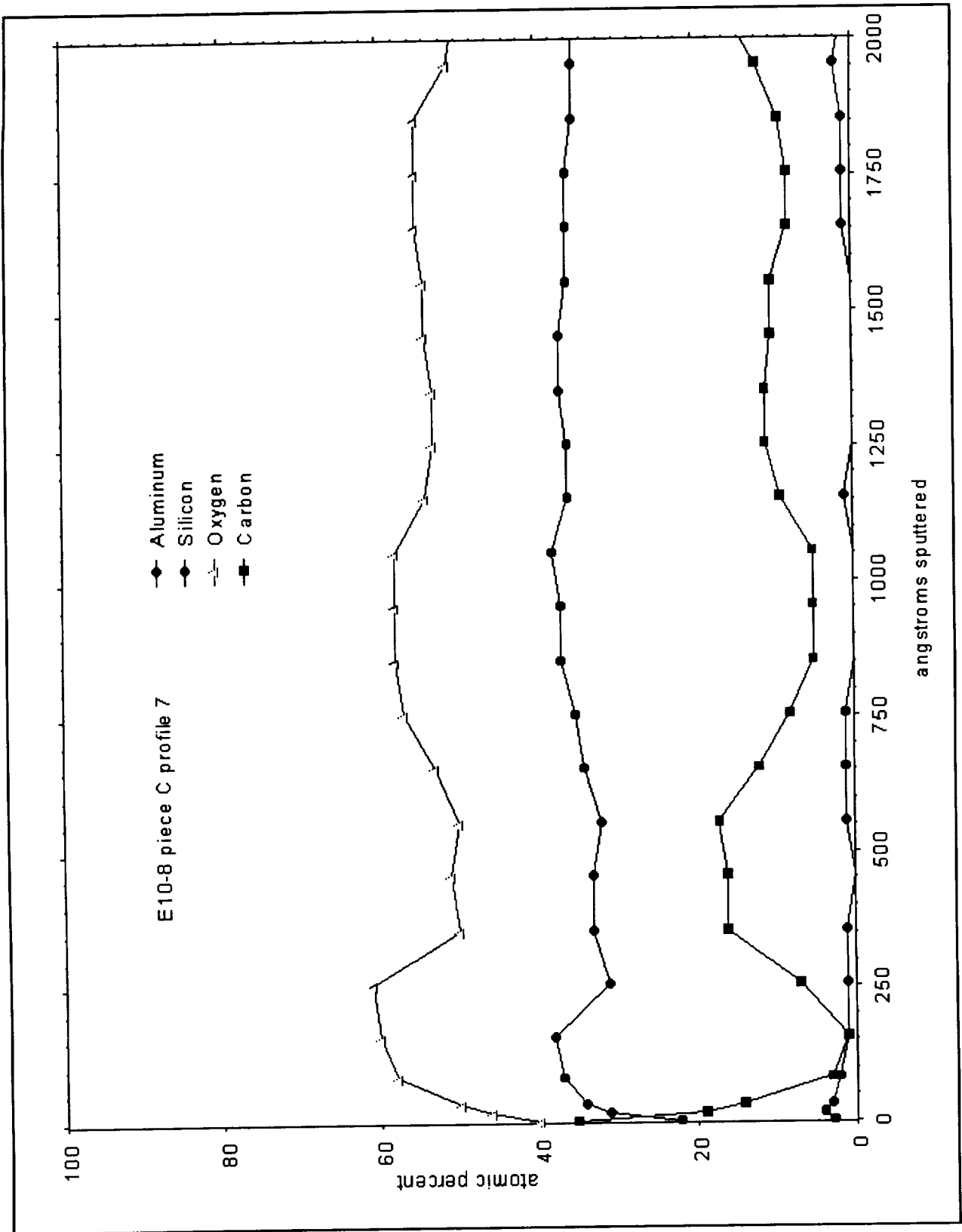


Figure B-11. Tray E10-8 piece C profile 7 (0 to 2000).

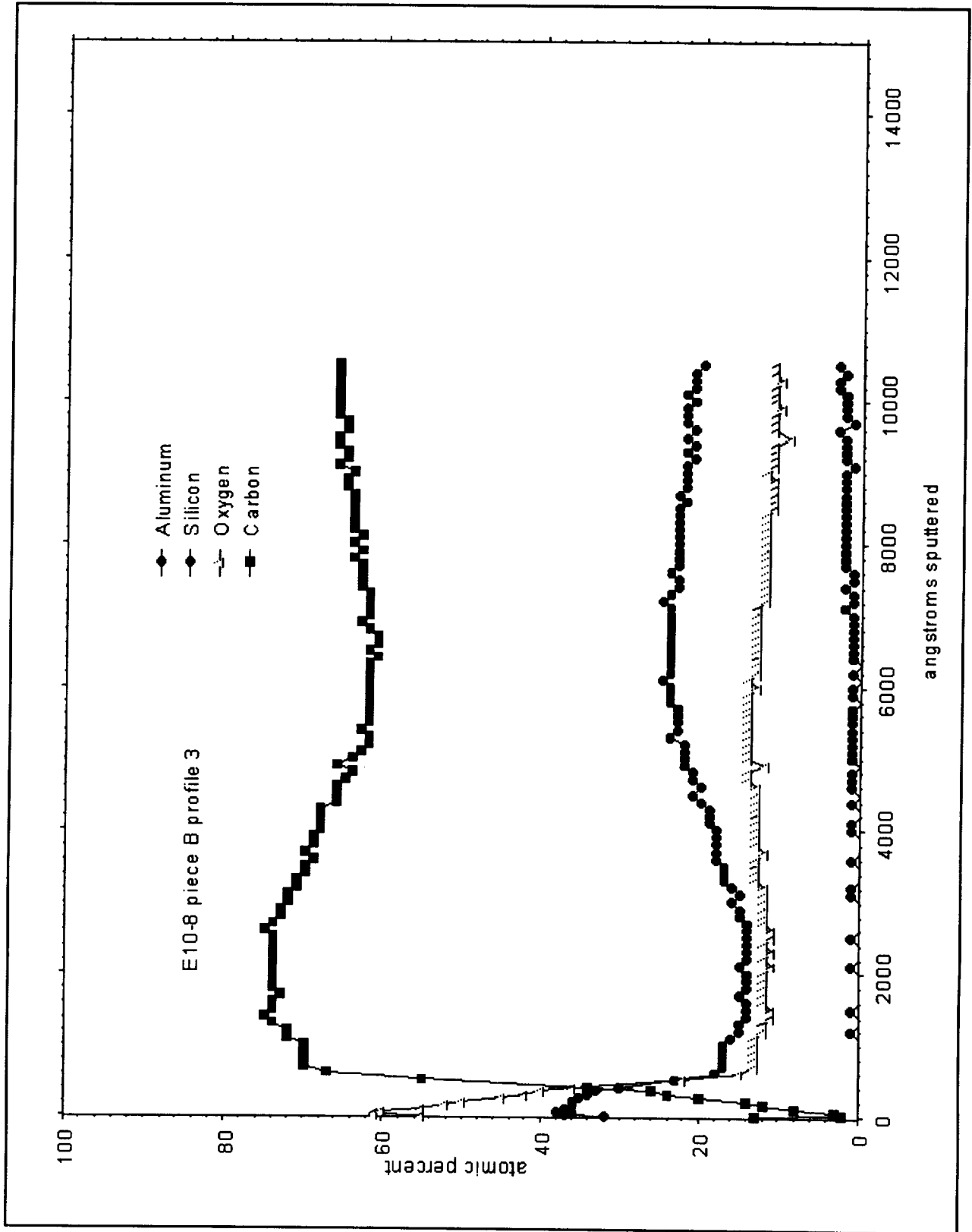


Figure B-14. Tray E10-8 piece B profile 3 (0 to 15000).

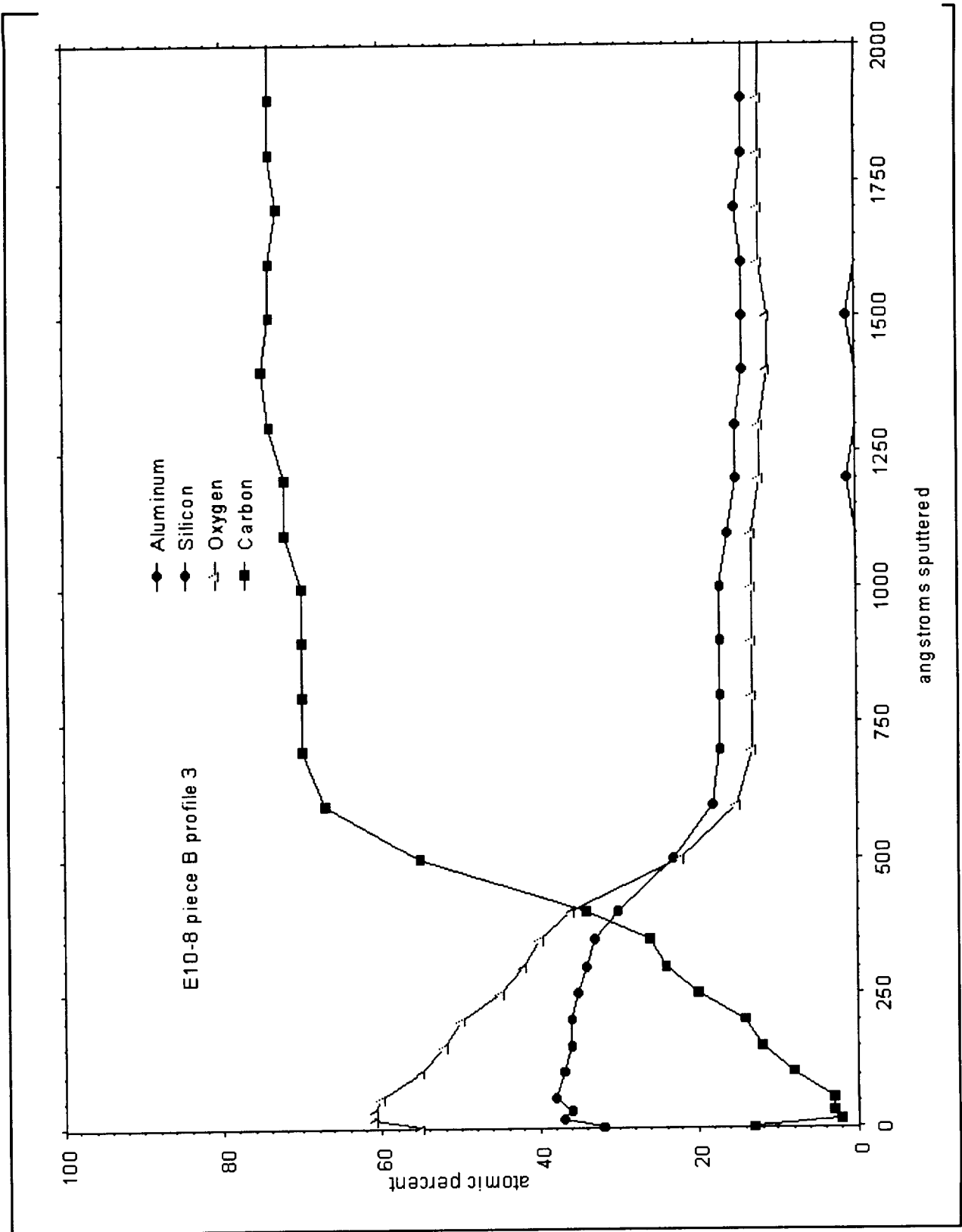


Figure B-15. Tray E10-8 piece B profile 3 (0 - 2000).

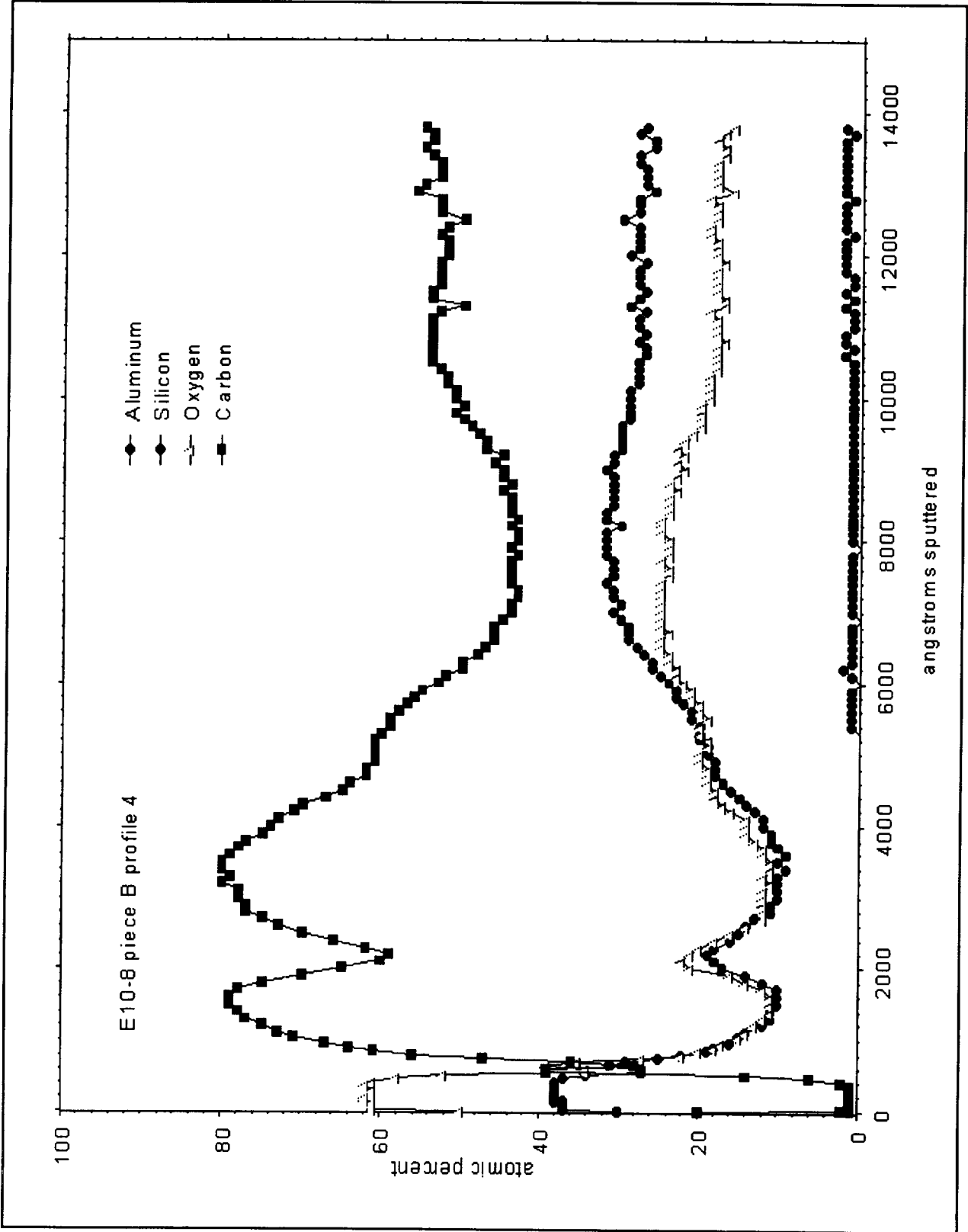


Figure B-16. Tray E10-8 piece B profile 4.

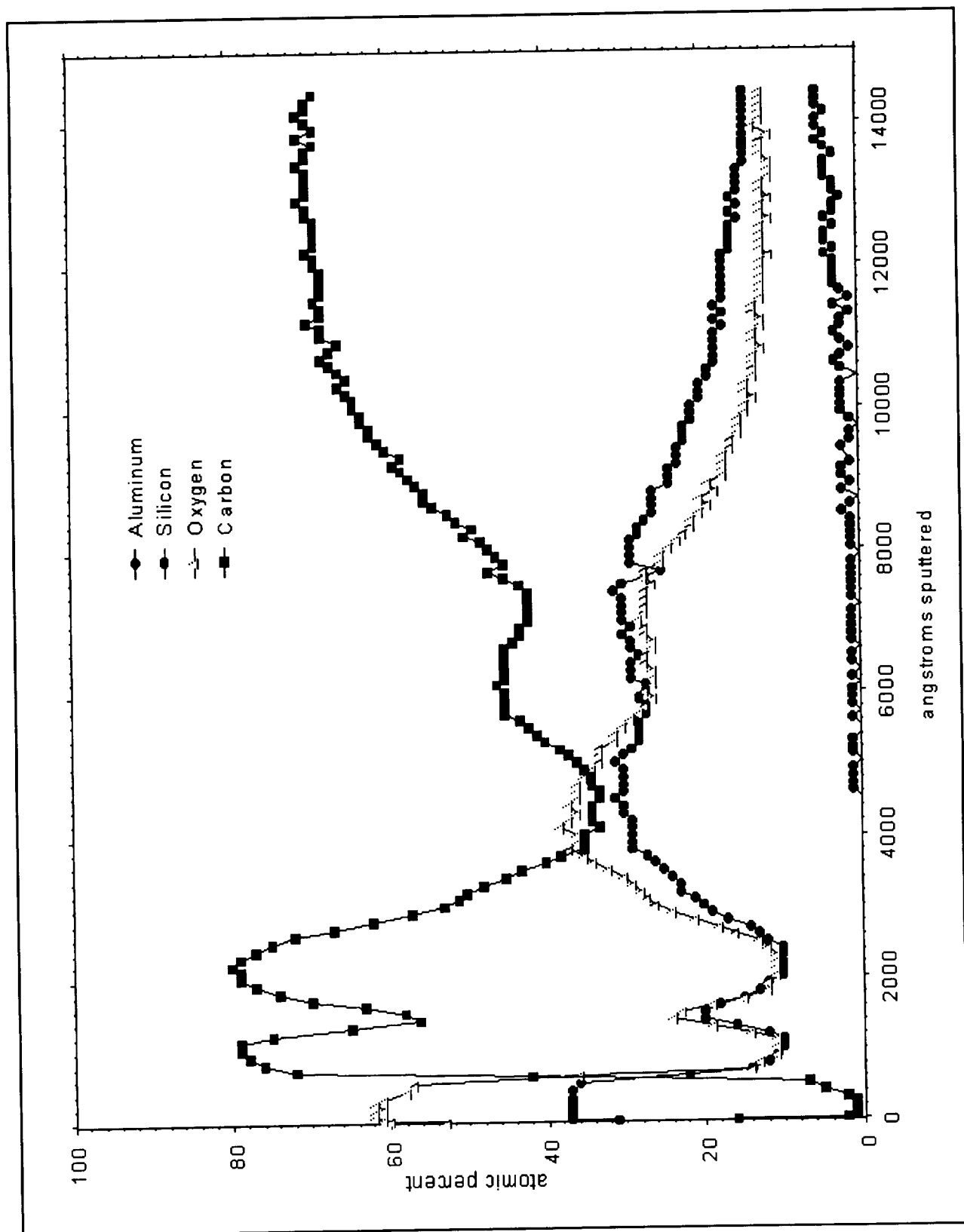


Figure B-17. Tray E10-8 piece B profile 1 (0 to 15000).

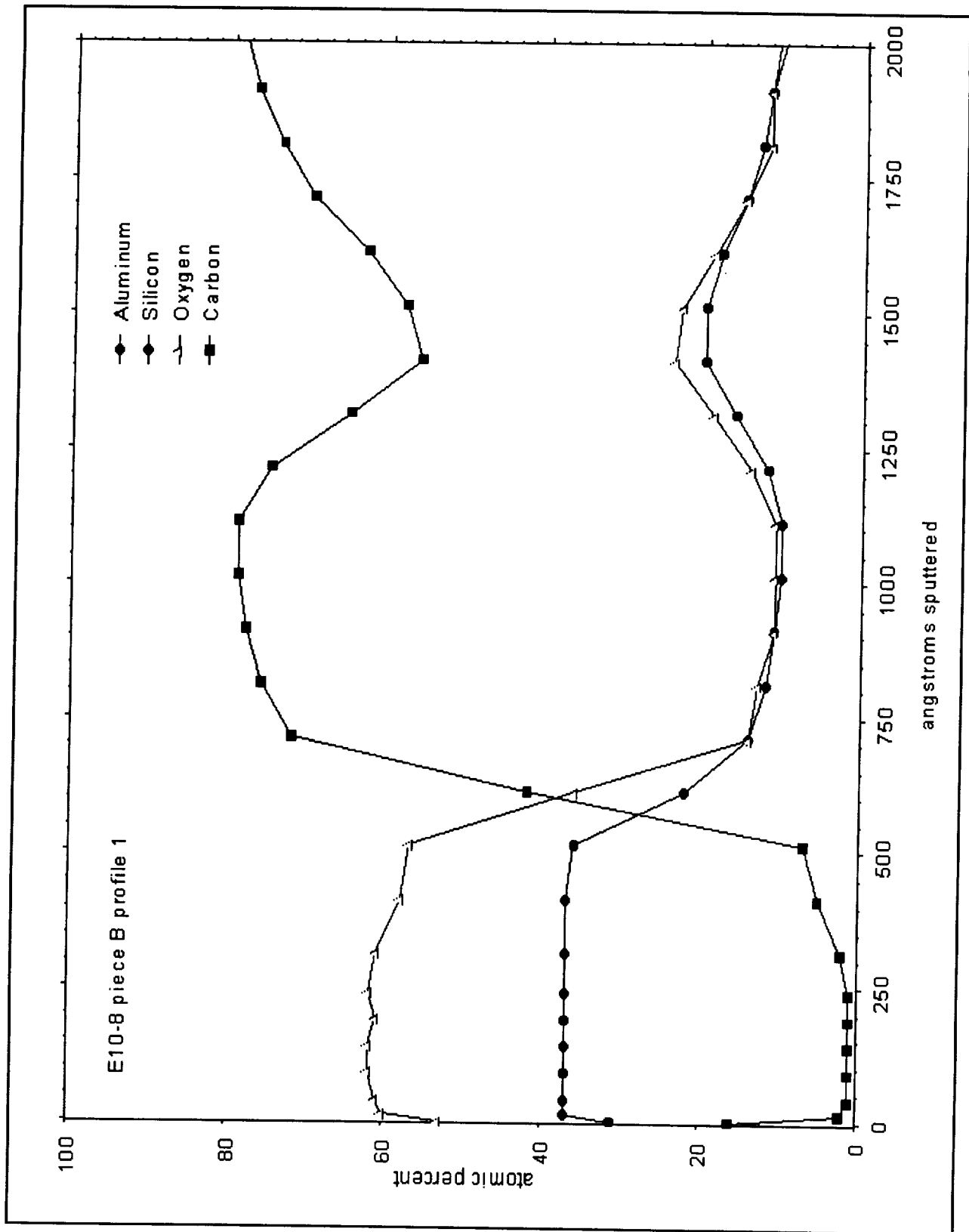


Figure B-18. Tray E10-8 piece B profile 1 (0 to 2000).

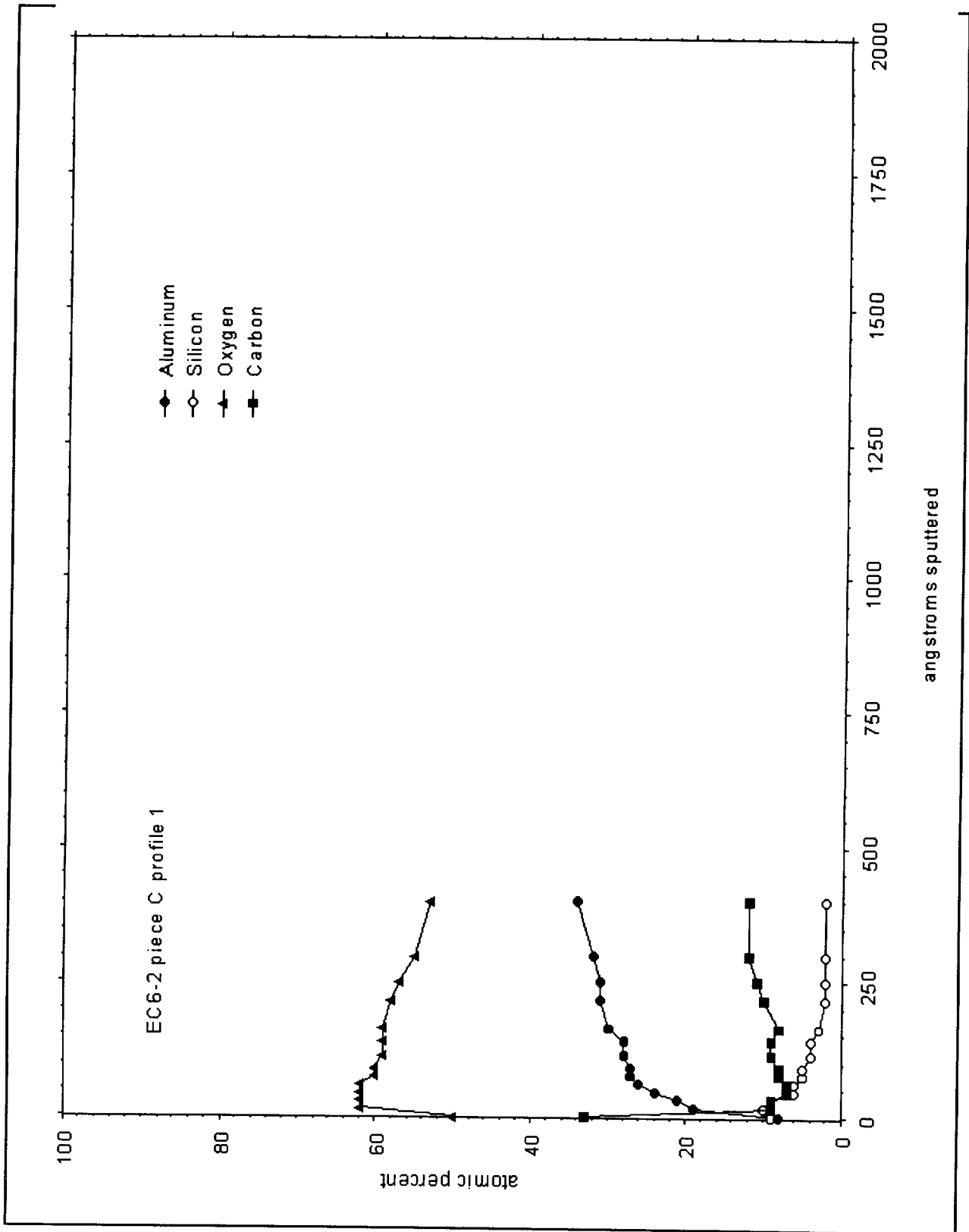


Figure B-20. Tray C6-2 piece C profile 1.

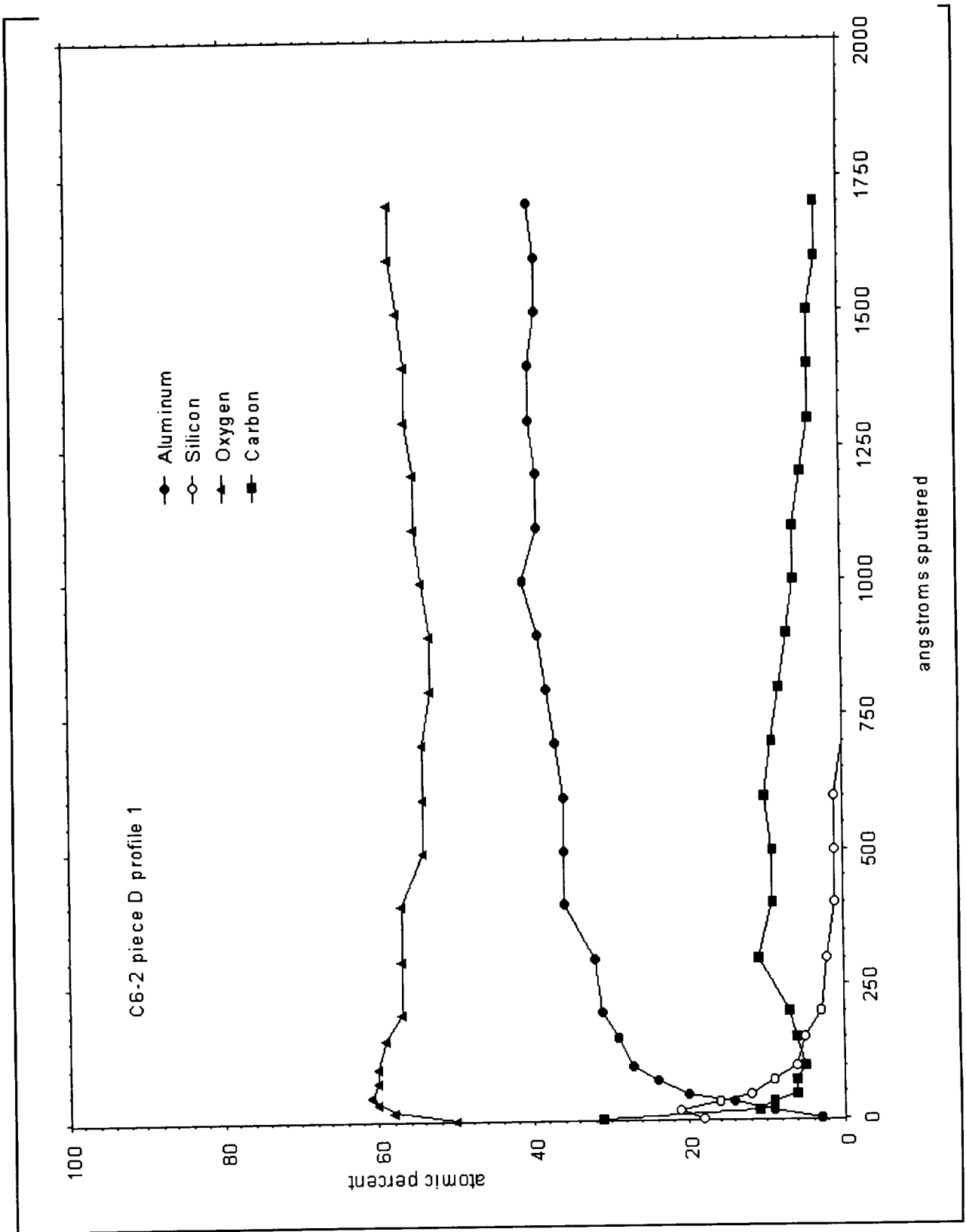


Figure B-21. Tray C6-2 piece D profile 1.

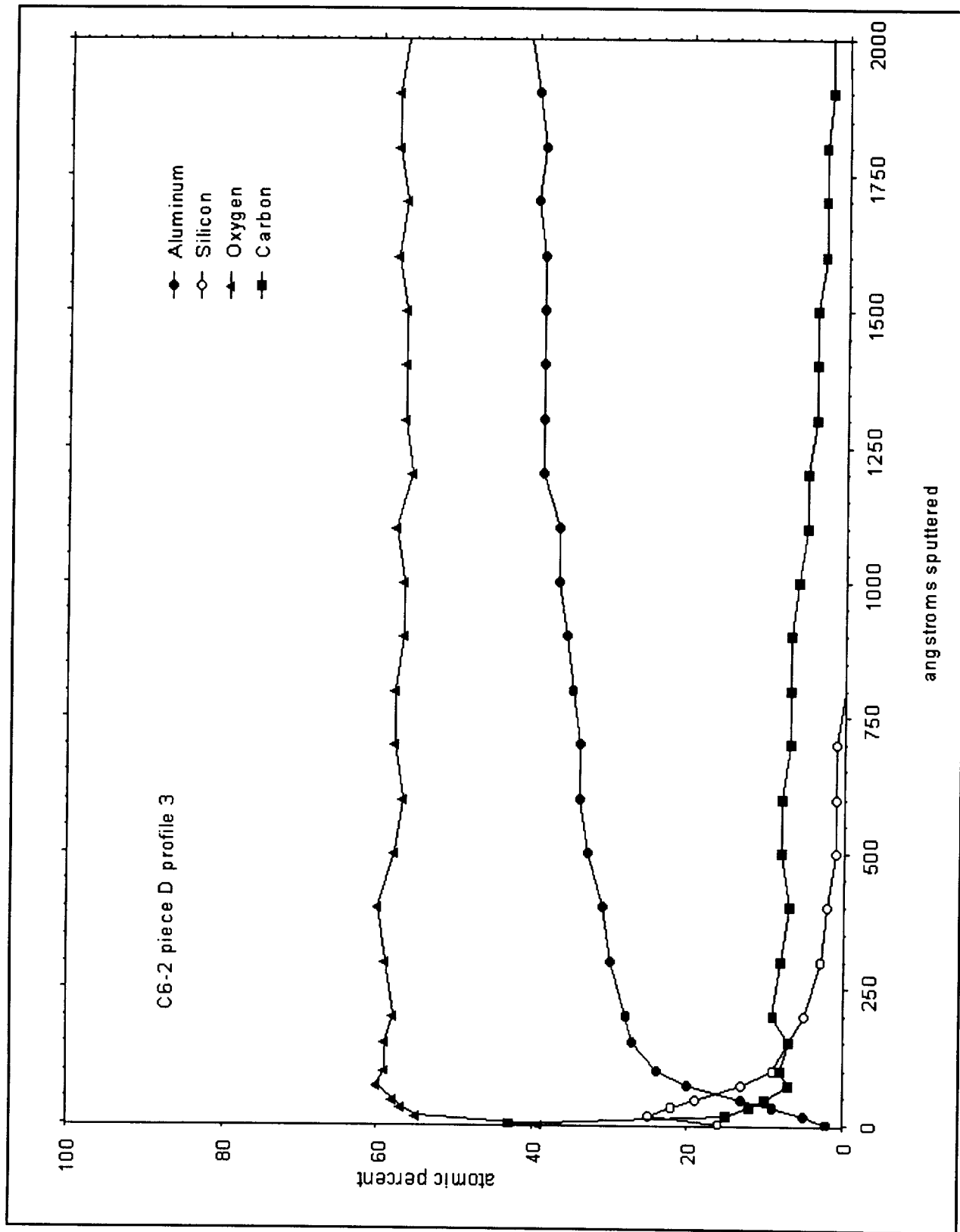


Figure B-22. Tray C6-2 piece D profile 3.

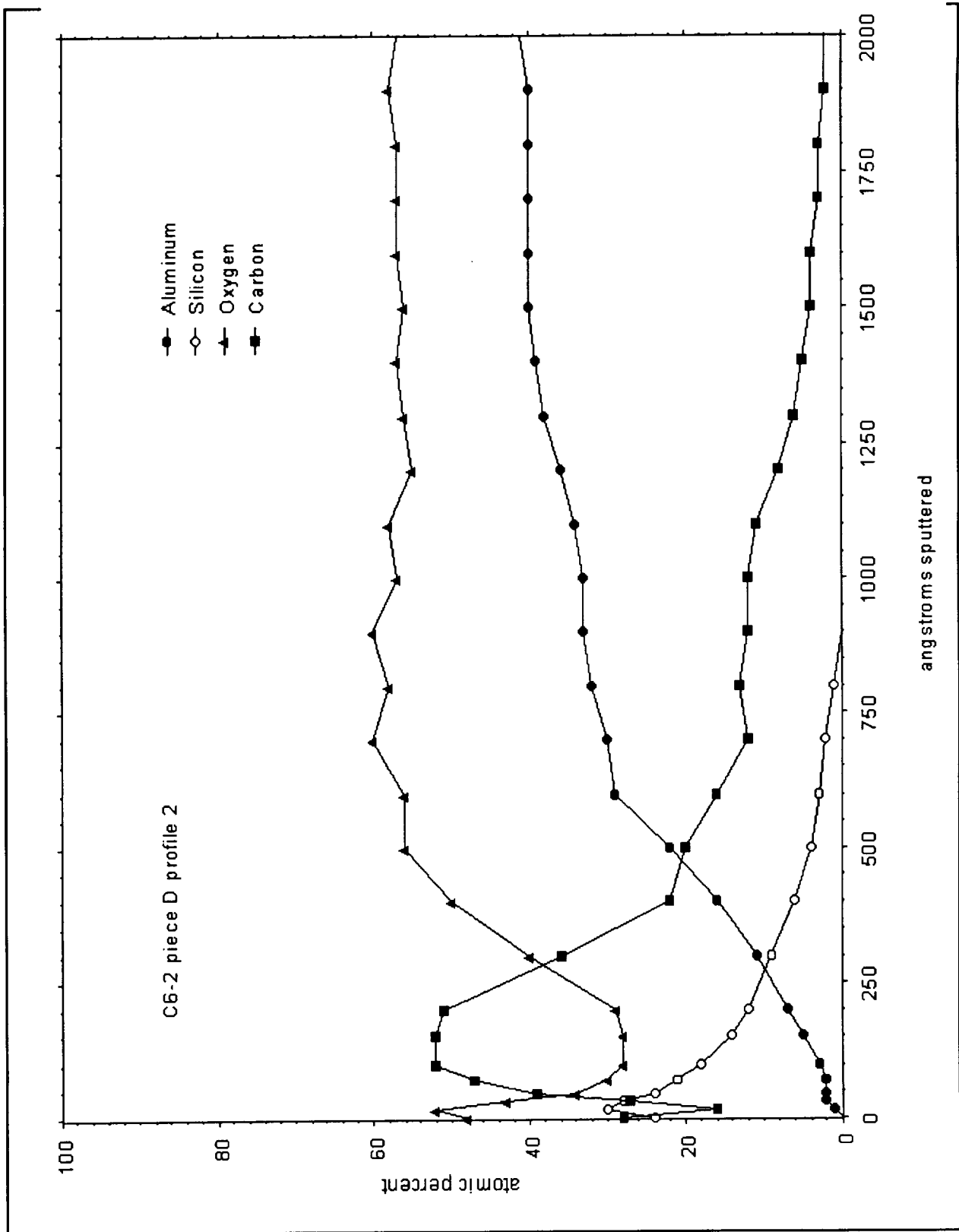


Figure B-23. Tray C6-2 piece D profile 2.

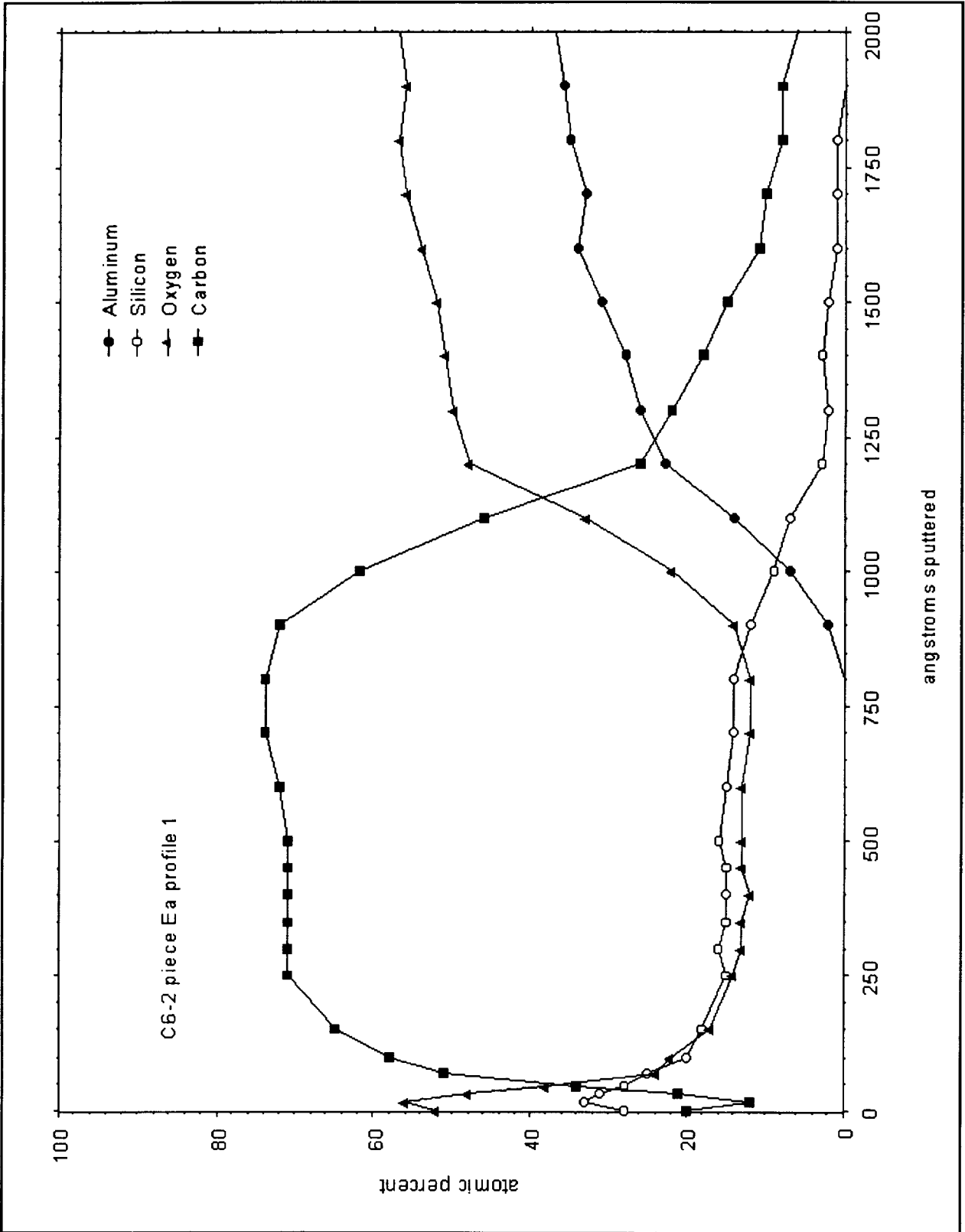


Figure B-24. Tray C6-2 piece Ea profile 1.

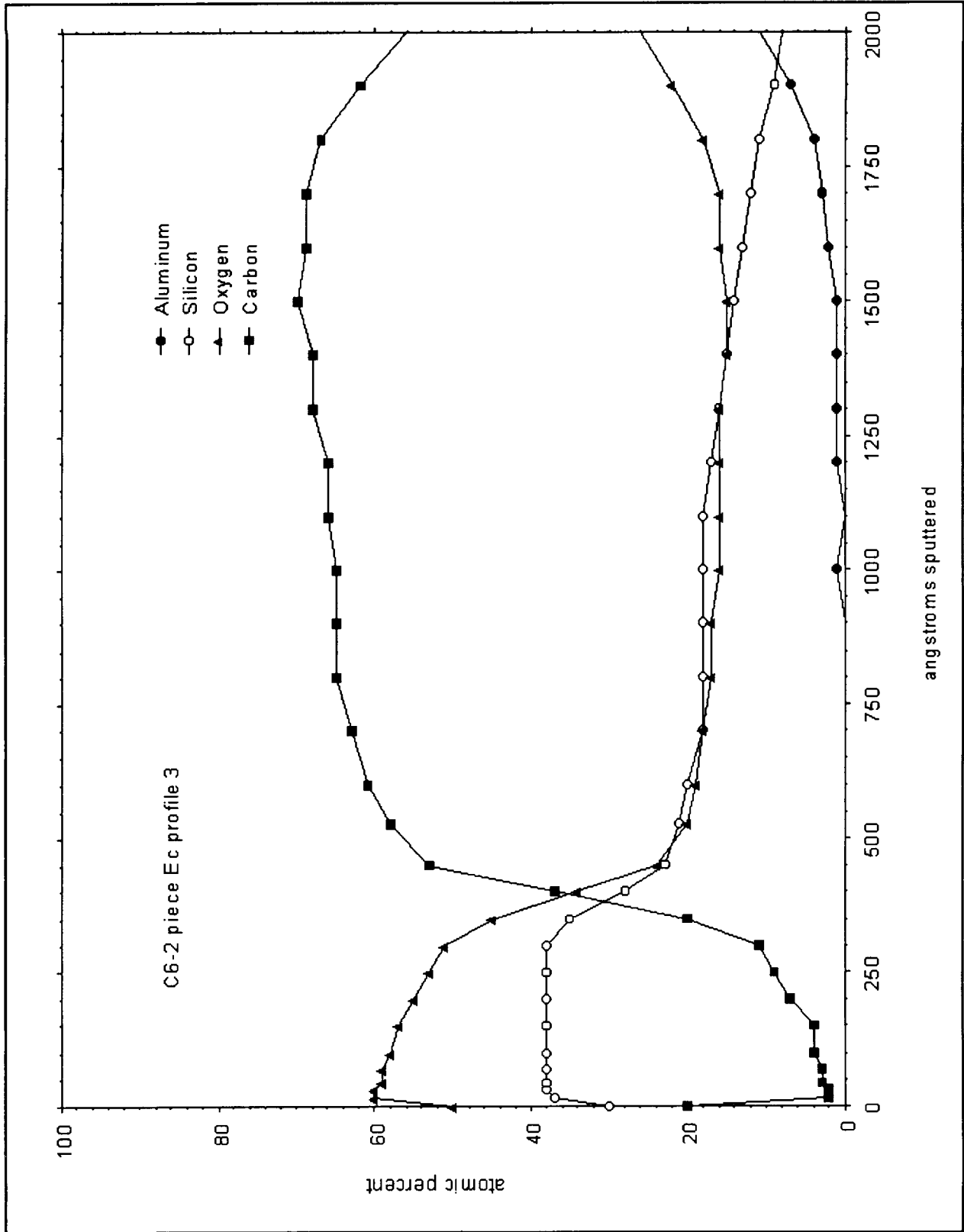


Figure B-25. Tray C6-2 piece Ec profile 3 (0 to 2000).

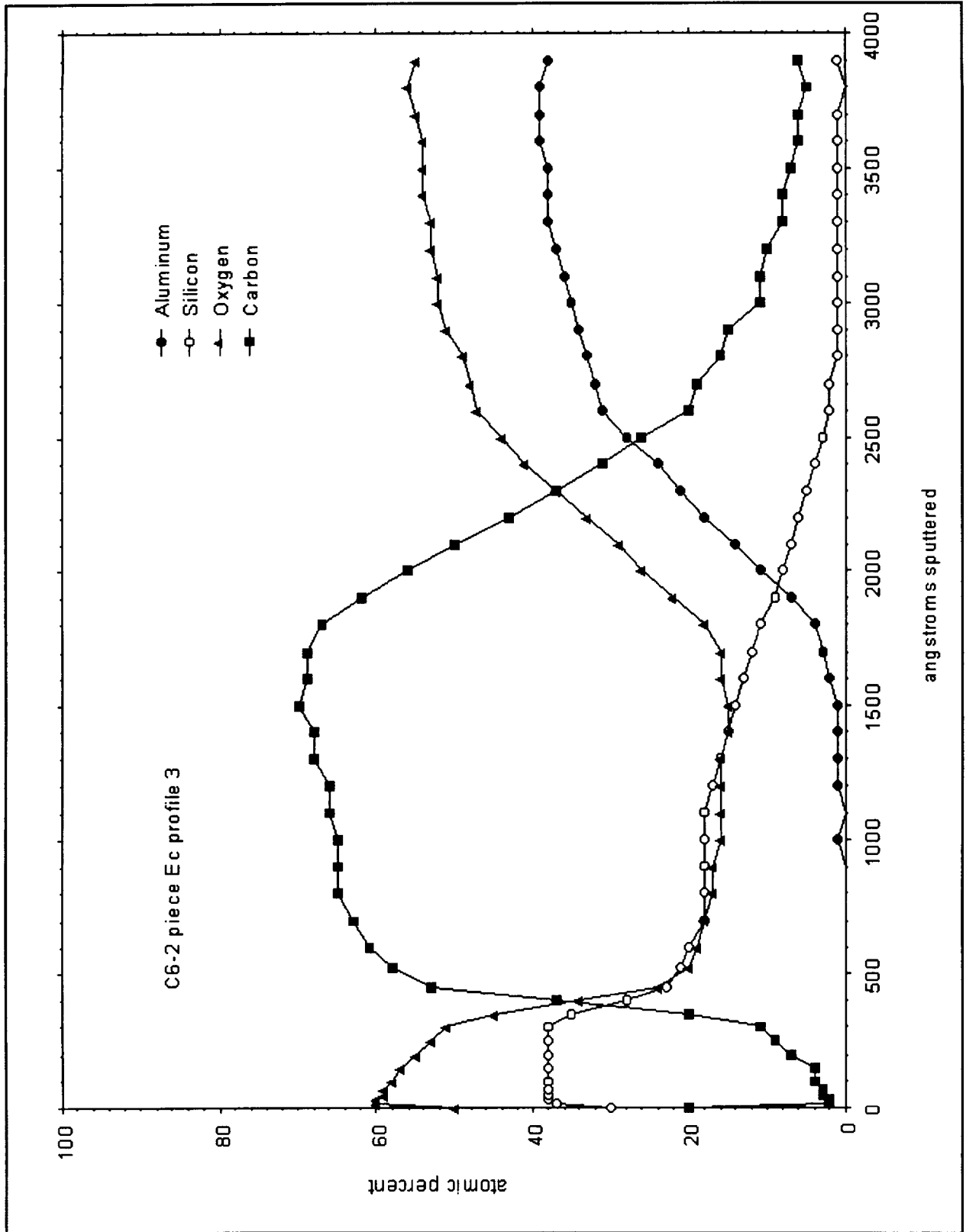


Figure B-26. Tray C6-2 piece Ec profile 3 (0 to 4000).

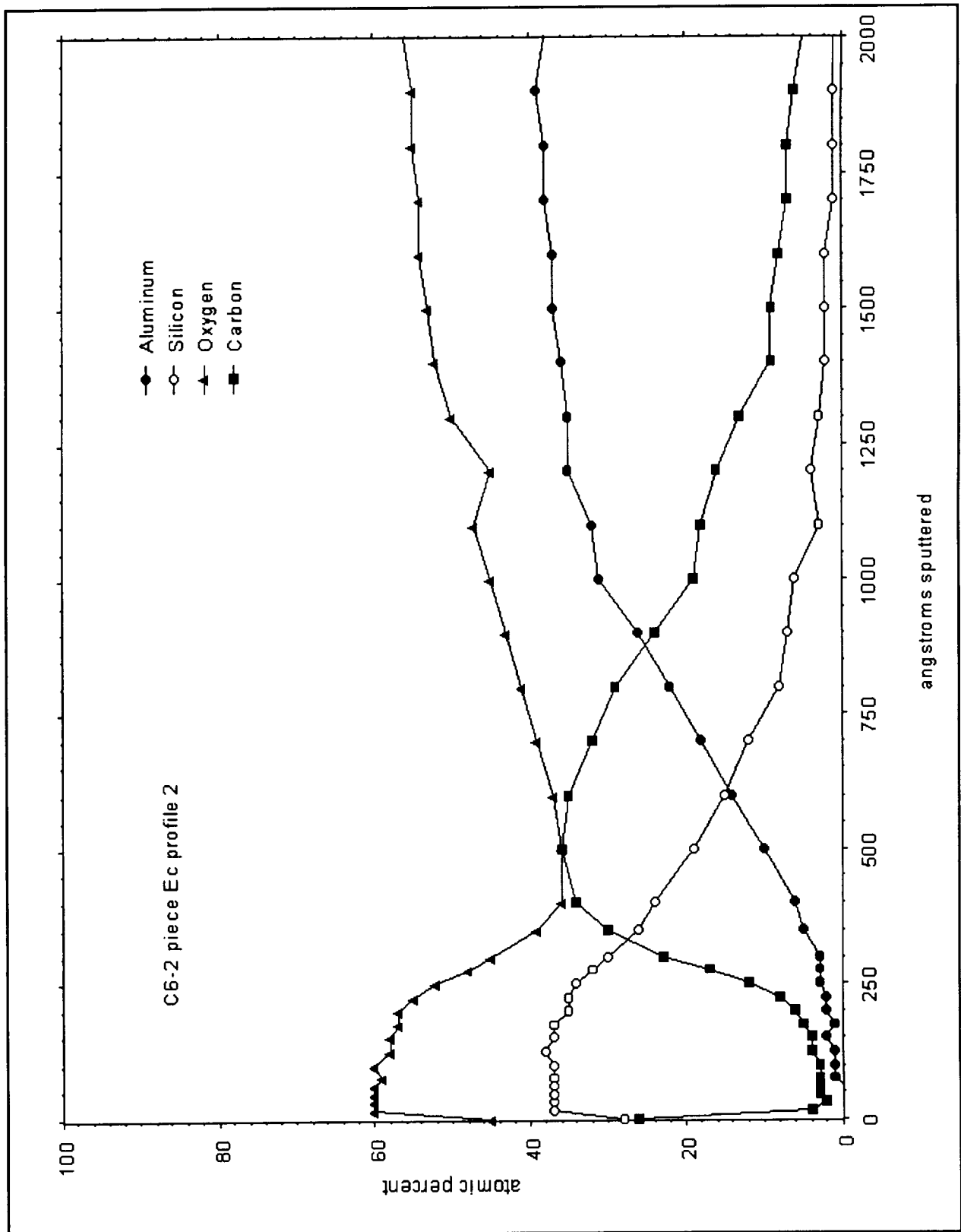


Figure B-27. Tray C6-2 piece Ec profile 2.

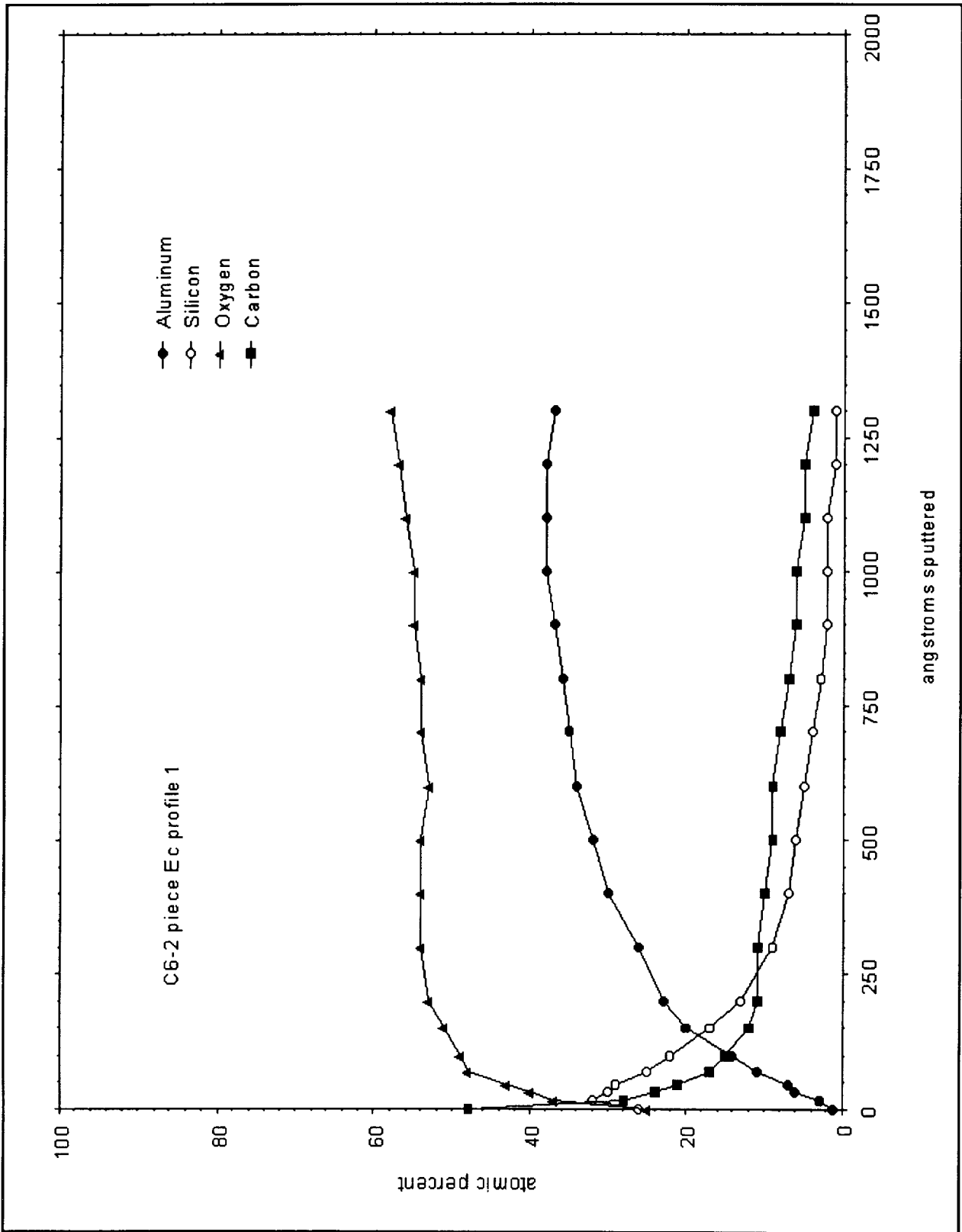


Figure B-28. Tray C6-2 piece Ec profile 1.

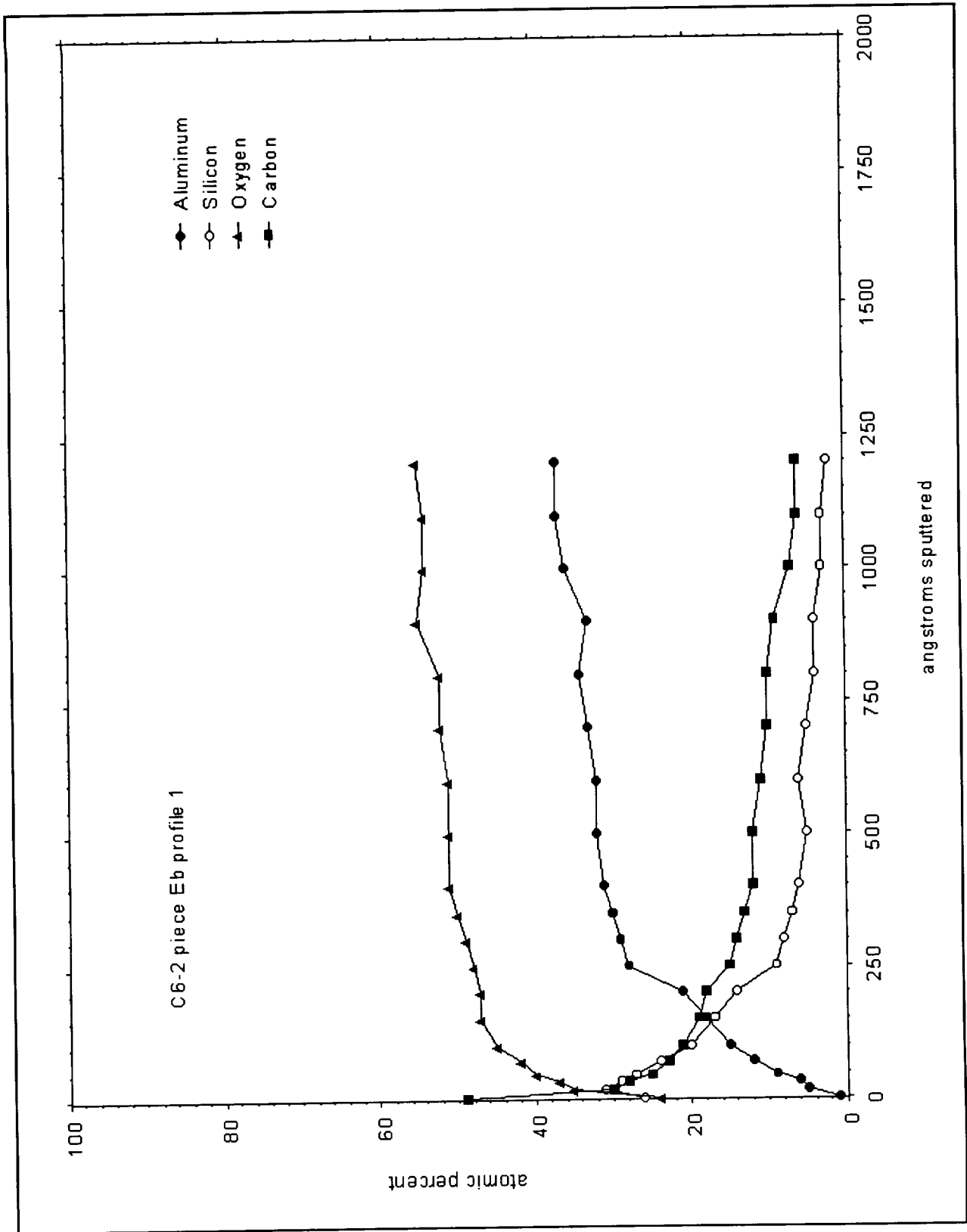


Figure B-29. Tray C6-2 piece Eb profile 1.

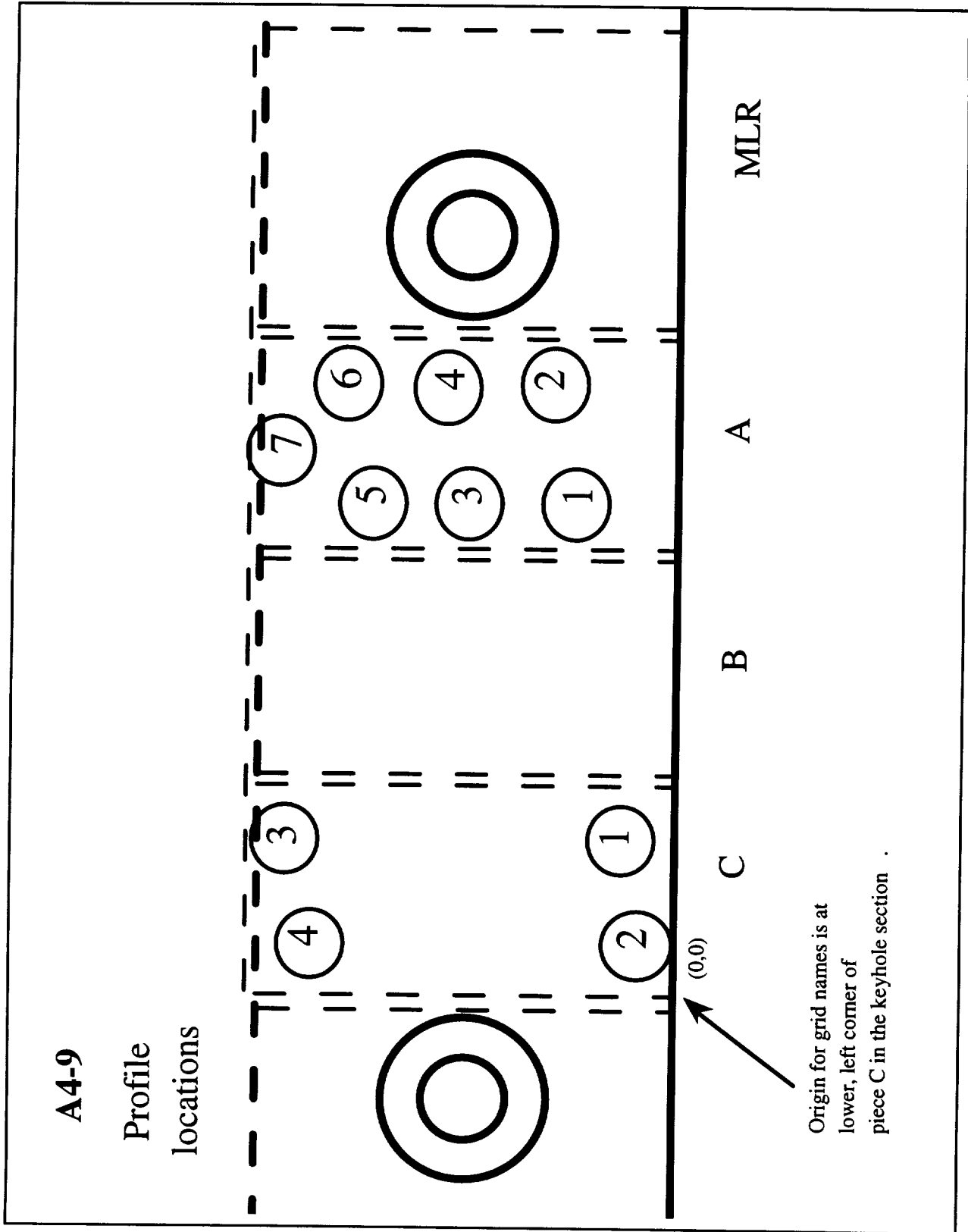


Figure B-30. Tray A4-9 Profile locations.

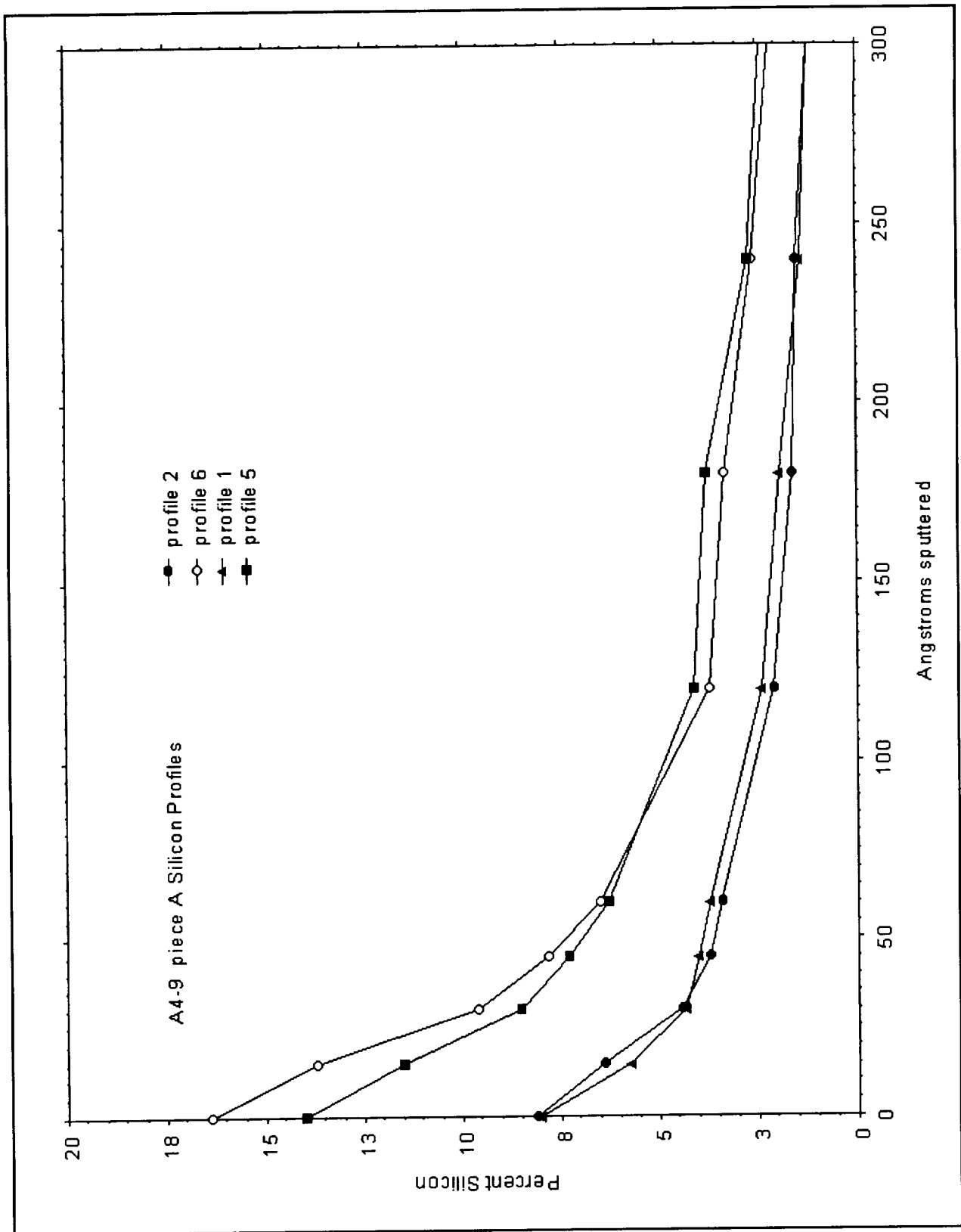


Figure B-31. Tray A4-9 piece A Silicon profiles.

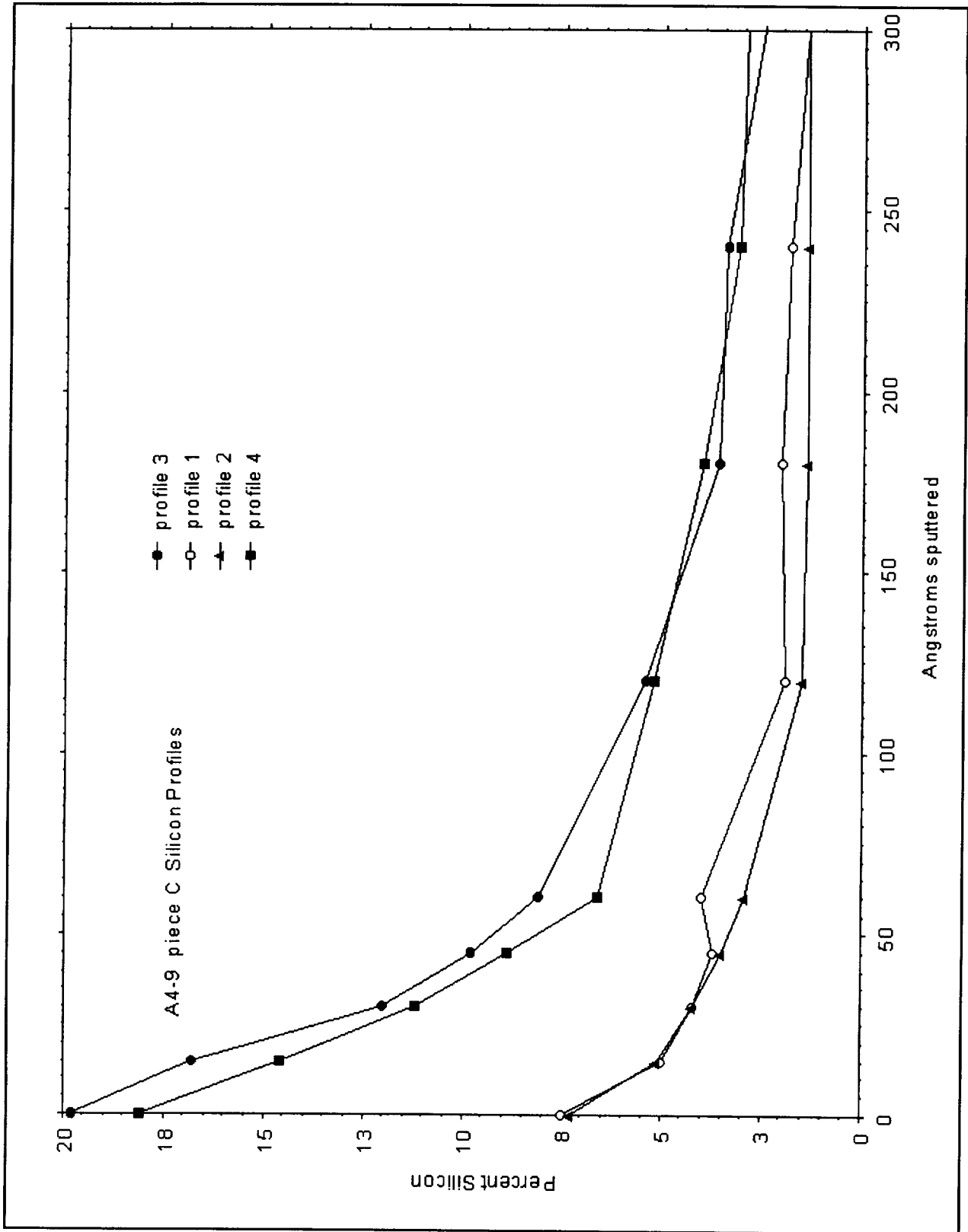


Figure B-32. Tray A4-9 piece C Silicon profiles.

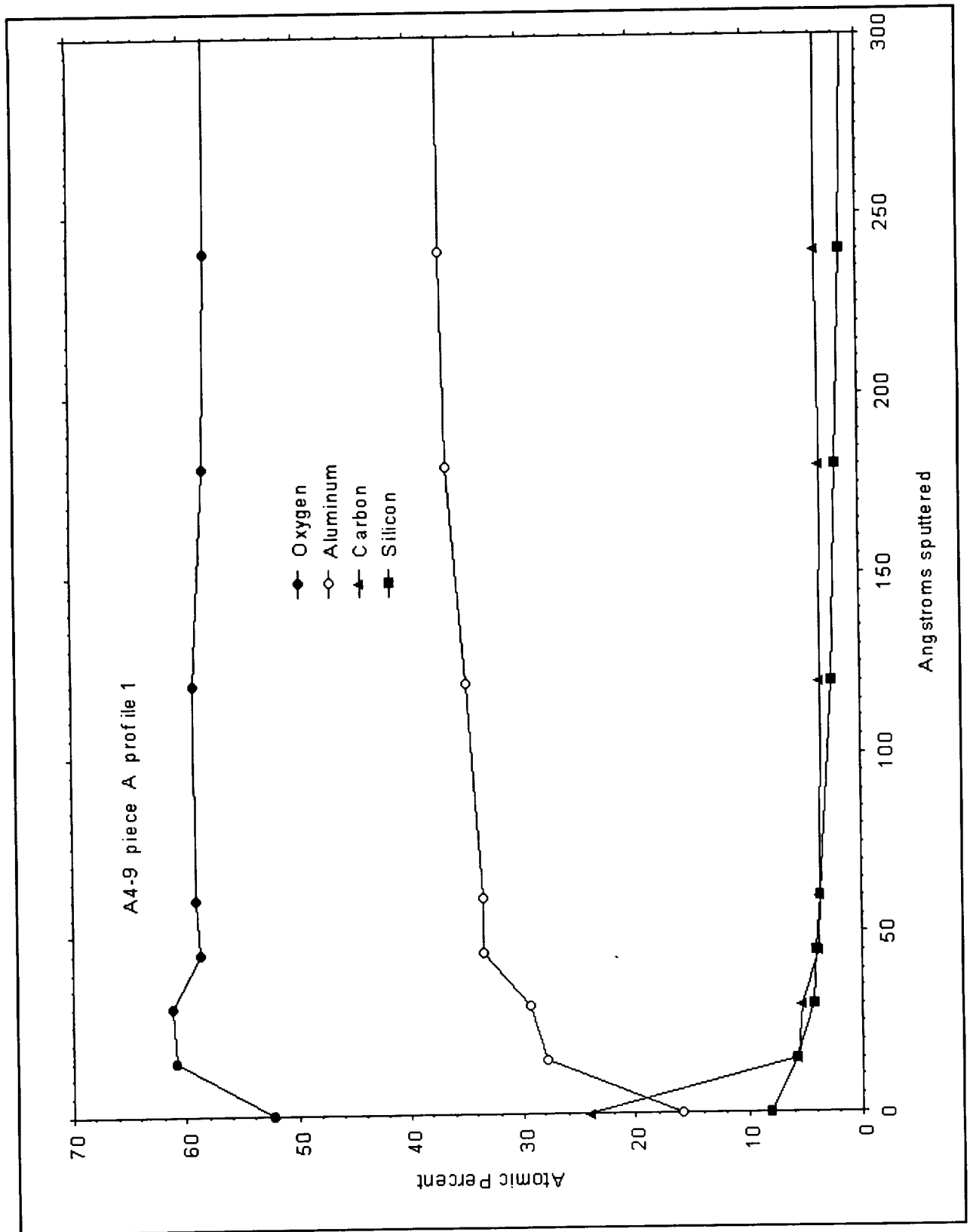


Figure B-33. Tray A4-9 piece A profile 1.

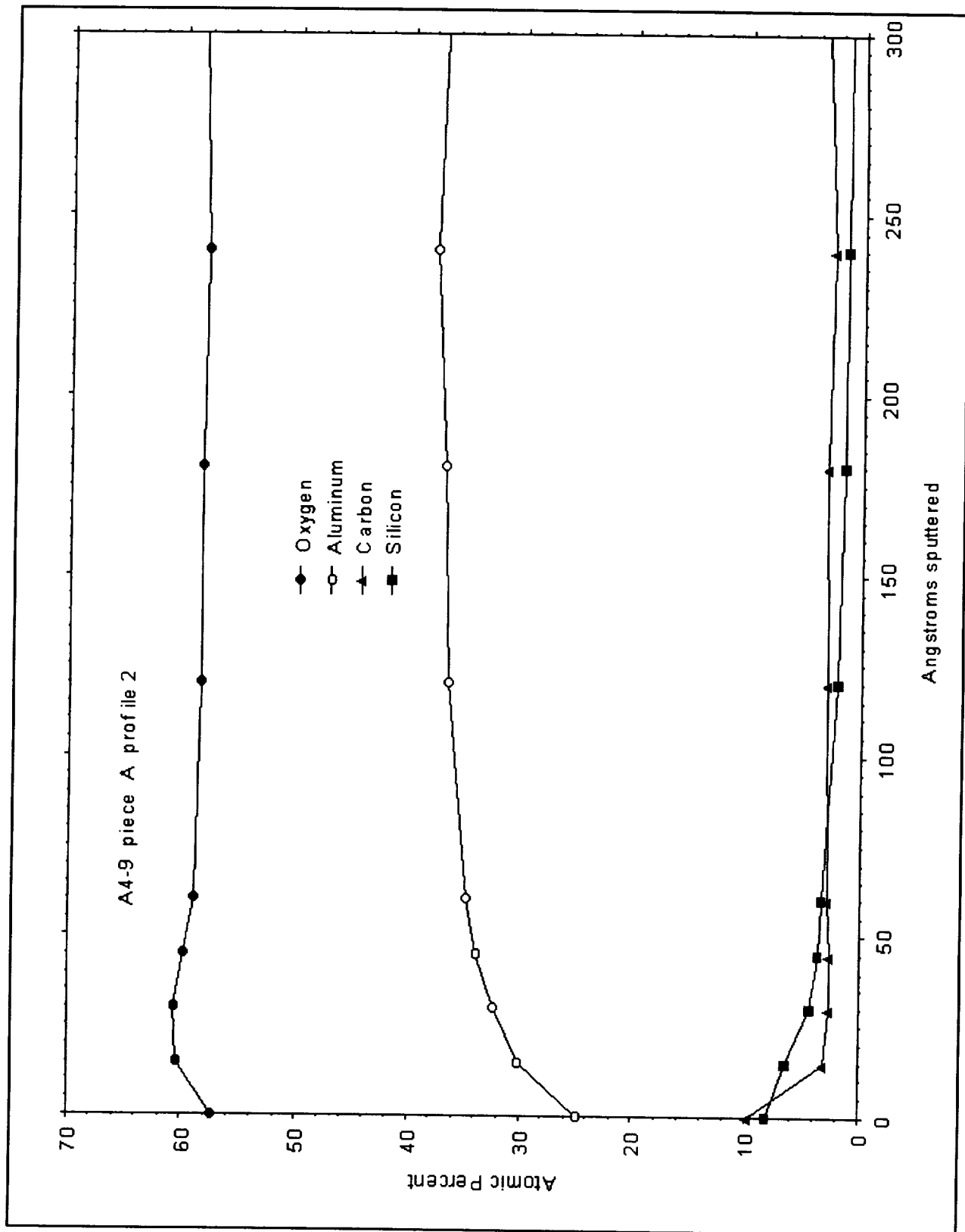


Figure B-34. Tray A4-9 piece A profile 2.

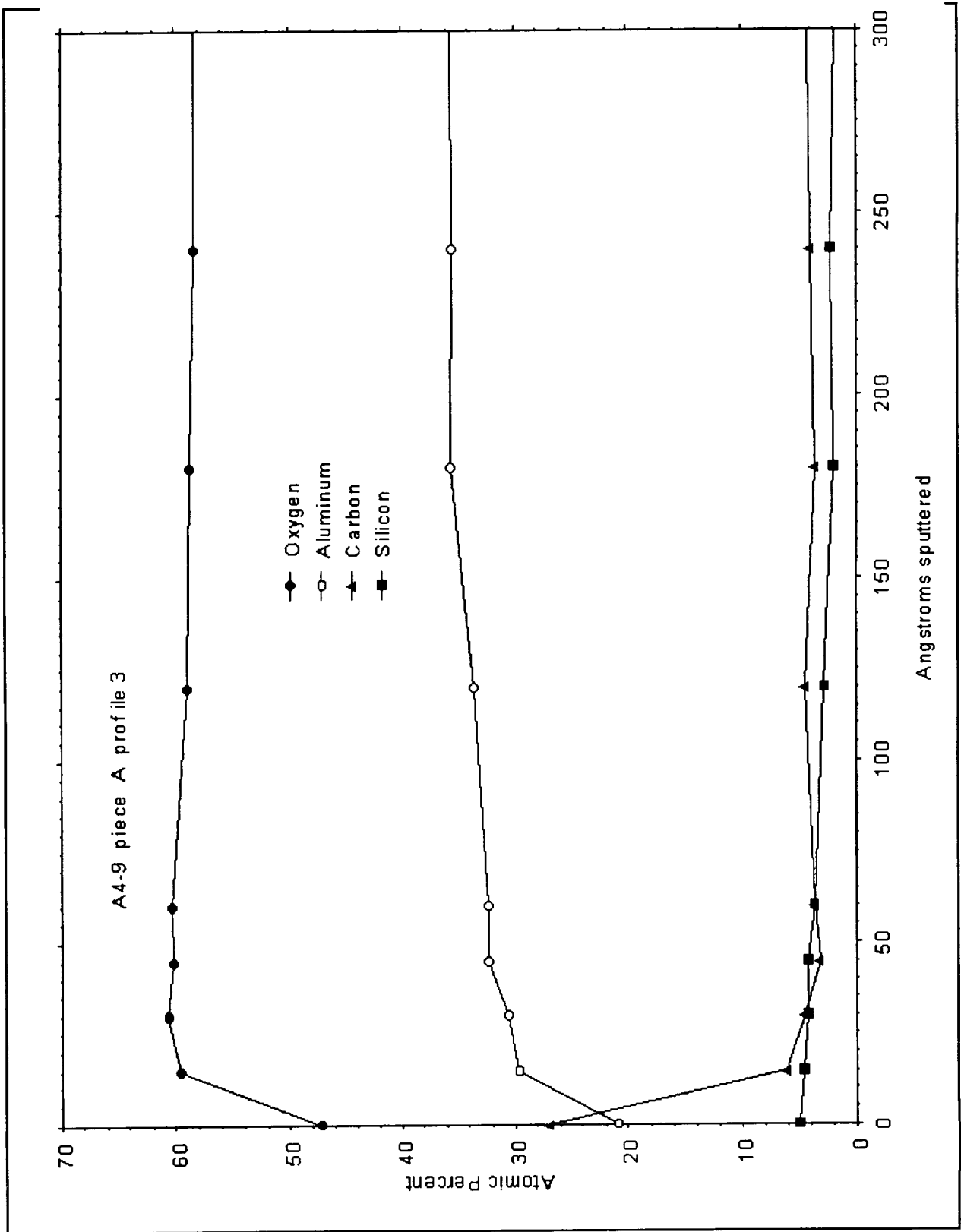


Figure B-35. Tray A4-9 piece A profile 3.

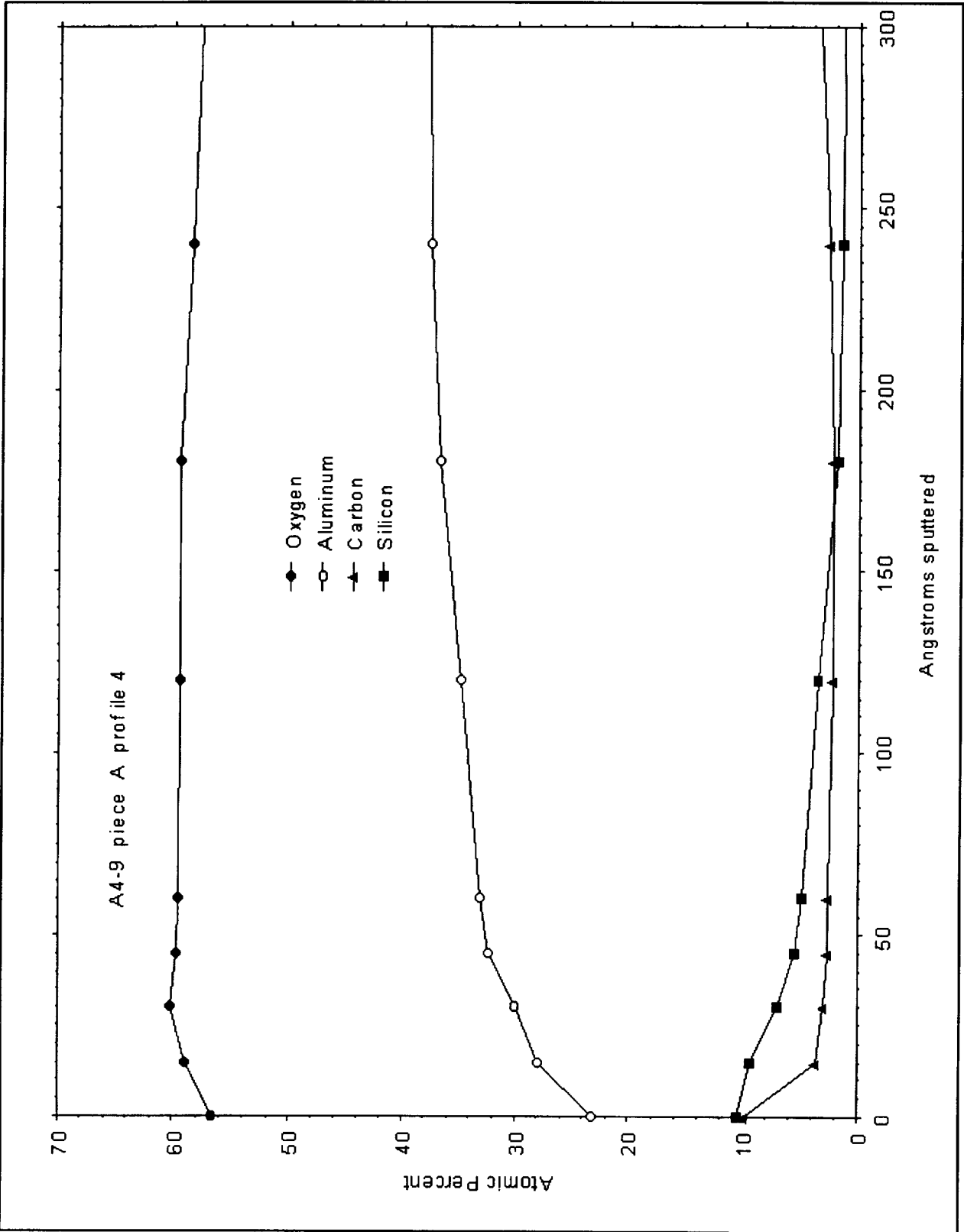


Figure B-36. Tray A4-9 piece A profile 4.

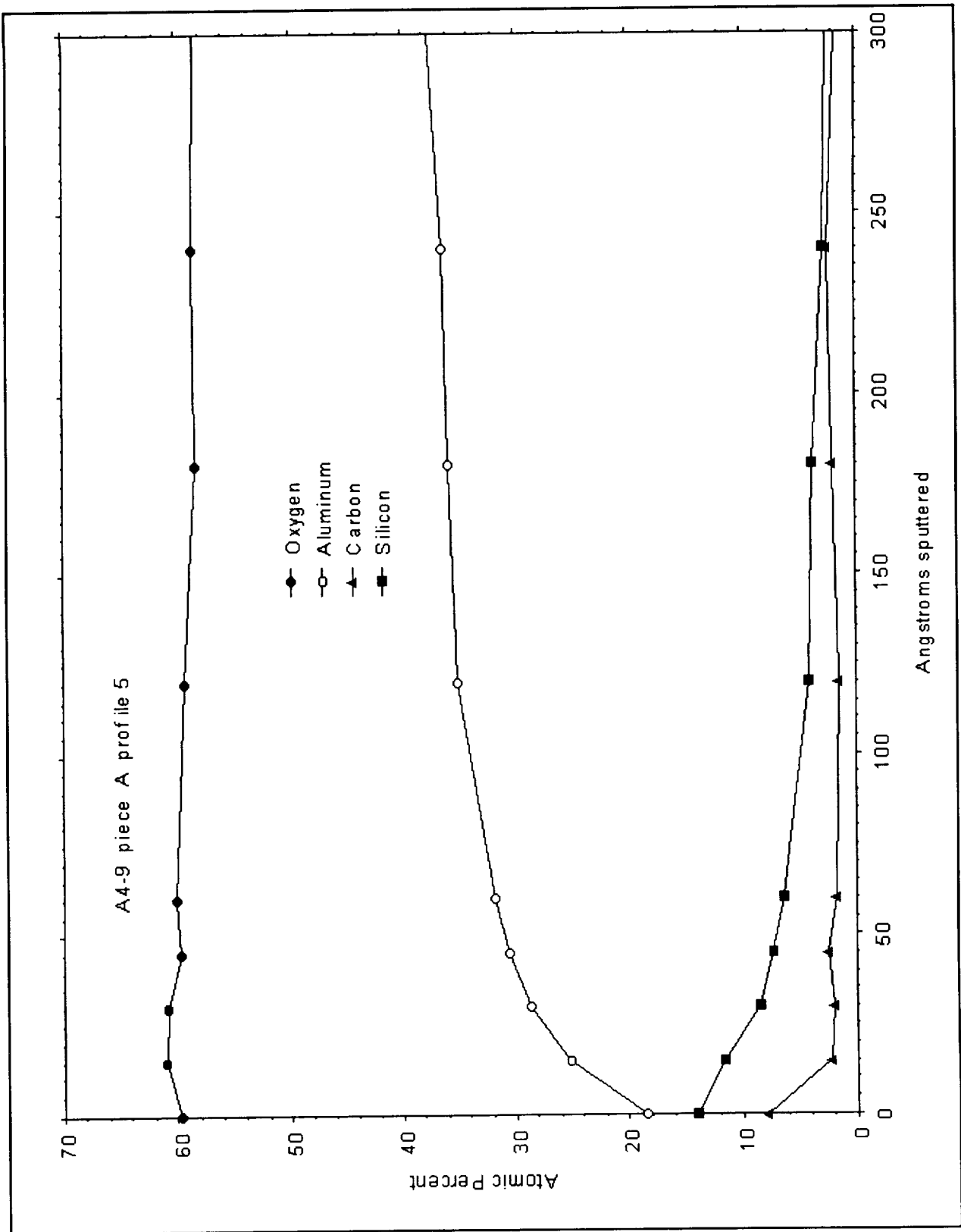


Figure B-37. Tray A4-9 piece A profile 5.

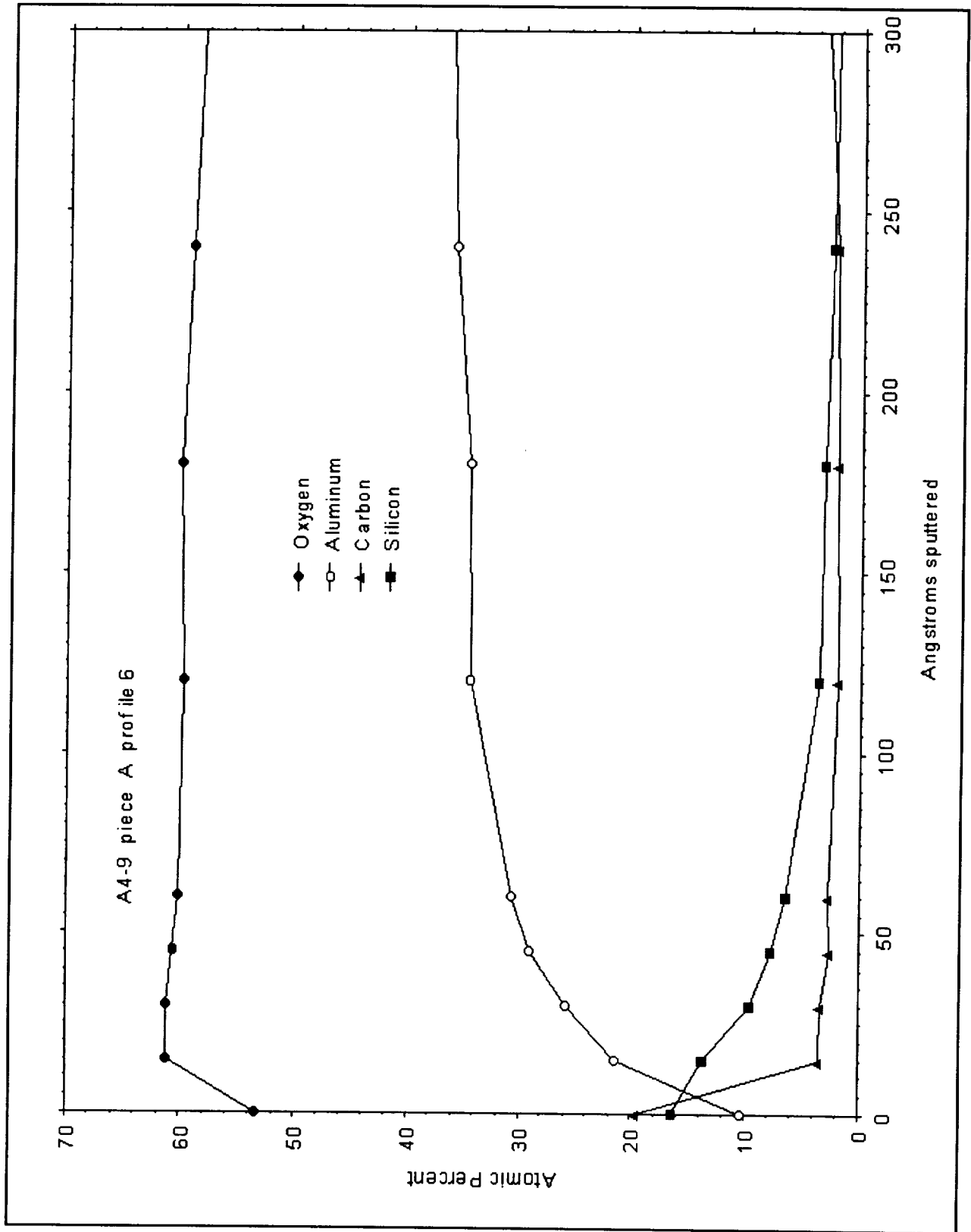


Figure B-38. Tray A4-9 piece A profile 6.

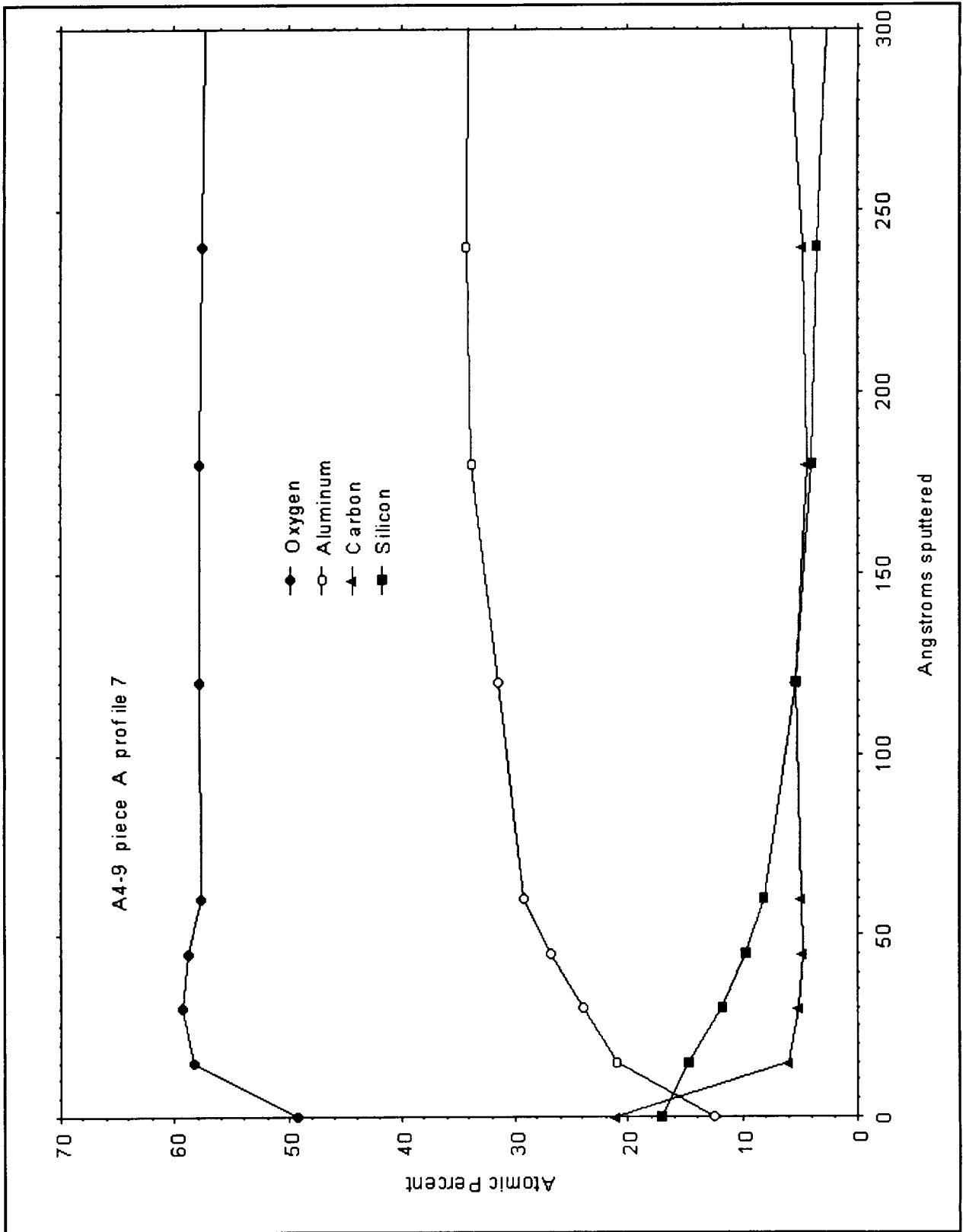


Figure B-39. Tray A4-9 piece A profile 7.

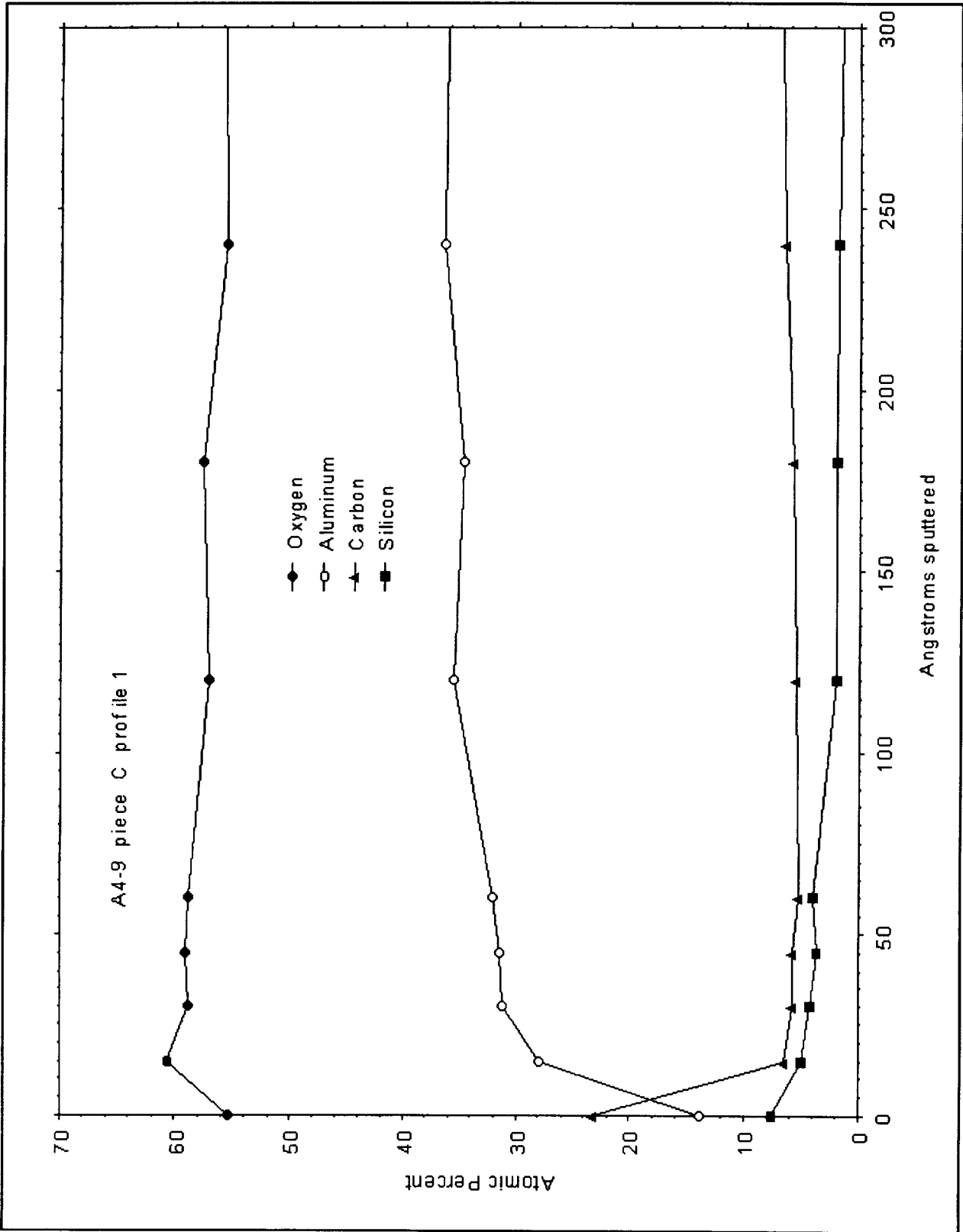


Figure B-40. Tray A4-9 piece C profile 1.

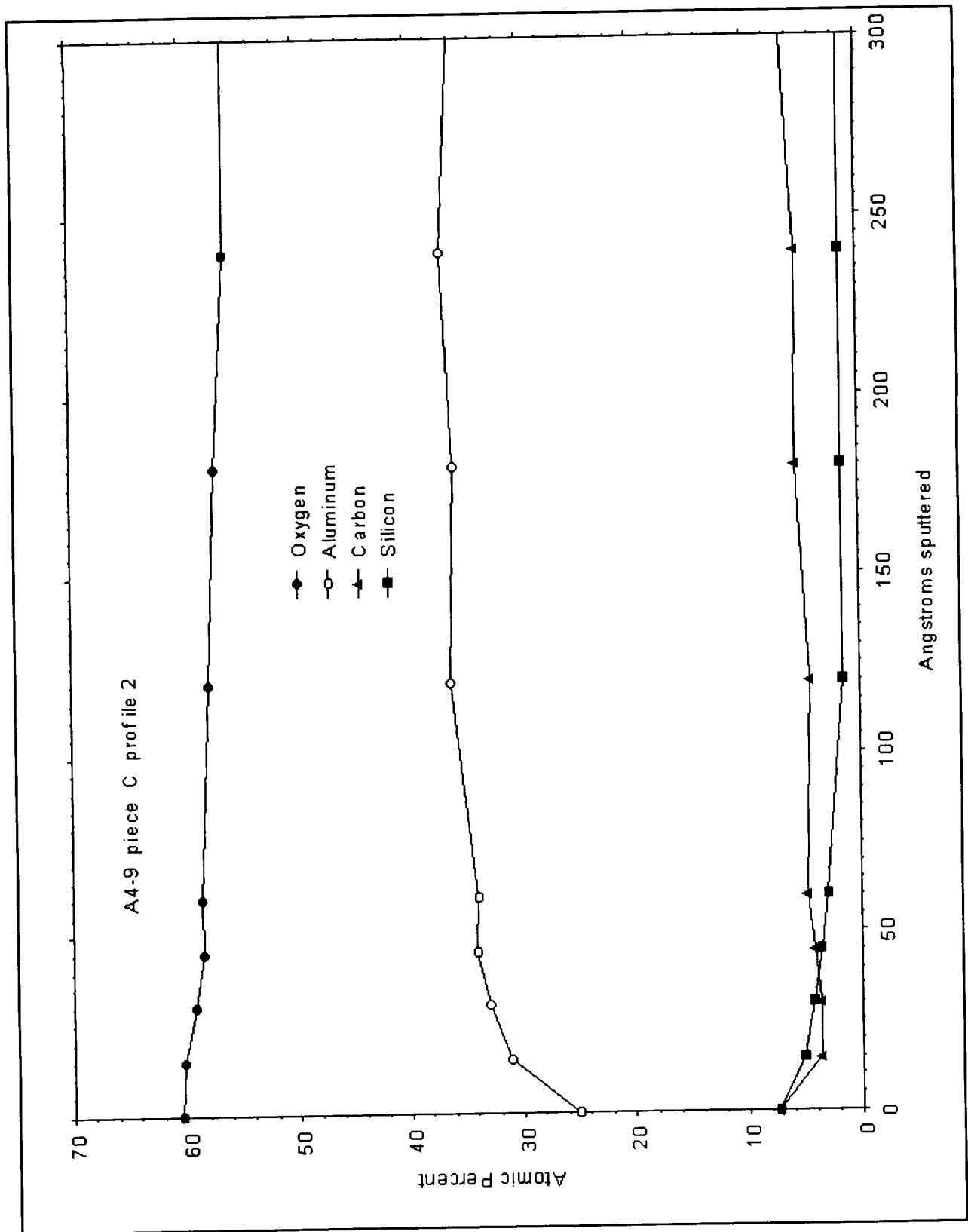


Figure B-41. Tray A4-9 piece C profile 2.

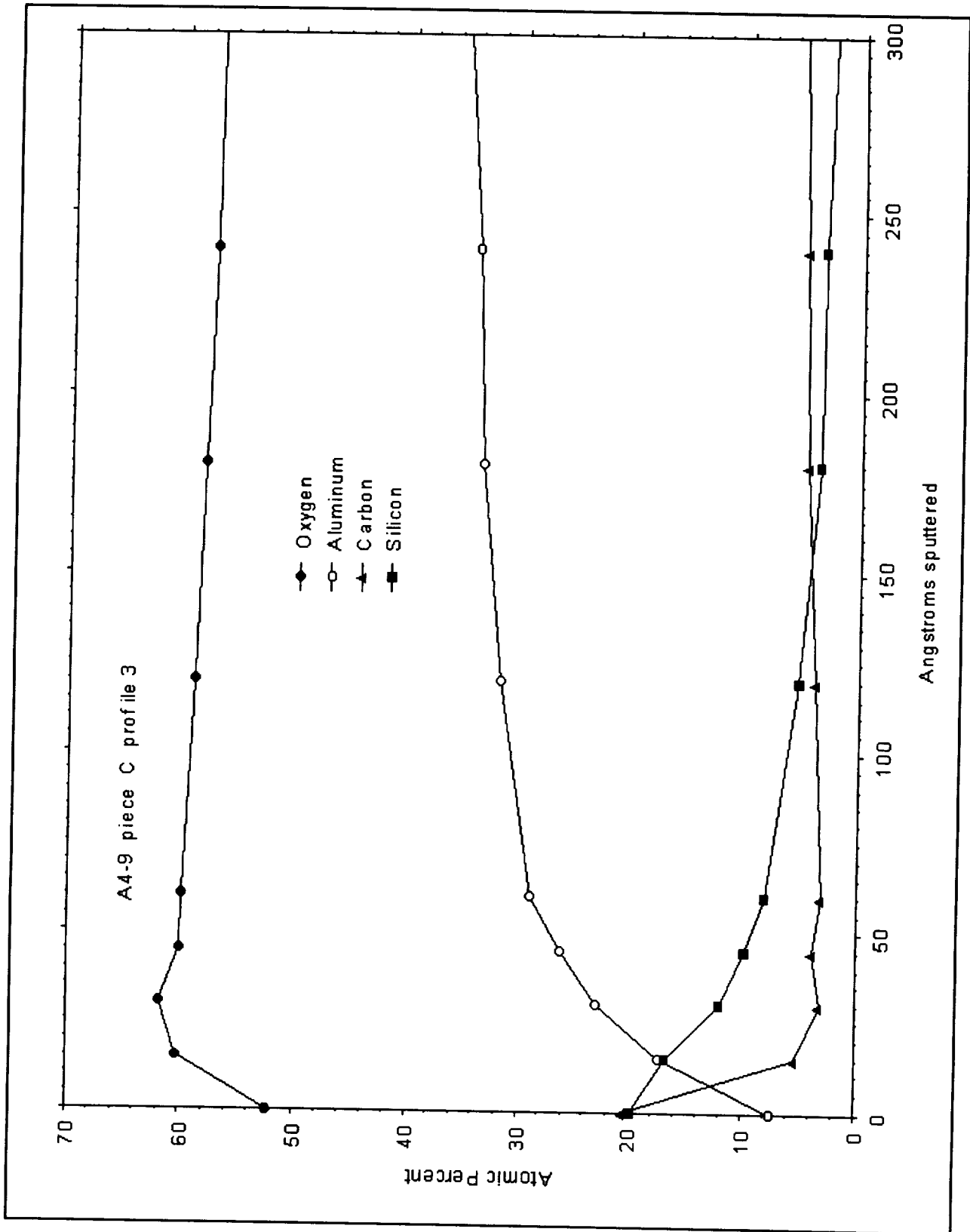


Figure B-42. Tray A4-9 piece C profile 3.

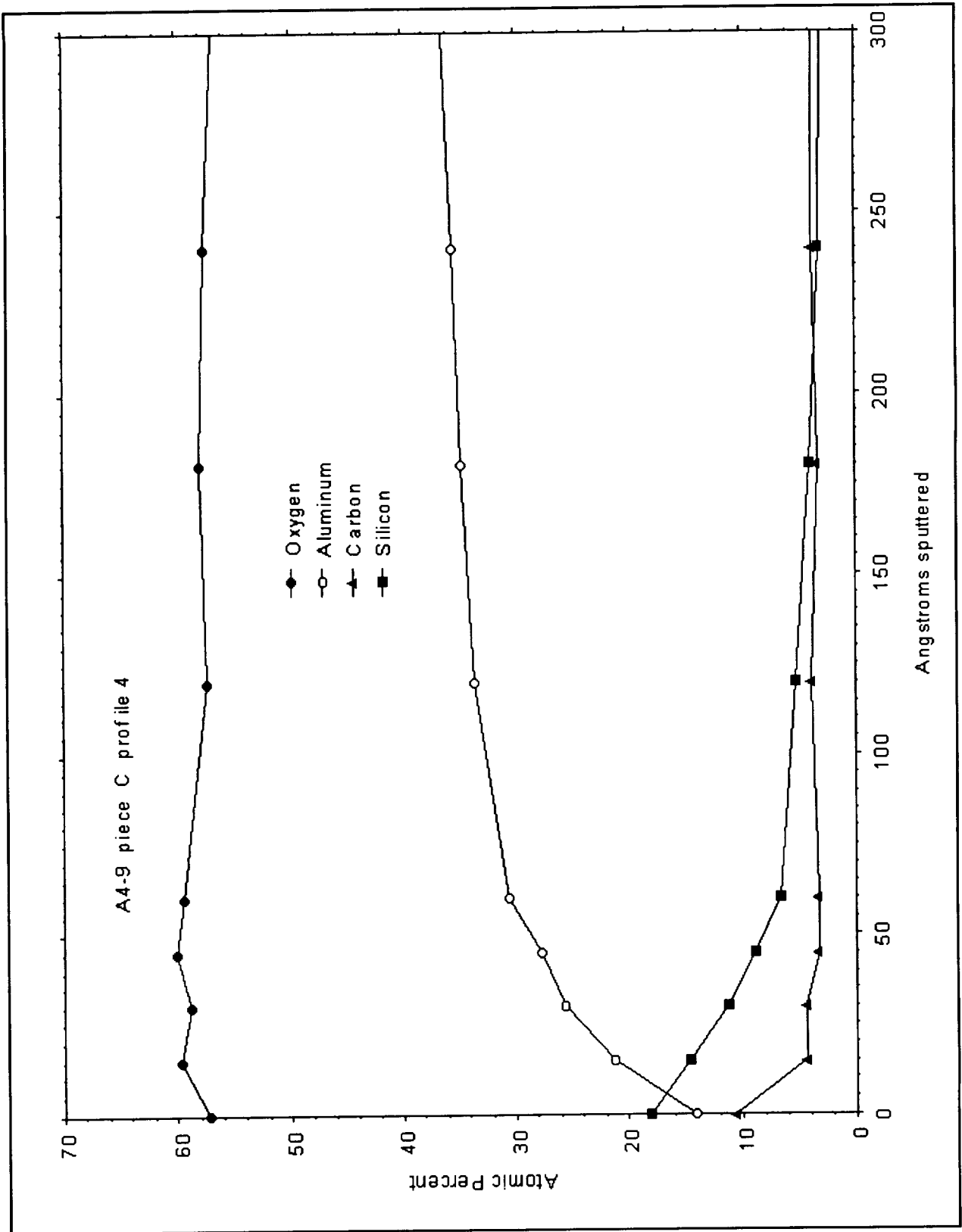


Figure B-43. Tray A4-9 piece C profile 4.

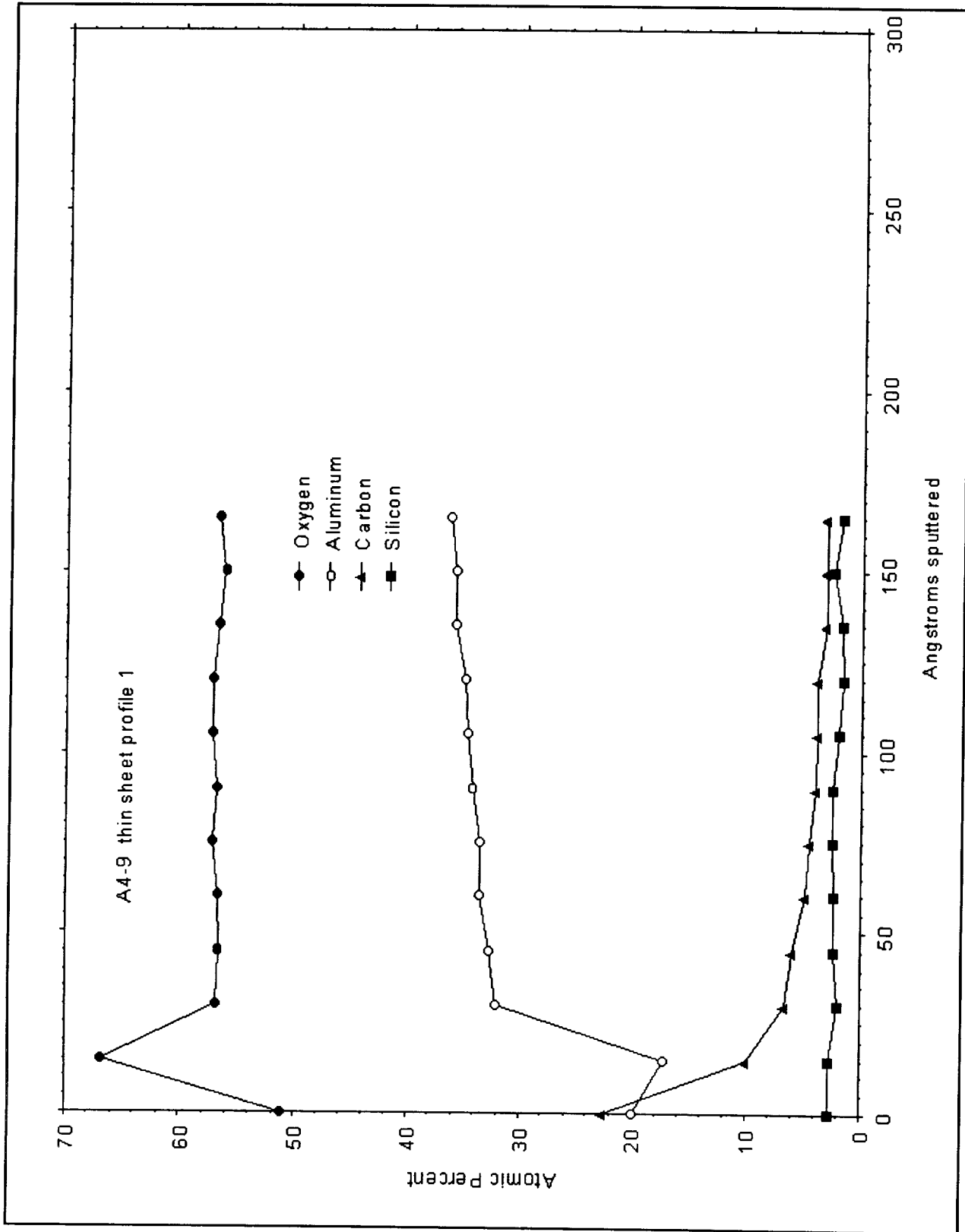


Figure B-44. Tray A4-9 thin sheet profile 1.

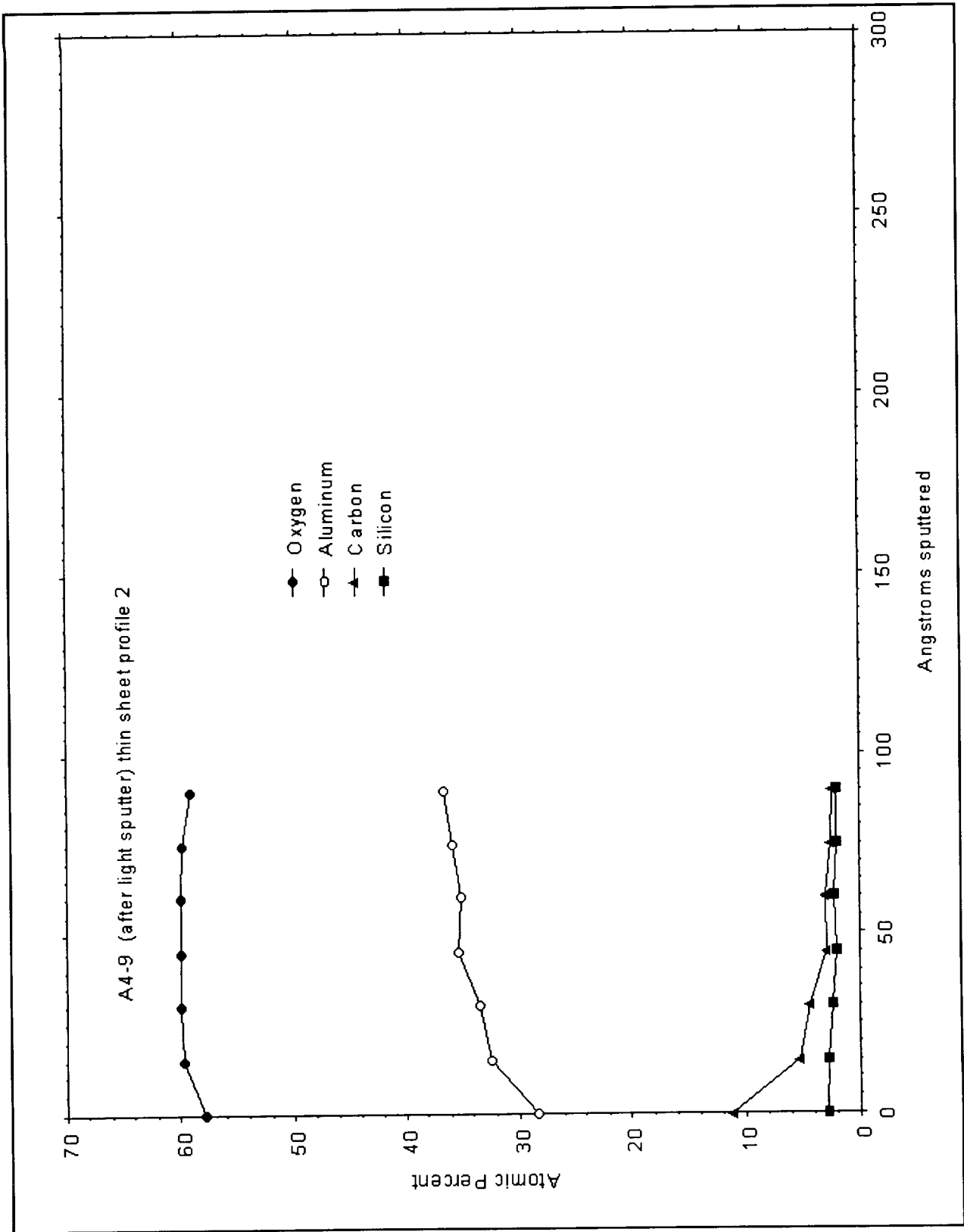


Figure B-45. Tray A4-9 thin sheet profile 2.

Appendix C

Plots of Solar UV and Atomic Oxygen Exposure Levels at Selected Locations on the LDEF Trays being Examined

Introduction

This appendix contains a number of cross sectional plots showing the Cumulative Equivalent Sun Hours (CESH) of solar exposure, or the fluence of atomic oxygen in atoms/cm², as functions of distance from the edge of the particular tray. Plots generally show exposure intensity from the edge of the tray to the surface immediately across from the base of the blanket vent hole. Each cross-section shows a constant exposure level initially. This portion of each plot represents the exposure on the lip of the particular tray. The x-axis caption "DISTANCE FROM BOTTOM EDGE (MM)" refers to distance from the edge of the tray lip in millimeters.

List of Figures

Figure C-1.	Cross-section for E10-7 surface showing Cumulative Equivalent Sun Hours as a Function of Location.	C4
Figure C-2.	Cross-section for E10-7 surface showing Atomic Oxygen Fluence as a Function of Location.	C5
Figure C-3.	Cross-section for C6-2 surface showing Cumulative Equivalent Sun Hours as a Function of Location.	C6
Figure C-4.	Cross-section for C6-2 surface showing Atomic Oxygen Fluence as a Function of Location.	C7
Figure C-5.	Cross-section for A4-1 surface showing Cumulative Equivalent Sun Hours as a Function of Location at Tray Vent (KEYHOLE).	C8
Figure C-6.	Cross-section for E10-7 surface showing Cumulative Equivalent Sun Hours as a Function of Location for Tray Surface near Tray Vent (KEYHOLE).	C9

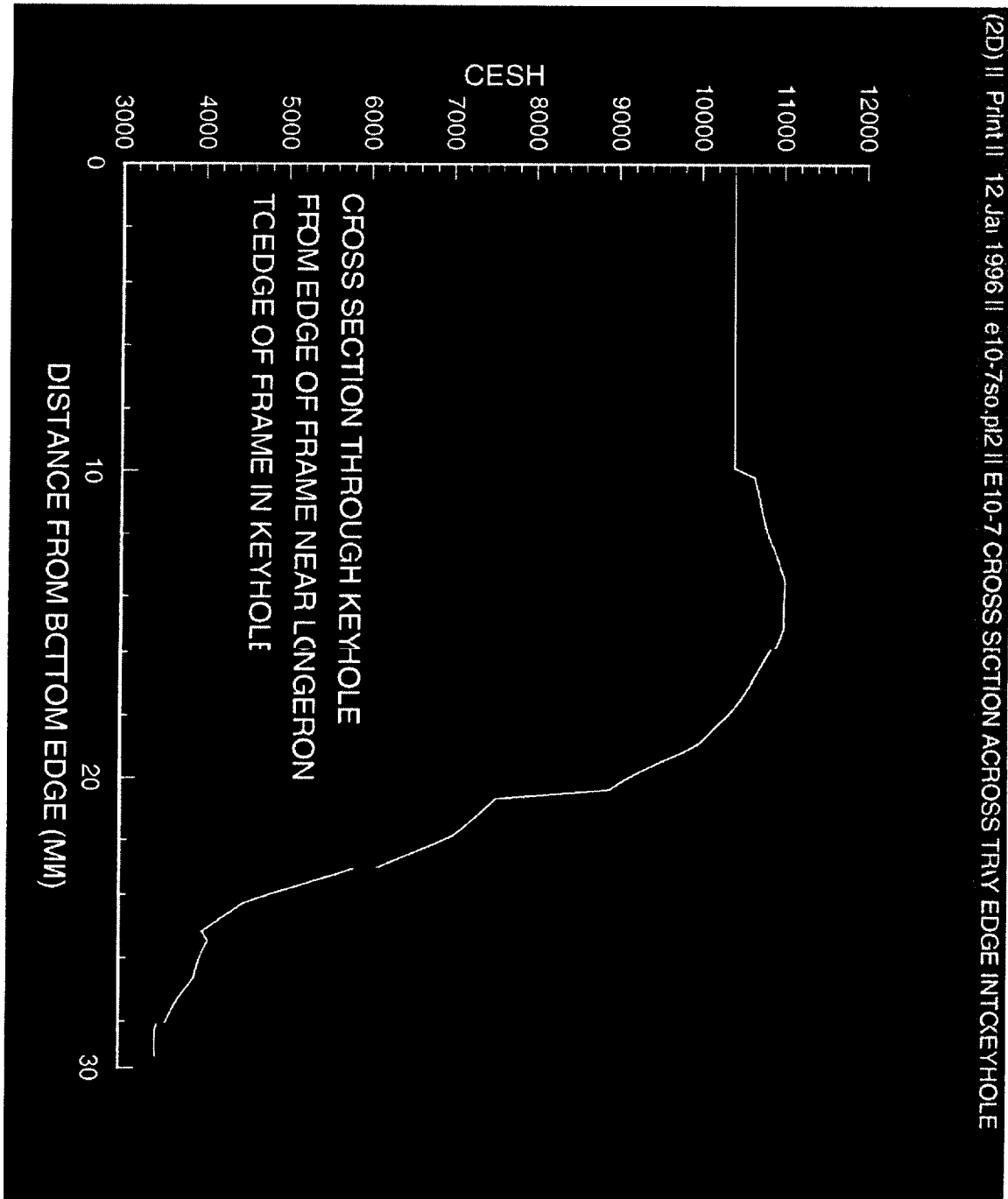


Figure C-1. Cross-section for E10-7 surface showing Cumulative Equivalent Sun Hours as a Function of Location.

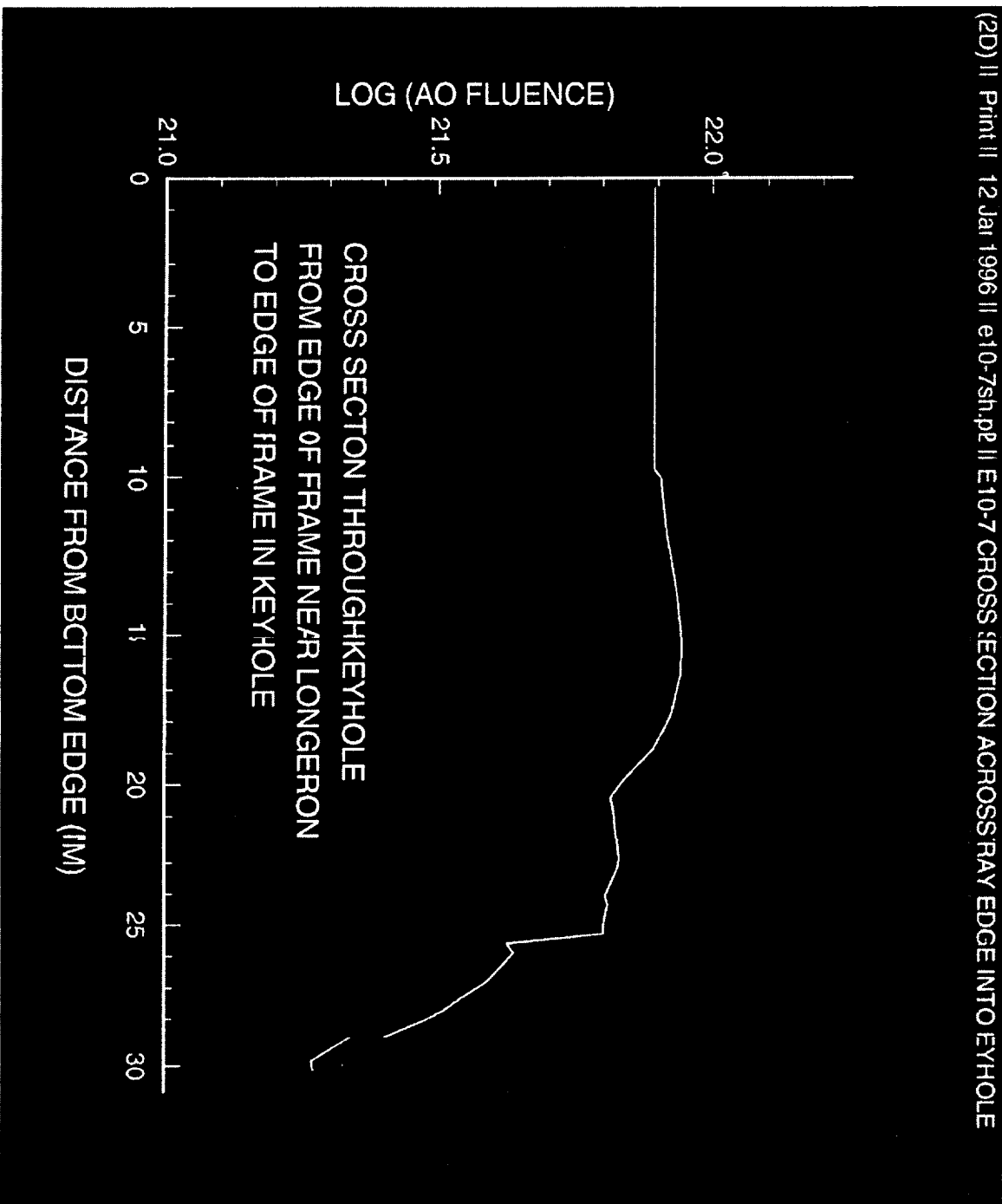


Figure C-2. Cross-section for E10-7 surface showing Atomic Oxygen Fluence as a Function of Location.

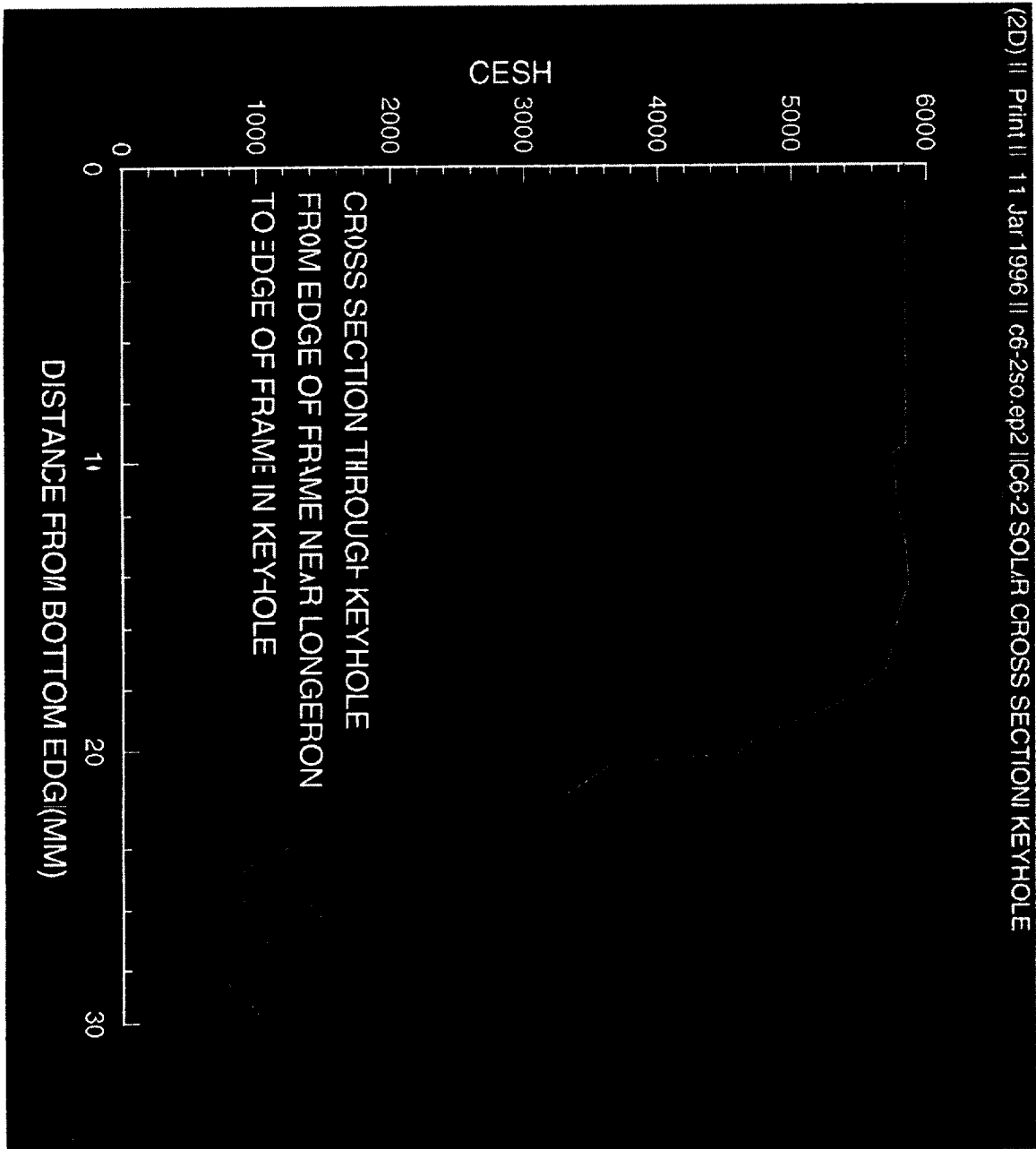


Figure C-3. Cross-section for C6-2 surface showing Cumulative Equivalent Sun Hours as a Function of Location.

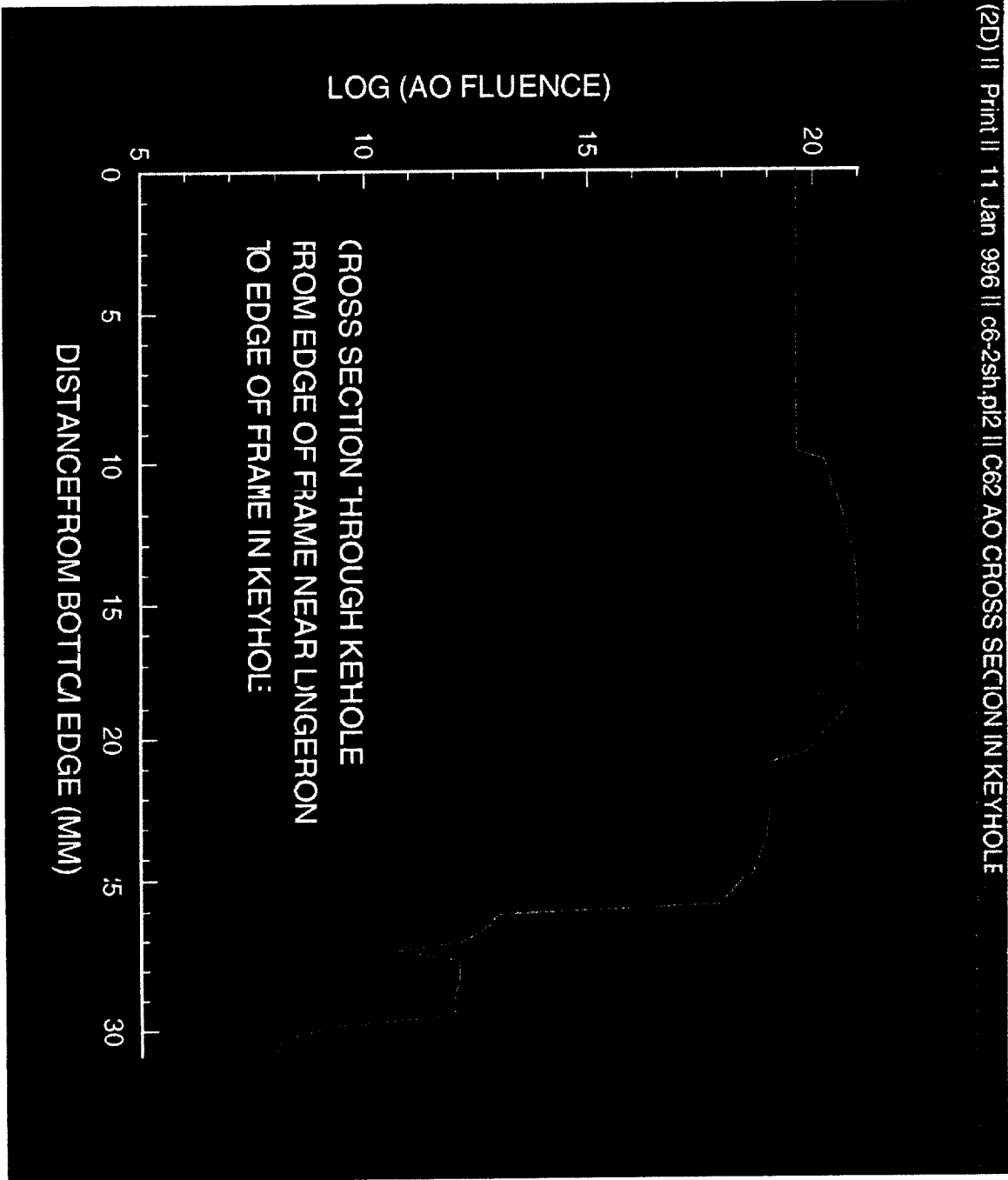


Figure C-4. Cross-section for C6-2 surface showing Atomic Oxygen Fluence as a Function of Location.

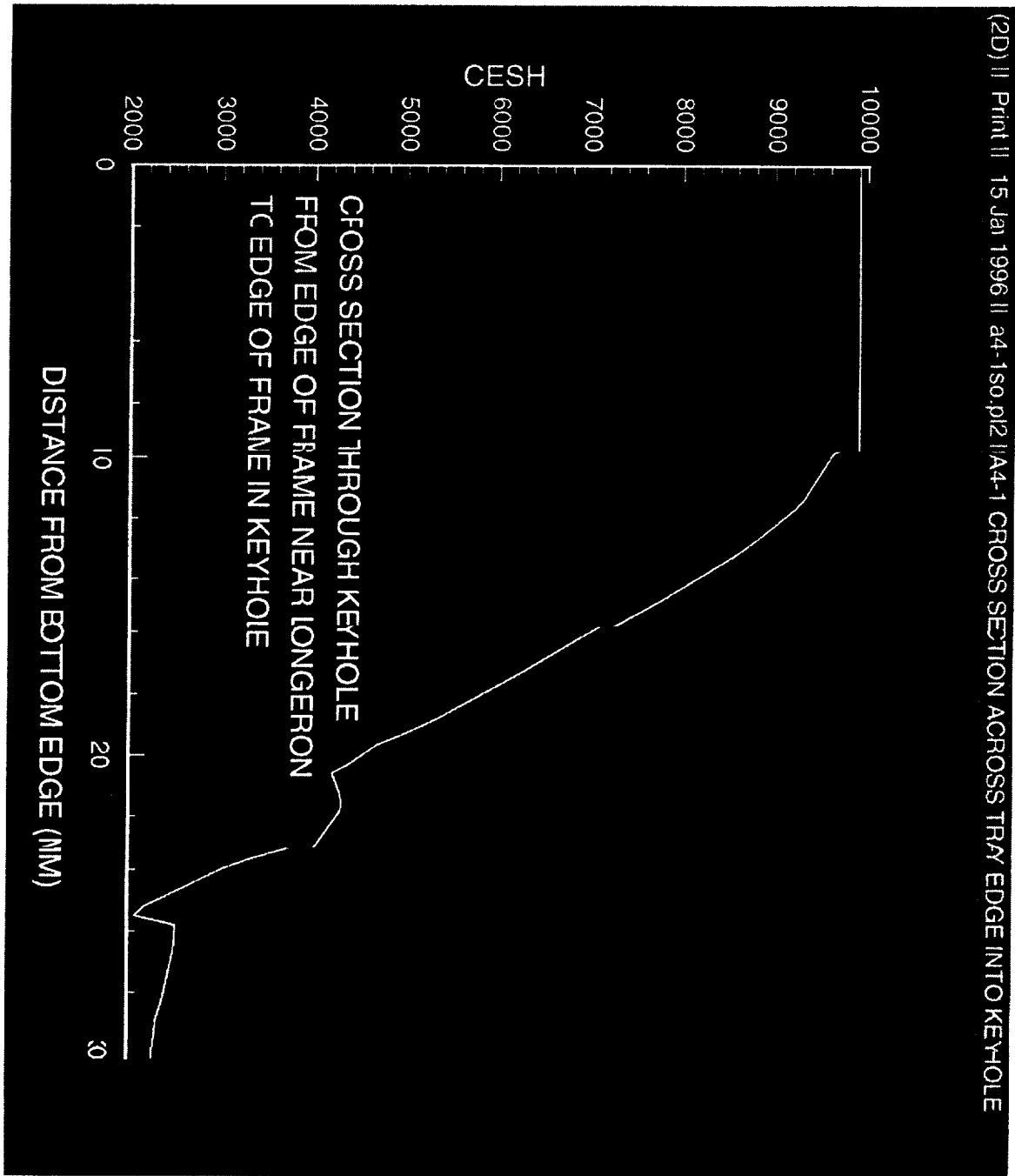


Figure C-5. Cross-section for A4-1 surface showing Cumulative Equivalent Sun Hours as a Function of Location at Tray Vent (KEYHOLE).

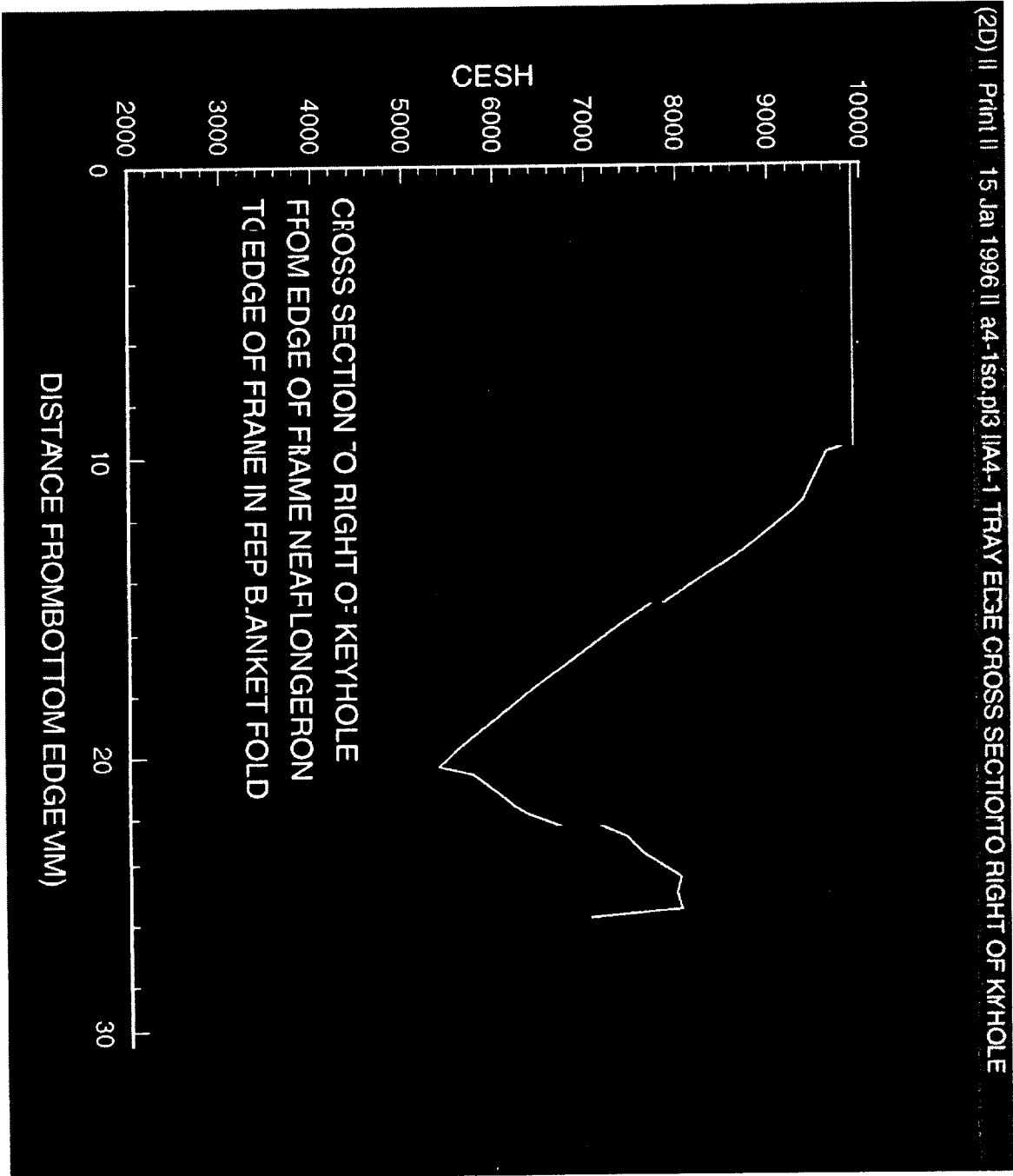


Figure C-6. Cross-section for E10-7 surface showing Cumulative Equivalent Sun Hours as a Function of Location for Tray Surface near Tray Vent (KEYHOLE).

Appendix D
SEM images from Tray E10-9

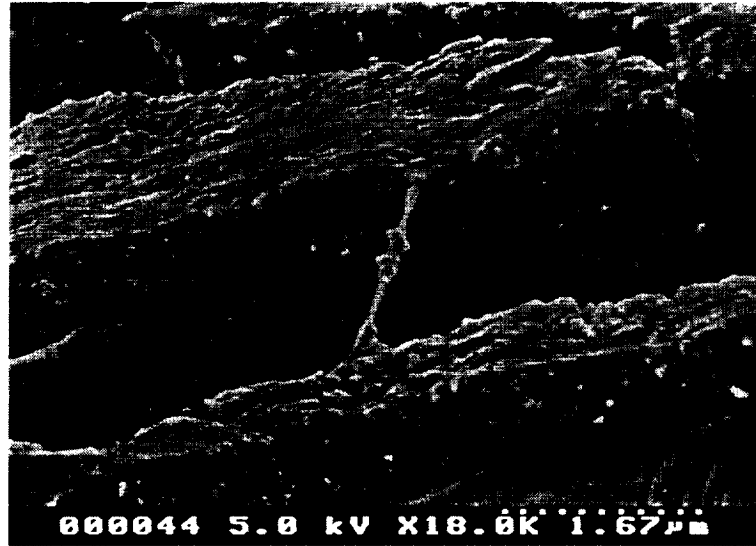
Introduction

These are a selected set of SEM images from E10-9 for areas showing deposits from the silicone gasket seal which contacted the tray surface, and for areas along the tray walls showing the contaminant layer from deposits due to on-orbit outgassing.

List of Figures

Figure D-1.	Tray E10-9 Surface in contact with Silicone Gasket.	D4
Figure D-2.	Tray E10-9 Surface in contact with Silicone Gasket.	D5
Figure D-3.	Tray E10-9 Surface in contact with Silicone Gasket.	D6
Figure D-4.	Tray E10-9 Layer from On-orbit Outgassing Deposits.	D7
Figure D-5.	Tray E10-9 Layer from On-orbit Outgassing Deposits.	D8
Figure D-6.	Tray E10-9 Layer from On-orbit Outgassing Deposits.	D9

Laboratory Bend Fracture 18000X



Laboratory Bend Fracture 50000X

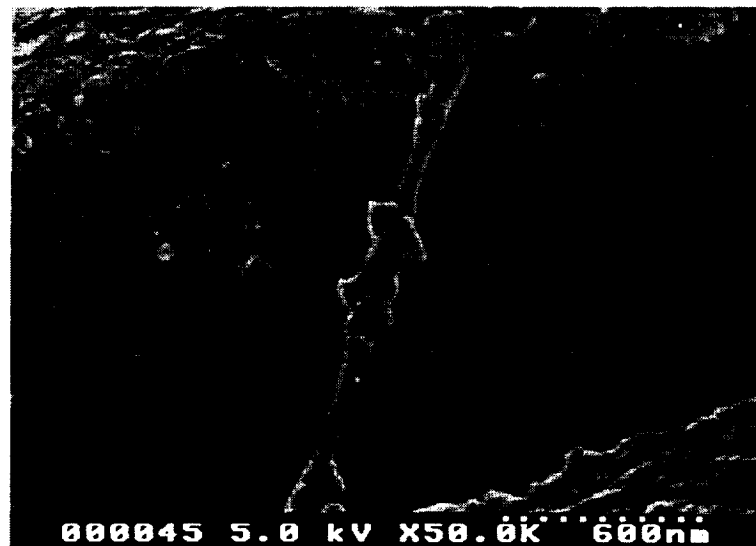
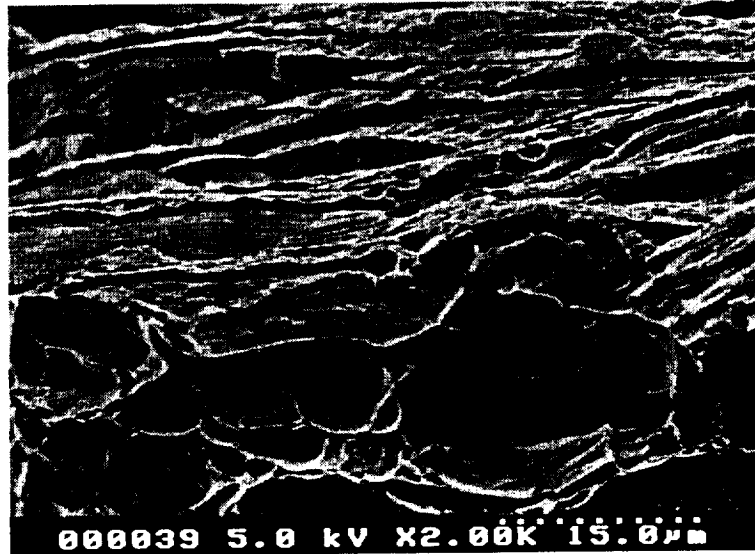


Figure D-1. Tray E10-9 Surface in contact with Silicone Gasket.

Laboratory Bend Fracture 2000X



Laboratory Bend Fracture 10000X

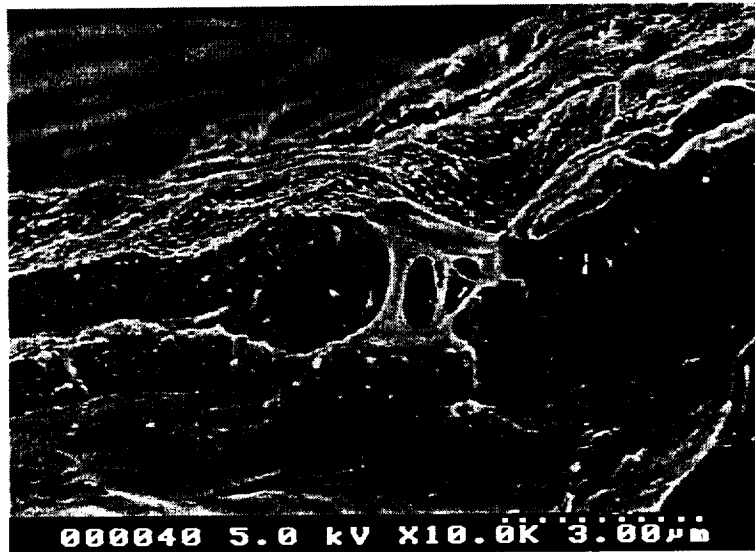
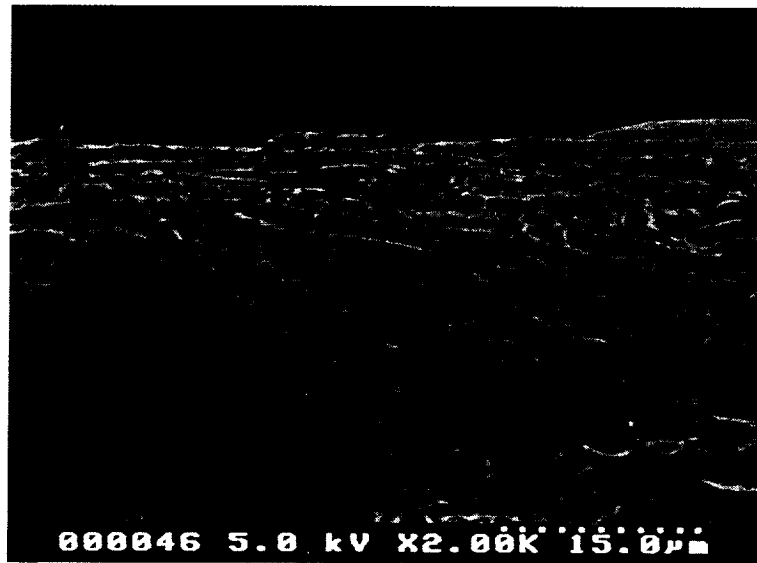


Figure D-2. Tray E10-9 Surface in contact with Silicone Gasket.

Laboratory Bend Fracture 2000X

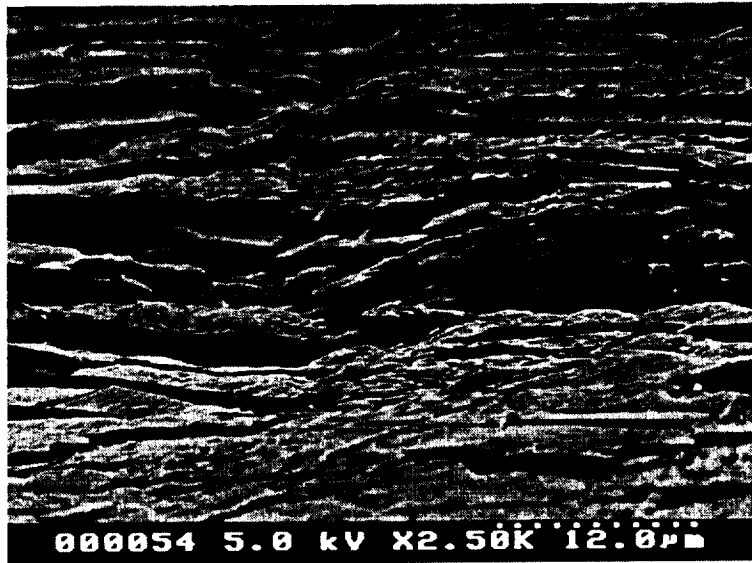


Laboratory Bend Fracture 10000X



Figure D-3. Tray E10-9 Surface in contact with Silicone Gasket.

Laboratory Bend Fracture 2500X



Laboratory Bend Fracture 10000X

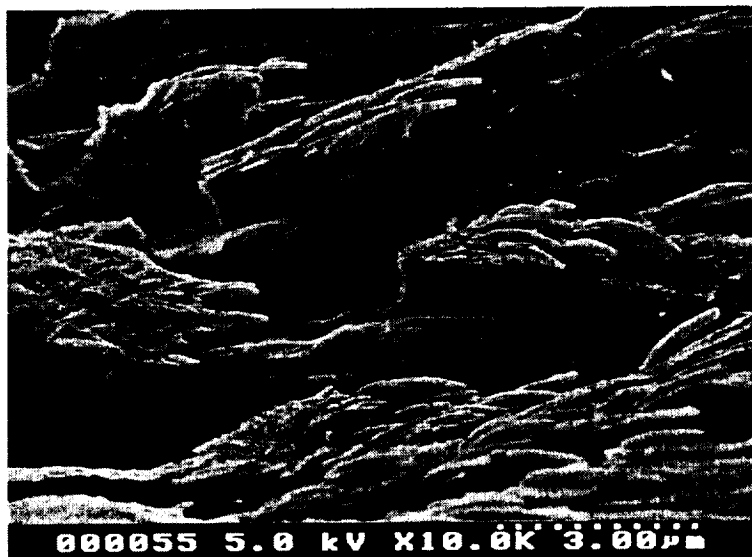


Figure D-4. Tray E10-9 Contaminant Layer from On-orbit Outgassing Deposits.

Laboratory Bend Fracture 50000X

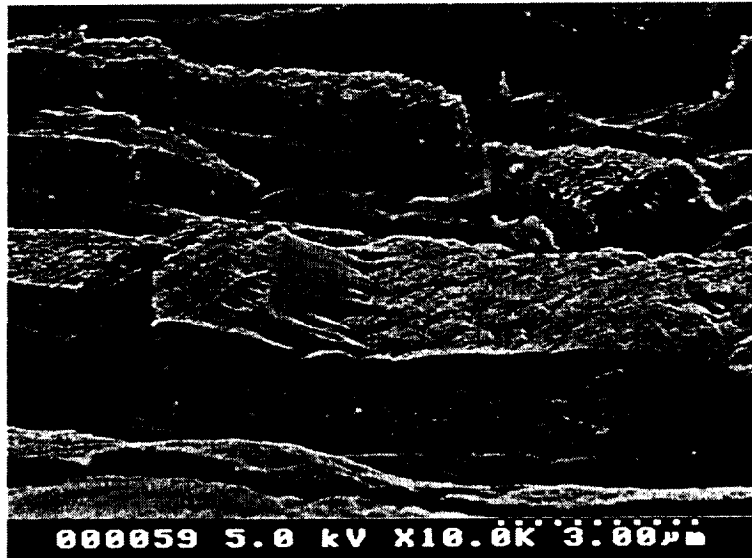


Laboratory Bend Fracture 150000X



Figure D-5. Tray E10-9 Contaminant Layer from On-orbit Outgassing Deposits.

Laboratory Bend Fracture 10000X



Laboratory Bend Fracture 50000X

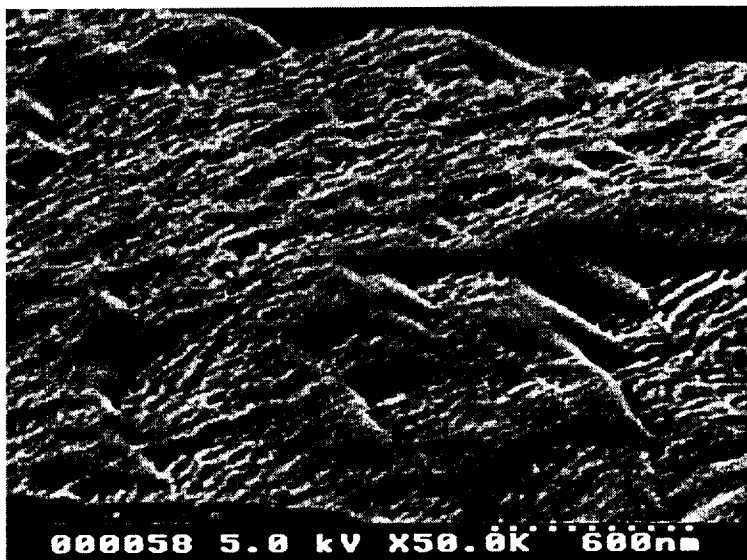


Figure D-6. Tray E10-9 Contaminant Layer from On-orbit Outgassing Deposits.

JANUARY 1998

MDC 97H0867R1

**CONTAMINATION DEPOSITED ON
LDEF SURFACES**

Nell Warnes

CONTAMINATION DEPOSITED ON LDEF SURFACES

Prepared for the
Boeing Defense and Space Group
Contract JQ4029

PREPARED BY:

Nell Warnes
Engineer
Materials and Processes
Space Station

APPROVED BY:

Cherie Jones
Manager
Materials and Processes
Space Station

ABSTRACT

Background

The Long Duration Exposure Facility (LDEF) carried experiment trays that were exposed to silicone based molecular contamination. The LDEF flew in a fixed orientation for 69 months in low earth orbit. This document examines the spread and the depth of the contamination onto the trays from the DC6-1104 silicone adhesive used to construct the trays and tray covers. The trays examined are E10, C6, and A4. The analysis performed for this report was conducted using NASA's NASTRAN/NASAN.

Discussion/Assumptions

The side walls of the LDEF trays have one primary source of contamination DC6-1104 silicone adhesive. It was used to attach Velcro to the aluminum frame. The analysis was performed assuming a constant source and receiver temperature. The MLI blankets effectively shield these areas, so no other sources of contamination were considered.

Summary and Conclusions

The results of this analysis are remarkably similar to pictures of the silicone deposition on the LDEF trays in terms of contamination shape. The depth of the contamination correlates well on tray slot A4-9. There is no data for a comparison of results at other locations, but the results the analyses are presented here.

KEYWORDS

DC6-1104™

Low Earth Orbit Environment

Contamination Deposition

Optical Properties Degradation

NASAN

LDEF

TABLE OF CONTENTS

Abstract	3
Keywords	4
Table of Contents	5
List of Tables.....	6
List of Figures	7
1.0 Background	8
2.0 Model	8
3.0 Temperature	23
4.0 Source rates	23
5.0 Results	27
6.0 Summary and Conclusions.....	30
References	37
Appendices	38

LIST OF TABLES

Table 1	Comparison of Surface Deposition at A4-9 from XPS to Depth of Deposition from NASAN	29
Table 2	Total Deposition at Typical Locations on E10-3, E10-8, and C6-2 from NASAN Model in Å.....	31

LIST OF FIGURES

Figure 1.	Drawing of LDEF thermal blanket assembly showing Velcro attachment locations and vent locations	10
Figure 2.	Cross-section drawing of details of the UHCRE trays showing orientation of blanket with respect to tray walls.....	11
Figure 3.	Vent location numbering system for tray E10	12
Figure 4.	Vent location numbering system for tray C6	13
Figure 5.	Vent location numbering system for tray A4.....	14
Figure 6.	Dimensional details for areas of trays near side blanket vents.....	15
Figure 7.	Cross-sectional detail of tray E10 side wall, frame holding thermal blankets, and cylinders holding experiment.....	16
Figure 8.	Dimensional details for areas of trays near Earth and space end blanket vents.	17
Figure 9.	Cross-sectional detail of tray E10 end wall, rivet, and frame holding thermal blankets.	18
Figure 10.	Geometry of E10-3 NASTRAN model.....	19
Figure 11.	Geometry of C6-2 NASTRAN model.....	20
Figure 12.	Geometry of A4-9 NASTRAN model	21
Figure 13.	Geometry of E10-8 NASTRAN model.....	22
Figure 14.	Daily averaged data from LDEF Thermal Measurement System	25
Figure 15.	DC6-1104 Adhesive: source temperature at 24 °C and receiver temperature at 10 °C	26
Figure 16.	Deposition on E10-3 NASTRAN model.....	32
Figure 17.	Deposition on C6-2 NASTRAN model	33
Figure 18.	Deposition on A4-9 NASTRAN model	34
Figure 19.	Deposition on A4-9 NASTRAN model	35
Figure 20.	Photograph of contamination on tray side wall.....	36

1.0 Background

The Long Duration Exposure Facility (LDEF) carried experiment trays that were exposed to contamination including silicone. This document examines the spread and the depth of the silicone contamination onto the Ultra Heavy Cosmic Ray experiment (UHCRE) trays from the DC6-1104 silicone adhesive used in construction of the trays and tray covers.

The tray side walls near the vent locations were selected for analysis to minimize exposure to silicone sources other than the DC6-1104 adhesive. Vent locations near the tray corners were exposed to tray cover gaskets as well as the DC6-1104 adhesive. This makes those vent locations unsuitable for this analysis, because of the multiple sources of contamination. Thermal control blankets physically block most of the possible contamination from the Space Shuttle.

The other non-metallic materials present are Z306 polyurethane black thermal control paint, MLI blankets, and Velcro fasteners. Z306 outgasses carbon based products, but contains no silicones. Ag/FEP blankets have a low-outgassing rate and should not effect the results presented here.

2.0 Model

The analysis for this report was performed using NASAN, a new molecular flux deposition program developed by NASA-JSC. It uses NASTRAN geometric files. This code is more time efficient than MOLFLUX and is currently the code used by the External Contamination Analysis and Integration Team (EC-AIT) for all International Space Station deposition assessment. An effort was made to retrieve MOLFLUX from the archives to do a comparative analysis. The software is no longer maintained and efforts to recompile the MOLFLUX software were unsuccessful. Comparisons of the two programs can be seen in the following reports: AIAA-97-0632 "Contamination Analysis Programs for the International Space Station" and MDC 97H0520 "Contamination Deposited On PG-1 Critical Surfaces From Node-1 Sources".

The following figures show the assembly of the trays. These drawings were used to construct the geometry of the NASTRAN models. Figure 1 shows the vent locations in relation to the Velcro attachment locations. A cross section of the tray and a close up of the tray wall and blanket junction can be seen in Figure 2. Figures 3-5 show the numbering system for the vents in the MLI blankets on trays E10, C6 and A4. This analysis centers

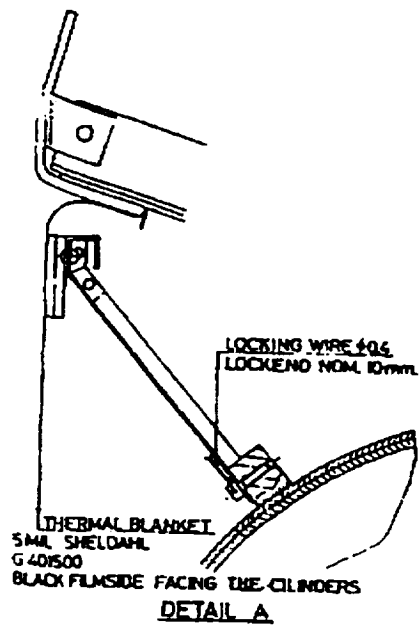
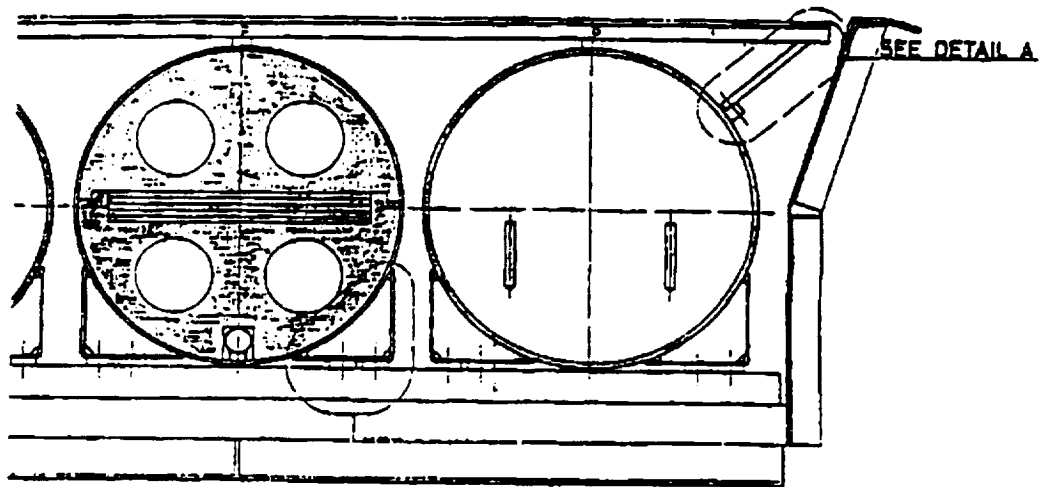


Figure 2. Cross-section drawing of details of the UHCRE trays showing orientation of blanket with respect to tray walls.

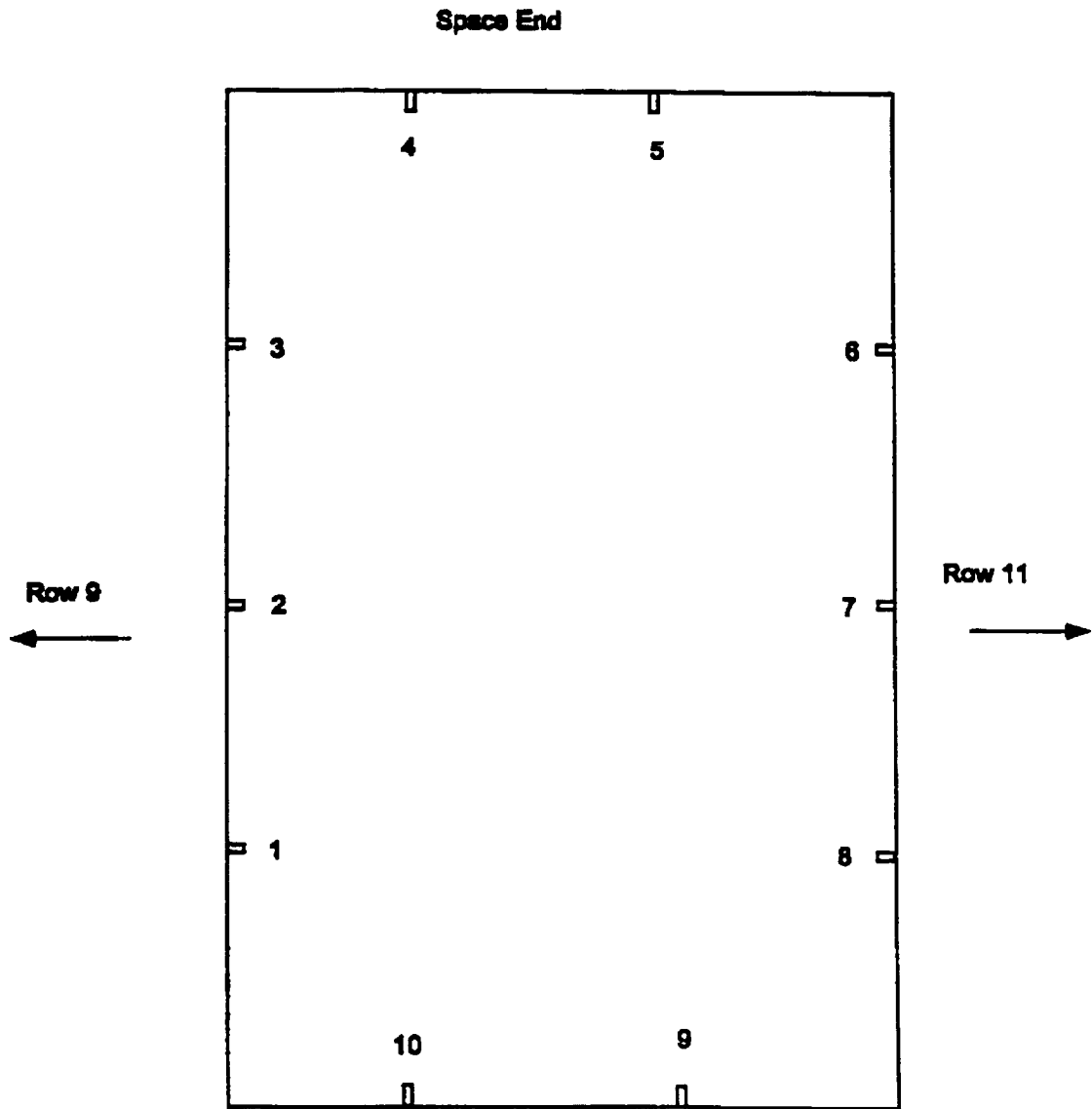


Figure 3. Vent location numbering system for tray E10.

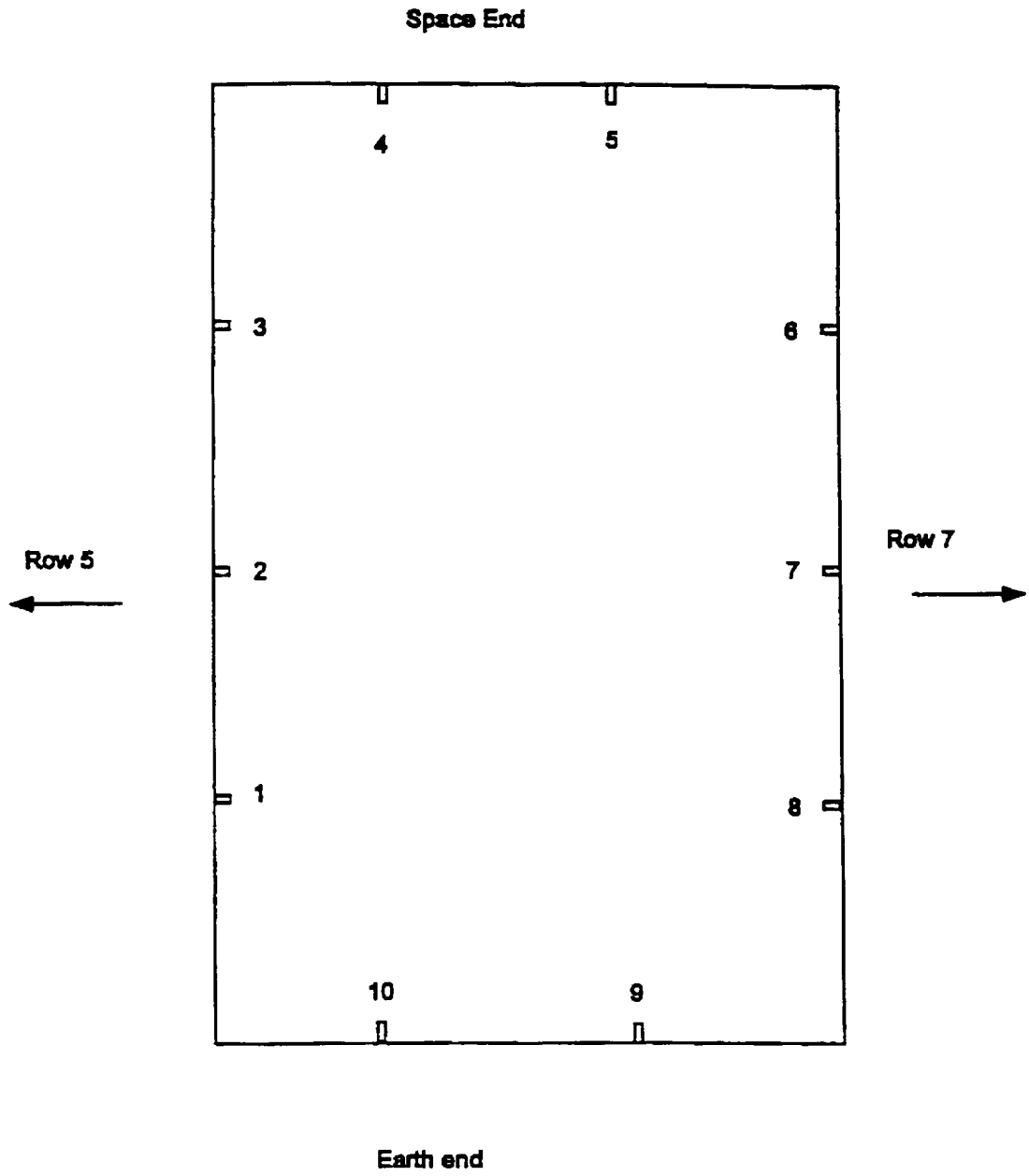


Figure 4. Vent location numbering system for tray C6.

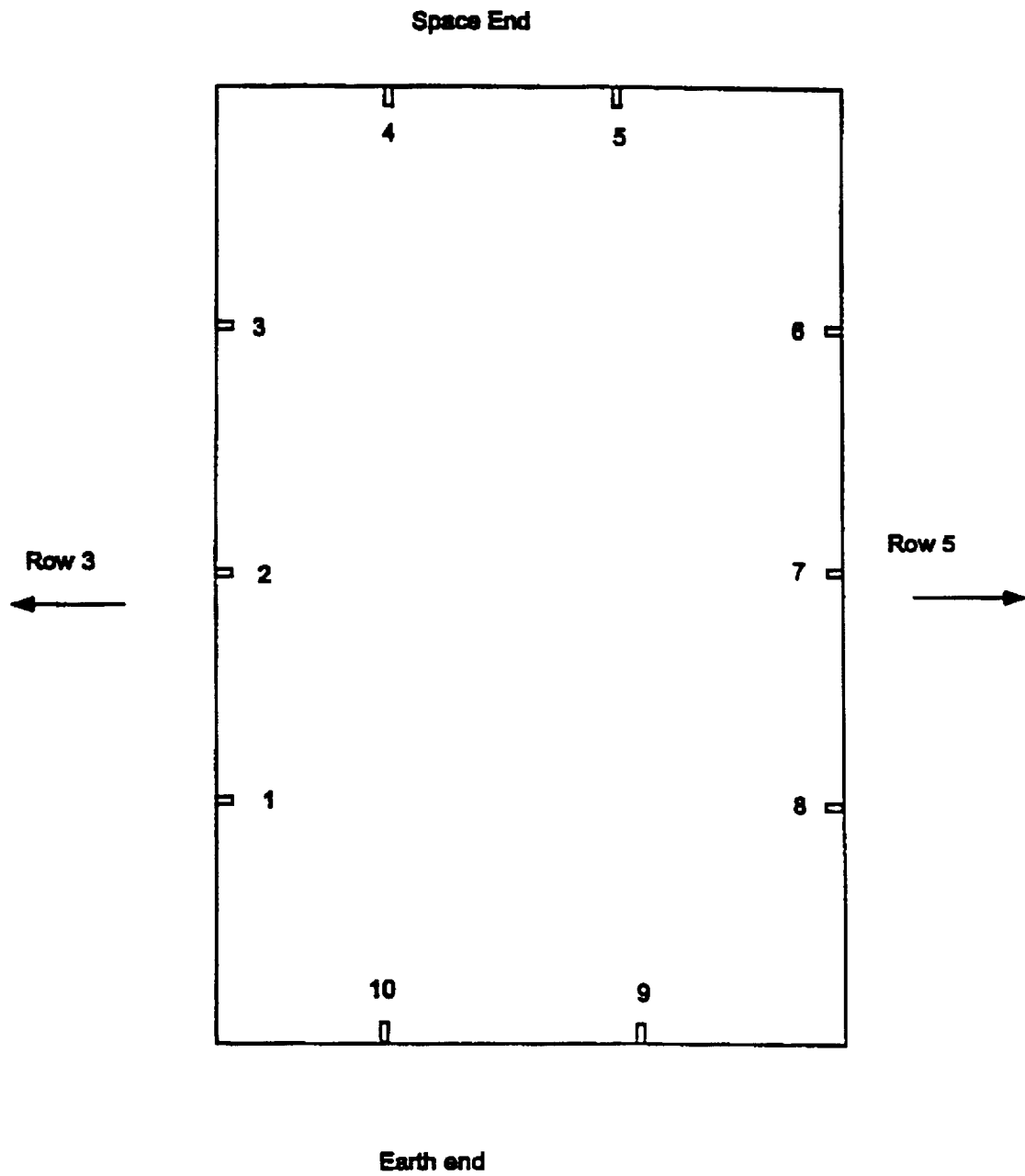
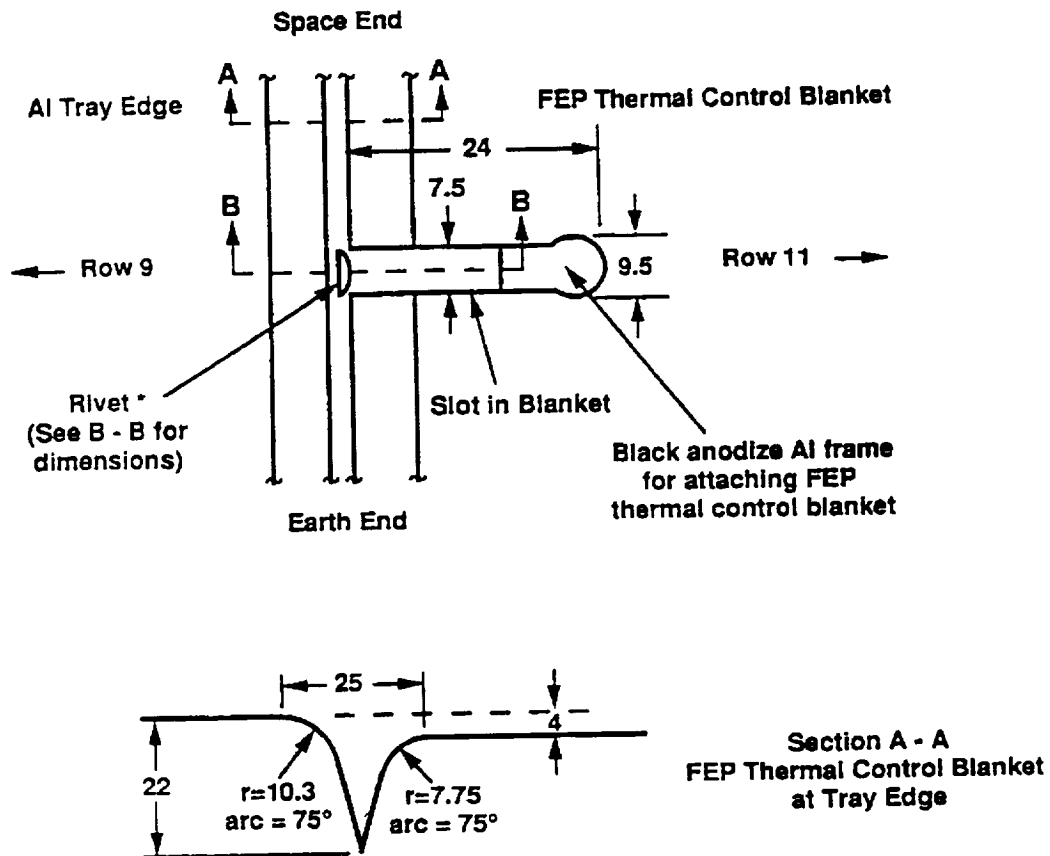


Figure 5. Vent location numbering system for tray A4.

Detail of E10 Tray and FEP Thermal Control Blanket
 at 6, 7, 8 (3, 2, 1 are symmetric facing row 11)
 (All dimensions in mm)



* location of rivet center relative to horizontal centerline of slot

- | | | | |
|---|----------|---|----------|
| 1 | 7 above | 6 | 8 below |
| 2 | no rivet | 7 | no rivet |
| 3 | 6 below | 8 | 3 above |

Figure 6. Dimensional details for areas of trays near side blanket vents.

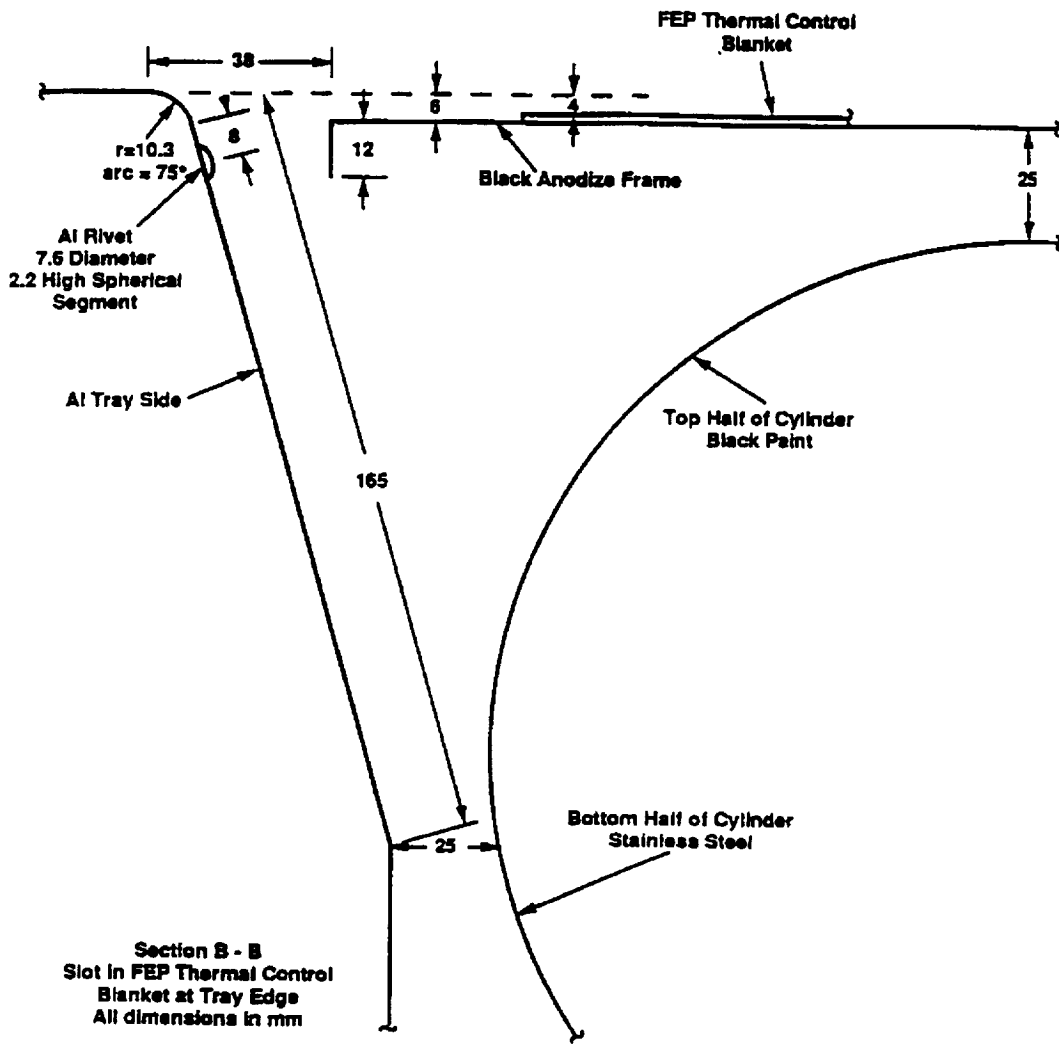
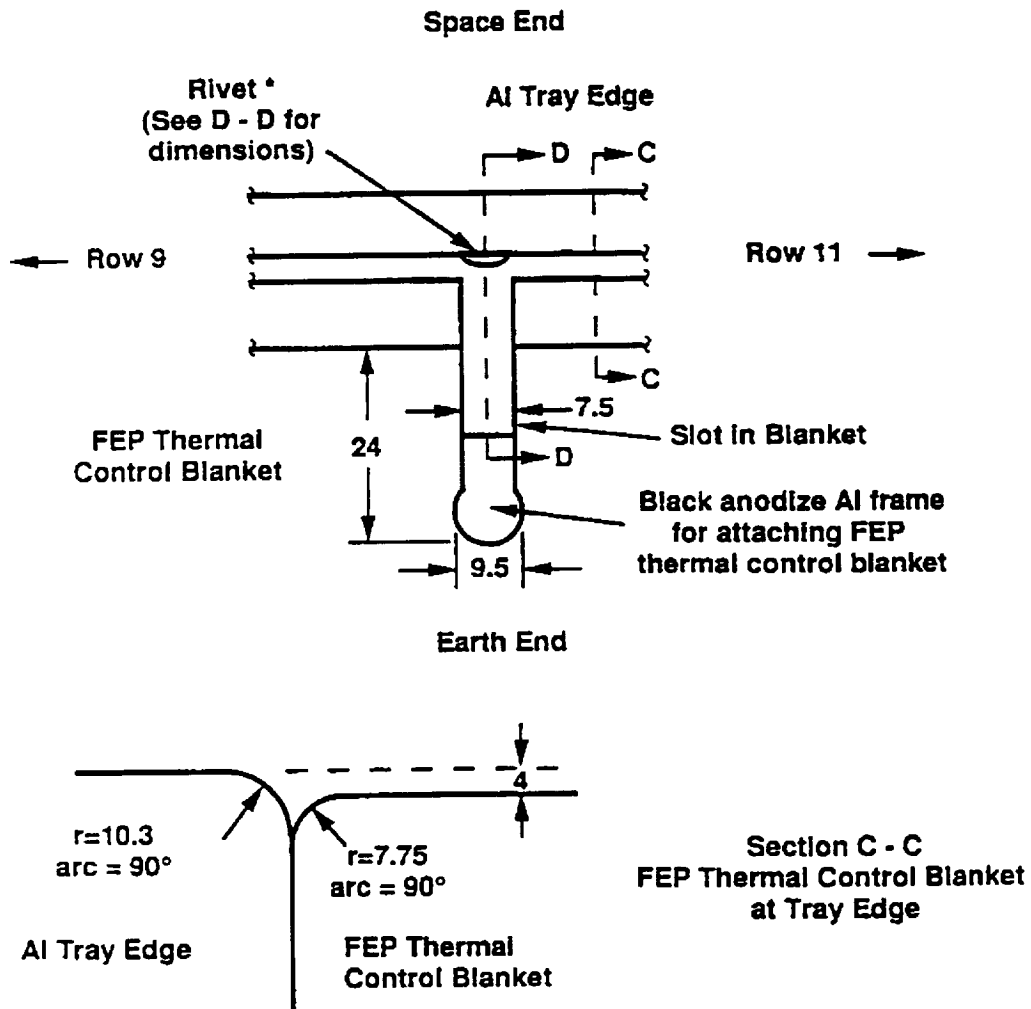


Figure 7. Cross-sectional detail of tray E10 side wall, frame holding thermal blankets, and cylinders holding experiment.

**Detail of E10 Tray and FEP Thermal Control Blanket
at 9 and 10 (5 and 4 are symmetric facing Earth End)
(All dimensions in mm)**



* location of rivet center relative to vertical centerline of slot

4	4 right	9	3 right
5	7 right	10	1 left

Figure 8. Dimensional details for areas of trays near Earth and space end blanket vents.

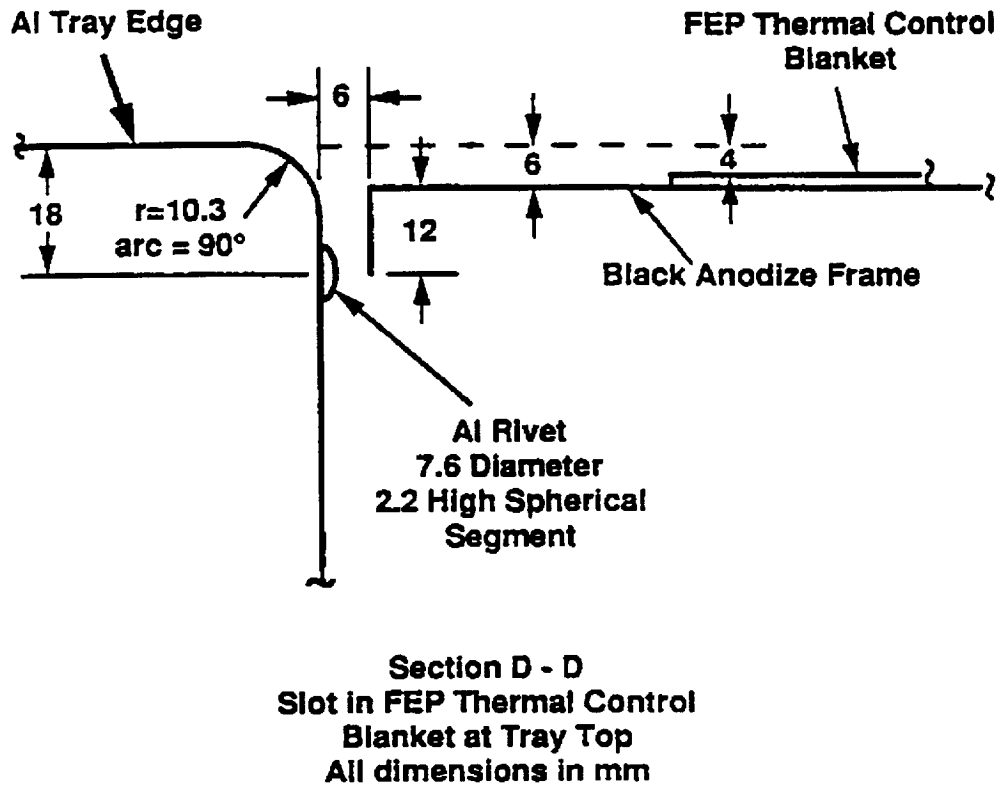
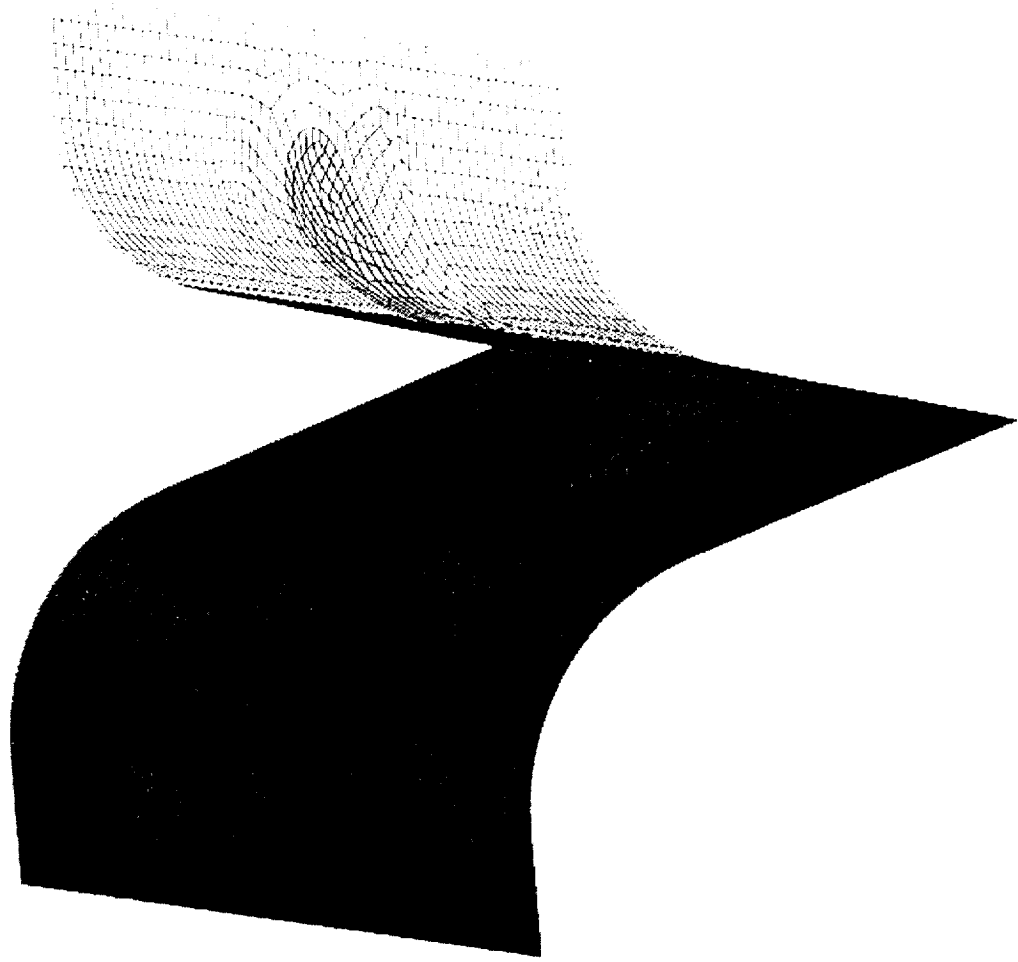


Figure 9. Cross-sectional detail of tray E10 end wall, rivet, and frame holding thermal blankets.



-  Rivet
-  Tray side wall
-  Slot
-  Thermal control blanket

Figure 10. Geometry of E10-3 NASTRAN model

Tray side wall
Slot
Thermal control blanket

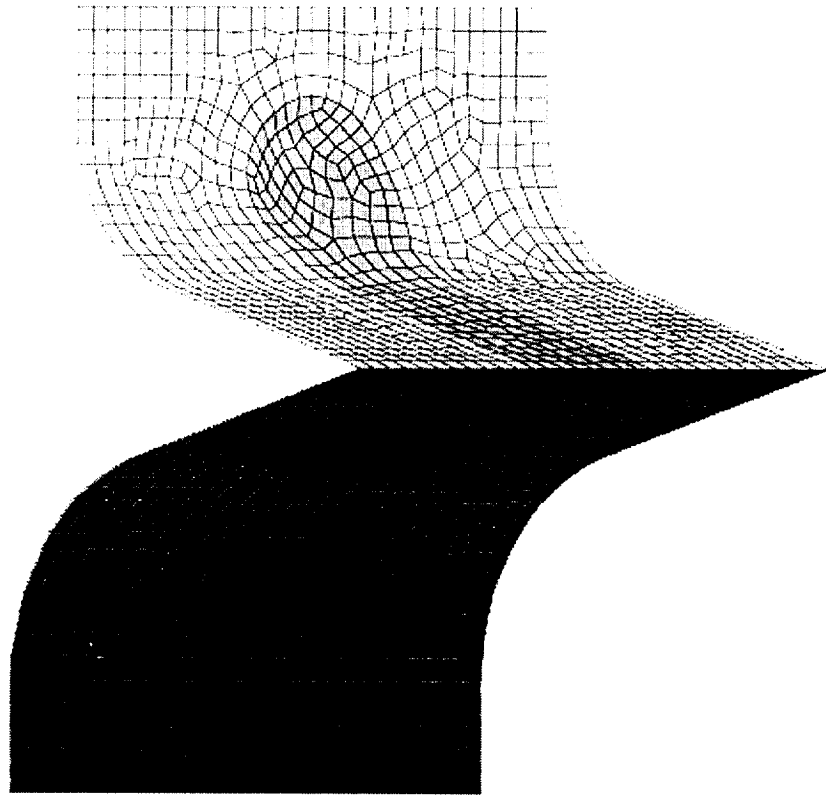


Figure 11. Geometry of C6-2 NASTRAN model

■ Rivet

■ Tray side wall

Slot

Thermal control blanket

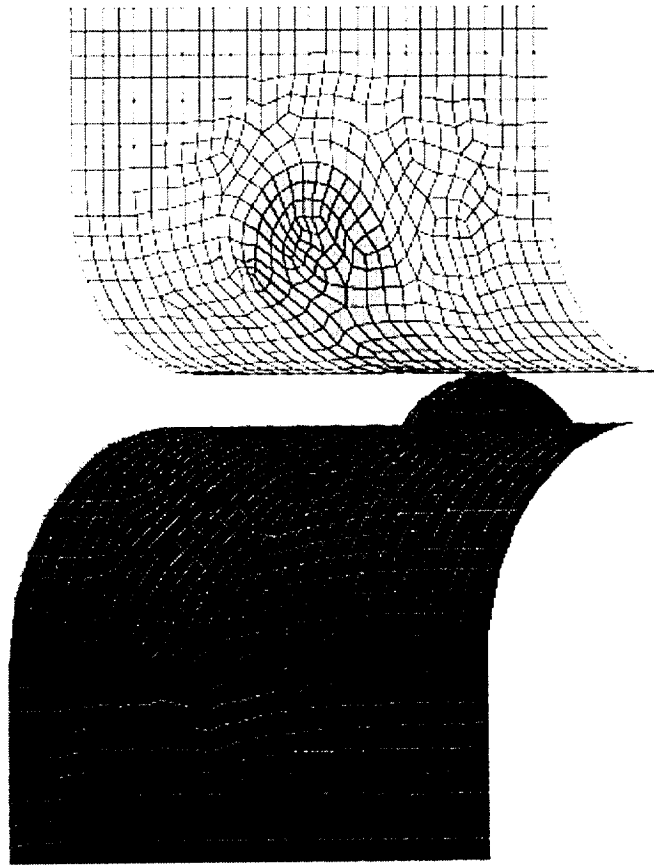


Figure 12. Geometry of A9-4 NASTRAN model



Figure 13. Geometry of E10-8 NASTRAN model

on vents E10-3, E10-8, C6-2, A4-9. The dimensional details were only available for tray E10; it was assumed that the other trays were similar in geometry, and NASTRAN models for C6-2 and A4-9 were created from these drawings. Figures 6-9 show the dimensions of the vent locations on tray E10. Figures 10-13 show the NASTRAN models for vents E10-3, E10-8, C6-2, and A4-9.

3.0 Temperatures

The thermal environment of LDEF is characterized by two set of temperatures: the interior temperature and the exterior temperature. DC6-1104, the source of silicone outgassing, was located underneath the thermal blankets and was considered to be at the internal temperature. The edge of the tray was exposed to space and was considered to be at the external temperature. The interior temperature ranged from 60 to 90 °F (15 to 30 °C). The external temperature ranged from 40 to 135 °F (5 to 60 °C). Figure 13 shows the daily average temperatures for a thermocouple located on an external structural member. Assuming a consistent average internal temperature of 70 F (25C) and using the temperatures presented in Figure 14 for the external temperature, the external temperature will only be lower than the internal temperature for about half the year

4.0 Source Rates

The outgassing rate for DC6-1104 was derived from the data gathered in Lockheed Martin Report WRDC-TR-89-4114 on contamination for source temperatures 125 °C and 75°C. These data were curve fit and documented in Memo EM2-E1-JWA-03. A function fit of the data in terms of frequency (f) versus time (t) is expressed as

$$f = A \ln(t) + b$$

where A and b are constants. The source rate was calculated by taking the derivative of the frequency (f) and multiplying by the TCQM (temperature controlled quartz crystal monitor) sensitivity, multiplying by the effusion cell view factor, and dividing by the sample area. The data were adjusted to reflect the temperatures . For a source

temperature of 24 °C and a receiver temperature of 10 °C, the outgassing rate equals $1.73 \times 10^{-5} \text{ g/cm}^2$ divided by time in seconds. Figure 15 shows this curve for the first 100 days.

Once A has been determined a curve for the rate is established. By integrating over the curve and evaluating the expression at 69 months, the duration of the LDEF flight, the outgassing rate used in this analysis was calculated at $9.1 \times 10^{-13} \text{ g/cm}^2/\text{s}$.

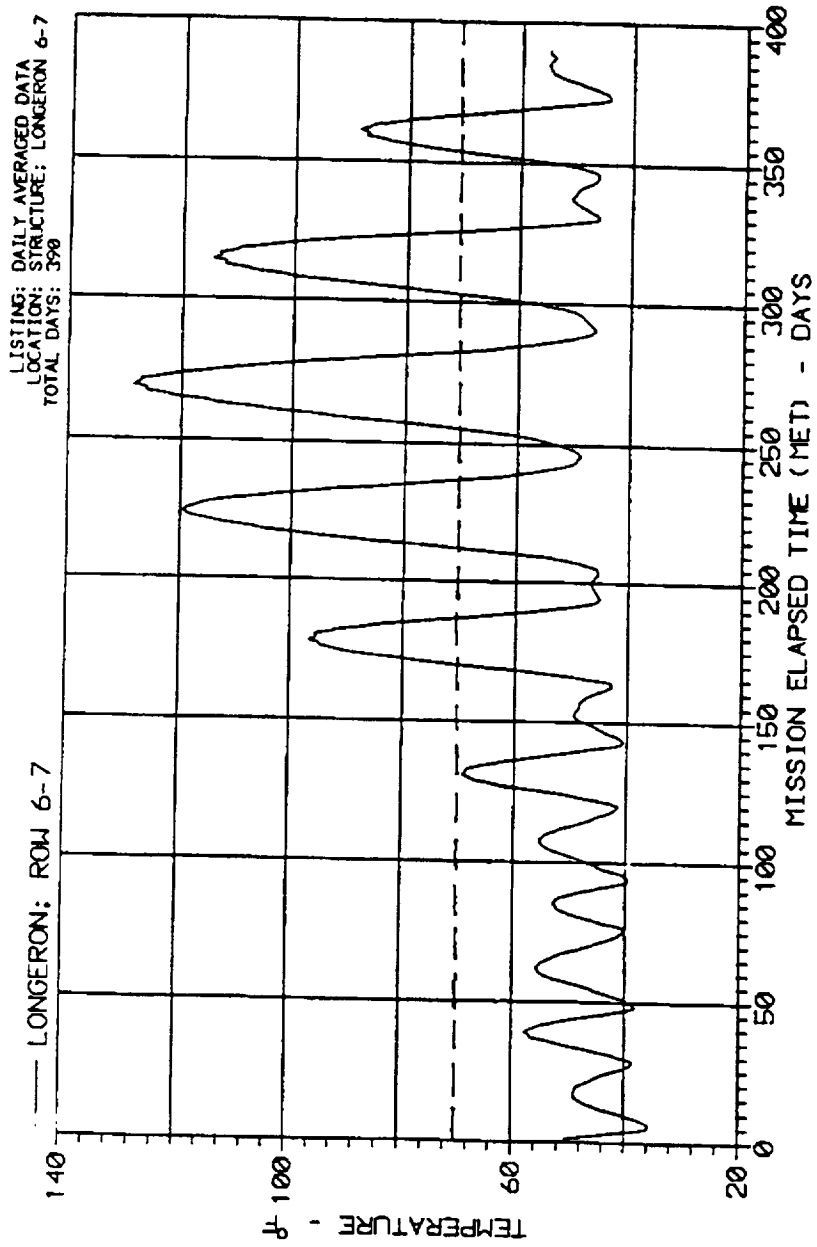
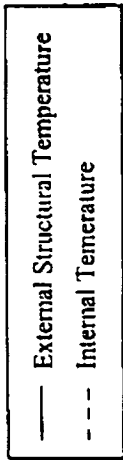


Figure 14. Daily Average Temperatures From LDEF Thermal Measurement System

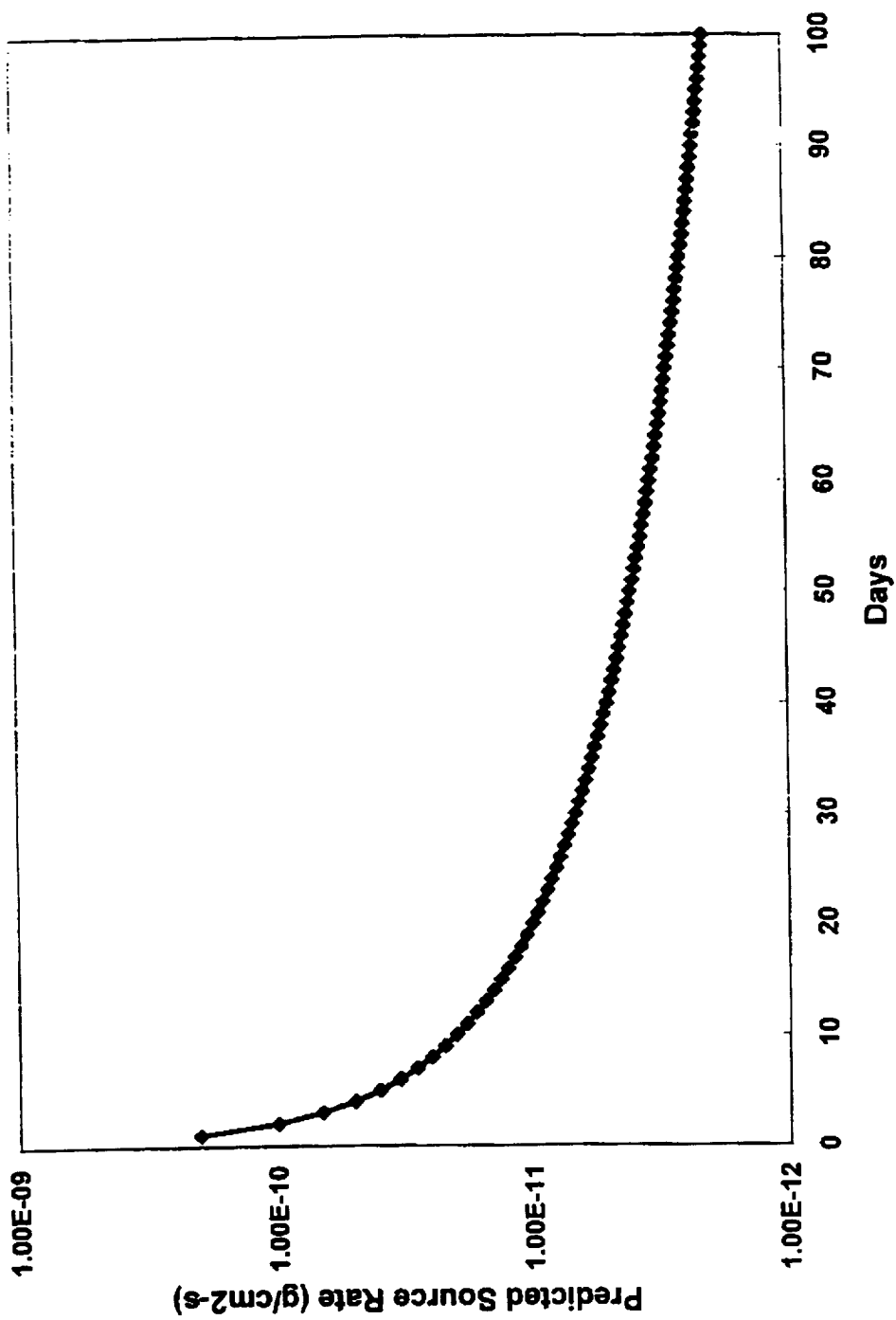


Figure 15. DC6-1104 Adhesive: Source Temperature at 24 °C and Receiver Temperature at 10 °C

5.0 Results

In order to compare the data provided in the Comparison Spacecraft Contamination Models with Well-Defined Flight Experiment Report with the results from the NASAN analysis, both results must be converted into angstroms of silicon at each site. By converting the atom percent in the XPS surface sampling volume to depth in angstroms of silicon on the surface of the tray and by taking a percentage the total deposition shown in the analysis to be angstroms of silicon, the two values can be compared. An example of the method of calculating the angstroms of silicon at coordinates (29.5, 6.0) on tray A4-9 will be shown here.

The XPS detects the X-ray photoelectrons emitted from a solid being bombarded with X-rays. The XPS spectrum consists of a plot of the number of electrons in each kinetic energy interval plotted against the electron kinetic energy. The energy of the X-rays is very well defined, so that chemical elements, and often their oxidation states, can be determined, by simply measuring the kinetic energy spectrum of the X-ray photoelectrons, which will be the difference between the energy of the X-ray and the electron binding energy of a particular electron shell in the parent atom. The extreme surface sensitivity of the XPS method results from the very short collision length of X-ray photoelectrons in solids; that is, the photoelectron can't escape the solid and retain kinetic energy information unless that photoelectron is created within a very few collision lengths of the surface.

Measurements of electron escape depths in the element Si indicate that 15 angstroms is the best and most recent value (C. J. Powell, M. P. Seah; "Precision, Accuracy and Uncertainty in Quantitative Surface Analysis by Auger-electron Spectroscopy and X-ray Photoelectron Spectroscopy," J. Vac. Sci. Technol., A8 (2), pp 735-768, March-April 1990). No escape depth measurements have been reported in the open literature for Al or Al_2O_3 . The escape depth used for analysis of the LDEF tray data is estimated as the escape depth of Si corrected by the $\text{Si}/\text{Al}_2\text{O}_3$ density ratio because the photoelectron collision length in a solid is proportional to the density of the solid.

The number of photoelectrons escaping from some distance, x , below the surface is a function of both the collision length and x . Thus, with an escape length of 15 angstroms, 2.3 grams per cubic centimeter for the density of Si, and 3.5×0.858 grams per cubic centimeter for the density of gamma alumina (corrected for the actual elemental composition measured by XPS as described in the next paragraph) we have,

$$T = \int_0^{100} \exp\left(\frac{-x \frac{2.3}{3.5(0.85)}}{15}\right) dx$$

$$T_s = \int_0^{50} \exp\left(\frac{-x \frac{2.3}{3.5(0.85)}}{15}\right) dx$$

$$\frac{T_s}{T} = 0.928$$

where T is the total signal from all depths, x , less than or equal to 100 angstroms and T_s is the total signal escaping from all depths less than or equal to 50 angstroms. Clearly, a sampling depth of 50 angstroms will account for 93 percent of the photoelectrons escaping from the sample, so 50 angstroms will be used as the sampling depth for the analysis reported here.

The actual elemental composition of the surface film as measured by XPS is different from that for pure, low-density, Al_2O_3 . The surface film elemental composition at coordinates (29.5, 6.0) on tray A4-9 corresponds to a formula weight of 18.287 amu compared to 20.4 amu for pure Al_2O_3 , so that the surface film sampled by XPS has a density 0.896 times that of the pure aluminum oxide (3.5 g/cc). The total mass (per square cm) of the surface film sampled by XPS is then,

$$50 \times 10^{-8} \text{ cm} \times 3.5 \text{ g/cm}^3 \times 0.896 = 1.57 \times 10^{-6} \text{ grams/cm}^2$$

The total mass of silicon in the film is calculated from the atomic weight of silicon and the surface atom percent silicon or,

$$\frac{27 \times \frac{8.3}{100}}{18.287} = 0.123 \text{ percent silicon by weight.}$$

The composition of the film must be separated from the first layer of the aluminum tray. The elements aluminum, carbon, and oxygen are present on the trays previous to exposure to the contamination. Using the control samples from the SPIFEX (Shuttle Plume Impingement Flight Experiment) Contamination Study, as a reference, we find that the Al₂O₃ surface is 22.7% aluminum, 33.3 % carbon and 43.8% oxygen. Assuming that all of the aluminum detected by XPS is part of the tray, the aluminum, carbon, and oxygen previously present can be subtracted from the XPS results to yield the contamination film. Given that contamination film is 6.578 amu and the surface film has a formula weight of 18.287 amu the following calculation can be made.

$$1.57 \times 10^{-6} \text{ grams/cm}^2 * 0.123 * \frac{18.287}{6.578} = 53.45 \times 10^{-8} \text{ g/cm}^2$$

The contamination derived through the NASAN analysis for this same position shows $19 \times 10^{-6} \text{ g/cm}^2$ of deposition. The silicon content of the deposition at this point can be determined by multiplying by the 8.3 percent shown in the XPS survey, to end up with $43 \times 10^{-8} \text{ g/cm}^2$ of silicon. The following table shows comparison of points from tray A4-9. Due to the initial assumption of a deposition depth of 50 Å, the margin of error in this derivation is around twenty to thirty percent.

Table 1. Comparison of Surface Deposition at A4-9 from XPS to Depth of Deposition from NASAN

Location	Percentage of silicon at the surface	Amount of deposition from XPS survey in g/cm ²	Amount of silicon from NASAN analysis in g/cm ²
(29.5, 6.0)	8.3	43 x 10 ⁻⁸	43 x 10 ⁻⁸
(24.5, 5.0)	7.0	45 x 10 ⁻⁸	6 x 10 ⁻⁸
(24.5, 14.0)	14.0	62 x 10 ⁻⁸	20 x 10 ⁻⁸
(29.5, 15.0)	15.3	69 x 10 ⁻⁸	55 x 10 ⁻⁸
(27.0, 19.0)	15.2	80 x 10 ⁻⁸	78 x 10 ⁻⁸
(29.5, 11.0)	8.9	58 x 10 ⁻⁸	37 x 10 ⁻⁸
(41.5, 17.0)	10.4	57 x 10 ⁻⁸	32 x 10 ⁻⁸
(37.0, 14.5)	13.2	63 x 10 ⁻⁸	366 x 10 ⁻⁸
(43.0, 13.0)	6.2	42 x 10 ⁻⁸	10 x 10 ⁻⁸
(41.5, 12.0)	5.6	39 x 10 ⁻⁸	8 x 10 ⁻⁸

Unfortunately, there have been no studies done to correlate XPS data with depth of deposition for thick layers of contamination. If the deposit layer is greater than 50 Å, then the XPS will not sample any of the substrate. Hence, the depth cannot be deduced from the XPS survey; a full depth profile is necessary to determine an estimate of the

depth of the contamination. A depth profile of several locations on E10-3, E10-8, and C6-2 would allow for comparative analysis to be done to determine a method of calculating the depth of a particular element from the XPS survey for thick layer contamination. The following table lists the amount of silicon present at various points on the surfaces of trays E10-3, E10-8 and C6-2.

6.0 Summary and Conclusions

The results of this analysis are remarkably similar to pictures of the silicone deposition on the LDEF trays in terms of contamination shape. The depth of the contamination correlates well on tray slot A4-9, with the exception of point (37.0, 14). This point is located on the rivet on the tray and is much closer to the source of the contamination, so it is reasonable to expect the contamination layer to be greater than 50 Å at that point. There are no data for a comparison of results at other locations, but the results of the analyses are presented here.

Table 2. Total Deposition at Typical Locations on E10-3, E10-8, and C6-2 from NASAN Model in Å

E-10-3 Total Deposition modeled with NASAN in Å	E-10-8 Total Deposition modeled with NASAN in Å	C6-2 Total deposition modeled with NASAN in Å
45	100	1100
83	2200	430
230	1700	2400
1900	28000	2400
5700	6300	3300
15000	29000	5400
12000	13000	9100
3600	1600	5000
8200	150000	10000
2200	100000	5900
120	43000	7500
76	27000	8500

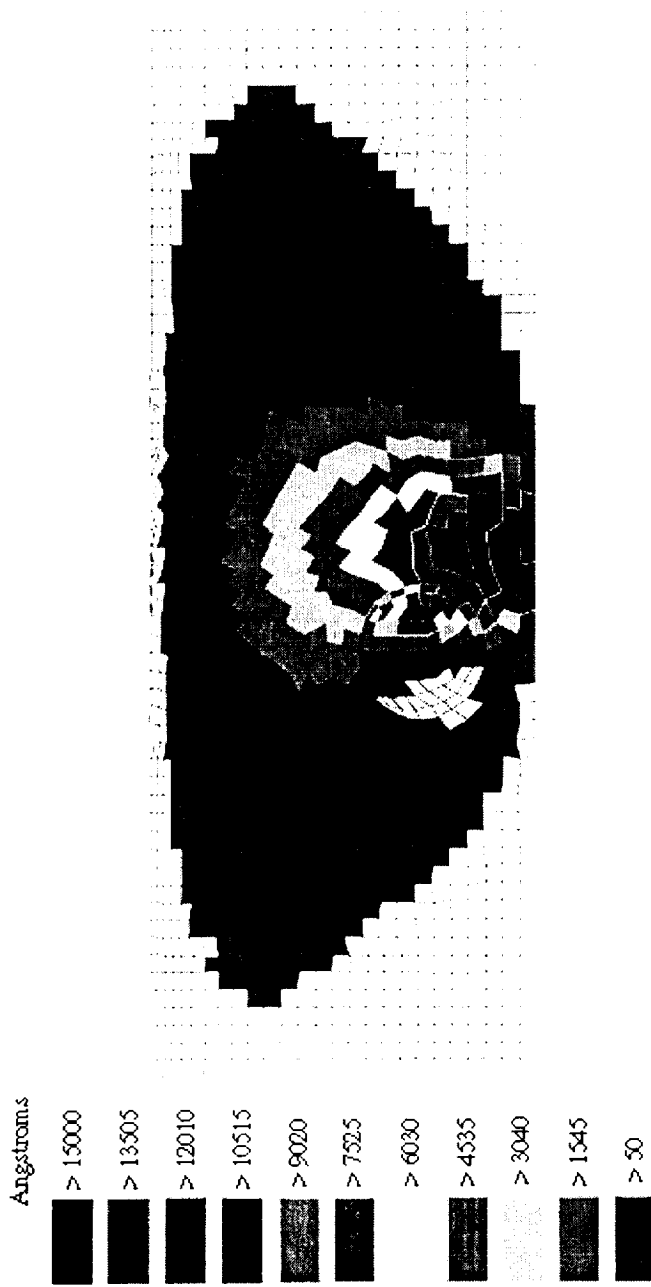


Figure 16. Deposition on E10-3 NASTRAN model

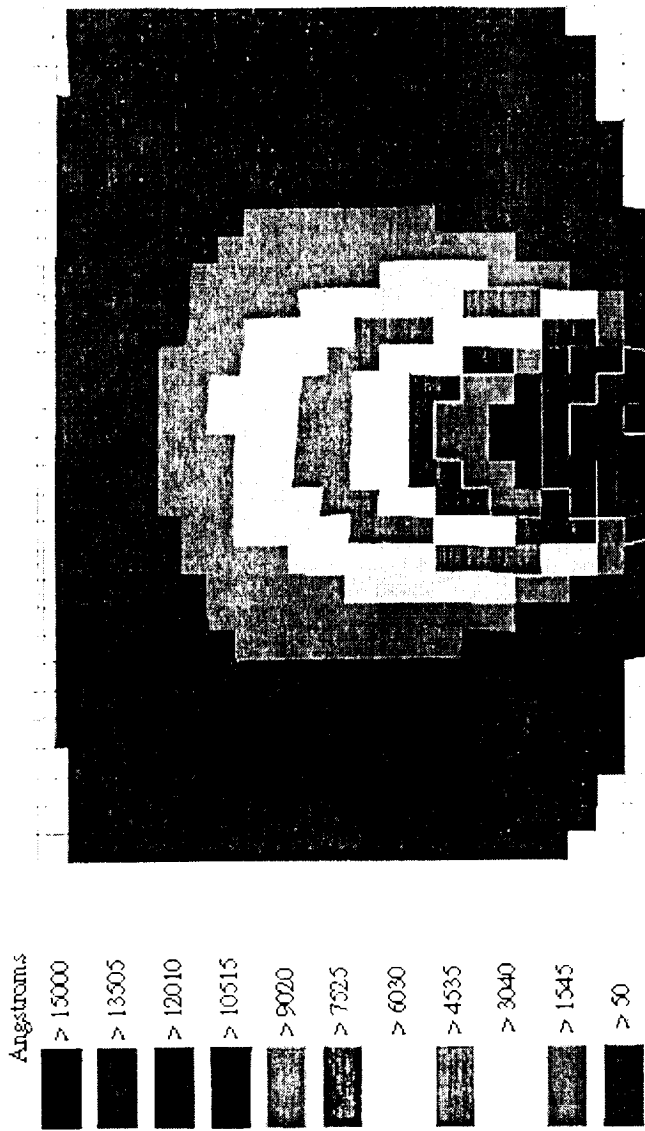


Figure 17. Deposition on C6-2 NASTRAN model

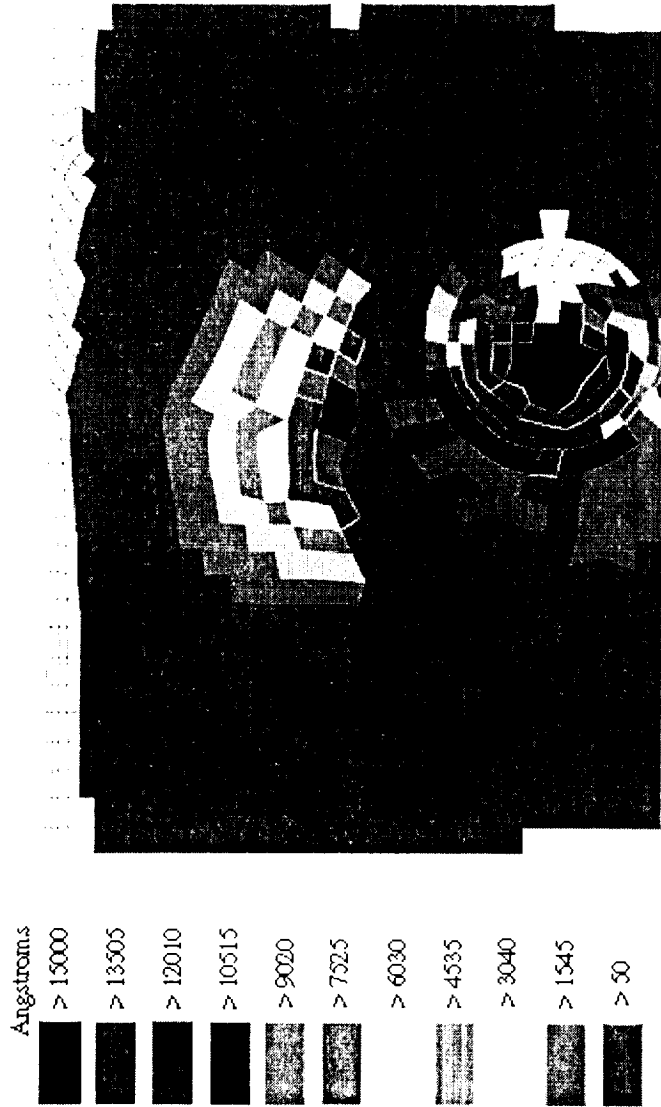


Figure 18. Deposition on A4-9 NASTRAN model

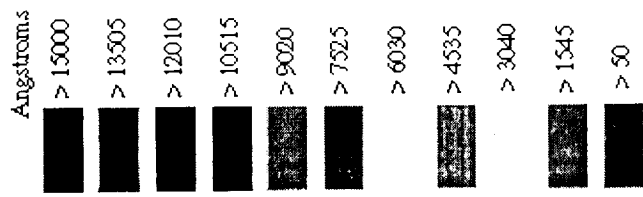


Figure 19. Deposition on E10-8 NASTRAN model

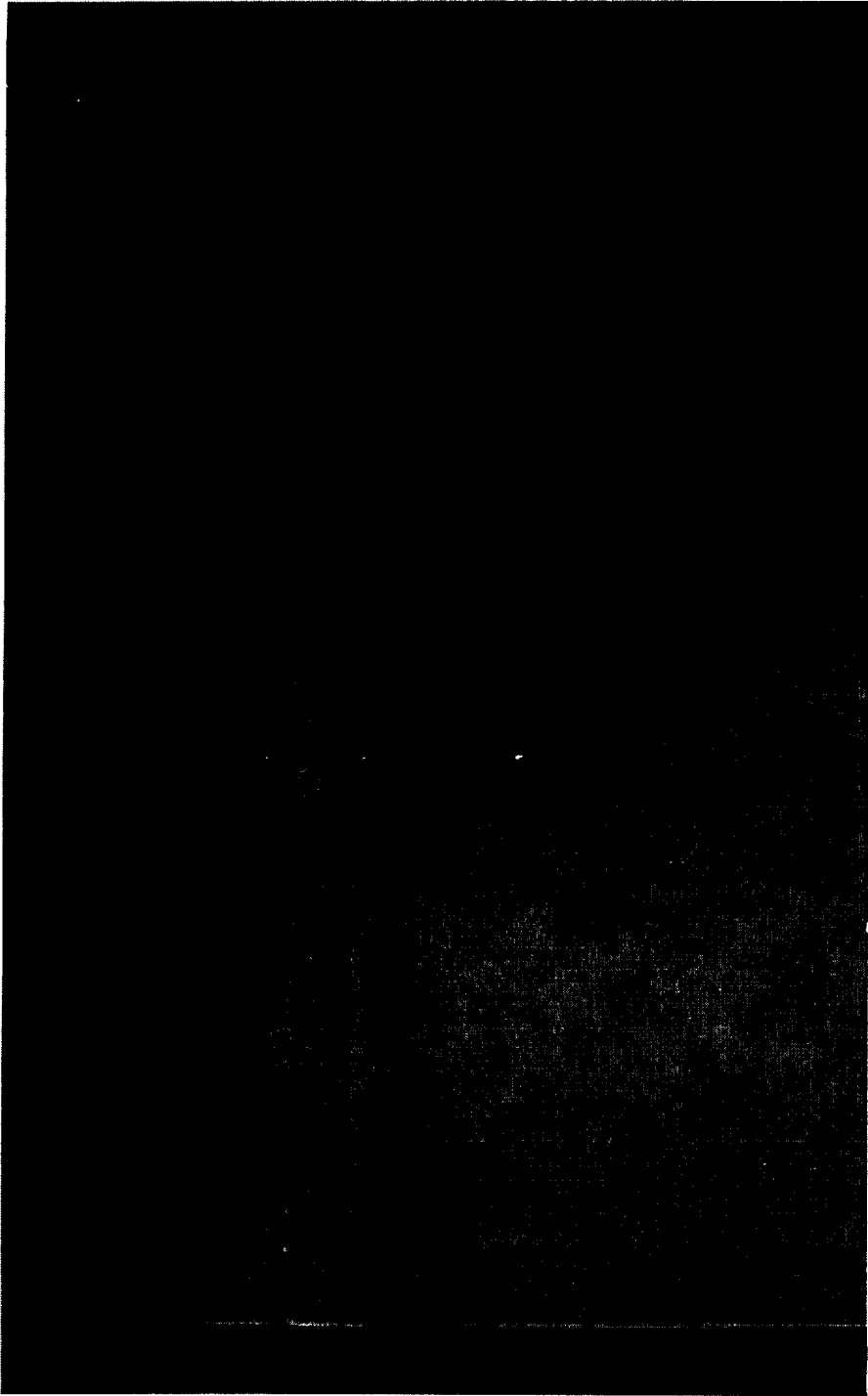


Figure 20. Photograph of concrete formwork, side wall.

References

1. Alred, John, "Outgassing Predictions for DC6-1104 Adhesive", Memorandum EM2-E1-JWA-03, 18 November 1997
2. Dursch, H. W., W.S. Spear, E. A. Miller, G.L. Bohnhoff-Hlavacek, and J. Edelman, "Analysis of Systems Hardware Flown on LDEF - Results of the Systems Special Investigation", NAS1-19247 April 1992
3. Fussell, John and Nell Warnes, "Contamination Deposited On PG-1 Critical Surfaces From Node-1 Sources", MDC 97H0520, April 1997.
4. Glassford, A. P. M. and J. W. Garrett, "Characterization of Contamination Generation Characteristics of Satellite Materials", Final Report WRDC-TR-89-4114, 22 November 1989.
5. Hakes, C. "Contamination Analysis Programs for the International Space Station", AIAA-97-0632, 35th Aerospace Sciences Meeting and Exhibit, Reno, Nevada, January 1997
6. Koontz, Steven, Orlando Melendez, Mike, Zolensky, and Carlos Soares, SPIFEX Contamination Studies, JSC 27399, May 1996.
7. Powell, C. J., M. P. Seah; "Precision, Accuracy and Uncertainty in Quantitative Surface Analysis by Auger-electron Spectroscopy and X-ray Photoelectron Spectroscopy," J. Vac. Sci. Technol., A8 (2), pp 735-768, March-April 1990.

Appendices

Appendix A. Data for DC6-1104 Outgassing Tests performed at Lockheed Martin-Sunnyvale

Appendix B. DC6-1104 Projections for Source Temperatures of 75°C and 125°C

APPENDIX A

**Data for DC6-1104 Outgassing Tests
performed at Lockheed Martin-Sunnyvale**



Memorandum

Date: November 18, 1997
Reference: EM2-E1-JWA-03

To: Keith Albyn Dept. NASA Bldg./ JSC-13
No.: Mail Code: EM2

From: John W. Alred Dept. A32 Bldg./ LM34GM Tel: 333-
No.: Mail Code: C87 7059

Subject: Outgassing Predictions for DC6-1104 Adhesive

Introduction

Ms. Nell Warnes and Mr. Carlos Soares of the Boeing ISS External Contamination Team requested that a prediction of the outgassing source rate for DC6-1104 adhesive be made based on the data available from Characterization of Contamination Generation Characteristics of Satellite Materials by Glassford and Garrett (WRDC-TR-89-4114, dated November 22, 1989). This memorandum documents the results of that analysis.

Description of Analysis

The Air Force Research Laboratory at Wright-Patterson Air Force Base issued a report entitled Characterization of Contamination Generation Characteristics of Satellite Materials by A. Glassford and J. Garrett (WRDC-TR-89-4114) on November 22, 1989. This report summarized a number of outgassing tests performed at Lockheed Martin-Sunnyvale. Much of the data in this reference is available locally in the Lockheed Martin computer systems. The data for the DC6-1104 adhesive was available for source temperatures of 75°C and 125°C and a receiver temperature of 90K. A program (EMBRACE), developed in March 1997, provides an excellent function fit to the measured data in terms of frequency (*f*) vs. time (*t*). The best functional form of this "curve-fit" has been found to be

$$f = a \cdot \ln(t) + b \tag{1}$$

where *a* and *b* are constants obtained from a variational technique that reduces the standard error (known as a "least-squares fit"). Each set of test data was fit using the function of Equation (1) for each TQCM temperature. The rate was calculated by taking the derivative of the frequency *f* and multiplying by the TQCM sensitivity, multiplying by the effusion cell view factor, and dividing by the sample area.

Hence,

$$\frac{df}{dt} = \frac{d}{dt} [a \cdot \ln(t) + b] = \frac{a}{t} \tag{2}$$

with a rate given by

$$\frac{dm}{dt} = \frac{\left(\frac{a}{t} \cdot A_{V.F.}\right)}{A_{Sample}} \quad (3)$$

The analysis procedure consisted of fitting the data to Equation (1) and using the value for a in Equation (3). The results for each test as a function of source temperature is presented in Appendix A.

For the DC6-1104 adhesive, the form of the curve calculated for the source rate data was

$$\frac{dm}{dt} = \frac{c}{t}; \quad (4)$$

where c is a constant and t is time (in seconds).

For a source temperature of 75°C and a receiver temperature of 90K, we calculated

$$c_{75^\circ\text{C}} = 0.001173 \text{ g/cm}^2 \quad (5)$$

For a source temperature of 125°C and a receiver temperature of 90K, we calculated

$$c_{125^\circ\text{C}} = 0.002048 \text{ g/cm}^2 \quad (6)$$

As a check of the curve fit, the regression coefficient for the 125°C case was 0.99952 and the regression coefficient for 75°C was 0.99973.

To complete this phase of the analysis, the curve-fit equations were used to project the data from 1-100 days. These projections are shown via plots contained in Appendix B.

Extension of the Data Analysis

The question was raised of extending the data from these tests to a source temperature of 24°C and a receiver temperature of 10°C. From Lockheed Martin Memorandum EM2-E1-JWA-01, dated November 5, 1997, the outgassing source rates for RTV-142 adhesive for source temperatures of 125°C, 90°C, and 75°C and receiver temperatures of 90K, -40°C, -10°C, and 25°C are presented. In Lockheed Martin Memorandum EM2-E1-JWA-02, dated November 18, 1997, a similar question was raised. To estimate the effect of a different source or receiver temperature, the values for the known sources and TQCM's at each time increment were taken and a function was fit to the curve generated by those points. The best fit for the RTV-142 data (regression coefficient of 0.99999) was found for the following function:

$$F(T) = d \cdot T^e + g; \quad (7)$$

where d , e , and g are constants determined from the data while T is the temperature in Kelvin. The process was then repeated at each time increment. Using this heritage of information modified with the actual DC6-1104 experimental data, values for the outgassing source rate of DC6-1104 at a source temperature of 24°C for receiver temperatures of 90K and 10°C were calculated. Using the curve-fit equation given in (4), we projected the data from 1-100 days. These plots are presented in Appendix C.

Reference: EM2-E1-JWA-03

For a source temperature of 24°C and a receiver temperature of 10°C, we calculated

$$c_{2rc} = 1.73 \times 10^{-03} \text{ g/cm}^2 \quad (8)$$

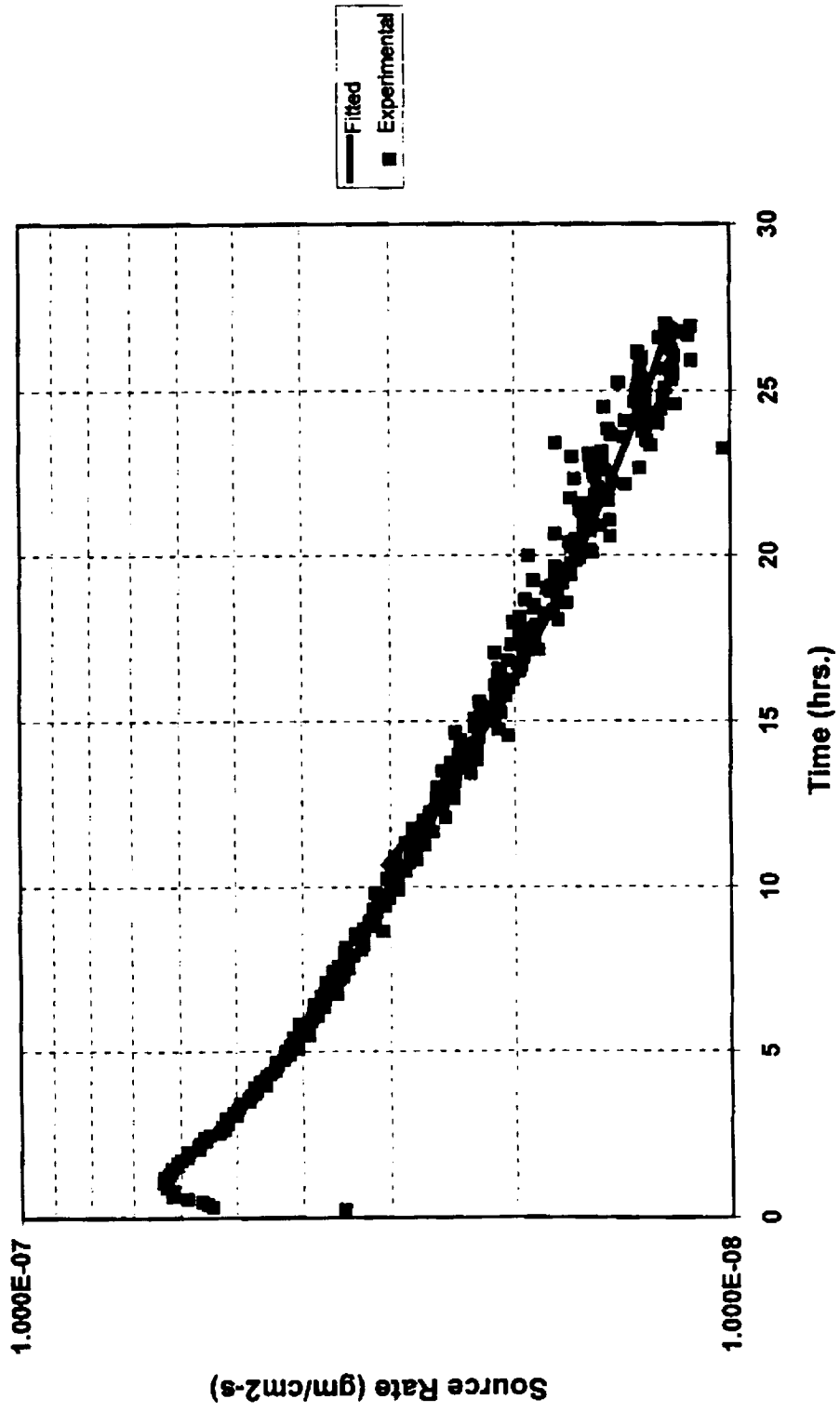
Prepared by:


John W. Alred; Engineering Specialist III
Engineering Analysis and Simulation Department

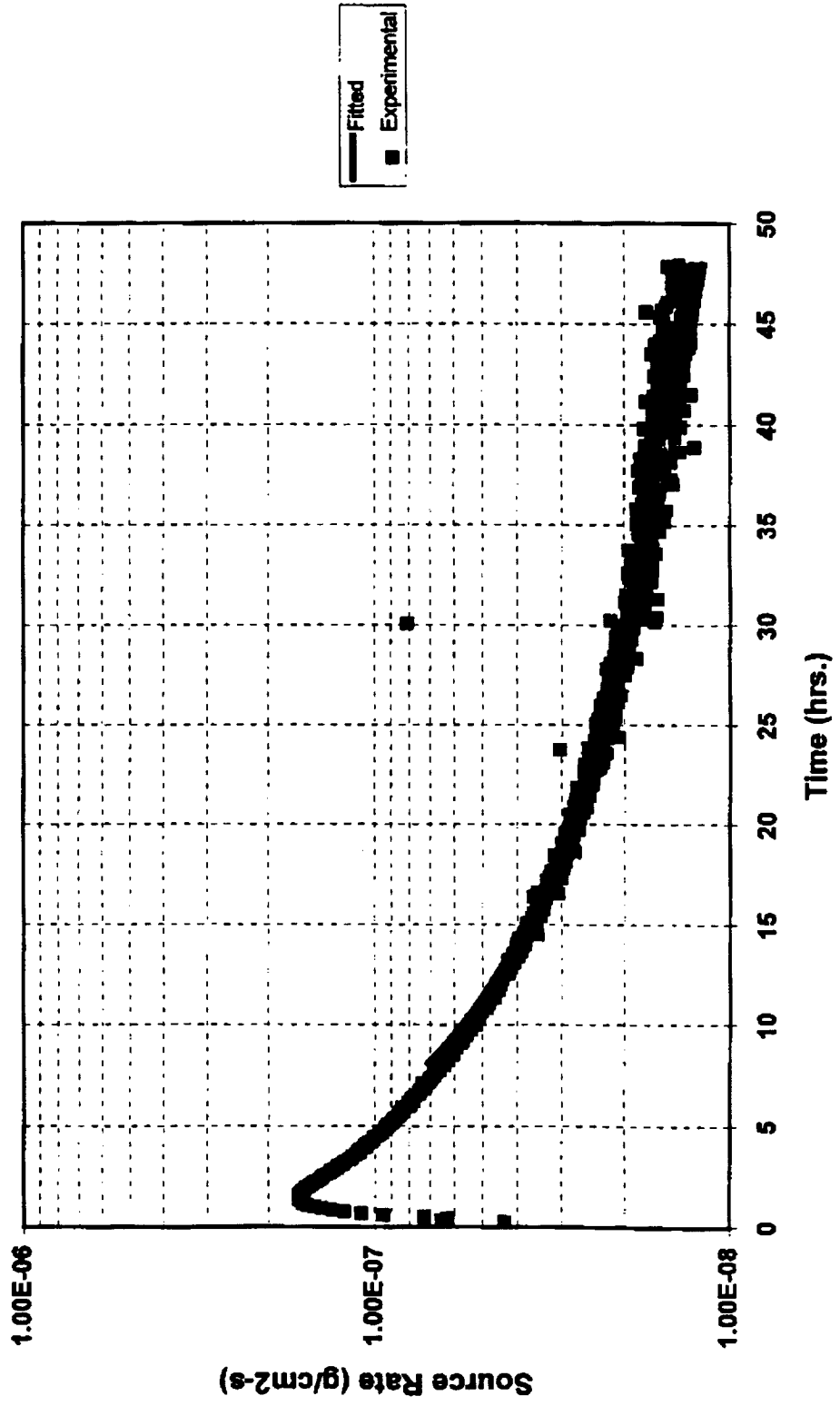
CC:

Tom Farrell/NASA ISS
Ron Mikatarian/Boeing
Carlos Soares/Boeing
Nell Warnes/Boeing
Bill Schoolmeyer/C87

DC6-1104 Adhesive @ 75°C



DC6-1104 Adhesive at 125°C

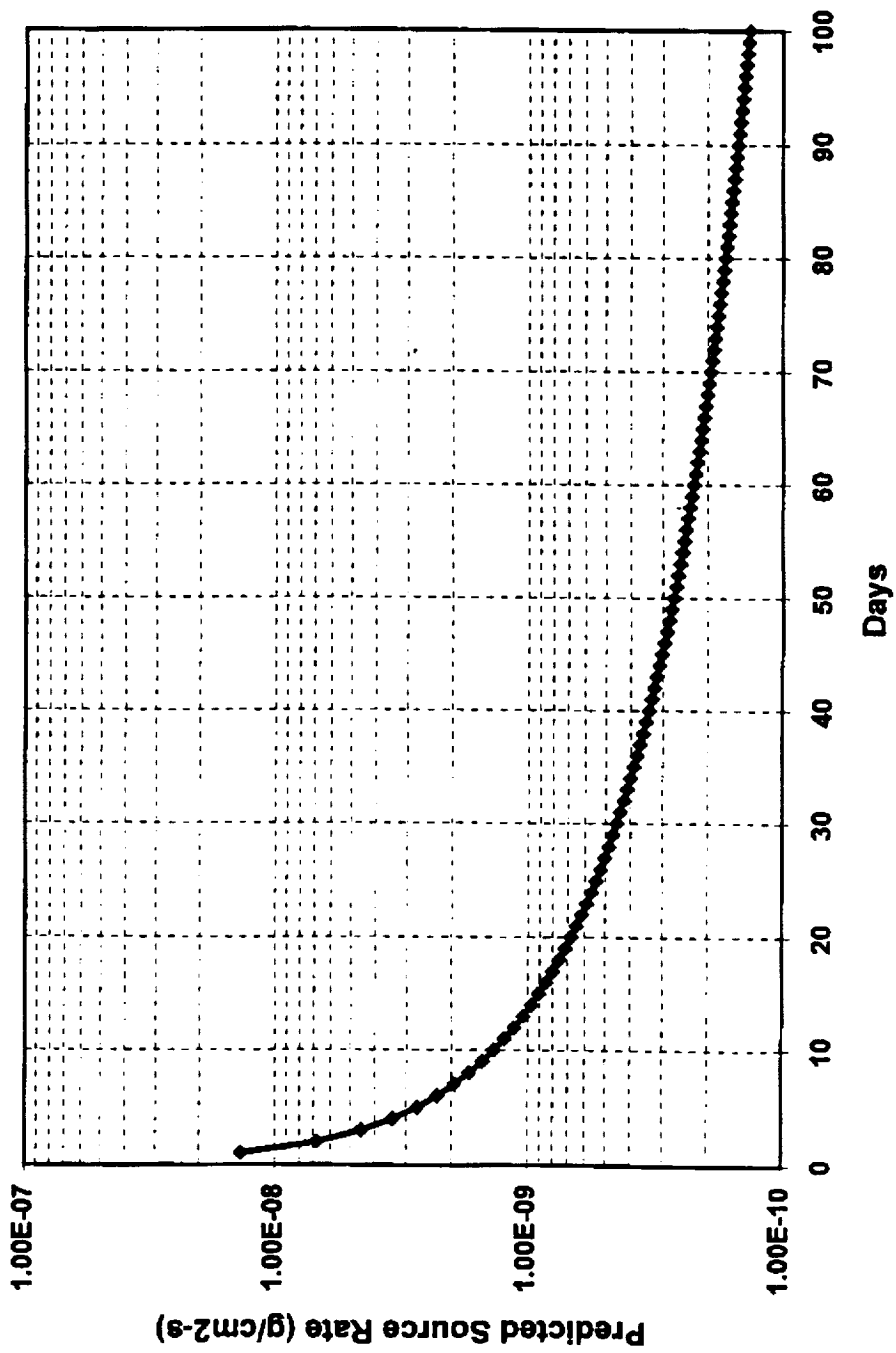


APPENDIX B

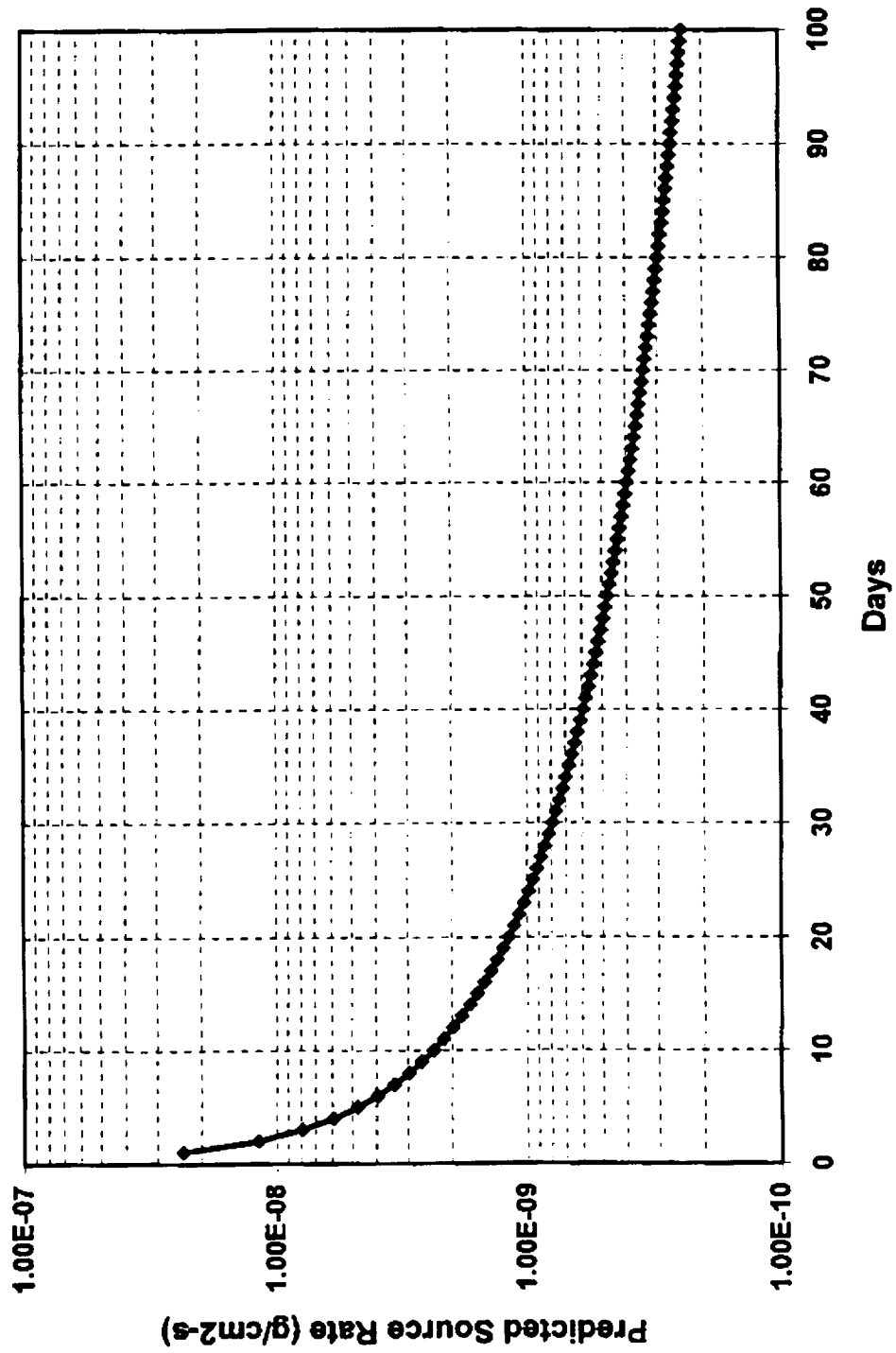
DC6-1104 Projections for Source Temperatures of 75°C and 125°C

B-1

DC6-1104 Adhesive :Source@ 75°C & Receiver@90K



DC6-1104 Adhesive :Source@ 125°C & Receiver@90K

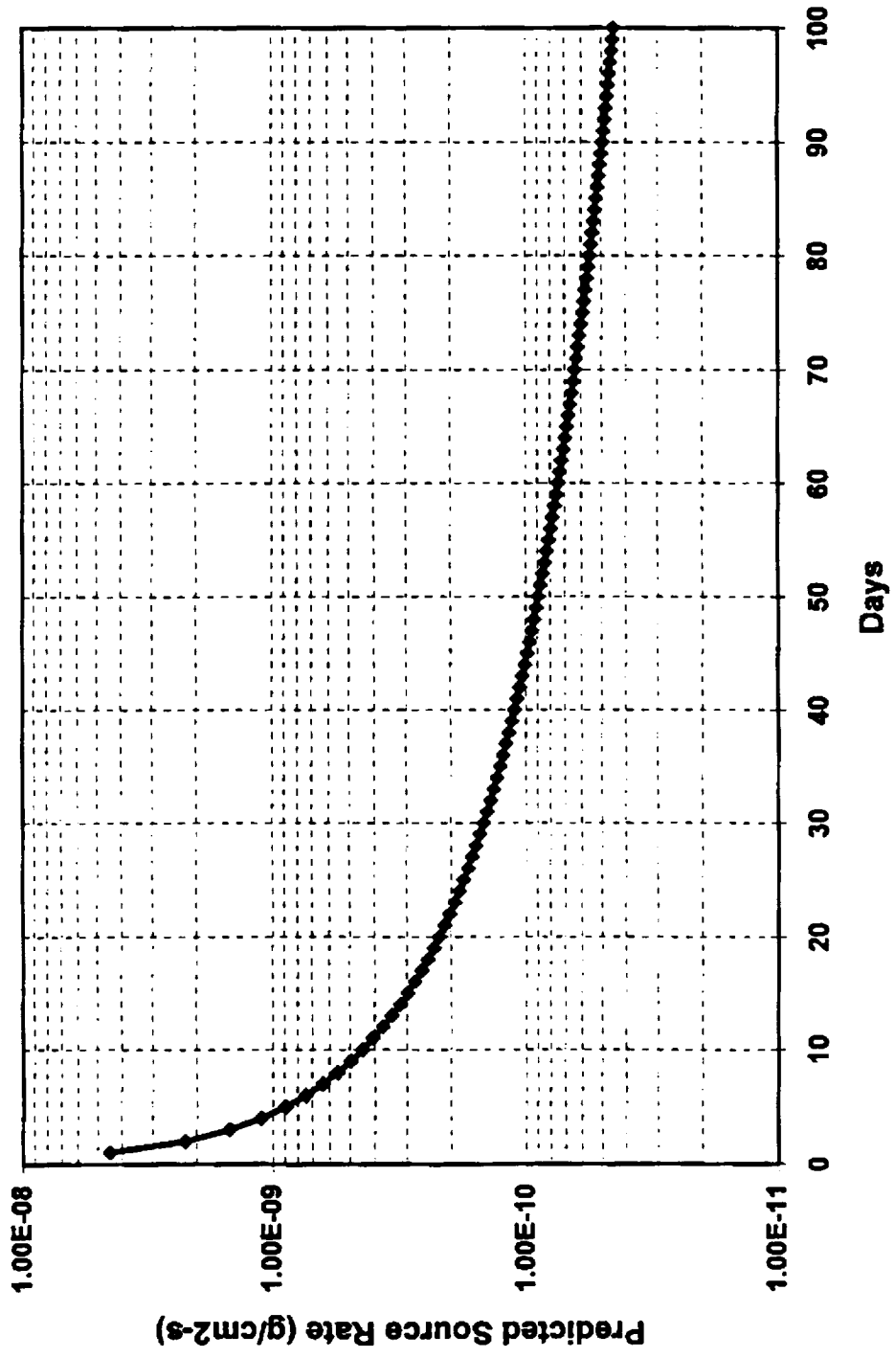


APPENDIX C

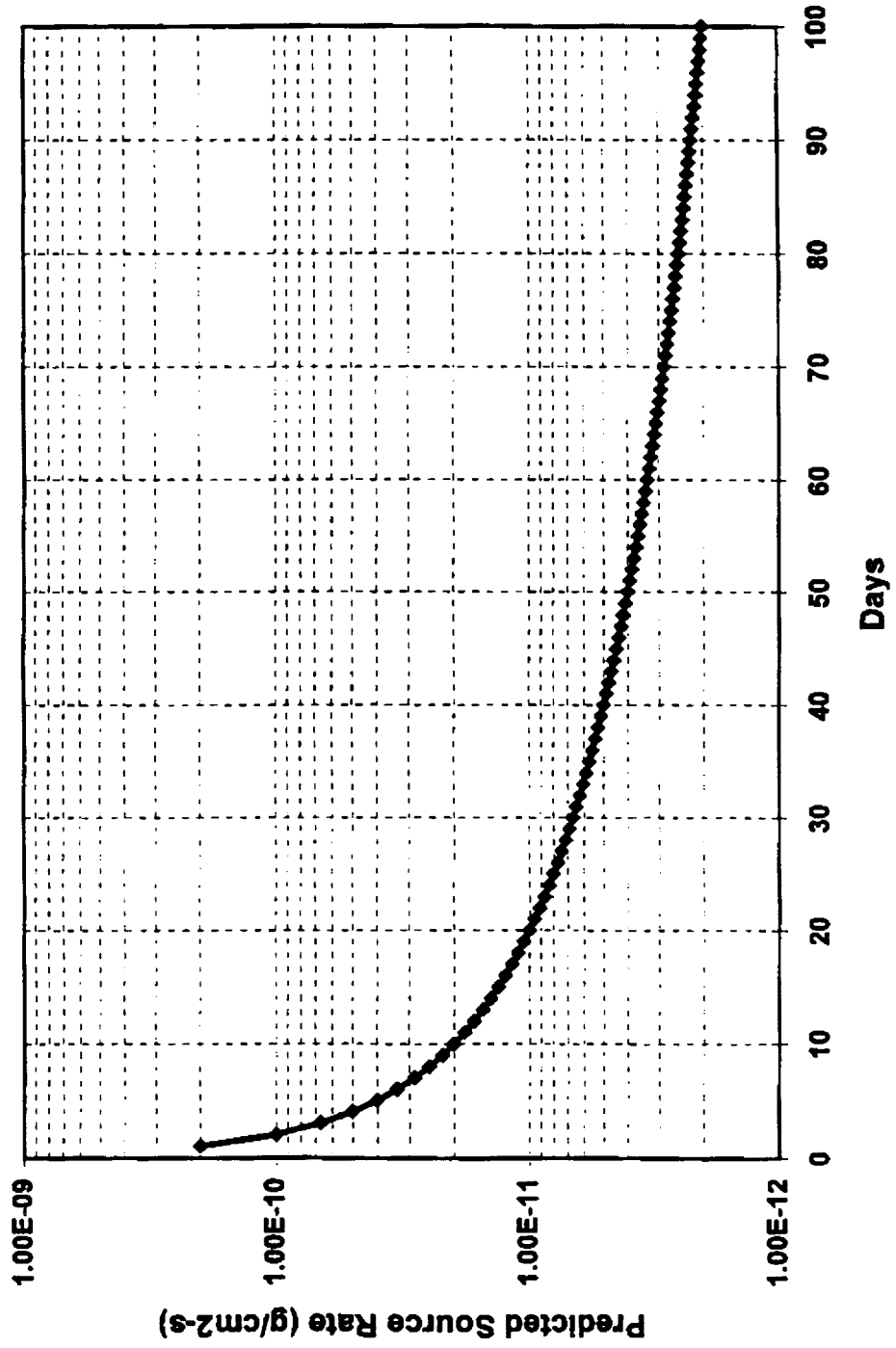
**DC6-1104 Projections for
Source Temperature of 24°C**

C-1

DC6-1104 Adhesive :Source@ 24°C & Receiver@90K



DC6-1104 Adhesive :Source@ 24°C & Receiver@ 10°C



FINAL REPORT

#ROR-B-9073-97

**“CONTAMINATION PREDICTION MODEL(ISEM) CALCULATION FOR
SELECTED LDEF TRAYS”**

**PURCHASE CONTRACT:
JJ9073**

**PART OF:
NAS8-040581**

**SUBMITTED TO:
THE BOEING COMPANY SPACE AND DEFENSE GROUP**

**SUBMITTED BY:
ROR ENTERPRISES, INC.
2455 W. SUMMER AVE
ATHOL, ID 83801**

**WORK ORDER CHARGE #:
5-9K466-5571-539640**

DATE:

10-27-97

APPROVED BY:

DR. RAY RANTANEN DATE

Table of Contents

<u>Section</u>	<u>Page</u>
1.0 Background.....	4
2.0 Modeling Objectives.....	4
3.0 Modeling Methodology.....	4
4.0 Macro Model.....	
5.0 Micro Model.....	6
5.1 Micro Model Geometry.....	6
5.2 Micro Model Sources and Temperatures.....	8
5.3 Micro Model Results.....	8
6.0 Deposition Predictions.....	9
7.0 Conclusions.....	13
8.0 References.....	14

Appendix A - Micro Model Computed Flux Tables

Table of Figures

<u>Figure</u>	<u>Page</u>
Figure 1 - Micro Model Geometry.....	15
Figure 2 - Thermal Blanket Keyhole Geometry.....	16
Figure 3 - Keyhole Modeling Approximation.....	17
Figure 4 - Basic TRASYS Geometry Model.....	18
Figure 5 - TRASYS Geometry Model with Computational..... Grid (+Z Axis View)	19
Figure 6 - TRASYS Geometry Model with Computational..... Grid (+Y Axis View)	20
Figure 7 - Flux Computation Point Row Locations.....	21
Figure 8 - Total Atomic Oxygen Flux Contours on Tray Wall.....	22
Figure 9 - Total Contaminant Flux Contours on Tray Wall.....	23
Figure 10 - Total Atomic Oxygen and Contaminant..... Flux Contours on Tray Wall	24
Figure 11 - Deposition Cross Sections Along Selected Rows	25
Figure 12 - Deposition along Keyhole Centerline.....	26
Figure 13 - Contaminant Deposition Contours on Tray Wall.....	27

1.0 Background

The Long Duration Exposure Facility (LDEF) was returned to Earth in early 1990 with a wealth of information regarding the orbital environment and its effects on various materials. In addition to the designed experiments, the structure of the spacecraft itself is providing significant clues and data regarding the space environment.

After removal of the experiment trays, numerous deposits on internal surfaces were noticed. Of particular interest to the contamination community were deposits on internal surfaces in close proximity to small apertures or openings in the external LDEF surface. These deposits exhibited patterns which seem peculiar to an environment where free molecular flow minimized collisional interaction.

2.0 Modeling Objectives

The purpose of this modeling effort is to use the Integrated Spacecraft Environments Model (ISEM) to model a portion of the LDEF for which careful deposition measurements will be made. The measured deposition can then be compared to the ISEM modeling results and the modeling accuracy determined.

3.0 Modeling Methodology

The modeling objectives require the modeling of a very small portion of one of the LDEF trays. The model will only model the local environment in the vicinity of the region of interest. This model will be referred to as the micro model.

As a prerequisite for the micro model, it is first necessary to determine whether or not the local environment to be modeled is significantly affected by other sources on the LDEF and the general interaction of the LDEF with the ambient atmosphere. This was accomplished by examining the results of a LDEF macro model which included the entire LDEF and included the modeling of all of the general sources as best they are known.

4.0 Macro Model

Work on the macro model which included the entire LDEF was accomplished prior to this current effort. It is referenced here as justification for the modeling approach which was used for the micro model.

For more extensive details regarding the work done previously on the LDEF macro model, please refer to references 1 and 2 listed in section 8.0 or the summary in Appendix B of the Preliminary report dated 4-20-97.

Based on the results of the LDEF macro model, the ambient is only slightly attenuated by the general LDEF environment. Also, the return flux of contaminants from overall LDEF sources to the location of the experiment tray (E10) are low compared to local effects. Consequently, it should not be necessary to account for the computed macro LDEF environment in the model setup for the micro model.

5.0 Micro Model

The micro model chosen for this study is for a small keyhole shaped aperture in a thermal blanket on the Ultra Heavy Cosmic Ray Experiment (UHCRE). The UHCRE was located on several trays at different locations on the LDEF. For the purposes of this modeling, a tray on row 10 (E10) was chosen. Row 10 was originally intended to be oriented at an angle of 30 degrees to the velocity (ram) vector. However, because of an 8 degree bias in the yaw angle, row 10 was oriented at an angle of 22 degrees to the velocity vector. As a consequence, surfaces in the plane of row 10 are believed to have received a fluence of atomic oxygen (AO) of approximately 8.7×10^{21} atoms/cm² over the 69 month mission³. The keyhole openings in the thermal blanket were located at intervals around the edge of the tray and allowed a limited direct ambient exposure (a function of the opening geometry relative to the velocity vector) to the tray wall beneath the blanket. A portion of the tray wall immediately above and below the thermal blanket openings showed obvious signs of contaminant deposition. It is the purpose of this effort to model the relevant molecular sources in the vicinity of one of the keyhole shaped openings and determine the flux and ultimately the deposition on the tray wall above and below the opening. Because row 10 was oriented at 22 degrees to the velocity vector and because of the orientation of the keyhole, it was only possible for the ambient to enter the keyholes on one side of the E10 tray. The micro model is for a keyhole on the side of tray E10 closest to row 11.

5.1 Micro Model Geometry

The geometry for tray wall, thermal blanket, and keyhole aperture were measured and supplied by Boeing personnel. Figure 1 shows a side view of the micro model geometry. The keyhole aperture is located in the thermal blanket and extends from the thermal blanket/tray wall intersection up and a little past the cylindrical bend in the blanket. Figure 2 shows the geometry of the keyhole in a planar view. Note that the portions of the keyhole aperture which are located on the flat slope and cylindrical section of the thermal blanket are designated in the figure.

The upper portion of the keyhole aperture is circular. The majority of this circular portion of the keyhole is in the cylindrical bend of the thermal blanket.

The compound geometry problem of a circular aperture superimposed on a cylinder is somewhat difficult to model using the Thermal Radiation Analysis System (TRASYS). A modified version of TRASYS is used by ISEM to model spacecraft geometries and to compute surface-to-surface formfactors and surface-to-point solid angles. The circular portion of the aperture which lies on the cylindrical part of the thermal blanket was modeled using discrete cylinder segments approximating the circular perimeter. The dimensions for this approximating technique are given in Figure 3. The area of the approximated aperture was made to match the computed area of the actual aperture. Figure 4 shows an oblique view of the TRASYS created geometry model.

ISEM requires the definition of a three dimensional modeling volume in which molecular collisional interactions are computed. For the micro model, the modeling volume is very small. The dimensions of the modeling volume were 80mm in X, 39mm in Y, and 30 mm in the Z dimension. The modeling volume was subdivided into incremental volumes measuring 4 by 3 by 2 mm in X, Y, and Z respectively. Figures 5 and 6 show the three dimensional modeling volume from the +Z and +Y views respectively. Figure 5 shows the model geometry angled such that the velocity vector is in the +X axis direction.

ISEM allows the user to designate any number of points within the modeling volume as flux computation points. For each flux computation point, the user designates the desired field-of-view (acceptance angle) and the direction vector of the field-of-view centerline. ISEM then computes the flux of each molecular species at each flux point by accumulating contributions from each incremental volume. The computed flux includes both direct and scattered components of each molecular species. For the micro model, 12 rows of flux computation points were placed on the LDEF tray wall. Each row contained 15 points. The flux computation points can be considered an array of 12 rows and 15 columns, with the 8th column aligned on the centerline of the keyhole. Because of the symmetrical nature of the problem, the array of computed flux values for each species were symmetrical about the 8th column. Figure 7 is a side view of the thermal blanket and tray wall geometry, with the flux computation point rows designated. The horizontal spacing of the flux computation points in the Y dimension was 2mm. The vertical spacing of the points along the tray wall surface is given in Figure 7. Each flux point was given a hemispherical field-of-view centered about the surface normal for the tray wall surface at that location.

5.2 Micro Model Sources and Temperatures

Although ISEM can model any number of ambient species, it seemed reasonable for the purposes of this study to only model the ambient atomic oxygen (AO). During the entire LDEF mission the predominant ambient species, in terms of number density, was AO. For the purposes of this analysis, the ambient density of AO was assumed to be 9×10^8 atoms/cm³. The ambient temperature was assumed to be 1303 degrees Kelvin. The temperatures of the modeled spacecraft surfaces were assumed to be 300 degrees Kelvin. The spacecraft velocity was assumed to be 7.69×10^5 cm/sec. The AO ambient density and temperature were computed using MSIS86 and are representative of ambient conditions relatively late in the mission when the AO flux was nearing its mission peak just before retrieval.

The internal volume underneath the thermal blanket was assumed to contain a number of outgassing contaminant sources. It was also assumed that since the exit apertures for the enclosed volume were a small fraction of the total internal surface area, on the average a contaminant molecule would make thousands bounces before finally reaching an exit aperture. The effect of this assumption is that the internal volume would have the effect of an integrating sphere which distributes the contaminant equally over all of the internal surfaces. Consequently, the internal outgassing can be characterized as a general background outgassing rate. The rate chosen for this initial modeling was 1×10^{-11} g/cm²/sec. If a contaminant molecular mass of 100 amu is assumed, this rate equates to 6.02×10^{10} molecules/cm²/sec. The thermal blanket was mounted on a framework which had a vertical surface in close proximity to the keyhole aperture. This surface was given the internal surface emission rate of 6.02×10^{10} molecules/cm²/sec. As an approximation for the remainder of the internal surfaces, the vertical surface was extended such that it backed the entire keyhole aperture.

5.3 Micro Model Results

The computed flux data for the micro model is summarized in the form of three flux contour plots. Prior to discussing specific implications of each plot, there are several general items which apply to all three plots.

Asymmetry about the vertical centerline in all three plots is an artifact of the contour plotting routine. The computed flux values were symmetrical about the vertical centerline.

The vertical distances given at the left of each plot are millimeters measured along the tray wall surface from the intersection of the thermal blanket with the tray wall. Because the tray wall bends at the top to form the tray lip, and because flux computation rows 10 through 12 are located on the cylindrical portion of the tray wall, the upper portion of the plot is not linear in the vertical dimension.

The intersection of the thermal blanket with the tray wall was located halfway between flux computation rows 5 and 6. Except within the keyhole, the intersection created a discontinuity in the data (i.e. the direct ambient is blocked by the outer surface of the thermal blanket, and the internal sources are blocked by the inside surface of the thermal blanket). The contour plotting routine naturally assumed a linear change between flux values in rows 5 and 6, which is only the case within the keyhole. To avoid confusion, the contour lines between flux rows 5 and 6 have been blacked out except in the keyhole.

Figure 8 shows the computed atomic oxygen (AO) iso-flux contours on the tray wall for the modeled conditions. The area of the tray wall above the blanket-wall intersection is exposed to direct AO flux (attenuated only by the cosine of the angle of the surface to the velocity vector), it is also exposed to direct surface reemitted AO flux from the portion of the thermal blanket which is within the field-of-view of each flux computation point. Also contributing to the total AO flux is the portion of the direct ambient AO which is scattered by collisions with the outgassing contaminant escaping through the keyhole and with surface reemitted AO. Likewise, scattered surface reemitted AO contributes a minor portion of the total AO flux. With the exception of a small portion of the keyhole which has a direct line-of-sight to the ambient AO, the portion of the tray wall below the thermal blanket receives AO flux via scattering. The relative contributions of each direct and scattered component of the AO can be examined in the flux component tables provided in Appendix A.

Figure 9 shows the computed contaminant iso-flux contours on the tray wall. For the modeled conditions, the contaminant flux on the tray wall below the thermal blanket intersection was a constant (within modeling limitations) of approximately $5E+10$ molecules/cm²/sec. The portion of the tray wall above the thermal blanket intersection received contaminant flux from the keyhole. The distribution of contaminant flux outside the keyhole appears (to the first approximation) to be cosine as would be expected.

For the modeled conditions, the limiting deposition parameter above the thermal blanket/tray wall intersection is the contaminant, if one assumes a one-to-one relationship between AO and contaminant molecules for the purposes of fixing the contaminant. Likewise, the limiting deposition parameter below the thermal blanket/tray wall intersection is the AO flux. In order to more easily visualize the deposition shape in the vicinity of the keyhole, a third contour plot, Figure 10, is provided which shows the contaminant iso-flux contours above the thermal blanket/tray wall intersection and the AO iso-flux contours below the intersection.

6.0 Deposition Predictions

The previously made flux values on the tray wall, outside and inside the keyhole, were used to predict the resulting deposition.

The amount of DC 61104 inside the experiment tray was reported to be 250 grams total. From Lockheed report WRDC-TR-89-4114, the VCM values for DC 61104 for the source at 125°C and receiver at 25°C was given as 0.0024%, and for the source at 75°C and receiver at 25°C it was .00025%. The value for the source at 125°C was used for a worst case analysis.

Assumptions made:

- 1) All of the VCM was released by the DC 61104 during the LDEF mission
- 2) All of the VCM deposited in areas around the keyhole
- 3) Sufficient atomic oxygen flux was present to fix the contaminants on the outside of the keyhole (flux was two to four orders of magnitude greater than the VCM flux)
- 4) ten keyholes each with an area of 1.85 cm² emitted the VCM

With these assumptions the maximum deposit predicted outside the keyhole was 28,464 angstroms for a deposit density of 1.12 g/cm³.

Measurements made by Boeing showed a deposit in this region of 10,000 angstroms. The worst case model prediction of 28,464 angstroms was next refined to account for attenuation of the contaminants emitted by the DC 61104 that are fixed inside the experiment volume due to atomic oxygen entering the 10 keyholes. Allowances for VCM differences and the fact that perhaps all of the VCM never came out of the DC 61104 over the life of the mission, were investigated. It was decided to stay with the VCM data that gave the most confidence, and determine what other mechanisms could be involved in the process of contaminants escaping out of the keyholes. Even though the DC 61104 source was not at the 125°C temperature of the VCM test, it was assumed the total amount available for VCM outgassing from this source would eventually come out a lower temperature over the life of the mission. The following is a brief summary of the calculations involved and the various results.

The rate of the VCM is 250 grams x .000024 (Lockheed data) divided by the mission timeline (1.8E+8 seconds) = 3.333E-11 g/s. Assuming all of this comes out the keyholes the rate is 3.333E-12 per hole or 1.8E-12 g/cm² for a keyhole size of 1.85 cm²

An independent analysis using pumping speed equations and partial pressures arrived at the same surface flux rate for the contaminant. The equations used were steady state where:

$P=Q/S$ where P is in Torr, Q is in Torr-liters per second and S is in liters/second.

The atomic oxygen total fluence is reported to be 8.7E+21 AO/cm² over the mission. The projected areas of the keyholes (normal to the AO flux) was calculated to be 8 cm² for this particular tray. Each individual contribution varied,

depending on the side of the tray the keyhole is located. The total AO entering the experiment volume is then = $6.96E+22$ AO atoms. Averaged over the mission ($1.8E+8$ seconds), this is $3.87E15$ AO/s. This flux entering the ten keyholes strikes different surfaces on initial impact and strikes a total area of near 150 cm^2 with an average flux level of $2.6E+13$ AO/cm²/s. This is near three orders of magnitude greater than the VCM surface flux rate. After this initial impact the first AO reflection sees a majority of the interior of the experiment. It was determined it sees all of the inside top surface, all of the sides, one half of the cylinders, one half of miscellaneous surfaces and 40% of the inside bottom. These equate to:

- top = 13400 cm^2
- sides = $8960 = 5570$
- 1/2 of cylinders = $10,900$
- 1/2 of misc. = $10,000$
- 40% of bottom = 5360

Total = $54,190\text{ cm}^2$.

The surfaces that the first reflected AO would impinge upon are determined by locating the flux of the first impact on the tray sides and bottom. This varies significantly between the ends and each side of the tray. The initial flux on the bottom inside can reemit to all the sides, the inside top of the experiment and bottom of the cylinders. The initial flux on the sides of the tray can emit to portions of the bottom, sides and top. Related to the total estimated area inside of $83,200\text{ cm}^2$, this is 65% of the total area. Since the VCM is assumed to be evenly distributed on all interior surfaces, this says 65% can be fixed by AO (at scattered fluxes of $2.6E+13\text{ cm}^2$) and can not come out of the keyholes. The remaining 35% can. This modifies the predictions for a worst case deposit immediately outside the keyhole to 9,963 angstroms which is very close to the measured value.

The AO fixed VCM on the interior is spread over a large surface area which should not result in a deposit layer greater than 12 angstroms and would therefore not be easily noticed.

If the VCM numbers for a 75°C source is used from the Lockheed report, then a deposit of 3000 angstroms maximum deposit is predicted for no attenuation and 1050 angstroms for attenuation due to VCM fixing in the experiment volume.

If a value for VCM is used, cited in the Boeing report (actually from an LDEF document), a total deposit of near 237,000 angstroms would result with no attenuation and 83,000 angstroms with attenuation due to AO fixing inside the experiment volume.

Since the pedigree and conditions of the CVCM measurements referenced in the LDEF report were not known, another source of VCM data was used. This data

came from Lockheed report WRDC-TR-89-4114. This VCM data was used to arrive at the baseline prediction of 9,963 angstroms.

The following tables summarize the overall results.

**SUMMARY PREDICTIONS-ANGSTROMS
MAXIMUM VALUES-CORRELATION TO MEASUREMENTS**

ISEM Model Prediction	Lockheed 125•C Source VCM Data	Lockheed 75•C Source VCM Data	LDEF VCM Data	Max. Measured (Best Estimate Via Telecon)
Worst Case Near Keyhole Angstroms	28,464	3,000	237,000	10,000
Refined Worst Case Near Keyhole Angstroms	<u>9,963</u>	1,050	83,000	10,000

**SUMMARY PREDICTIONS-ANGSTROMS
OFF CENTERLINE-CORRELATION TO MEASUREMENTS**

ISEM Model Prediction Worst Case Refined	Lockheed 125•C Source VCM Data	Measured (Best Estimate Via Telecon)
Near Centerline	9963	10,000
~ One cm up from Centerline	3000	~1000
~ Two cm up from Centerline	80	50-200
~ Three cm up from Centerline	30	20-50
~ One cm over to side Row 7	250	50-200
~1.5 cm over to side Row 7	35	20-50

The relative deposition values predicted as a function of distance away from the centerline near the keyhole match the measurements made on the deposits fairly well.

Figure 11 shows profiles of the predicted VCM deposition levels, normalized to the maximum at the center, for different cross sections up from the centerline.

Figure 12 shows the same data for a cross section up and below the center from the zero centerline. The first three points in Figure 12 correspond to a region inside where the atomic oxygen flux is less than the contaminant flux and is primarily scattered oxygen. The other data points correspond to regions that the atomic oxygen flux is greater than the contaminant flux by 2 to 4 orders of magnitude.

Figure 13 summarizes the predicted deposition levels on the tray wall utilizing the refined worst case(i.e. Lockheed 125 • C data). The value of 8000 angstroms corresponds to the first iso-contour line plotted. The actual maximum value, slightly below it, is 9963 angstroms.

7.0 Conclusions

The deposition in the vicinity of the modeled keyhole aperture undoubtedly occurred over the entire span of the LDEF mission. During the early portion of the mission, the internal outgassing rates would have been at a maximum, but the AO fluxes would have been near a minimum due to the maximum altitude. However, because the AO flux still would have been much larger than the contaminant flux on the tray wall above the opening, significant contaminant fixing likely occurred in this region the entire mission.

A major unknown in the deposition computation is the actual fixing mechanism. For the region above the keyhole aperture there appeared to be an abundance of AO flux available for contaminant fixing even if the process was very inefficient. However, contaminant fixing on the tray wall inside the aperture was very dependent on the efficiency of the fixing process. For the inside surface, the contaminant was plentiful and the flux of AO onto the surface, outside of a small area of direct AO ambient flux, is dependent on the scattered AO flux. Consequently, the deposition pattern and thickness inside the aperture is strongly affected by the efficiency of the fixing process.

If the contaminant outgassing rate had a strong time dependence, then most of the outgassing would have taken place early in the mission when the AO flux was at a mission minimum. In that case, the internal deposition pattern would likely be somewhat more confined than if the outgassing rate was still strong during the latter portion of the mission when the AO flux was higher. This is because the strong contaminant outgassing combined with the higher fluxes of AO later in the mission would cause a broader area of contaminant fixing by virtue of the larger scatter fluxes. The deposition pattern above the keyhole aperture should be unaffected by the time dependence of the contaminant outgassing rate because all through the mission the AO flux on that portion of the tray wall was considerably larger than the contaminant flux.

Under the assumption that all of the VCM leaves the DC 61104 during the mission and comes out of a total of ten keyholes, the model predictions are a factor of three higher than the measured values. This is reasonable agreement

considering the uncertainties of the amount of VCM that actually was released by the DC 61104. However, by estimating the amount of VCM that was trapped inside the experiment tray by AO, the predictions came within less than one percent of the measured values. After this first refinement step it was not deemed necessary to continue any other refinements.

It is felt this baseline prediction accuracy is fortuitous because of the unknowns in the source characteristics (more than an order of magnitude in reported VCM) and the fact that the silicone gasket material was not modeled as a source.

If the LDEF reported VCM value is used then it is apparent that not all of the VCM would be allowed to escape, since this value is a factor of almost ten too high. Compared to the worst case, refined value of VCM (Lockheed data) that gave a prediction of 9963 angstroms, only a fraction of 0.125 came out of the DC 61104 based on the LDEF VCM values.

It was encouraging to see the predicted relative deposition levels, up and to the side of the keyhole, matched the variation in measured values fairly well. This creates confidence that ISEM, with its direct and scattered AO and contaminant flux routines, was a good model for the task.

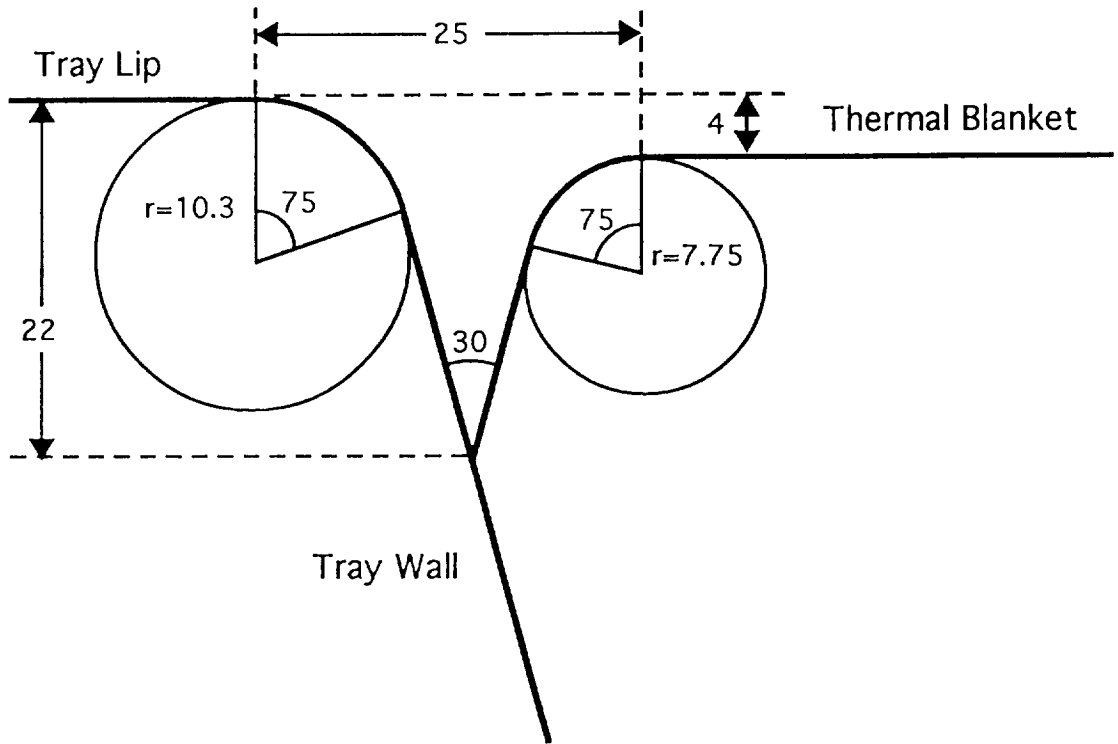
It is estimated that the results could have varied by as much as one order of magnitude in any direction based upon the source VCM uncertainties, but the educated guess as to what to use came very close to measured values.

In summary, the worst case baseline (Lockheed 125°C VCM) predicted 28,464 angstroms and the refined baseline predicted 9,963 angstroms for the maximum deposit outside the keyhole. This corresponds to the 10,000 angstroms measured at this location.

This type of model correlation is required on returned flight samples to build confidence in the different models prediction capabilities and to find ways to make the models more accurate. It is recommended this type of analysis be implemented wherever possible.

8.0 References

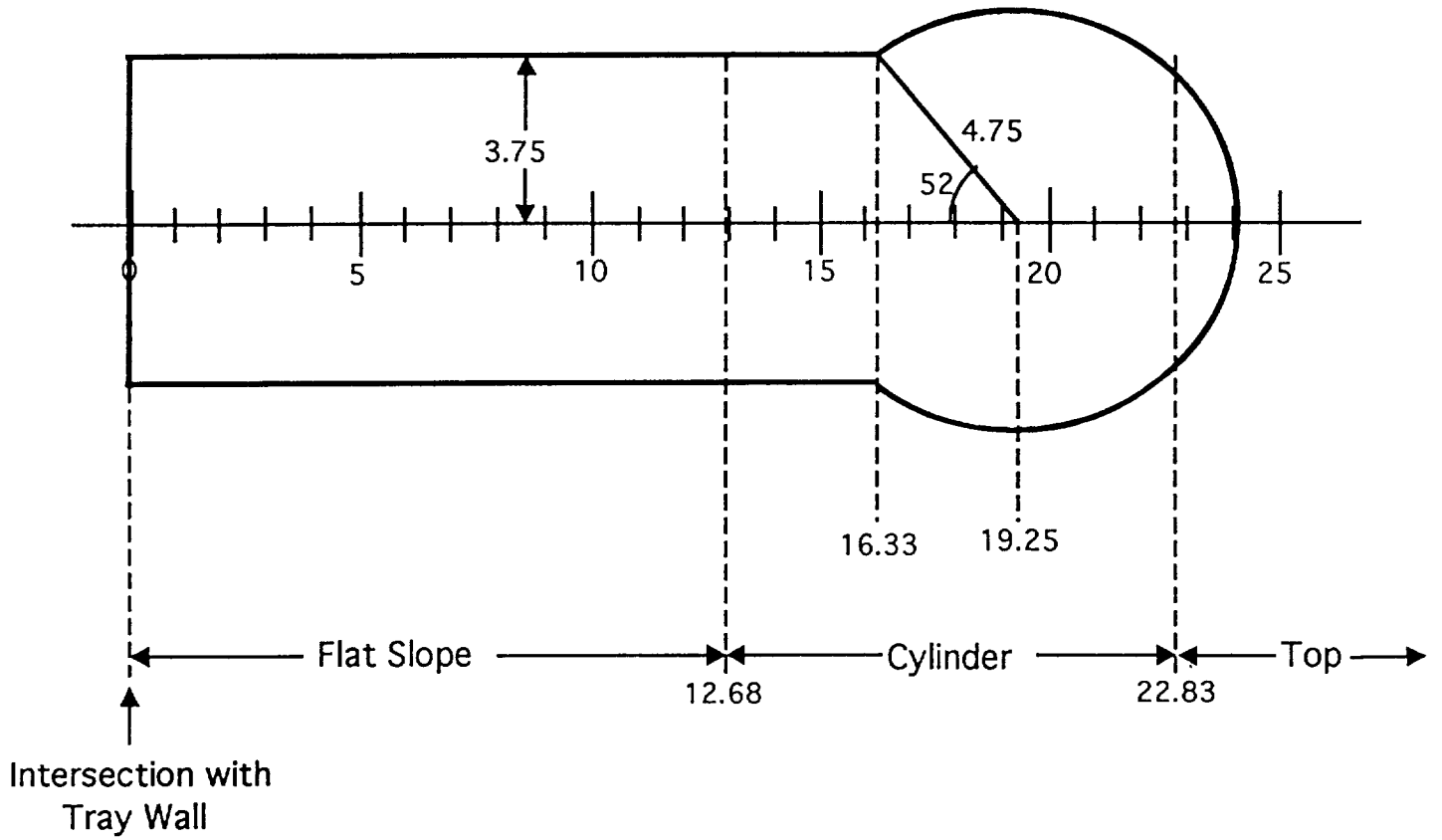
- 1 T. Gordon, Dr. R.O. Rantanen, "LDEF Modeling", SEA No. 493-003- 1, NASA Contract NAS8-38146, January 22, 1991.
- 2 Dr. R.O. Rantanen, T. Gordon, "LDEF Experiment AO171 Contamination Modeling", ROR-MSFC-1-93, NASA Contract NASA PO L31641D for Dr. Ann Whitaker, MSFC, October 1, 1993.
- 3 R. Bourassa, J.R. Gillis, "LDEF Atomic Oxygen Fluence Update", pg 59, LDEF Materials Workshop '91, NASA Conference Publication 3162, Part 1, November 19-22, 1991.



All Linear Dimensions Given in Millimeters

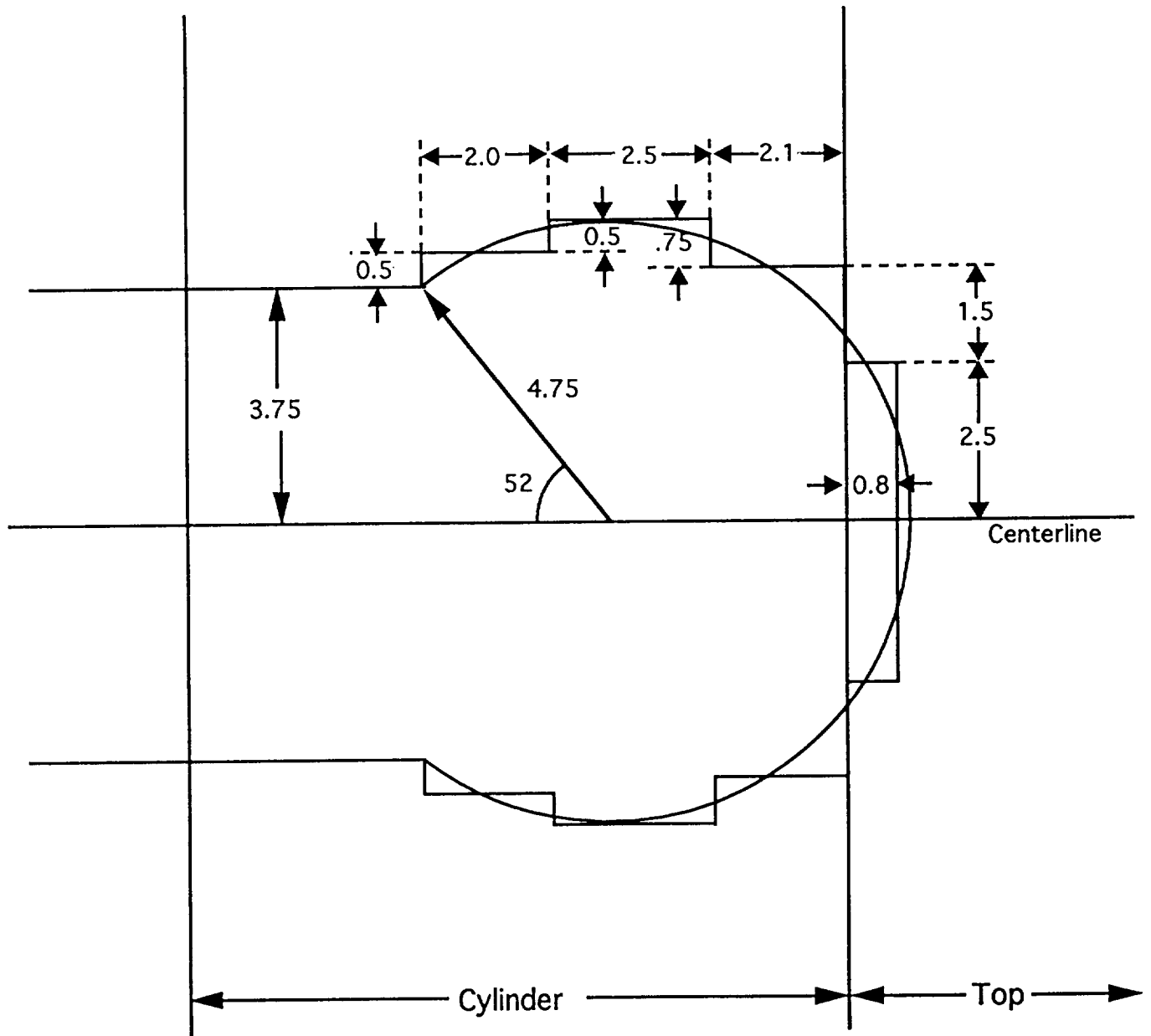
Geometry -- Side View

Figure 1 - Micro Model Geometry



All Linear Dimensions in Millimeters

Figure 2 - Thermal Blanket Keyhole Geometry



All Dimensions in Millimeters
 Area of Approximation Equals Area of Actual Keyhole

Figure 3 - Keyhole Modeling Approximation

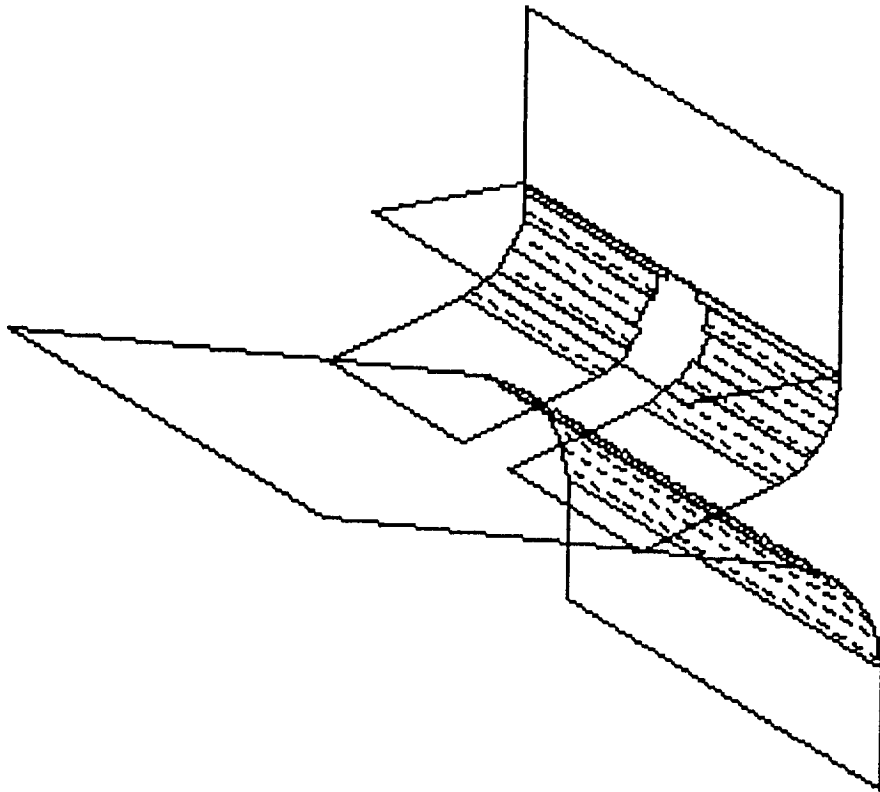


Figure 4 - Basic TRASYS Geometry Model

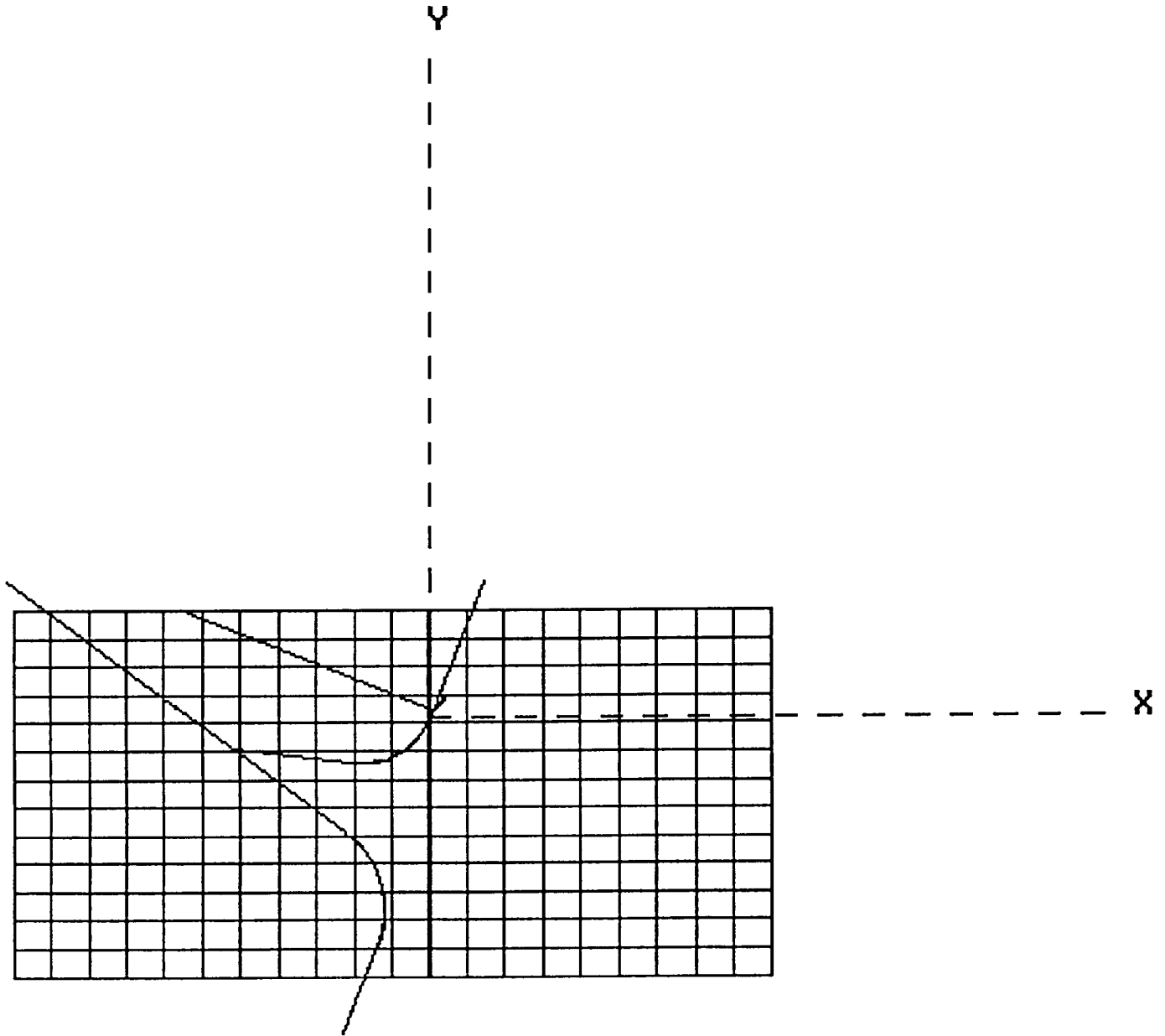


Figure 5 - TRASYS Geometry Model with Computational Grid
(+Z Axis View)

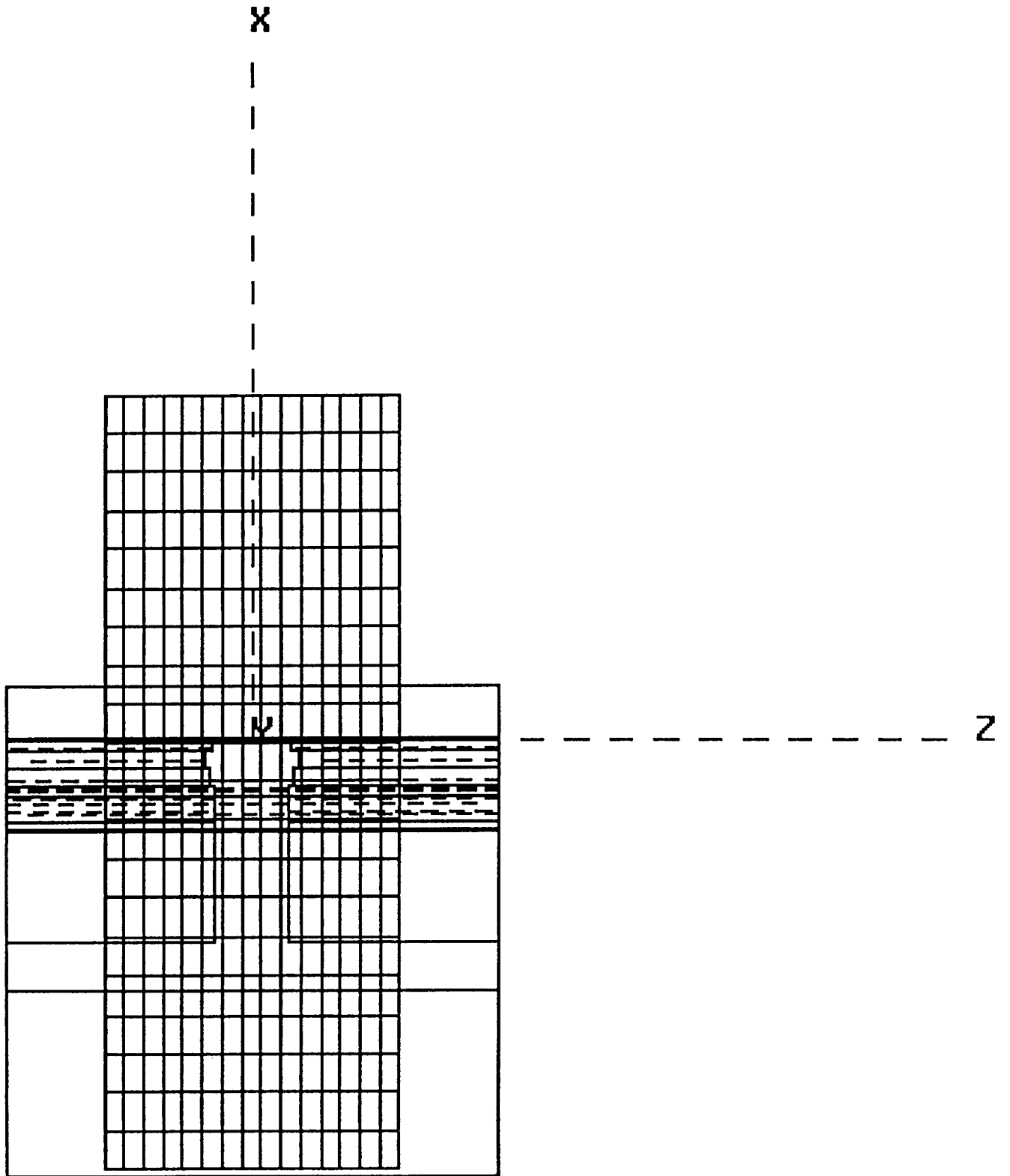
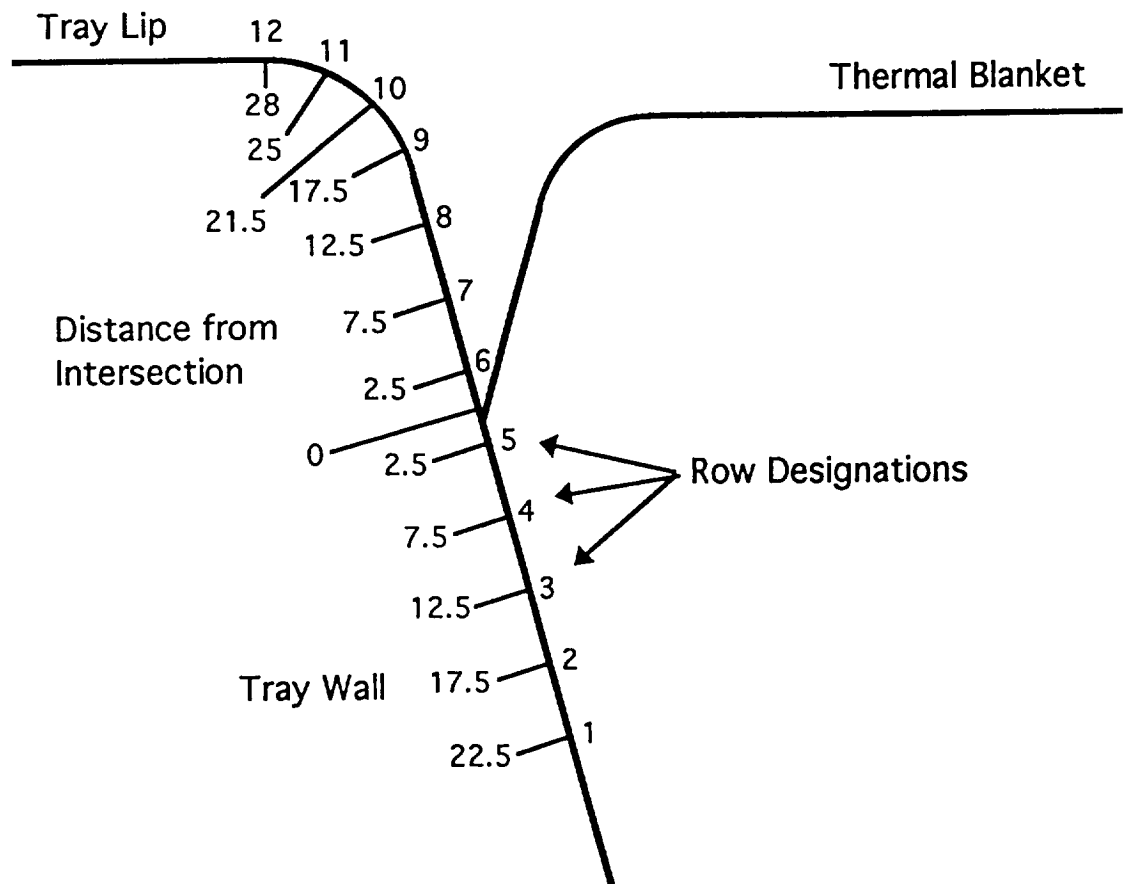


Figure 6 - TRASYS Geometry Model with Computational Grid
(+Y Axis View)



All Linear Dimensions Given in Millimeters

Row locations measured along surface from intersection of thermal blanket and tray wall

Each row contains 15 flux computation points spaced at 2mm intervals, centered about keyhole centerline

Figure 7 - Flux Computation Point Row Locations

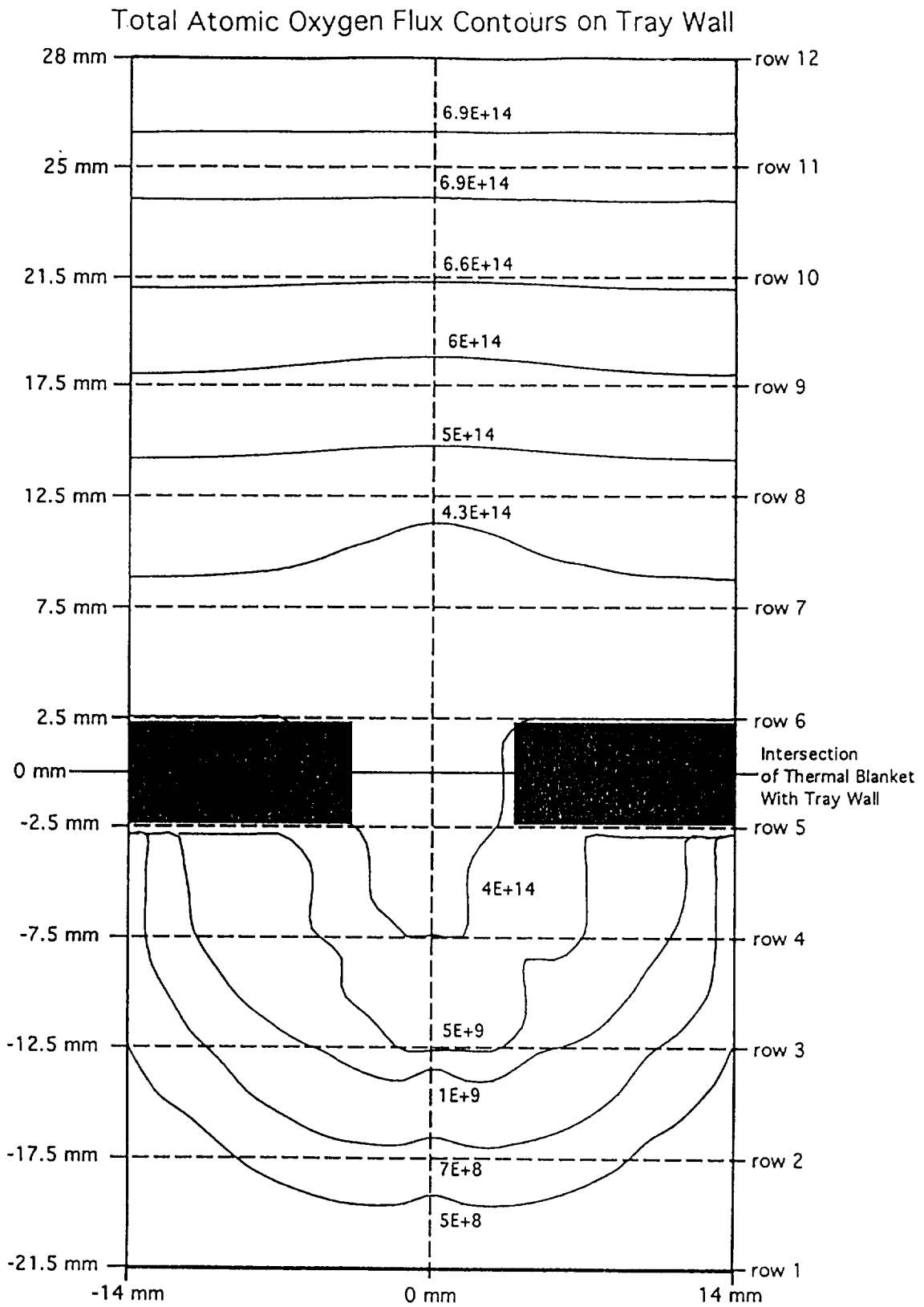


Figure 8 - Total Atomic Oxygen Flux Contours on Tray Wall

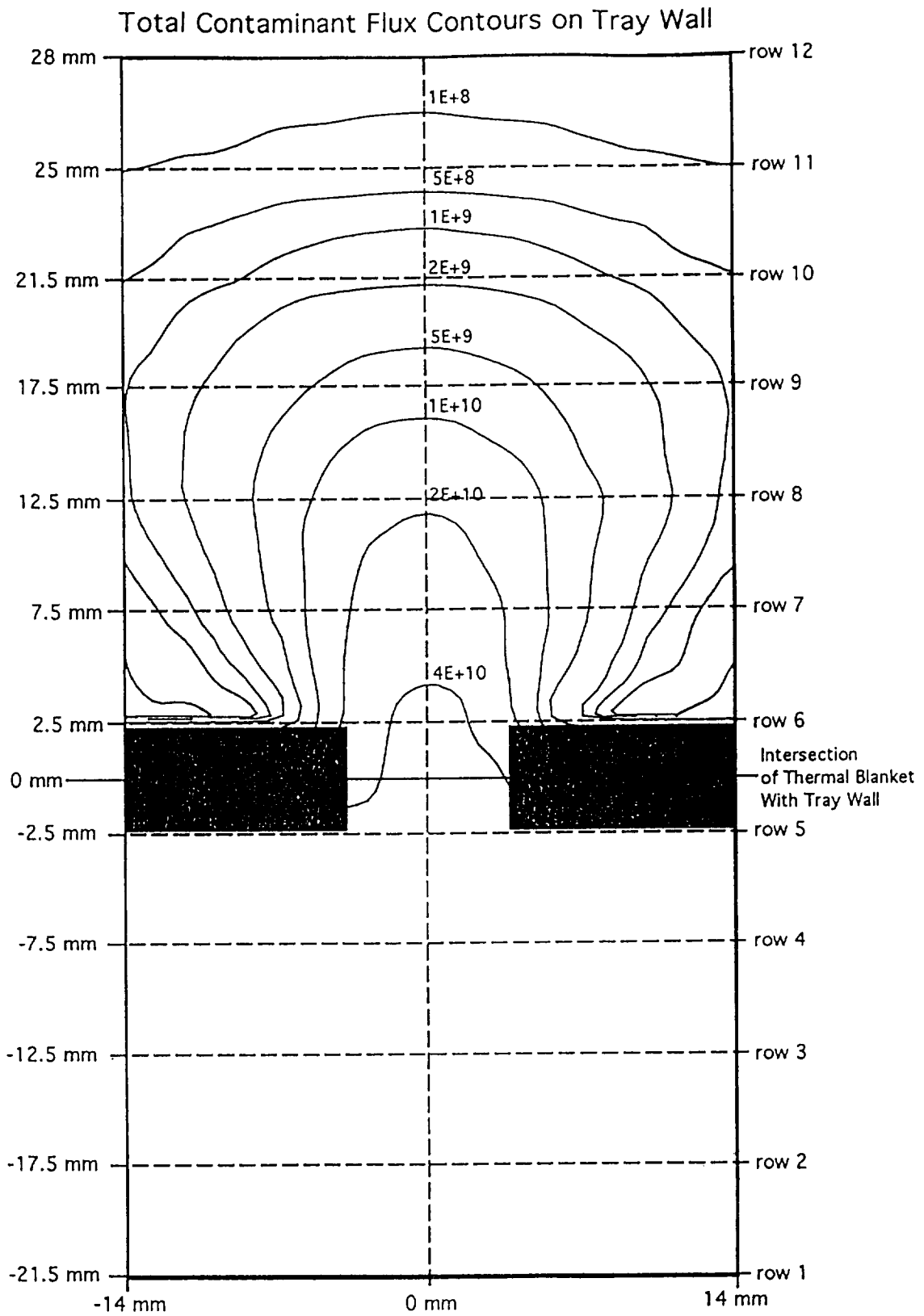


Figure 9 - Total Contaminant Flux Contours on Tray Wall

Total Atomic Oxygen & Contaminant Flux Contours on Tray Wall

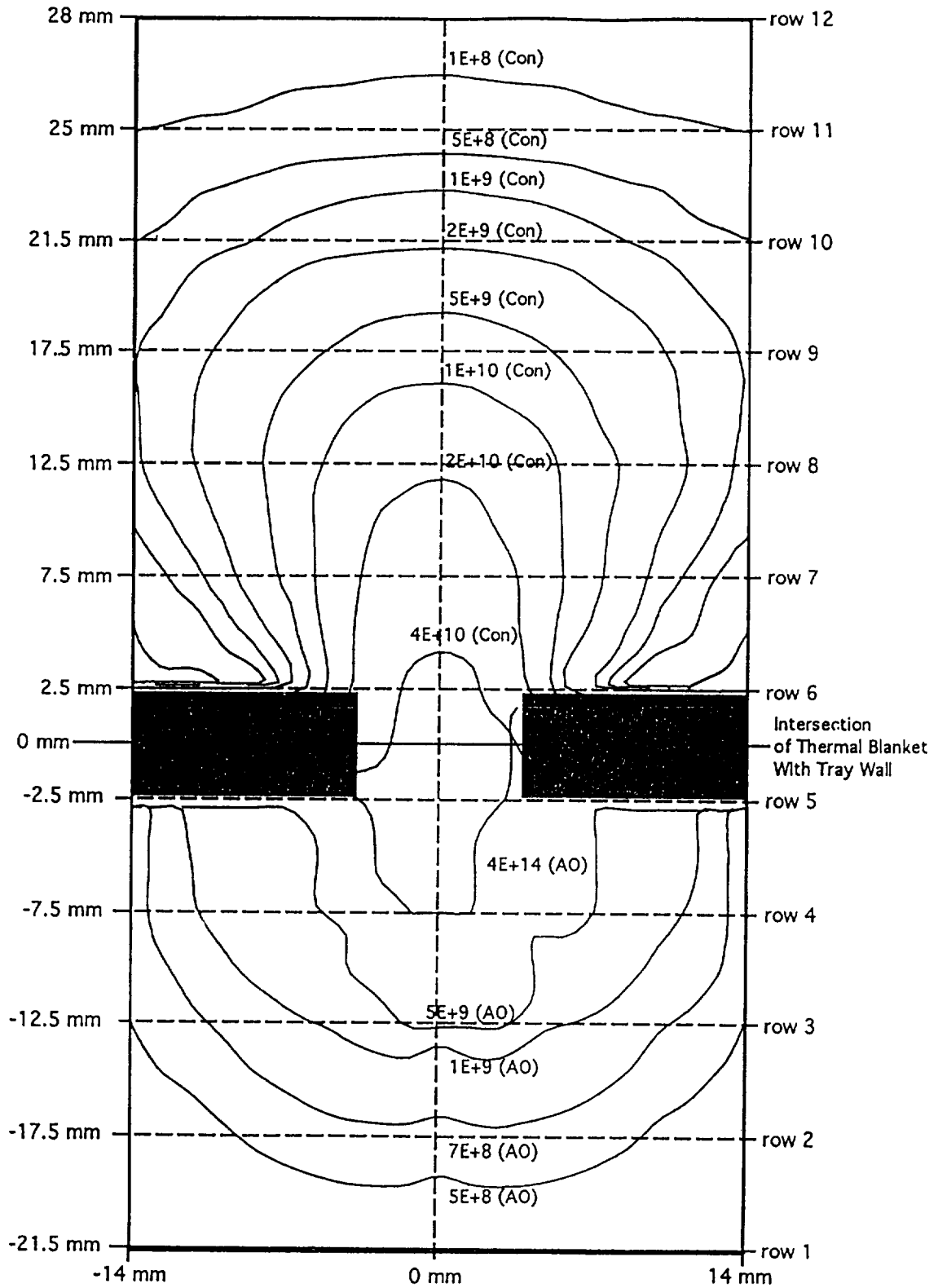


Figure 10 - Total Atomic Oxygen and Contaminant Flux Contours on Tray Wall

Deposition Along Lines Perpendicular to Keyhole Centerline
(Normalized to Maximum Value)

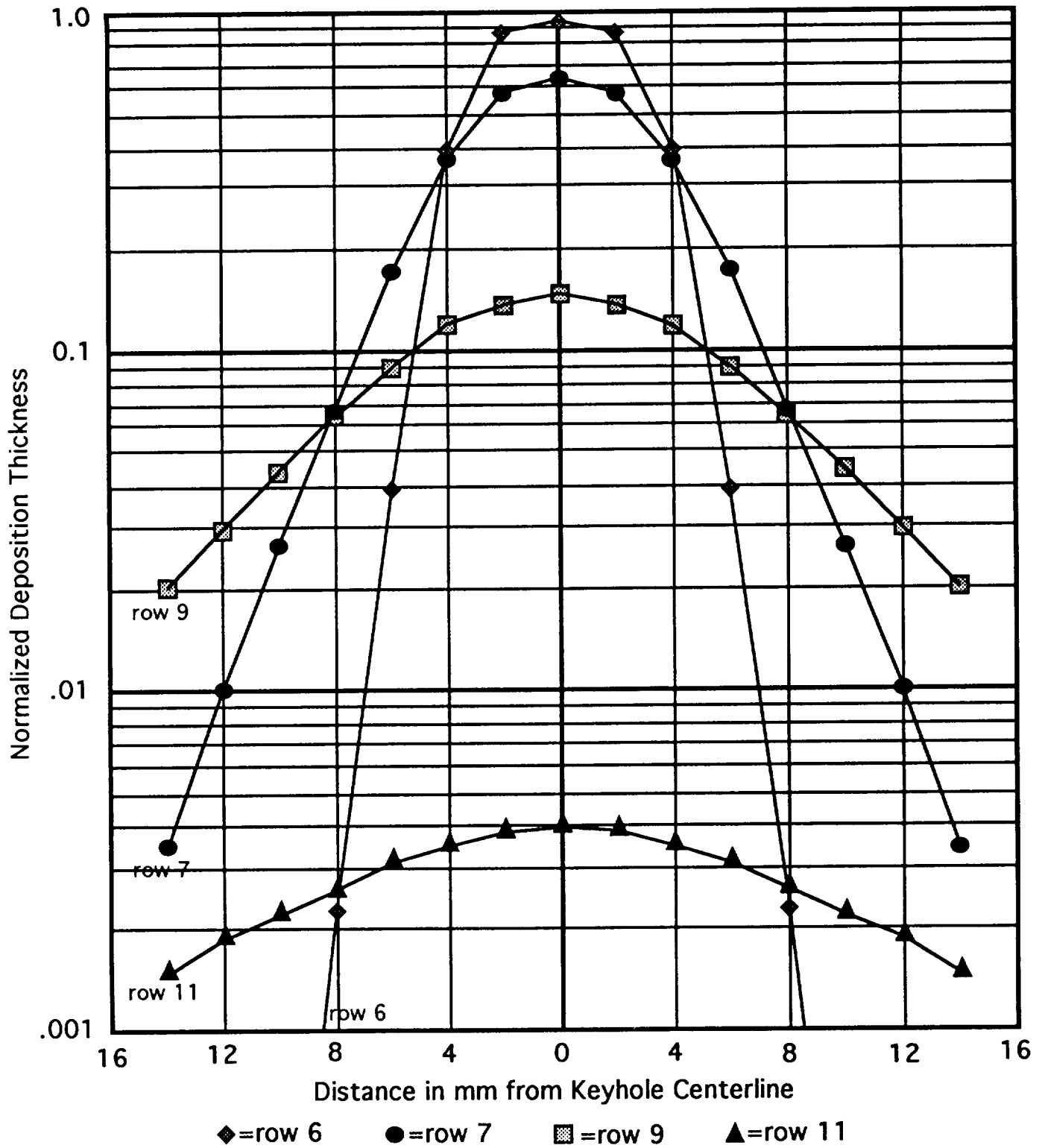
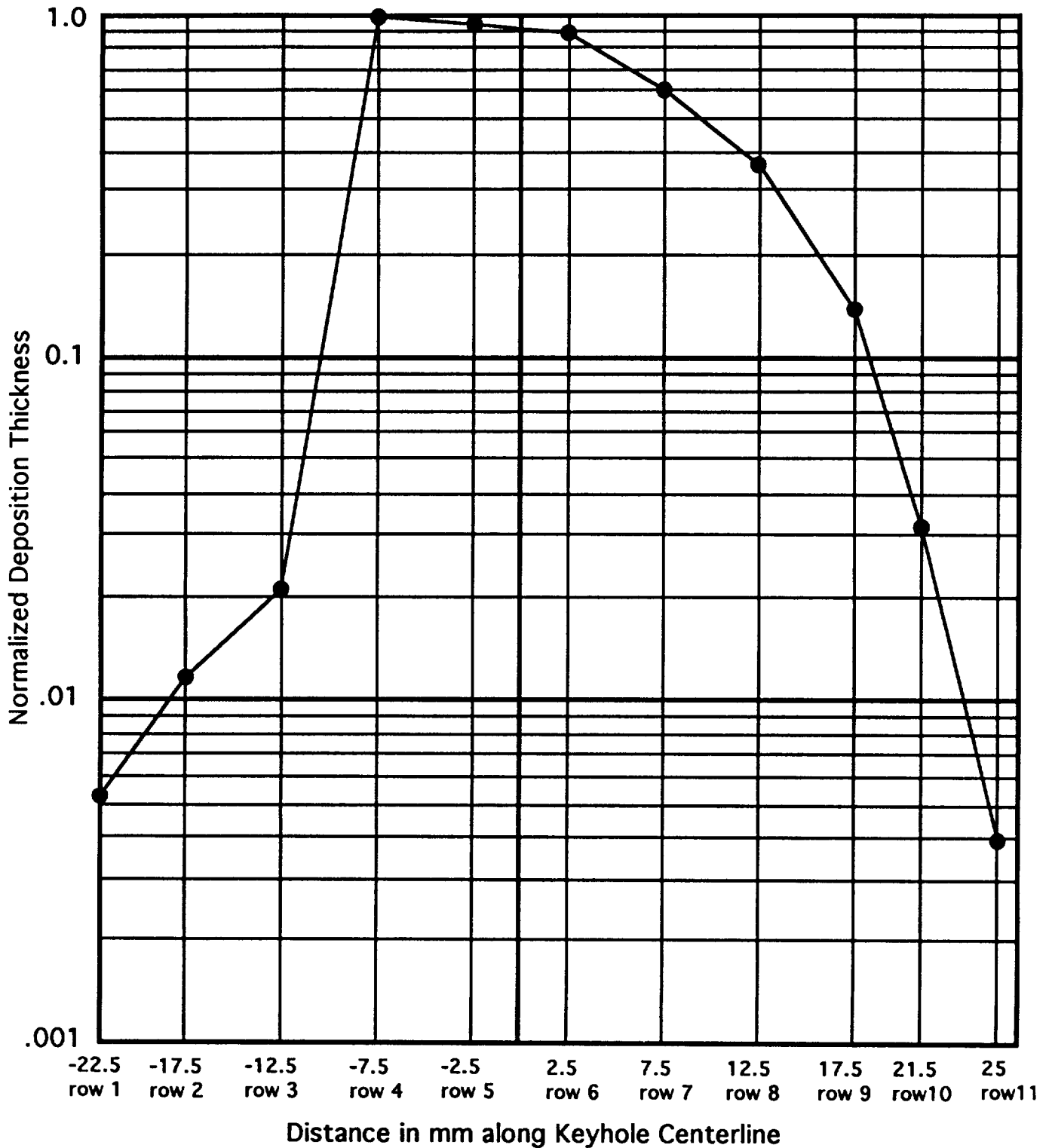


Figure 11 - Deposition Cross Sections Along Selected Rows

Deposition Along Keyhole Centerline
(Normalized to Maximum Value)



Zero Represents Intersection of Thermal Blanket and Tray Wall

Figure 12 - Deposition Along Keyhole Centerline

Contaminant Deposition Contours on Tray Wall

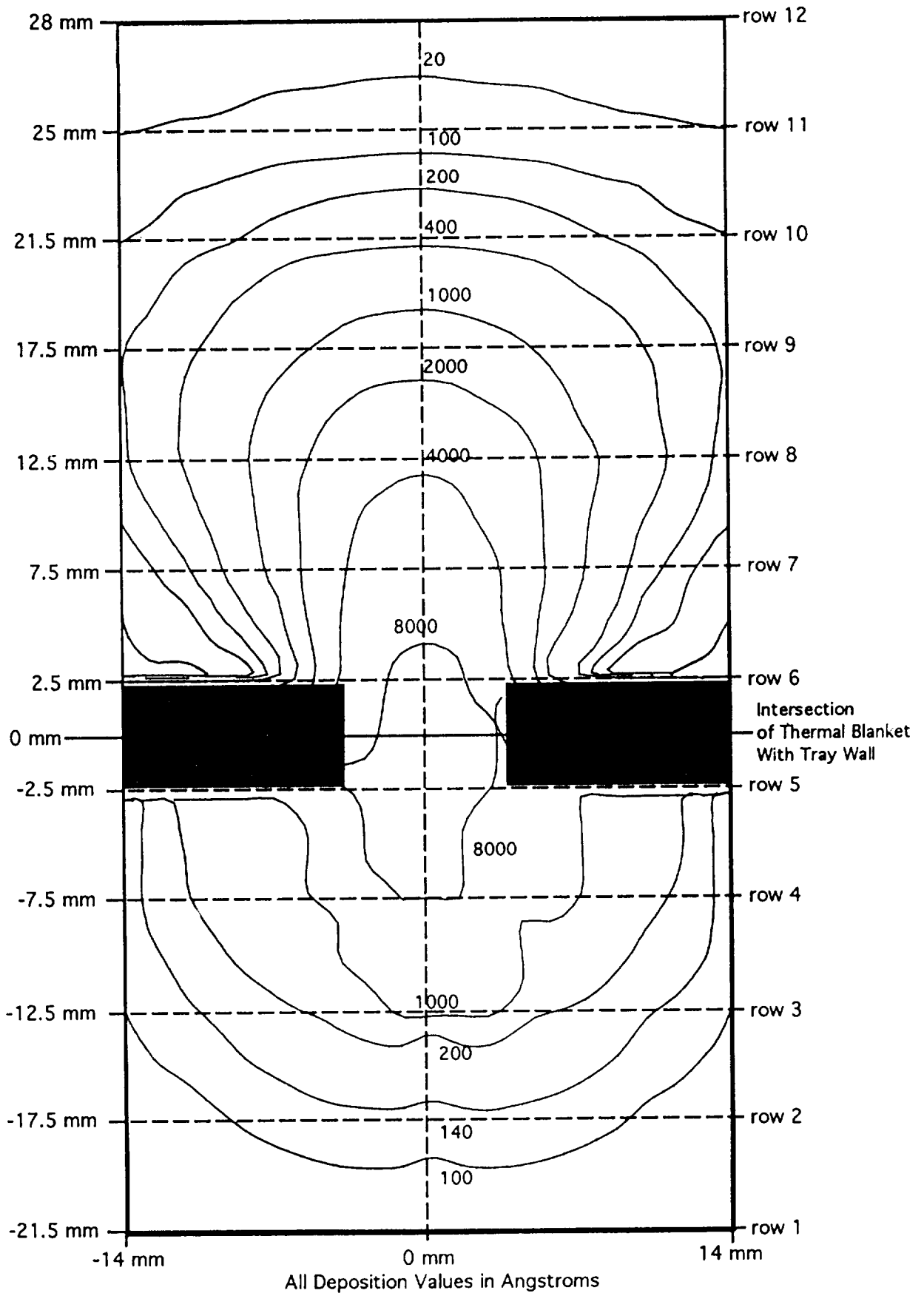


Figure 13 - Deposition Contours on Tray Wall

Appendix A

Computed Flux Tables

Forward

This appendix contains 8 tables of computed flux values resulting from the micro model ISEM run.

The array of flux computation points was comprised of 12 rows and 15 columns of points. The within each row the computed flux values are symmetrical about the value in column 8 because of the geometry symmetry. Consequently, only the first 8 columns are provided. The leftmost number is the row designation (see Figure 7).

ISEM computes and keeps track of molecular species by collisional status. For example, once an ambient molecule collides with a surface emitted molecule, it is tracked as a new species (because it likely now has different velocity characteristics from the uncollided ambient molecules). Because of this capability, ISEM can separate flux components into different source and collisional status categories. The table headings are explained below.

<u>Title</u>	<u>Explanation</u>
Total AO Flux	sum of all AO flux
Direct AO Flux	unscattered ambient AO flux
Direct Surface Reemitted AO Flux	unscattered surface reemitted AO flux
Scatter Direct AO Flux	scattered ambient AO flux
Scattered Surface Reemitted AO Flux	scattered surface reemitted AO flux
Total Contaminant Flux	sum of all contaminant flux
Direct Contaminant Flux	unscattered surface emitted contaminant flux
Scattered Contaminant Flux	scattered contaminant flux

TOTAL AO FLUX

row

12	0.67E+15							
11	0.70E+15							
10	0.67E+15	0.67E+15	0.67E+15	0.67E+15	0.66E+15	0.66E+15	0.66E+15	0.66E+15
9	0.59E+15	0.59E+15	0.59E+15	0.59E+15	0.58E+15	0.58E+15	0.57E+15	0.57E+15
8	0.45E+15	0.45E+15	0.45E+15	0.45E+15	0.44E+15	0.44E+15	0.43E+15	0.43E+15
7	0.42E+15							
6	0.42E+15							
5	0.54E+09	0.94E+09	0.15E+10	0.20E+10	0.30E+10	0.42E+15	0.42E+15	0.42E+15
4	0.60E+09	0.88E+09	0.11E+10	0.14E+10	0.18E+10	0.25E+10	0.42E+15	0.42E+15
3	0.50E+09	0.61E+09	0.72E+09	0.86E+09	0.96E+09	0.11E+10	0.12E+10	0.11E+10
2	0.34E+09	0.40E+09	0.46E+09	0.54E+09	0.60E+09	0.64E+09	0.65E+09	0.60E+09
1	0.18E+09	0.19E+09	0.21E+09	0.24E+09	0.28E+09	0.29E+09	0.30E+09	0.27E+09

DIRECT AO FLUX

row

12	0.67E+15							
11	0.69E+15							
10	0.62E+15							
9	0.55E+15							
8	0.42E+15							
7	0.42E+15							
6	0.42E+15							
5	0.00E+00	0.00E+00	0.00E+00	0.00E+00	0.00E+00	0.42E+15	0.42E+15	0.42E+15
4	0.00E+00	0.00E+00	0.00E+00	0.00E+00	0.00E+00	0.00E+00	0.42E+15	0.42E+15
3	0.00E+00							
2	0.00E+00							
1	0.00E+00							

DIRECT SURFACE REEMITTED AO FLUX

row									
12	0.00E+00								
11	0.12E+14	0.13E+14							
10	0.41E+14	0.42E+14	0.42E+14	0.41E+14	0.40E+14	0.39E+14	0.38E+14	0.38E+14	0.38E+14
9	0.46E+14	0.45E+14	0.44E+14	0.41E+14	0.37E+14	0.33E+14	0.29E+14	0.28E+14	0.28E+14
8	0.33E+14	0.33E+14	0.32E+14	0.29E+14	0.26E+14	0.21E+14	0.18E+14	0.16E+14	0.16E+14
7	0.56E+13	0.56E+13	0.54E+13	0.50E+13	0.44E+13	0.37E+13	0.30E+13	0.28E+13	0.28E+13
6	0.00E+00								
5	0.00E+00								
4	0.00E+00								
3	0.00E+00								
2	0.00E+00								
1	0.00E+00								

SCATTER DIRECT AO FLUX

row									
12	0.71E+10	0.86E+10	0.87E+10	0.87E+10	0.87E+10	0.86E+10	0.84E+10	0.82E+10	0.82E+10
11	0.90E+10	0.11E+11	0.11E+11	0.11E+11	0.11E+11	0.11E+11	0.11E+11	0.10E+11	0.10E+11
10	0.94E+10	0.11E+11							
9	0.10E+11	0.12E+11	0.12E+11	0.12E+11	0.12E+11	0.11E+11	0.11E+11	0.11E+11	0.11E+11
8	0.56E+10	0.43E+10	0.34E+10	0.28E+10	0.22E+10	0.17E+10	0.18E+10	0.15E+10	0.15E+10
7	0.43E+10	0.46E+10	0.45E+10	0.43E+10	0.42E+10	0.41E+10	0.39E+10	0.37E+10	0.37E+10
6	0.24E+10	0.28E+10	0.29E+10	0.31E+10	0.34E+10	0.37E+10	0.40E+10	0.38E+10	0.38E+10
5	0.22E+09	0.40E+09	0.63E+09	0.87E+09	0.14E+10	0.22E+10	0.29E+10	0.29E+10	0.29E+10
4	0.25E+09	0.37E+09	0.48E+09	0.62E+09	0.83E+09	0.12E+10	0.17E+10	0.17E+10	0.17E+10
3	0.20E+09	0.25E+09	0.29E+09	0.36E+09	0.43E+09	0.49E+09	0.56E+09	0.51E+09	0.51E+09
2	0.13E+09	0.15E+09	0.17E+09	0.20E+09	0.22E+09	0.24E+09	0.25E+09	0.23E+09	0.23E+09
1	0.69E+08	0.72E+08	0.79E+08	0.90E+08	0.10E+09	0.11E+09	0.11E+09	0.10E+09	0.10E+09

SCATTERED SURFACE REEMITTED AO FLUX

row									
12	0.75E+10	0.90E+10	0.90E+10	0.89E+10	0.89E+10	0.87E+10	0.85E+10	0.83E+10	
11	0.96E+10	0.11E+11							
10	0.10E+11	0.12E+11	0.12E+11	0.12E+11	0.12E+11	0.11E+11	0.11E+11	0.11E+11	
9	0.11E+11	0.13E+11	0.13E+11	0.12E+11	0.12E+11	0.12E+11	0.11E+11	0.11E+11	
8	0.61E+10	0.48E+10	0.39E+10	0.32E+10	0.25E+10	0.19E+10	0.19E+10	0.15E+10	
7	0.45E+10	0.48E+10	0.47E+10	0.45E+10	0.44E+10	0.42E+10	0.40E+10	0.37E+10	
6	0.25E+10	0.30E+10	0.31E+10	0.33E+10	0.36E+10	0.38E+10	0.41E+10	0.39E+10	
5	0.32E+09	0.54E+09	0.83E+09	0.11E+10	0.16E+10	0.24E+10	0.30E+10	0.30E+10	
4	0.35E+09	0.51E+09	0.62E+09	0.76E+09	0.93E+09	0.13E+10	0.18E+10	0.18E+10	
3	0.30E+09	0.36E+09	0.43E+09	0.50E+09	0.54E+09	0.57E+09	0.61E+09	0.57E+09	
2	0.20E+09	0.25E+09	0.29E+09	0.35E+09	0.38E+09	0.40E+09	0.40E+09	0.38E+09	
1	0.11E+09	0.12E+09	0.14E+09	0.15E+09	0.17E+09	0.18E+09	0.18E+09	0.17E+09	

TOTAL CONTAMINANT FLUX

row									
12	0.31E+06	0.39E+06	0.42E+06	0.44E+06	0.46E+06	0.47E+06	0.47E+06	0.46E+06	
11	0.73E+08	0.94E+08	0.11E+09	0.13E+09	0.16E+09	0.17E+09	0.19E+09	0.20E+09	
10	0.50E+09	0.63E+09	0.86E+09	0.11E+10	0.13E+10	0.15E+10	0.16E+10	0.17E+10	
9	0.10E+10	0.15E+10	0.22E+10	0.32E+10	0.44E+10	0.59E+10	0.68E+10	0.72E+10	
8	0.89E+09	0.15E+10	0.28E+10	0.51E+10	0.86E+10	0.14E+11	0.17E+11	0.19E+11	
7	0.17E+09	0.49E+09	0.13E+10	0.33E+10	0.84E+10	0.18E+11	0.28E+11	0.31E+11	
6	0.13E+07	0.19E+07	0.25E+07	0.11E+09	0.19E+10	0.19E+11	0.42E+11	0.45E+11	
5	0.45E+11	0.46E+11	0.47E+11	0.48E+11	0.48E+11	0.49E+11	0.49E+11	0.49E+11	
4	0.47E+11	0.49E+11	0.50E+11	0.50E+11	0.51E+11	0.51E+11	0.51E+11	0.52E+11	
3	0.49E+11	0.50E+11	0.51E+11	0.52E+11	0.51E+11	0.52E+11	0.52E+11	0.53E+11	
2	0.47E+11	0.49E+11	0.50E+11	0.50E+11	0.49E+11	0.49E+11	0.50E+11	0.51E+11	
1	0.37E+11	0.39E+11	0.41E+11	0.40E+11	0.38E+11	0.39E+11	0.40E+11	0.41E+11	

DIRECT CONTAMINANT FLUX

row									
12	0.00E+00								
11	0.72E+08	0.94E+08	0.11E+09	0.13E+09	0.16E+09	0.17E+09	0.19E+09	0.20E+09	0.20E+09
10	0.50E+09	0.63E+09	0.86E+09	0.11E+10	0.13E+10	0.15E+10	0.16E+10	0.17E+10	0.17E+10
9	0.99E+09	0.15E+10	0.22E+10	0.32E+10	0.44E+10	0.59E+10	0.68E+10	0.72E+10	0.72E+10
8	0.89E+09	0.15E+10	0.28E+10	0.51E+10	0.86E+10	0.14E+11	0.17E+11	0.19E+11	0.19E+11
7	0.17E+09	0.49E+09	0.13E+10	0.33E+10	0.84E+10	0.18E+11	0.28E+11	0.31E+11	0.31E+11
6	0.00E+00	0.00E+00	0.00E+00	0.11E+09	0.19E+10	0.19E+11	0.42E+11	0.45E+11	0.45E+11
5	0.45E+11	0.46E+11	0.47E+11	0.48E+11	0.48E+11	0.49E+11	0.49E+11	0.49E+11	0.49E+11
4	0.47E+11	0.49E+11	0.50E+11	0.50E+11	0.51E+11	0.51E+11	0.51E+11	0.52E+11	0.52E+11
3	0.49E+11	0.50E+11	0.51E+11	0.52E+11	0.51E+11	0.52E+11	0.52E+11	0.53E+11	0.53E+11
2	0.47E+11	0.49E+11	0.50E+11	0.50E+11	0.49E+11	0.49E+11	0.50E+11	0.51E+11	0.51E+11
1	0.37E+11	0.39E+11	0.41E+11	0.40E+11	0.38E+11	0.39E+11	0.40E+11	0.41E+11	0.41E+11

SCATTERED CONTAMINANT FLUX

row									
12	0.31E+06	0.39E+06	0.42E+06	0.44E+06	0.46E+06	0.47E+06	0.47E+06	0.46E+06	0.46E+06
11	0.40E+06	0.51E+06	0.56E+06	0.61E+06	0.65E+06	0.67E+06	0.68E+06	0.66E+06	0.66E+06
10	0.42E+06	0.54E+06	0.63E+06	0.71E+06	0.79E+06	0.84E+06	0.88E+06	0.85E+06	0.85E+06
9	0.73E+06	0.94E+06	0.12E+07	0.14E+07	0.16E+07	0.20E+07	0.19E+07	0.22E+07	0.22E+07
8	0.93E+06	0.12E+07	0.15E+07	0.18E+07	0.20E+07	0.22E+07	0.11E+07	0.81E+06	0.81E+06
7	0.11E+07	0.16E+07	0.21E+07	0.30E+07	0.39E+07	0.56E+07	0.74E+07	0.71E+07	0.71E+07
6	0.13E+07	0.19E+07	0.25E+07	0.39E+07	0.56E+07	0.76E+07	0.84E+07	0.81E+07	0.81E+07
5	0.15E+07	0.20E+07	0.31E+07	0.40E+07	0.51E+07	0.78E+07	0.86E+07	0.83E+07	0.83E+07
4	0.83E+06	0.12E+07	0.16E+07	0.22E+07	0.31E+07	0.34E+07	0.37E+07	0.44E+07	0.44E+07
3	0.11E+07	0.15E+07	0.18E+07	0.23E+07	0.26E+07	0.25E+07	0.23E+07	0.27E+07	0.27E+07
2	0.61E+06	0.74E+06	0.84E+06	0.14E+07	0.20E+07	0.17E+07	0.19E+07	0.18E+07	0.18E+07
1	0.21E+06	0.24E+06	0.39E+06	0.51E+06	0.72E+06	0.51E+06	0.62E+06	0.57E+06	0.57E+06

**FINAL REPORT
ADDENDUM**

#ROR-B-9073-97

**"CONTAMINATION PREDICTION MODEL(ISEM) CALCULATION FOR
SELECTED LDEF TRAYS"**

ADDENDUM- MODELING OF TRAYS C6 AND A4

**PURCHASE CONTRACT:
JJ9073**

**PART OF:
NAS8-040581**

**SUBMITTED TO:

THE BOEING COMPANY SPACE AND DEFENSE GROUP**

**SUBMITTED BY:
ROR ENTERPRISES, INC.
2455 W. SUMMER AVE
ATHOL, ID 83801**

**WORK ORDER CHARGE #:
5-9K466-5571-539640**

DATE:

1-13-97

APPROVED BY:

Final Addendum

Modeling of LDEF Tray E10 Slots 6,7,8

The previously presented modeling was representative of the slots 6, 7, and 8 on LDEF tray E10. These keyhole shaped apertures are on the side of the tray closest to row 11. Modeling of a slot representative of this side of the tray E10 was picked because the tray wall closest to row 11 had a direct AO flux and showed the most significant deposition. For results of the E10 modeling see figures 11, 12 and 13 in the Final Report.

Modeling of LDEF Tray C6 Slots 1,2,3

A new modeling effort, representative of LDEF tray C6 slots 1, 2, and 3 is presented here. Slots 1, 2, and 3 are located on the side of tray C6 closest to row 5. LDEF settled in orbit with an 8 degree yaw angle. The yaw angle was in the direction such that plane of row 6 was rotated 8 degrees into the wake direction (relative to the ram). One might surmise that because of the yaw angle, no direct AO flux would impinge on the wall of tray C6. However, the 8 degree yaw angle is well within the angular spread of the AO due to the ambient thermal distribution (see the analysis in Appendix B of the original report, Figures 6.9, 6.10, and 6.11). Consequently, the portion of the C6 tray wall above the plane of the thermal blanket received sufficient direct ambient AO flux to fix all of the outgassed contaminant received on that portion of the tray wall (assuming an AO to contaminant fixing ratio of 1 to 1).

Much of the C6 tray analysis is identical to the previous E10 analysis, but there are also some significant differences. Modeling parameters which were considered identical to the E10 analysis included;

- 1) The geometry of the keyhole shaped aperture and relative location to the tray wall.
- 2) The source rate of the outgassing contaminant within the tray.
- 3) The molecular mass of the contaminant.

Differences for the C6 analysis included;

1) As previously mentioned, the ambient angle of incidence for the AO is essentially parallel to the plane of the thermal blanket for the C6 analysis. This resulted in only a portion of the tray wall receiving direct AO flux, and consequently reduced the size of the deposition relative to the E10 analysis.

2) Although the source rate for the contaminant inside the tray of C6 was modeled as being the same as for E10, the fraction of contaminant fixing inside the tray by AO entering the tray apertures was much less in the C6 analysis due to the difference in the ambient angle of incidence. This resulted in larger contaminant fluxes exiting through the keyholes in the C6 analysis. Essentially all of the AO which could enter the tray apertures is either surface reemitted or scattered. The computed internal fixing percentage of the contaminant for the C6 analysis was 10% (compared to 65% in the E10 analysis).

LDEF Tray C6 Analysis Results

The analysis resulted in an area of deposition on the C6 tray wall at the keyhole locations, centered well above the intersection of the thermal blanket and the tray wall. The maximum computed deposition thickness was approximately 3500 angstroms. A plot of computed deposition iso-contours is shown in the following Figure 14. The deposition on the tray wall along the keyhole centerline is given in Figure 15.

Modeling of LDEF Tray A4 Slots 1 through 6

The plane of A4 was oriented 158 degrees from the ram side of the LDEF vehicle. Consequently, it received no direct flux of ambient AO. Published AO fluence calculations give a mission fluence value for row 4 of 9×10^4 AO atoms¹. However, these calculations obviously ignored molecular scattering. ISEM macro modeling (see figures 7.2.2-4 in appendix B of our initial report) showed a range of scattered AO flux for row 4 from a high of 5×10^8 atoms/cm²/s at the beginning of the mission to a low of 8×10^6 atoms/cm²/s during the middle of the mission and then back up to 6×10^7 atoms/cm²/s at the end of the mission. Assuming that for most of the mission, the AO scattered flux value was close to the mission middle value of 8×10^6 atoms/cm²/s we will assume an average flux over the mission of 2×10^7 atoms/cm²/s. For the A4 analysis, the following assumptions were made;

- 1) The mission averaged scattered AO flux onto row 4 was assumed to be 2×10^7 atoms/cm²/s.
- 2) Internal fixing of contaminant inside tray due to AO entering tray apertures was considered insignificant for tray A4.

- 3) All of the same assumptions, as for the E10 & C6 analysis, regarding contaminant mass and density were applied to the A4 analysis.
- 4) Scattered AO was assumed to have the same contaminant fixing efficiency (namely 1 to 1) as direct AO.

¹ Bourassa, R.J., and Gillis, J.R., "LDEF Atomic Oxygen Fluence Update", NASA Conference Publication 3162, Part 1, LDEF Materials Workshop '91, November 19-22, 1991.

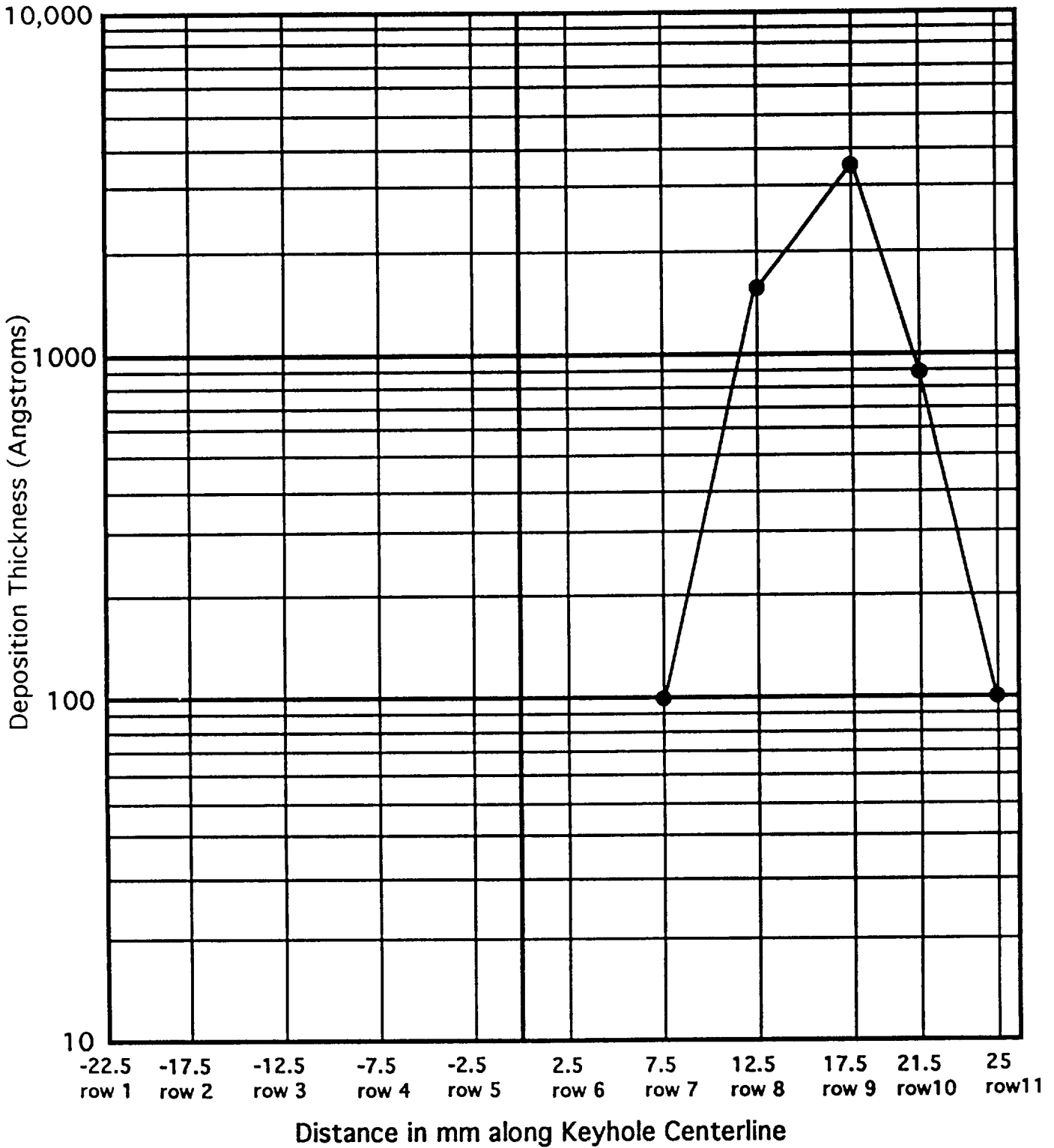
LDEF Tray A4 Analysis Results

The deposition area on the tray wall near the keyhole slots is severely AO limited. Since the AO flux above the blanket/tray wall intersection is uniform, the resulting computed deposition is also very uniform. The computed deposition thickness for the uniform coating is approximately 65 angstroms. A deposition thickness contour plot for this case was not made because the 65 angstrom uniform coating covered nearly the entire modeled portion of the tray wall above the blanket/tray wall intersection. Only flux points in row 12 and the extreme ends of row 11 had deposition thicknesses of less than the 65 angstroms, and they had values of essentially zero. The deposition thickness on the tray wall along the centerline of the keyhole is shown in Figure 16.

Summary Table for ISEM Deposition Computations

<u>Keyhole Locations</u>	<u>Maximum Deposition</u> (angstroms)
Tray E10 Slots 6,7,8	10,000
Tray C6 Slots 1,2,3	3,500
Tray A4 Slots 1-6	65

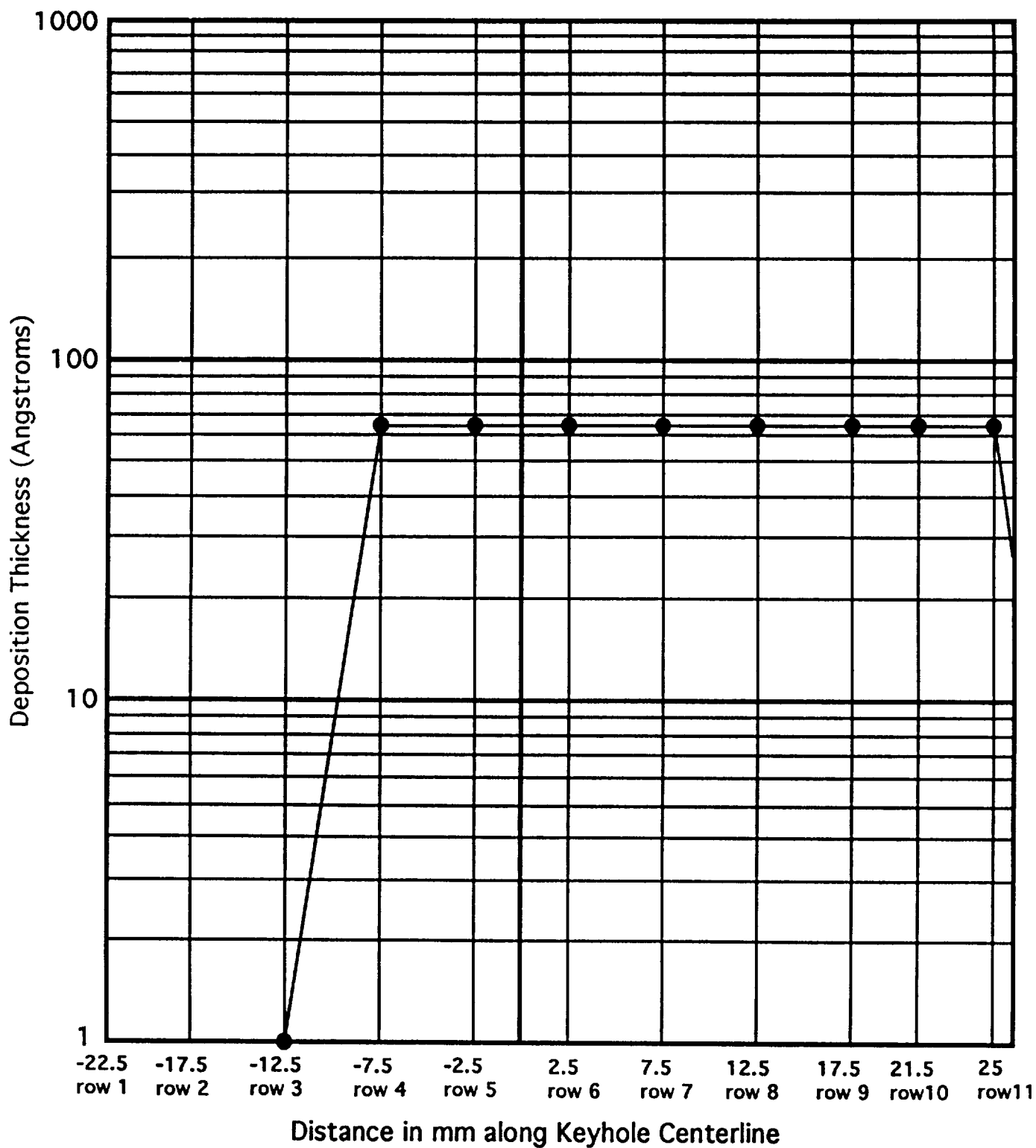
Deposition Along Keyhole Centerline (Angstroms)



Zero Represents Intersection of Thermal Blanket and Tray Wall

Figure 15 - Deposition Along Keyhole Centerline for C6

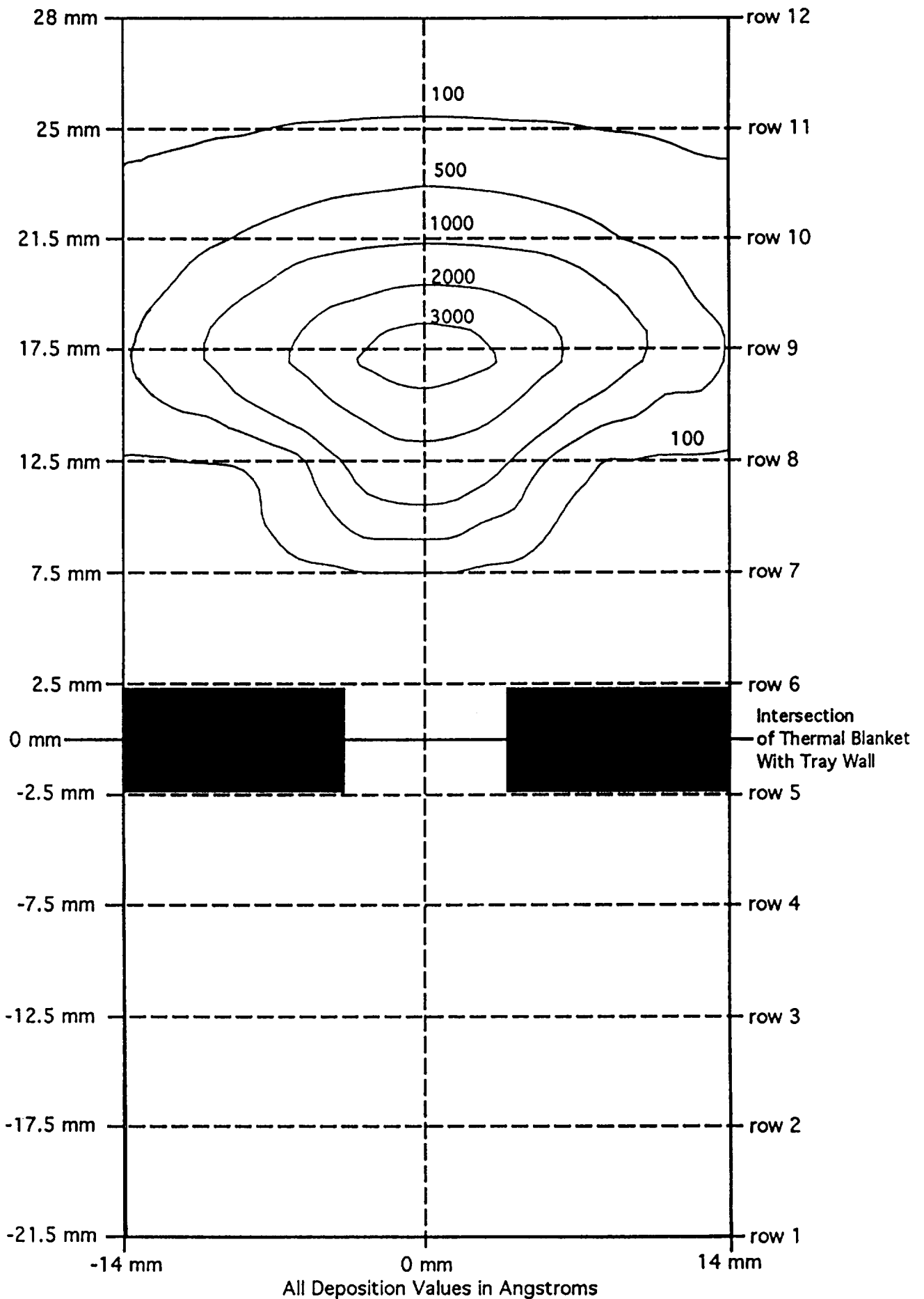
Deposition Along Keyhole Centerline (Angstroms)



Zero Represents Intersection of Thermal Blanket and Tray Wall

Figure 16 - Deposition Along Keyhole Centerline for A6

Figure 14 - C6 Contaminant Deposition Contours on Tray Wall



REPORT DOCUMENTATION PAGE

Form Approved
OMB No. 0704-0188

Public reporting burden for this collection of information is estimated to average 1 hour per response, including the time for reviewing instructions, searching existing data sources, gathering and maintaining the data needed, and completing and reviewing the collection of information. Send comments regarding this burden estimate or any other aspect of this collection of information, including suggestions for reducing this burden, to Washington Headquarters Services, Directorate for Information Operation and Reports, 1215 Jefferson Davis Highway, Suite 1204, Arlington, VA 22202-4302, and to the Office of Management and Budget, Paperwork Reduction Project (0704-0188), Washington, DC 20503

1. AGENCY USE ONLY (Leave Blank)		2. REPORT DATE September 1998	3. REPORT TYPE AND DATES COVERED Contractor Report (Final)	
4. TITLE AND SUBTITLE Comparison of Spacecraft Contamination Models with Well-Defined Flight Experiment			5. FUNDING NUMBERS NAS8-40581	
6. AUTHORS Dr. G. H. Pippin				
7. PERFORMING ORGANIZATION NAME(S) AND ADDRESS(ES) Boeing Information Space & Defense Systems P.O. Box 3999 Seattle, WA 98124			8. PERFORMING ORGANIZATION REPORT NUMBER M-894	
9. SPONSORING/MONITORING AGENCY NAME(S) AND ADDRESS(ES) National Aeronautics and Space Administration Washington, DC 20546-0001			10. SPONSORING/MONITORING AGENCY REPORT NUMBER NASA/CR-1998-208800	
11. SUPPLEMENTARY NOTES Prepared for the Marshall Space Flight Center for NASA's Space Environments and Effects (SEE) Program <u>Technical Monitor: Miria Finckenor</u>				
12a. DISTRIBUTION/AVAILABILITY STATEMENT Unclassified-Unlimited Subject Category 29 Standard Distribution			12b. DISTRIBUTION CODE	
13. ABSTRACT (Maximum 200 words) "Comparison of Spacecraft Contamination Models with Well-Defined Flight Experiment" report presents analyzed surface areas on particular experiment trays from the Long Duration Exposure Facility (LDEF) for silicone-based molecular contamination. The trays for examination were part of the Ultra-Heavy Cosmic Ray Experiment (UHCRE). These particular trays were chosen because each tray was identical to the others in construction, and the materials on each tray were well known, documented, and characterized. In particular, a known specific source of silicone contamination was present on each tray. Only the exposure conditions varied from tray to tray. The results of post-flight analyses of surfaces of three trays were compared with the predictions of the three different spacecraft molecular contamination models. Phase one tasks included 1) documenting the detailed geometry of the hardware; 2) determining essential properties of the anodized aluminum, Velcro™, silverized Teflon™, silicone gaskets, and DC6-1104™ silicone adhesive materials used to make the trays, tray covers, and thermal control blankets; 3) selecting and removing areas from each tray; and 4) beginning surface analysis of the selected tray walls. Phase two tasks included 1) completion of surface analysis measurements of the selected tray surface, 2) obtaining auger depth profiles at selected locations, and 3) running versions of the ISEM, MOFLUX, and PLIMP (Plume Impingement) contamination prediction models and making comparisons with experimental results.				
14. SUBJECT TERMS materials, contamination, space materials properties			15. NUMBER OF PAGES 287	
			16. PRICE CODE A13	
17. SECURITY CLASSIFICATION OF REPORT Unclassified	18. SECURITY CLASSIFICATION OF THIS PAGE Unclassified	19. SECURITY CLASSIFICATION OF ABSTRACT Unclassified	20. LIMITATION OF ABSTRACT Unlimited	